

# University of Southampton Research Repository ePrints Soton

Copyright © and Moral Rights for this thesis are retained by the author and/or other copyright owners. A copy can be downloaded for personal non-commercial research or study, without prior permission or charge. This thesis cannot be reproduced or quoted extensively from without first obtaining permission in writing from the copyright holder/s. The content must not be changed in any way or sold commercially in any format or medium without the formal permission of the copyright holders.

When referring to this work, full bibliographic details including the author, title, awarding institution and date of the thesis must be given e.g.

AUTHOR (year of submission) "Full thesis title", University of Southampton, name of the University School or Department, PhD Thesis, pagination

### UNIVERSITY OF SOUTHAMPTON

Faculty of Human and Social Sciences

### Dynamic Modelling of Blood Glucose Concentration in People With Type 1 Diabetes

by

Sean Michael Ewings

Thesis submitted for the degree of Doctor of Philosophy
December 2012

# UNIVERSITY OF SOUTHAMPTON ABSTRACT

#### FACULTY OF SOCIAL AND HUMAN SCIENCES

Mathematics

Doctor of Philosophy

# DYNAMIC MODELLING OF BLOOD GLUCOSE CONCENTRATION IN PEOPLE WITH TYPE 1 DIABETES

by Sean Michael Ewings

The behaviour of blood glucose concentration (BGC) in free-living conditions is not well understood in people with type 1 diabetes; in particular, the effect of different types of activity experienced in everyday life has not been fully investigated. Better understanding of the effect of major disturbances to BGC can improve treatment regimes and delay or prevent complications associated with diabetes. The current research investigates approaches to modelling BGC, based on blood glucose, physical activity, food and insulin data collected from a Diabetes UK study.

Exploratory analysis of the study data found that BGC is non-stationary and exhibits strong autocorrelation, which varies among and within individuals. Analysis of BGC in the frequency domain also highlights indistinct low-frequency periodicities. However, BGC measurements alone are not enough to predict BGC over several hours using autoregressive models.

Dynamic linear models are used to model BGC empirically using inputs from measured physical activity, and estimates of glucose and insulin absorption after food intake and injections, respectively, derived from physiological models in the literature. Dynamic linear models are used for parameter learning and predicting BGC over several hours: the models show some capability for predicting BGC for up to one hour, in particular highlighting periods of low and high BGC, but parameter estimates do not comply with established physiological knowledge.

A new semi-empirical compartmental model is developed to impose a structure that incorporates well-established physiology. A set of differential equations are converted into a probabilistic Bayesian framework, suitable for simultaneous, model-wide parameter estimation and prediction. A simulation study is conducted to determine the feasibility of using Markov chain Monte Carlo methods as a means for parameter estimation, and test performance in the predictive space. The methods show an ability to estimate a subset of the parameters simultaneously with good coverage, robustness to parameter misspecification, and insensitivity to specification of prior distributions.

The current research represents a new paradigm for analysing mathematical models of BGC, and highlights important practical and theoretical issues not previously addressed in the quest for an artificial pancreas as treatment for type 1 diabetes.

# Contents

1	Intr	oducti	on
	1.1	Type	1 Diabetes
		1.1.1	Treatment
			1.1.1.1 Insulin Therapy
		1.1.2	Hyperglycaemia
		1.1.3	Hypoglycaemia
	1.2	Type 2	2 Diabetes
	1.3	Other	Types of Diabetes
	1.4	Motiva	ation
	1.5	Resear	rch Overview and Contributions
		1.5.1	Thesis Structure
	1.6	Summ	ary 1
<b>2</b>	Res	earch l	Background 1:
	2.1	Metab	oolic Processes
		2.1.1	Role of Food
		2.1.2	Role of the Pancreas
		2.1.3	Role of the Liver
		2.1.4	Role of the Kidneys
		2.1.5	Role of the Brain
		2.1.6	Role of Muscles
		2.1.7	Role of Hormones
		2.1.8	Role of Fatty Acids
		2.1.9	Role of Glucose Transporters
		2.1.10	Implication of Type 1 Diabetes
	2.2	Exerci	se Physiology
		2.2.1	Whole-Body Changes
		2.2.2	Adenosine Triphosphate
		2.2.3	Carbohydrates as a Source of Energy
		2.2.4	Fats (lipids) as a Source of Energy
		225	Other Sources of Energy 25

		2.2.6	Hormonal Response to Exercise
		2.2.7	Implication of Type 1 Diabetes
	2.3	Other	Factors Affecting BGC
		2.3.1	Renal Clearance
		2.3.2	Temporal Effects
		2.3.3	Miscellaneous
	2.4	Physio	ological Review: Summary
	2.5	Modell	ling Techniques
		2.5.1	Compartmental Modelling
		2.5.2	Glucose Tolerance Tests
		2.5.3	Continuous Glucose Monitors
		2.5.4	Percentage of Maximal Oxygen Consumption
	2.6	Diabet	ses Modelling
		2.6.1	Glucose-Insulin Dynamics: Bergman's Minimal Model
		2.6.2	Glucose-Insulin Dynamics: Other Compartmental Models
		2.6.3	Glucose-Insulin Dynamics and Physical Activity
		2.6.4	Empirical Modelling of BGC
		2.6.5	Artificial Pancreas
	2.7	Modell	ling Review: Summary
		~	
3			ection and Exploratory Analysis
	3.1		tes UK Study
	3.2		Glucose Concentration Data
		3.2.1	MiniMed Calibration
	3.3		al Activity Data
	3.4	Food I	Diary
		3.4.1	Modelling the Digestive System
	3.5		Diary
		3.5.1	Modelling Insulin Injection
	3.6		ling Limitations
	3.7		Collection: Summary
	3.8	Time S	Series Methods
		3.8.1	Stochastic Processes
		3.8.2	Stochastic Processes in the Time Domain
			3.8.2.1 Autocovariance and Autocorrelation
			3.8.2.2 Simple Stochastic Models
			3.8.2.3 Autoregressive Moving-Average Models
			3.8.2.4 Extensions of ARMA models
		3.8.3	Estimation in the Time Domain

		3.8.4	Stochastic Processes in the Frequency Domain 5
		3.8.5	Estimation in the Frequency Domain
		3.8.6	Analysis of the Periodogram
			3.8.6.1 Smoothing the Periodogram
			3.8.6.2 Tapering
		3.8.7	Autoregressive Spectral Estimation
	3.9	BGC V	Variation in the Time Domain
		3.9.1	BGC AR Model
		3.9.2	BGC AR Prediction
			3.9.2.1 Results
		3.9.3	Conclusions
	3.10	BGC V	Variation in the Frequency Domain 6
		3.10.1	Results
		3.10.2	Conclusions
	3.11	Summ	ary 6
4	Dvr	amic I	Modelling of Blood Glucose Concentration 7
_	4.1		nic Linear Models
		4.1.1	Structure of a DLM
		4.1.2	Updating Procedure
		4.1.3	Unknown System Error Variance
		4.1.4	Unknown Observation Error Variance
		1,1,1	4.1.4.1 Time-Varying Observation Error Variance
		4.1.5	K-step Forecasting
		4.1.6	Filtering and Smoothing
			Reference Analysis
	4.2		of Blood Glucose Concentration
		4.2.1	First-order Polynomial Model
		4.2.2	One-Step Regression DLM
			4.2.2.1 Results
			4.2.2.2 Double-Discount DLM
			4.2.2.3 Sensitivity Analysis
			4.2.2.4 Model Diagnostics
			4.2.2.5 Filtered DLM of BGC
			4.2.2.6 Conclusions
	4.3	Sampl	ing the DLM of Blood Glucose Concentration
	5	4.3.1	Full, Individual Conditional Sampling
			4.3.1.1 Results
		432	Full Joint Conditional Sampling 10

			4.3.2.1 Results
			4.3.2.2 Conclusions
	4.4	Many-	Step Regression DLM
		4.4.1	12-Step BGC Prediction
		4.4.2	24-Step BGC Prediction
		4.4.3	48-Step BGC Prediction
		4.4.4	Conclusions
	4.5	Summ	ary
		4.5.1	Discussion
5	Sto	chastic	Modelling of Glucose-Insulin Dynamics in Free-Living Con-
	ditio	ons for	People with Type 1 Diabetes 119
	5.1	Develo	opment of the Minimal Model
		5.1.1	Stochastic Minimal Model
		5.1.2	Physical Activity Minimal Model
	5.2	PA Mo	odel and Free-Living Data
		5.2.1	Results
		5.2.2	Modified PA Model
	5.3	Stocha	astic Modified PA Model
		5.3.1	Posterior Distribution of the SPA model
	5.4	Simula	ation Study of MCMC and the SPA Model
		5.4.1	Practical MCMC Considerations
			5.4.1.1 Initialisation
			5.4.1.2 Tuning
		5.4.2	Results
		5.4.3	Model Verification
			5.4.3.1 Results
		5.4.4	Robustness
			5.4.4.1 Results
		5.4.5	Conclusions
	5.5	Summ	ary
6	Con	clusio	ns and Future Work 151
	6.1	Conclu	sions
		6.1.1	Contributions
	6.2	Future	e Work
	6.3	Summ	ary
$\mathbf{A}$	Bay	esian I	Methods 157

В	Dou	ıble <b>-</b> Di	scount DLM Structure	159			
$\mathbf{C}$	C Sampling-Based Methods						
	C.1	Monte	Carlo Integration	161			
	C.2	Marko	v Chains	162			
		C.2.1	Metropolis-Hastings Algorithm	162			
		C.2.2	Gibbs Sampling	163			
	C.3	Impler	menting MCMC	164			
		C.3.1	Proposal Density	164			
		C.3.2	Verification	164			
Re	efere	nces		167			

# List of Tables

2.1	Metabolic processes relating to BGC. The first three are anabolic processes (com-	
	plex substances formed from simpler substances), and the remaining are catabolic	
	pathways (complex substances broken down into simpler ones)	14
2.2	Selected organs, tissues and cells involved in blood glucose production and uptake	15
2.3	Function of various hormones on BGC	19
2.4	Function of glucose transporters	19
2.5	Parameters of the minimal model	28
3.1	Variables recorded by the SenseWear armband	41
3.2	Examples of approximate METs for various activities; values taken from Ainsworth	
	et al. (2000)	41
3.3	Parameters of the Lehmann and Deutsch (1992) digestion model	44
3.4	Parameters of the Tarin et al. (2005) insulin model	47
3.5	AIC of autoregressive models for change in BGC	62
4.1	FOP model error properties for selected values of discount factor, $\lambda$ ; all values	
	rounded to 3sf. Mean squared error (MSE), mean absolute deviation (MAD) and	
	log-likelihood ratio (LLR) as defined in section 4.1.3. Starred $(*)$ entries, where	
	given, indicate minimum values for MAD and MSE, and the maximum value for LLR. $$	85
4.2	One-step regression model error properties for selected values of discount factor, $\lambda$ ; all	
	values rounded to 3sf. Mean squared error (MSE), mean absolute deviation (MAD) $$	
	and log-likelihood ratio (LLR) as defined in section 4.1.3. Starred (*) entries, where	
	given, indicate minimum values for MAD and MSE, and the maximum value for LLR. $$	86
4.3	Reference model error properties for selected values of discount factor, $\lambda$ ; all values	
	rounded to 3sf. Mean squared error (MSE), mean absolute deviation (MAD) and	
	log-likelihood ratio (LLR) as defined in section 4.1.3. Starred $(*)$ entries, where	
	given, indicate minimum values for MAD and MSE, and the maximum value for LLR.	91
5.1	Relationship of model and equation parameters for the minimal model	120
5.2	Parameters for the Roy and Parker (2007) model. Parameters $p_i$ are assumed known	
	and taken from the original Bergman et al. (1979) model. The set of parameters $a_i$	
	are fitted using various studies; see Roy and Parker (2007) and references within	125

5.3	Parameter values used to generate BGC time series for simulation study.			137
5.4	CRPS values under scenarios given in section 5.4.4			149

# List of Figures

2.1	Glucose production from exogenous sources and the metabolic pathways	14
2.2	Internal glucose storage and utilisation	15
2.3	Diagram of the pancreas; image reproduced from http://www.webmd.com/digestive-	
	disorders/picture-of-the-pancreas, last accessed $02/10/12$	16
2.4	Minimal model of blood glucose metabolism; G represents BGC, $\mathbf{I}_p$ is plasma insulin	
	concentration, $I_a$ is active insulin concentration and parameters $k_1, \ldots, k_6$ represent	
	rates of exchange between compartments. Reproduced from Bergman et al. (1979).	28
2.5	Two-compartment glucose subsystem of Dalla Man et al. (2007). Variables and	
	parameters as described in text	30
2.6	Basic structure of artificial pancreas	34
3.1	Example of Guardian BGC measurements over 24 hours	39
3.2	Example of the one-step change in BGC time series, with times of calibration, for an	
	individual in the DUK study	40
3.3	Activity armband output over a 24-hour period for an individual in the DUK study:	
	(i) skin temperature; (ii) longitudinal acceleration	42
3.4	Metabolic equivalent units (METs) over a 24-hour period for an individual in the	
	DUK study	42
3.5	Estimated glucose absorption over a 24-hour period for one individual in the DUK	
	study using the Lehmann and Deutsch model	45
3.6	Estimated insulin absorption over a 24-hour period for one individual in the DUK	
	study using the Tarin et al. model	48
3.7	Glucose and insulin absorption over a 24-hour period for one individual in the DUK	
	study using the Lehmann and Deutsch and Tarin et al. models, respectively	48
3.8	Subject A's measured BGC time series	59
3.9	Autocorrelation coefficient against respective lag for BGC of Subject A. Dotted lines	
	represent theoretical 95% confidence intervals given by $\pm \frac{2}{\sqrt{n}}$	60
3.10	Autocorrelation coefficient against respective lag for BGC for two different individ-	
	uals in the DUK study. Dotted lines represent theoretical $95\%$ confidence intervals	
	given by $\pm \frac{2}{\sqrt{n}}$	60
3.11		61

3.12	Sample autocorrelation function for change in BGC of Subject A. Dotted lines rep-	
	resent theoretical 95% confidence intervals given by $\pm \frac{2}{\sqrt{n}}$	61
3.13		
	lines represent theoretical 95% confidence intervals given by $\pm \frac{2}{\sqrt{n}}$	62
3.14	AR(1) model residuals for change in BGC of Subject A	63
3.15	Correlogram of the AR(1) model residuals for change in BGC of Subject A	64
3.16	Measured BGC and one-step (five minutes) ahead prediction for BGC using $\operatorname{ARIMA}(1,1,1)$	0)
	model for Subject A	65
3.17	Measured BGC and 48-step (four hours) ahead prediction for BGC using $\operatorname{ARIMA}(1,1,0)$	
	model for Subject A	66
3.18	Periodogram for change in BGC of Subject A with taper proportion 0.1 and Daniell	
	smoothers of spans 7 and 11	68
3.19	Periodogram for change in BGC of Subject A using ASE	68
4.1	Measured BGC and FOP DLM predicted BGC for $\lambda = 0.01$ and $\lambda = 1.$	84
4.2	One-step (five minutes) ahead prediction of BGC and measured BGC, with $95\%$	
	credible intervals. Extreme values of intervals omitted for clarity	87
4.3	Predicted BGC (solid line) and 95% credible intervals for standard DLM ( $\delta=1$ ; blue	
	lines) and double discount model ( $\delta$ as described in the text, representing increased	
	uncertainty at time 21.12; red lines)	88
4.4	METs parameter estimates for varying discount factor: (i) $\lambda = 1$ ; (ii) $\lambda = 0.96$ ; (iii)	
	$\lambda = 0.5$ ; (iv) $\lambda = 0.1$	89
4.5	METs parameter estimates for varying initial values: (i) $\theta = (0,0,0,0)$ ; (ii) $\theta =$	
	$(100, 100, 100, 100)$ ; (iii) $\theta = (-100, -100, -100, -100)$ ; (iv) $\theta = (100, -100, 100, -100)$	. 90
4.6	Measured BGC and predicted BGC for reference analysis approach, with $95\%$ cred-	
	ible intervals	92
4.7	Time series of reference model forecast variance	92
4.8	Time series of filter model one-step BGC prediction errors	93
4.9	Partial autocorrelation function of filter model errors	93
4.10	Reference model errors against measured BGC	94
4.11	Reference filter model output for BGC and measured BGC	95
4.12	Parameter estimates for the reference filter model: (i) constant parameter; (ii) car-	
	bohydrate parameter; (iii) insulin parameter; (iv) METs parameter	96
4.13	Predicted BGC in the absence of insulin based on filter model results	97
4.14	Predicted BGC and measured BGC using parameter predictions from previous 24-	
	hour period	98
4.15	Representative MCMC output for full, individual conditional distribution sampling	
	of DLM parameters: (i) the constant parameter at time $t=1$ and (ii) $t=800$ ; (iii)	
	the carbohydrate parameter at $t = 100$ ; (iv) the insulin parameter at time $t = 500$ .	102

4.16	MCMC output for observation error precision, $\phi$ , under full, individual conditional	
	distribution sampling of DLM parameters	103
4.17	Representative MCMC trace plots, sampled values for: (i) constant parameter at	
	time t=0; (ii) carbohydrate parameter at time t=50; (iii) insulin parameter at time	
	t=100; (iv) METs parameter at time t=500	105
4.18	MCMC trace plot for observation error precision, $\phi$	105
4.19	Means (solid lines) and $95\%$ quantiles (dotted lines) from MCMC output for: (i)	
	constant parameter; (ii) carbohydrate parameter; (iii) insulin parameter; (iv) METs	
	parameter	106
4.20	12-steps (one hour) ahead predicted BGC (solid line) and measured BGC (dotted	
	line): (i) time series $g_{[1]}$ , as given in (4.4.1); (ii) time series $g_{[12]}$	109
4.21	24-hour window of compiled 12-step predicted BGC from all time series, $g_{[n]}$ , and	
	measured BGC. Red circles indicate points in time series $g_{[1]}$	109
4.22	(i) Function $I_t^{(1)}(\cdot)$ (4.4.2) applied to 12-step predicted BGC (black dots) and mea-	
	sured BGC (red dots); (ii) function $I_t^{(2)}(\cdot)$ applied to 12-step predicted and measured	
	BGC	110
4.23	Parameter estimates for 12-step predictive model: (i) constant parameter; (ii) car-	
	bohydrate parameter; (iii) insulin parameter; (iv) METs parameter	110
4.24	24-steps (two hours) ahead predicted BGC (solid line) and measured BGC (dotted	
	line): (i) time series $g_{[1]}$ , as given in (4.4.1); (ii) time series $g_{[24]}$	112
4.25	24-hour window of compiled 24-step predicted BGC from all time series, $g_{[n]}$ , and	
	measured BGC. Red circles indicate points in time series $g_{[1]}$	112
4.26	(i) Function $I_t^{(1)}(\cdot)$ (4.4.2) applied to 24-step predicted BGC (black dots) and mea-	
	sured BGC (red dots): (ii) function $I_t^{(2)}(\cdot)$ applied to 24-step predicted and measured	
	BGC	113
4.27	Parameter estimates for 24-step predictive model: (i) constant parameter; (ii) car-	
	bohydrate parameter; (iii) insulin parameter; (iv) METs parameter	113
4.28	48-steps (four hours) ahead predicted BGC (solid line) and measured BGC (dotted	
	line): (i) time series $g_{[1]}$ , as given in (4.4.1); (ii) time series $g_{[48]}$	114
4.29	24-hour window of compiled 48-step predicted BGC from all time series, $g_{[n]}$ , and	
	measured BGC. Red circles indicate points in time series $g_{[1]}$	114
4.30	(i) Function $I_t^{(1)}(\cdot)$ (4.4.2) applied to 48-step predicted BGC (black dots) and mea-	
	sured BGC (red dots); (ii) function $I_t^{(2)}(\cdot)$ applied to 48-step predicted and measured	
	BGC	115
4.31	Parameter estimates for 48-step predictive model: (i) constant parameter; (ii) car-	
	bohydrate parameter; (iii) insulin parameter; (iv) METs parameter	115
<u>ር</u> 1	Minimal model of almost insulin him time (2) and 1 ft 1 (2)	
5.1	Minimal model of glucose-insulin kinetics: (i), model of glucose metabolism; (ii),	190
	model of insulin kinetics. Reproduced from Bergman et al. (1979, 1981)	120

5.2	Directed acyclic graph of the Andersen and Højbjerre (2005) model	23
5.3	Glucose (i) and insulin absorption (ii) (from the digestion and insulin models) and	
	relative PVO <sub>2</sub> <sup>max</sup> (iii) for Subject A	26
5.4	PA model predicted of BGC and measured BGC for Subject A	26
5.5	Integrated exercise intensity from the PA model for Subject A	27
5.6	Hepatic contribution to BGC from the PA model for Subject A	27
5.7	Blood insulin concentration from the PA model for Subject A	28
5.8	BGC profiles for two different basal glucose values, $G_b=4.44$ mmol/l and $G_b=4.17$ mmol/l.	128
5.9	Renal clearance for a range of BGC. Recreated from Arleth et al. (2000)	30
5.10	The modified physical activity model for glucose-insulin kinetics, where PA indicates	
	the relationships affected by physical activity	30
5.11	Measured BGC and modified PA model results for BGC	.31
5.12	Directed acyclic graph of the extended model	34
5.13	(i) Estimated glucose and (ii) insulin absorption (from the digestion and insulin	
	models) and (iii) relative PVO $_2^{max}$ for one day of Subject A's records	37
5.14	MCMC trace plot for $p_5$ from a long chain	40
5.15	MCMC trace plots for $p_1$ based on three different starting values: (i) $p_1^{(0)} = 0$ , (ii)	
	$p_1^{(0)}=-10$ (iii) $p_1^{(0)}=-3.35$ (the true value, as indicated by the red line in each plot). 1	41
5.16	Measured BGC and MCMC output	42
5.17	Means and 95% credible intervals for $p_1$ from each Markov chain in the simulation	
	study; the horizontal line represents the value of $p_1$ used to generate the simulations. 1	43
5.18	Means and 95% credible intervals for $p_2$ from each Markov chain in the simulation	
	study; the horizontal line represents the value of $p_2$ used to generate the simulations. 1	43
5.19	Means and 95% credible intervals for $p_{10}$ from each Markov chain in the simulation	
	study; the horizontal line represents the value of $p_{10}$ used to generate the simulations. 1	44
5.20	Means and 95% credible intervals for $\tau_i$ from each Markov chain in the simulation	
	study; the horizontal line represents the value of $\tau_i$ used to generate the simulations.	45
5.21	Means and 95% credible intervals for $\tau_{g^*}$ from each Markov chain in the simulation	
	study; the horizontal line represents the value of $\tau_{g^*}$ used to generate the simulations. 1	45
5.22	Means and 95% credible intervals for each missing observation under scenario A $1$	47
5.23	Means and 95% credible intervals for each missing observation under scenario B $1$	47
5.24	Means and 95% credible intervals for each missing observation under scenario C (first	
	block)	48
5.25	Means and 95% credible intervals for each missing observation under scenario C $$	
	(second block)	48

# Declaration of Authorship

I, SEAN MICHAEL EWINGS, declare that the thesis entitled

# DYNAMIC MODELLING OF BLOOD GLUCOSE CONCENTRATION IN PEOPLE WITH TYPE 1 DIABETES

and the work presented in it are my own and has been generated by me as the result of my own original research.

I confirm that:

- 1. This work was done wholly or mainly while in candidature for a research degree at this University;
- 2. Where any part of this thesis has previously been submitted for a degree or any other qualification at this University or any other institution, this has been clearly stated;
- 3. Where I have consulted the published work of others, this is always clearly attributed;
- 4. Where I have quoted from the work of others, the source is always given. With the exception of such quotations, this thesis is entirely my own work;
- 5. I have acknowledged all main sources of help;
- 6. Where the thesis is based on work done by myself jointly with others, I have made clear exactly what was done by others and what I have contributed myself;
- 7. None of this work has been published before submission.

Signed	 		 	 		 		 											
Date.	 																		

# Acknowledgements

I would firstly like to thank my supervisors, Dr. Sujit Sahu and Dr. Andy Chipperfield, for their guidance, enthusiasm and encouragement throughout. I am also grateful for the support of EPSRC and the work of Diabetes UK and all those involved in the study, particularly Dr. John Joseph Valletta.

I owe a very large thank you to my family, Paul, Maeve, Fiona and Holly, and fiancée, Izi; their unwavering belief and support was invaluable and I cannot thank them enough.

Finally, a thank you also to all the brilliant people at the university I have shared offices and cake with through the years; it has been an enormous pleasure.

## List of Abbreviations

AIC Akaike information criterion

AIDA Automated Insulin Dosage Advisor

AP Artificial pancreas
AR Autoregressive

ARIMA Autoregressive integrated moving average

ARMA Autoregressive moving average
ASE Autoregressive spectral estimation

ATP Adenosine triphosphate

BGC Blood glucose concentration CGM Continuous Glucose Monitor

CRPS Continuous ranked probability score

CSII Continuous subcutaneous insulin infusion

DCCT Diabetes Care and Control Trial

DAG Directed acyclic graph
DE Differential equation

DIAS Diabetes Advisory System

DKA Diabetic ketoacidosis
DLM Dynamic linear model

DP Dormand-Prince

DUK Diabetes UK

EDIC Epidemiology of Diabetes Interventions and

Complications

FFA Free fatty acid

FOP First-order polynomial

 $\begin{array}{ll} \operatorname{GI} & \operatorname{Glycaemic\ index} \\ \operatorname{GL} & \operatorname{Glycaemic\ load} \\ \operatorname{GLUT} & \operatorname{Glucose\ transporter} \\ \operatorname{HbA}_{1c} & \operatorname{Glycated\ haemoglobin} \end{array}$ 

IF Interstitial fluid

IVGTT Intravenous glucose tolerance test

KADIS Karlsburger Diabetes Management System

LLR Log-likelihood ratio
MA Moving average

MAD Mean absolute deviation
MCMC Markov chain Monte Carlo
MDI Multiple daily injections
MET Metabolic equivalent of task

MH Metropolis-Hastings

MM Minimal Model

MPC Model predictive control

MSE Mean squared error

OGTT Oral glucose tolerance test

PA model Physical activity minimal model

PCr Phosphocreatine

PDM Principal dynamic mode

PID Proportional-integral-derivative

PVO<sub>2</sub><sup>max</sup> Percentage of maximal oxygen consumption

SCMH Single-component Metropolis-Hastings

SGLT Sodium-glucose transport protein

TG Triglyceride

# Chapter 1

# Introduction

Diabetes mellitus (usually referred to as diabetes) is a chronic metabolic disorder characterised by prolonged high blood glucose concentration (hyperglycaemia). Glucose is a vital energy source for the body, particularly the brain, and its concentration in blood is maintained within strict limits by various hormones. Insulin is crucial in this process, as it is the only hormone that allows cells to take up glucose from the blood to meet energy requirements. Diabetes is caused by reduced sensitivity to, or insufficient secretion of, insulin. Defective insulin response results in hyperglycaemia, which is associated with increased morbidity and mortality.

Worldwide prevalence of all forms of diabetes is approximately 180 million (World Health Organisation, 2008), which is estimated to more than double by 2030 (Wild et al., 2004). There is no cure, and day-to-day management is the responsibility of the individual. Serious short- and long-term health complications are common due to the unpredictable nature of treatment. Greater understanding of how different factors affect blood glucose concentration (BGC) can help improve current treatment programmes, and decrease the mental, physical and financial burden on individuals and health services.

There are two predominant forms of diabetes, type 1 and type 2; the current work is primarily focused on type 1 diabetes. This chapter discusses its causes, treatment and complications, leading to the motivation for the current project and its potential contributions to understanding and managing diabetes. The chapter also introduces key concepts used throughout the thesis.

### 1.1 Type 1 Diabetes

Type 1 diabetes<sup>1</sup> is a chronic autoimmune disease where an individual loses the ability to produce insulin. The hormone is normally created in  $\beta$ -cells found in regions of the

 $<sup>^{1}</sup>$ also referred to as insulin-dependent or juvenile-onset diabetes, though these are no longer defining characteristics.

pancreas called the islets of Langerhans. In people with type 1 diabetes, the  $\beta$ -cells are destroyed, leaving no means for the uptake and utilisation of blood glucose (glucose metabolism); the individual is thus deprived of a vital source of energy.

The  $\beta$ -cells are destroyed by the body's own immune system, specifically by a T-cell mediated response (Roep, 2003). The autoimmune reaction may be triggered by an infection, where the body's attack on virus-infected cells is also directed against  $\beta$ -cells. There is evidence that enterovirus infections are linked to type 1 diabetes more strongly than other environmental factors (Hyoty, 2002). Other research has focused on genetic predisposition to type 1 diabetes; genetic susceptibility stems from genes in the human leukocyte antigen region (Donner et al., 1997). An ongoing collaborative article from the Online Mendelian Inheritance in Man website<sup>2</sup> documents other work studying genetic factors in type 1 diabetes.

Type 1 diabetes tends to present in people under the age of 30. The onset can be quick, from a few days to a few weeks. When insulin-producing mechanisms are destroyed, a number of physiological processes become unregulated. This results in the over-production of ketones, which increase blood acidity (a process known as diabetic ketoacidosis, DKA). Left untreated, type 1 diabetes will result in coma and eventually death.

Type 1 diabetes accounts for approximately 15% of known cases of diabetes in the UK, equivalent to around 250-300,000 people. The incidence of type 1 diabetes over the period 1996-2005 remained relatively constant in the UK (Gonzalez et al., 2009); however, there is evidence of increasing incidence around the world in 0-14 year-olds (Onkamo et al., 1999), and other studies have found increasing prevalence in different countries, e.g., Akesen et al. (2011); Ehehalt et al. (2012).

#### 1.1.1 Treatment

There is currently no widely available cure for any form of diabetes. A pancreas transplant is a highly invasive and expensive procedure, requiring a post-transplant lifetime of immunosuppressant drugs. Pancreas transplants are usually only carried out in individuals that are undergoing/have undergone other organ transplants. Islet cell transplant is less invasive, where cells from donor pancreases are infused into the individual to replace the lost insulin function. The method has produced promising preliminary results (Shapiro et al., 2000), with the development of the Edmonton Protocol (Shapiro et al., 2006) designed to investigate the potential of a standardised approach to treatment in an international, multi-centre trial. However, the method is still hampered by the need for immunosuppressants and potentially multiple donors for one individual's treatment.

<sup>&</sup>lt;sup>2</sup>http://www.ncbi.nlm.nih.gov/omim/222100, last accessed 12/01/2012

Developments in stem cell research offer a route for curing diabetes that potentially eliminates the need for immunosuppressants. Promising results have been seen in small, preliminary studies, e.g., Couri et al. (2009), though traditional stem cell therapy does not overcome the underlying problems of autoimmunity. However, particular forms of stem cells have been shown to change immune activity; Zhao et al. (2012) presented results from a small trial demonstrating reduced autoimmunity maintained over several months. Stem cell research in diabetes is, however, in its infancy, and any potential cure remains in the distant future.

Current treatment regimes for diabetes are based on careful management of BGC. For people without diabetes, BGC ranges between  $\sim$ 4-7 mmol/l (also reported as  $\sim$ 75-120 mg/dl, where 18 mmol/l  $\sim$  1 mg/dl; the units mmol/l will be used here) in the fasting state, with post-prandial (after meal) peaks up to  $\sim$ 10 mmol/l. For people with type 1 diabetes, the aim is to maintain BGC within these ranges through insulin therapy (discussed in section 1.1.1.1).

Assessing insulin requirements to maintain healthy BGC (euglycaemia) is an individualised practice, dependent on various physiological and lifestyle factors. Age, gender, body mass index and duration of diabetes all relate to insulin needs (Muis et al., 2006); other important factors include insulin sensitivity (the body's ability to respond to insulin) and hormonal secretion (e.g., the response to physical or mental stress). It is well established that food and physical activity are the dominant external factors affecting the behaviour of BGC (as discussed later). The individual must assess their insulin needs according to these external factors, and their own experience, on an injection-by-injection basis. Choosing an appropriate insulin dosage is usually aided by a small number of finger-prick blood tests each day; these provide a measure of BGC at a particular moment in time, but offer no indication of stability or direction of change.

Long-term control of BGC is assessed during routine visits to a care facility, using a number of different methods. In particular, a blood test for glycated haemoglobin ( $HbA_{1c}$ ) offers an indication of BGC over the preceding 2-3 months. The  $HbA_{1c}$  blood test measures the extent to which glucose molecules have attached themselves to haemoglobin on red blood cells, where elevated readings suggest recurrent or prolonged hyperglycaemia.

#### 1.1.1.1 Insulin Therapy

Treatment with exogenous insulin began in the early 1920's, when Fredrick Banting and colleagues identified insulin and extracted it from animals for human injection. Diabetes was no longer an abruptly fatal illness, but early patients suffered pain, swelling and other allergic reactions, as well as unpredictable BGC (Bliss, 1982). Animal insulin has since been superseded by synthetic human insulin (also known as insulin

analogues), which rarely cause an allergic response; such insulin can also be altered to achieve different absorption and metabolism. A history of the major advancements in insulin production is discussed in Teuscher (2007).

Currently, the most common treatment programme is the multiple daily injection (MDI), or basal-bolus, regime, where exogenous insulin is delivered into the subcutaneous tissue using insulin pens or syringes. The programme is designed to mimic the response of a healthy pancreas, but at the cost of more insulin injections per day: a once-daily injection of basal insulin allows low-level metabolism of glucose throughout the day, while a bolus of fast-acting insulin is taken with each meal to help metabolise exogenous glucose. The amount of insulin taken with meals is based on an estimate of the amount of carbohydrate being consumed (carbohydrate counting) and recent and/or impending exercise.

Continuous subcutaneous insulin infusion (CSII), where insulin is delivered via a pump device and cannula, also aims to mimic the action of a healthy pancreas. While the cannula must be replaced every few days, the method helps to reduce the number of injections needed. In England and Wales, insulin pumps are generally only available to those experiencing severe difficulties in reaching and maintaining HbA<sub>1c</sub> targets, as indicated by the National Institute of Health and Clinical Excellence guidelines<sup>3</sup>. Pump use is limited due to cost and the training required for the user to successfully implement the regime (Pickup and Keen, 2001). However, the benefits of this method of treatment have been demonstrated: a meta-analysis showed improved HbA<sub>1c</sub> and mean BGC compared to conventional therapy, with no increase in adverse effects (Weissberg-Benchell et al., 2003).

CSII may be open- or closed-loop. In an open-loop system, the user is still responsible for selecting appropriate doses of insulin based on finger-prick blood tests, as with the MDI regime. A closed-loop system is the ideal as it removes the individual from the maintenance of euglycaemia. However, the system requires a BGC monitor to be worn continuously, and computational software to relay the information from the monitor as signals for action from the insulin pump. The combination of pump, monitor and software is often referred to as an artificial pancreas; this is discussed further in section 1.4.

For both MDI and CSII, insulin is delivered into subcutaneous tissue. This represents a compromise for insulin delivery; the tissue is easily accessible, but represents a "compartmental mismatch" (Buse et al., 2002): diffusion and absorption from subcutaneous tissue does not faithfully recreate the conditions associated with a healthy pancreas, with regard to the ratio of insulin concentration in the periphery and liver. However, other methods for insulin delivery are not widely used. Intravenous delivery is used in the health care environment, but is difficult outside of this. Inhaled insulin is

<sup>&</sup>lt;sup>3</sup>http://www.nice.org.uk/Guidance/TA151#documents, last accessed 11/01/2012

not generally available, in part due to fears over long-term complications of the lungs. Oral administration of insulin is currently not possible as it is broken down by digestive juices, rendering it unusable.

Whichever treatment programme is used, the ultimate aim is to achieve eugly-caemia. Due to the complex nature of BGC, maintaining euglycaemia is a daily challenge. Establishing a suitable insulin regimen is essentially a trial-and-error process for every individual, even with the support of a professional health care team. It is hugely important that BGC is maintained within the physiologically desirable range, as poor control of BGC can lead to a number of short- and long-term complications, discussed in the following two sections.

### 1.1.2 Hyperglycaemia

Extreme hyperglycaemia over a short period of time can cause life-threatening DKA. Frequent and prolonged hyperglycaemia damages blood vessels and results in a number of complications over a longer period of time. The Diabetes Care and Control Trial (DCCT; a 9-year clinical study) demonstrated that intensive blood glucose control<sup>4</sup> can reduce the risk of eye, kidney and nerve damage in the longer-term (DCCT Research Group, 1993). The follow-up study, the Epidemiology of Diabetes Interventions and Complications (EDIC), also showed that intensive control can reduce the risk of cardiovascular events, such as heart attack and stroke (DCCT/EDIC Study Research Group, 2005). Treatment aims to maintain euglycaemia and hence avoid these complications, but is itself associated with problems.

### 1.1.3 Hypoglycaemia

Hypoglycaemia, or low BGC, is a side effect of insulin therapy. The inexact nature of treatment means that BGC may fall below normal levels (generally 4 mmol/l is considered to be the threshold for hypoglycaemia). The brain is then starved of its primary energy source, and the individual will experience a hypoglycaemic reaction. Symptoms, and their severity, depend on the individual's recent history of hypoglycaemic reactions, and the severity of the hypoglycaemia. Failure to deal with hypoglycaemia may result in unconsciousness, and potentially death.

In a healthy pancreas, low BGC will stimulate the secretion of glucagon from pancreatic  $\alpha$ -cells and a concomitant suppression of insulin; this stimulates the liver to release glucose into the blood. However, injected insulin cannot be suppressed, and

<sup>&</sup>lt;sup>4</sup>The "intensive control" trialled by the DCCT involved upwards of four finger-prick blood tests a day, at least three injections of insulin per day (which could be adjusted according to food, physical activity and current BGC), monthly visits to a health care team, and more frequent contact via telephone to review their regimen. The control group consisted of people on one or two injections per day.

will continue to encourage blood glucose uptake and suppress the release of glucagon. Furthermore, glucagon response may be diminished over time in people with diabetes, weakening the body's ability to counteract hypoglycaemia (Liu et al., 1993). The secretion of epinephrine, which helps stimulate hepatic glucose release and triggers symptoms of hypoglycaemia, may also be attenuated in the presence of nerve damage.

Recent hypoglycaemic events may result in loss of awareness of future events, as hypoglycaemia lowers glycaemic thresholds for autonomic and symptomatic response (LeRoith et al., 2003). Thus, when several hypoglycaemic events occur over a short period of time, the body will only begin to respond to more severe hypoglycaemia, if at all. This can impact upon quality of life, due to fear of unexpected hypoglycaemia. The DCCT trial showed that while intensive control helped to reduce HbA<sub>1c</sub>, it also resulted in a three-fold increase in hypoglycaemic events. It appears that by making a concentrated effort to avoid hyperglycaemia, individuals run an increased risk of hypoglycaemia.

Other side effects of treatment are relatively uncommon. Repeated injections in the same site can lead to hard lumps (hyperlipotrophy) forming under the skin, which can disrupt insulin absorption; it is recommended that injection sites are rotated to avoid unpredictable absorption, which can result in hypo- or hyperglycaemia (Saez-de Ibarra and Gallego, 1998).

### 1.2 Type 2 Diabetes

Type 2 diabetes<sup>5</sup> is generally associated with genetic and lifestyle factors, particularly obesity and sedentary lifestyle (Zimmet, 1982; Ohlson et al., 1988; Hu, 2003). Defective insulin response manifests in the form of lowered insulin sensitivity (where tissues are less responsive to insulin, thus diminishing the body's capacity to metabolise blood glucose) and/or relatively-reduced insulin secretion. Onset is gradual and can go unnoticed for many years, with potentially 40% of type 2 diabetes cases unidentified (Thomas et al., 2005).

Type 2 diabetes tends to present in adults over the age of 40, though changes in lifestyle has resulted in increased incidence in younger adults and children are increasing (Fagot-Campagna et al., 2001). It is estimated that more than 2.5 million people in the UK have type 2 diabetes. The Centers for Disease Control and Prevention (part of the US health service) note that the number of Americans with type 2 diabetes tripled in the period 1980 to 2006, from 5.6 million to 16.8 million, and led them to label it "an epidemic" 6.

<sup>&</sup>lt;sup>5</sup>also referred to as non-insulin dependent or adult-onset diabetes, though these are no longer defining characteristics.

<sup>&</sup>lt;sup>6</sup>http://www.cdc.gov/nccdphp/publications/aag/ddt.htm, last accessed 12/01/2012

Generally, the first course of treatment is to make lifestyle changes, as dietary improvements and increased physical activity can help improve insulin sensitivity. If this is unsatisfactory, oral drugs may be prescribed. Failure to achieve euglycaemia with these approaches means exogenous insulin may be required, as with type 1 diabetes.

### 1.3 Other Types of Diabetes

There are various other types of diabetes, which are generally less common. Gestational diabetes can occur in pregnant women when the increased insulin demands placed on the body during pregnancy are not met. Gestational diabetes is temporary and the problem usually resolves itself after the baby is born. However, it needs careful management during the course of pregnancy to ensure the short- and long-term health of mother and child. Other rarer forms of diabetes also exist, such as secondary diabetes mellitus, caused by any drug or disease that damages the pancreas or  $\beta$ -cells.

The current project will focus on type 1 diabetes; however this does not discount applicability to other types of diabetes, particularly those that require exogenous insulin.

### 1.4 Motivation

Diabetes is a major public health issue. The National Diabetes Audit (NHS Information Centre, 2011), based on English GP practices, estimated there were 24,000 more deaths in the diabetes population compared to the general population in the 2007-08 cohort. Soedamah-Muthu et al. (2006) reported mortality rates of 8 per 1,000 person-years in the type 1 diabetes group, compared to 2.15 per 1,000 person-years in the control group. It is a growing worldwide problem, and the burden on health services is already substantial. The National Health Service in the UK spends approximately 10% of its budget annually on treatment for all forms of diabetes (Diabetes UK, 2008). The American Diabetes Association estimates similar levels of spending in U.S. healthcare, corresponding to \$147bn in 2007. Thus, diabetes attracts a great amount of research interest that will only escalate given its increasing prevalence.

For those with diabetes, maintaining euglycaemia is a daily challenge, with insulin needs having to be balanced against various lifestyle factors. The repercussions of poor BGC control can present in the short- and long-term, and may result in eye, nerve and kidney damage, as well as cardiovascular events such as heart attack and stroke. Effective treatment can prevent, delay or slow the progress of these complications.

 $<sup>^7 \</sup>rm http://www.diabetesarchive.net/advocacy-and-legal$ resources/cost-of-diabetes.jsp, last accessed <math display="inline">13/09/2012

The DCCT study demonstrated that intensive treatment can be effective in preventing longer-term complications, albeit at the risk of more frequent hypoglycaemic episodes. However, not all aspects of the treatment are realistic in the long-term; in particular, the weekly and monthly consultations with various health care specialists are generally not viable due to time and financial constraints. Thus, effective treatment must rely more on the individual or on other more cost-effective methods. To this end, much work has focused on understanding the factors which affect BGC and how they manifest.

It is well established that food, insulin and physical activity are the major factors affecting BGC. In the diabetes literature, much recent work has focused on describing glucose-insulin dynamics in the blood under these external disturbances. Many of the underlying modelling strategies used in such work are attributable to landmark research undertaken by Bergman and colleagues (Bergman et al., 1979, 1981; Toffolo et al., 1980), who developed a "minimal model" to be used for estimating insulin sensitivity (the work was predominantly concerned with type 2 diabetes). The minimal model compartmentalised the body by separating out the most important features of the body's response to a glucose load, though originally made no consideration of food intake, insulin injections or physical activity.

Compartmental models (discussed in section 2.5.1) have long been a popular approach to describing glucose-insulin dynamics, with prominent examples found in Sorensen (1985), and computer packages AIDA (Lehmann and Deutsch, 1992) and DIAS (Hejlesen et al., 1997). These models have been extended to account for processes that were previously overlooked, e.g., the models of Bergman et al. and Sorensen have been extended by Derouich and Boutayeb (2002) and Hernandez-Ordonez and Campos-Delgado (2008), respectively, to include the effects of physical activity. More recently, compartmental models have been used in the development of software as part of an artificial pancreas. It is interesting to note, however, that in a review of diabetes modelling, experienced authors Lehmann and Deutsch suggest that "compartmental model-based computational techniques may have relatively little utility for generating glycaemic prediction and offering decision support in routine clinical practice" (Lehmann and Deutsch, 1998).

The concept of the artificial pancreas generates much of the current diabetes modelling literature, despite the fact that the necessary insulin pump and BGC monitor are not part of the current standard treatment protocol for diabetes. Furthermore, the various proposed control algorithms in the literature have only been tested using simulated BGC profiles. The approach has yet to demonstrate long-term efficacy, cost-effectiveness, and most crucially, safety. In contrast, there appears to be much less focus on improving the MDI treatment regime that is most commonly used in diabetes management.

Despite advances in understanding glucose metabolism, diabetes research is still hampered by a lack of free-living data. Data collected in a clinical setting may have very limited relevance to the daily life of an individual. This is particularly notable in the case of physical activity; attempts to adequately incorporate activity into models of glucose-insulin dynamics have been based on data collected from unrealistic, simplified and/or artificial experiments, or from non-diabetic subjects. A number of different approaches to quantifying exercise have been proposed, each with their own advantages and limitations. The percentage of maximum oxygen uptake (PVO<sub>2</sub><sup>max</sup>; discussed in section 2.5.4) has been used in a number of studies, e.g., Lenart and Parker (2002) and Hernandez-Ordonez and Campos-Delgado (2008), and is based on the approximate linear relationship between oxygen consumption and energy expenditure. However, measuring PVO<sub>2</sub><sup>max</sup> requires specialist equipment only found in a clinical environment. Breton (2008) proposed the use of heart rate as an indication of exercise duration and intensity. This has only been trialled within a very strict clinical environment, and has yet to be used in the free-living environment.

Recently developed devices, such as the BodyMedia SenseWear armband (Andre et al., 2006) which estimates physical activity as a multiple of resting metabolic rate, offer an opportunity to quantify both the duration and intensity of activity outside of the clinical setting. As such, these devices can be a crucial component in understanding how activity affects BGC in free-living conditions. It is worth highlighting the importance of people with diabetes being able to safely incorporate physical activity into their daily routine; the benefits in the general population are well-documented, and regular physical activity is also associated with better glycaemic control and enhanced insulin sensitivity for people with diabetes (Waden et al., 2005; Herbst et al., 2006; Riddell and Iscoe, 2006).

### 1.5 Research Overview and Contributions

The proposed research seeks to combine data from SenseWear devices with detailed, free-living data on BGC, food and insulin for the purpose of improving current treatment regimes, without recourse to continuous glucose monitors and insulin pumps, and potential treatment regimes based on an artificial pancreas. The research will draw on knowledge from a number of separate disciplines relevant to diabetes; this includes work that describes the digestion of food, absorption of injected insulin, and the effects of physical activity.

The current work has two main aims: the first is to investigate more precisely how the effects of physical activity manifest in the behaviour of BGC; this has the potential

<sup>&</sup>lt;sup>8</sup>Free-living data is a term used throughout to refer to data that is collected from an individual's everyday environment without impediment

to help those with diabetes safely incorporate physical activity into daily life, and enjoy the health benefits without the dangers of hypo- or hyperglycaemia. The second aim is to build a model that can accurately predict BGC over periods of several hours. Prediction over four hours (or more) are of particular interest, as this represents a reasonable amount of time between finger-prick tests as part of the MDI regime. Such a model could then be included in current treatment regimes by guiding the insulin therapy decision-making process.

An appropriate predictive and/or descriptive model of BGC would help reduce the risk of the short- and long-term complications associated with diabetes, and reduce the burden on individuals and health services. The proposed work thus offers the potential for a relatively inexpensive and immediate improvement in diabetes care. Furthermore, better understanding of the role of physical activity would further develop the push for an artificial pancreas, by providing a more physiologically-accurate representation of the glucoregulatory system under the stimuli experienced by individuals with type 1 diabetes in their normal daily environment.

#### 1.5.1 Thesis Structure

The thesis is divided as follows:

- Chapter 2 reviews relevant literature in physiology and mathematical modelling. The work highlighted here helps guide modelling strategies used throughout the rest of the current work;
- Chapter 3 discusses in detail the unique data which drives the current project. Practical modelling issues regarding the food and insulin data are highlighted and overcome with the use of physiological models taken from the literature. The chapter also introduces and uses simple time series analysis methods, including analysis in the time and frequency domains, to better understand the nature of free-living BGC data. The exploratory measures inform the more complex modelling strategies used in later chapters;
- Chapter 4 uses dynamic linear models, not previously used in diabetes modelling, to predict BGC from food, insulin and physical activity data. These models are also used to explore the role of physical activity in the behaviour of BGC. Long-term predictions of BGC (over several hours) take the form of either forecasting the profile of BGC or forecasting periods of hypo- and hyperglycaemia. The models presented here are one of few empirical approaches used to predict the behaviour of BGC;

- Chapter 5 uses a more detailed semi-empirical compartmental model to further investigate the role of physical activity in the behaviour of BGC. The chapter describes the potential problems in many of the current diabetes modelling strategies with regard to free-living data, highlighting the danger of building models based on inappropriate data from non-diabetic subjects or simulations. A new model, with food, insulin and physical activity inputs, is presented to overcome limitations of current models. The performance of the new model is tested using the free-living data previously described. The chapter presents a simulation study designed to test the feasibility of a Bayesian approach and modern, computationally-intensive statistical methods to simultaneously estimate model parameters, and predict BGC. This is the first time the descriptive capabilities of compartmental models have been tested with free-living data;
- Chapter 6 summarises the work of the previous chapters and makes recommendations for future work in the area.

### 1.6 Summary

Type 1 diabetes is a worldwide problem, whose treatment and associated complications represent a great cost to individuals and health services. Current treatment methods such as MDI are limited due to the variable nature of BGC, and intensive treatment to limit hyperglycaemia results in more frequent hypoglycaemic episodes. The development of an artificial pancreas is ongoing, and attempts to model BGC are limited by a lack of appropriate and relevant data, particularly with regard to physical activity. New technology, such as the BodyMedia SenseWear® device, provide a means of quantifying activity in free-living conditions, and hence may be used to assess and model the effect of exercise on BGC. This opens the possibility of data-driven models for BGC using food intake, insulin and physical activity as explanatory variables, and testing compartmental models developed using artificial data.

# Chapter 2

# Research Background

The following chapter is a review of research in diabetes, and other relevant fields, that provides context to the current work. The chapter is split into two sections: the first is a review of the literature on relevant physiology and the effect of diabetes on the body's internal processes, and the second is a review of the diabetes modelling literature. Understanding the relevant underlying physiology is vital for modelling the behaviour of blood glucose concentration (BGC), particularly if the model is to be accurate, viable and interpretable by potential end-users, i.e., clinicians and people with diabetes. The second section presents the motivations and objectives of research related to the current work, and how modelling approaches are guided by the physiology presented in the first section. The review includes discussion of limitations in the research and how the current work may improve the body of knowledge.

### Physiological Review

This section looks at the different factors that affect BGC, and how diabetes impacts on these. The roles of various organs, tissues, cells and hormones and their relationships (collectively called the glucoregulatory system) are discussed with respect to their influence on blood glucose homeostasis (self-regulation). The second half of this section focuses on the body's response to physical activity, highlighting the practical and theoretical difficulties in modelling this response.

### 2.1 Metabolic Processes

Blood glucose is a vital source of energy for the body, whose regulation is maintained via various metabolic pathways, summarised in Table 2.1. Glucose in the body is derived from digestion of the nutrients carbohydrate, fat and protein; Figure 2.1 shows the processes by which the body converts food to glucose. Reserves of glucose are

stored as glycogen in the liver and muscles, and excess glucose is converted to fat for storage in adipose tissue. BGC is maintained within strict limits by various hormones (discussed later) that stimulate metabolic processes responsible for either uptake to, or release from, the glucose stores; Figure 2.2 shows how blood glucose is maintained by these processes. The role of blood glucose in providing the means for energy synthesis is summarised in Table 2.2, and is discussed in more detail throughout the following sections.

Table 2.1: Metabolic processes relating to BGC. The first three are anabolic processes (complex substances formed from simpler substances), and the remaining are catabolic pathways (complex substances broken down into simpler ones).

Process	Definition
Glycogenesis	Creation of glycogen from glucose
Gluconeogenesis	Creation of glucose from non-carbohydrate substrates
Lipogenesis	Creation of triglycerides from glucose
Glycolysis	Breakdown of glucose for energy
Glycogenolysis	Breakdown of glycogen to glucose
Lipolysis	Breakdown of triglyceride into fatty acids and glycerol

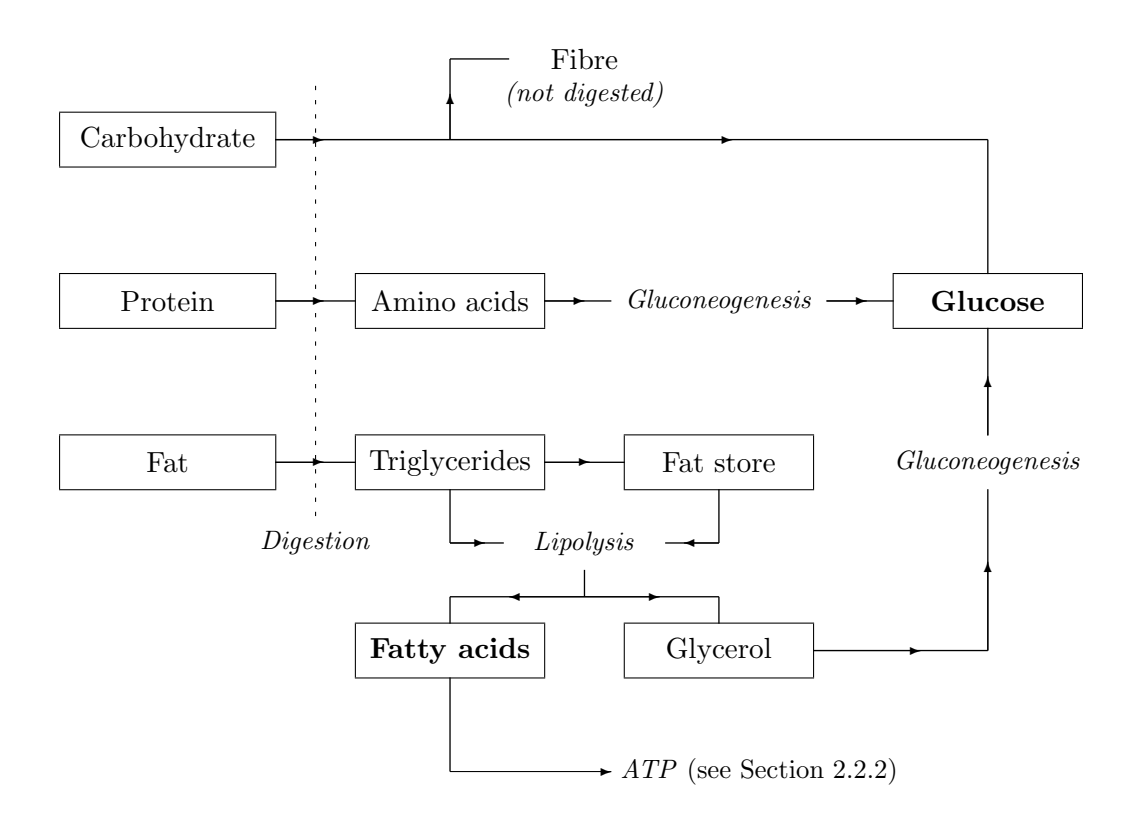


Figure 2.1: Glucose production from exogenous sources and the metabolic pathways.

<sup>&</sup>lt;sup>1</sup>Reference to energy or energy synthesis in this work refers to free energy, i.e., energy derived from chemical reactions that can be used by a cell for work.

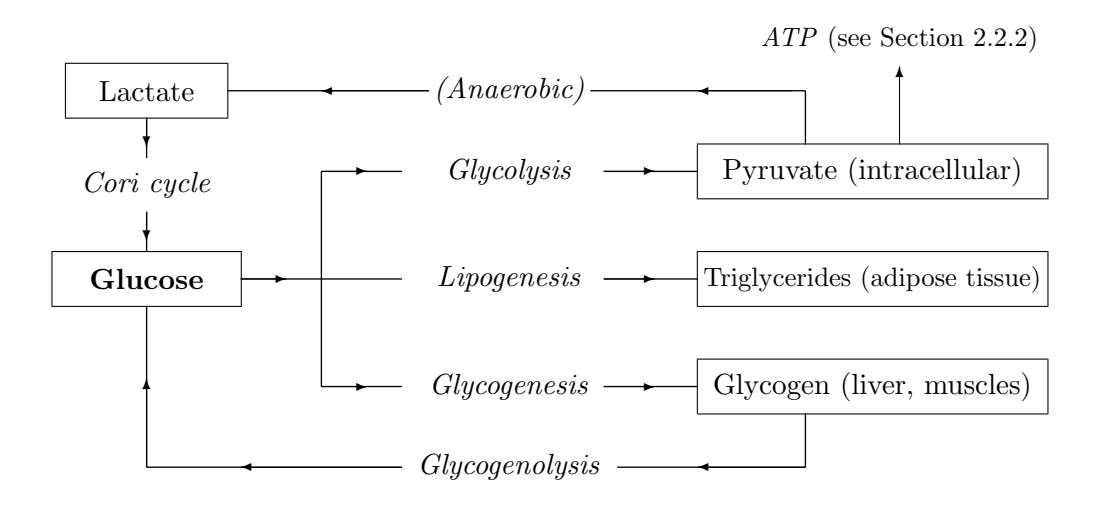


Figure 2.2: Internal glucose storage and utilisation.

Table 2.2: Selected organs, tissues and cells involved in blood glucose production and uptake.

Organ/tissue/cell	Source or sink	Via process
Brain	Sink	Insulin-independent uptake
Liver	Source / sink	Glycogenolysis, gluconeo. / Glycogenesis
Kidneys	Source / sink	Gluconeogenesis / Filtration
Intestines	Source	Digestion
Muscles	Sink	Glycogenesis
Adipose tissue	Source / sink	Lipolysis / Lipogenesis
Red blood cells	Sink	Insulin-independent uptake

#### 2.1.1 Role of Food

Carbohydrates are the most accessible source of energy for the body, and are generally split into three types: monosaccharides (e.g., glucose), disaccharides (e.g., lactose), and polysaccharides (also known as complex carbohydrates, e.g., starch). The digestion of carbohydrate, from mouth to intestines, is the process by which the body breaks down the more chemically complex carbohydrates into simpler monosaccharides. These molecules can then be absorbed into the bloodstream and used as a source of energy by various cells, organs and tissues.

The type of carbohydrate ingested determines the rate of digestion, and thus how quickly it increases BGC. The glycaemic index (GI) was developed by Jenkins et al. (1981) as a way of grouping foods that displayed similar effects on BGC. High GI foods, e.g., honey, raise BGC relatively quickly, while low GI foods, e.g., pasta, exhibit a slower, longer effect on BGC. The index was designed to help people with type 2 diabetes avoid rapid increases in BGC, and hence reduce the strain on impaired insulin production/action.

The glycaemic load (GL) extends the idea of the GI by also considering the quan-

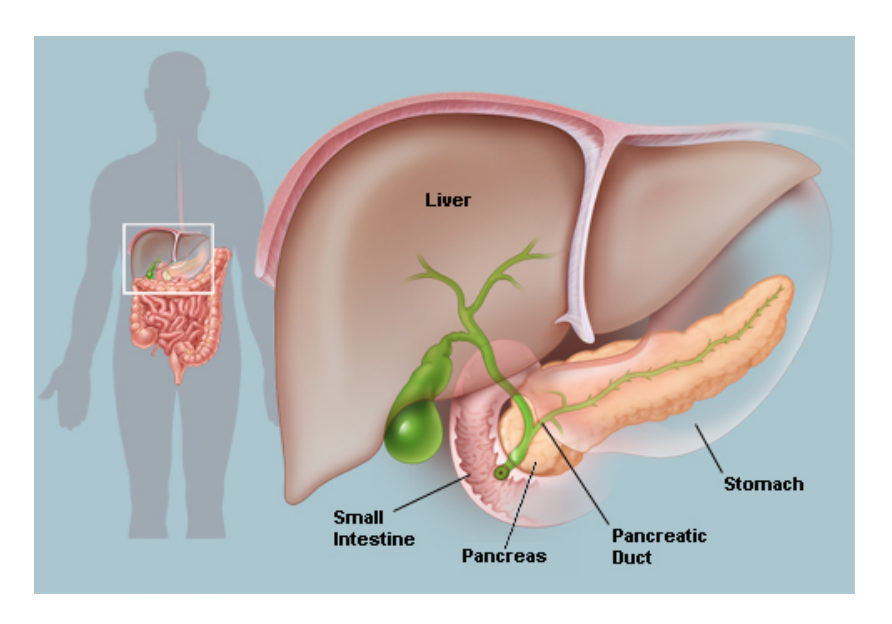


Figure 2.3: Diagram of the pancreas; image reproduced from http://www.webmd.com/digestive-disorders/picture-of-the-pancreas, last accessed 02/10/12

tity of carbohydrate consumed, thus giving a better description of the effect of food on BGC after consumption. The GI, and hence GL, is limited by not considering interand intra-person variability, and also fails to account for the effect of mixed meals (meals containing other nutrients): it has been suggested that consumption of fats and proteins affect the digestive process, e.g., fat slows the gastric emptying process (Kroop et al., 1979); however, Wolever and Bolognesi (1996) argue that the suggested effects of fat and protein are based on unrealistic meal comparisons. The American Diabetes Association summarise that the quantity of carbohydrate is the most important indicator of post-prandial BGC behaviour, but that the GI can play a useful role (Sheard et al., 2004).

#### 2.1.2 Role of the Pancreas

The pancreas (see Figure 2.3) plays a vital role in controlling BGC. The hormones glucagon and insulin are secreted by the  $\alpha$ - and  $\beta$ -cells, respectively, found in regions of the pancreas called the islets of Langerhans. These hormones regulate BGC by stimulating different metabolic pathways.

Insulin secretion is stimulated by rising BGC, as often occurs after meals, and by certain substances, such as amino acids. It primarily stimulates the anabolic pathways, in particular encouraging glycogenesis and lipogenesis in the liver. Insulin enables blood glucose metabolism by insulin-sensitive tissues, such as muscles, hence reducing BGC. Insulin has a fat-preserving effect, encouraging the use of carbohydrate rather than fat as an energy source, by inhibiting lipolysis and gluconeogenesis.

Insulin works by binding to receptors on cells, activating a number of chemical reactions that result in the translocation of glucose transporters (section 2.1.9) to the

cell membrane. The transporters aid the movement of glucose in the blood across cell membranes. Once insulin has effected its action, it may be degraded by the cell or released back into the blood where it is cleared by the liver or kidneys.

The effect of insulin on blood glucose uptake varies according to circumstance: insulin-independent uptake dominates during fasting, but insulin-dependent uptake becomes more prominent after meals. Hovorka et al. (2001) note that this results in nonlinear insulin action: raising basal insulin levels by 50% during fasting has a small effect on total glucose uptake, but the same increase during times of insulin-dependent dominance has a far greater effect on uptake.

Glucagon has the opposite effect of insulin. Its release is stimulated by low BGC, and inhibited by insulin. Glucagon stimulates the liver to release glucose via the catabolic pathways glycogenolysis (primarily) and gluconeogenesis; it thus helps to raise BGC. Conversely, glucagon secretion encourages secretion of insulin, so that the body is able to metabolise recently liberated glucose.

#### 2.1.3 Role of the Liver

Insulin stimulates the liver to convert glucose to glycogen for storage; this is the single largest pool of stored glucose in the body. When fasting, the liver helps maintain euglycaemia by releasing glucose into the blood via glycogenolysis and gluconeogenesis. The ratio at which these metabolic pathways provide glucose depends on the glycogen stores in the liver. Glycogenolysis is generally the dominant method of glucose production, but during/after exercise, or after long periods of fasting, the glycogen stores in the liver become depleted; gluconeogenesis is then the primary pathway for glucose production. Gluconeogenesis is slower to produce glucose than glycogenolysis, and may result in demand outstripping production and a subsequent decrease in BGC.

Hepatic glycogen depletion results in increased post-prandial glucose uptake in the liver to replenish stores. If hepatic glycogen stores are full, excess glucose in the liver is used in the synthesis of fatty acids. These are released in to the blood where they may then be stored in other tissue as triglycerides. When glucose reserves are low, the liver can produce ketones by metabolising fatty acids. At low levels, ketones are not harmful and can be used by the brain and kidneys as an alternative source of energy.

# 2.1.4 Role of the Kidneys

Net renal glucose output is small in the fasting state, but the kidneys have been shown to be a significant organ in the uptake and release of blood glucose. Stumvoll et al. (1995) reported that the kidneys account for around 20% (average) of blood glucose uptake, and approximately 28% (average) of glucose released into the blood in their sample of healthy individuals. During epinephrine infusion (up to levels designed to

mimic those seen during hypoglycaemia), the kidneys increased output to account for 40% of glucose appearance. This increase accounted for almost all of the raised glucose appearance. Stumvoll et al. (1995) note that there seems to be little scope for glycogen storage in the kidneys, so glucose production is assumed to be dominated by gluconeogenesis.

#### 2.1.5 Role of the Brain

The brain relies on the constant supply of blood glucose for its source of energy, and accounts for approximately 50% of basal glucose uptake (Naylor et al., 1995). Glucose uptake in the brain is insulin-independent. The brain cannot use fatty acids for creating energy, though during fasting it can use ketones to reduce demand on blood glucose.

#### 2.1.6 Role of Muscles

Muscles store glucose as glycogen, thus providing an immediate energy source at the onset of exercise. If glycogen stores become depleted, muscular blood glucose uptake increases; increased uptake may also be seen post-exercise as the stores of glycogen are replenished. Muscles do not release glucose into the blood, but during exercise may release gluconeogenic precursors; in particular, pyruvate is converted in to alanine (an amino acid) and released in to the blood. It is then transported to the liver, where it is converted back into pyruvate and then glucose. Increased production of alanine also occurs when glucose stores are low and the muscle begins to break down protein reserves for energy. Lactate is also released by muscle and transported to the liver, where it may be converted to glucose as part of the Cori cycle.

#### 2.1.7 Role of Hormones

In addition to insulin and glucagon, a number of other hormones aid blood glucose homeostasis; their roles are summarised in Table 2.3. It is worth noting that insulin is the only hormone that always reduces BGC. The role of hormones is discussed more thoroughly by Ganong (2005) and Pocock and Richards (2006).

#### 2.1.8 Role of Fatty Acids

Fat is stored in adipose tissue, predominantly in the form of triglycerides (TGs); these consist of fatty acids bound by glycerol. When TGs are broken down (lipolysis) they release the fatty acids (becoming free fatty acids, FFAs) and glycerol in to the blood. FFAs are then oxidised for energy in muscle(s) or the liver, while glycerol may be converted to glucose in the liver. At rest, FFAs dominate muscle energy synthesis as fat yields more energy by mass (~9.4kcal/g) than carbohydrate (~4.2kcal/g) or protein

Table 2.3: Function of various hormones on BGC.

Hormone(s)	Stimulus for Secretion	Effect
Somatostatin	Rising BGC and amino	Inhibits both insulin and glucagon se-
	acids	cretion
Glucocorticoid	Low BGC; stress	Primary aim is to preserve glycogen
hormones (e.g,		stores; stimulates lipolysis (fatty acid
cortisol)		liberation) and gluconeogenesis; anti-
		insulin effect (inhibits glucose uptake)
		on adipose tissue
Growth Hormone	Low BGC, significant	Anti-insulin effect on muscles; stim-
	during fasting	ulates glycogenolysis in the liver and
		lipolysis
Catecholamines	Low BGC, particularly	Stimulate glycogenolysis and lipoly-
(e.g., epinephrine)	when glucagon response	sis; inhibit insulin secretion
	is impaired; stress	
Thyroid hormones	Various, though seems to	Complex: low concentration may in-
	be unrelated to BGC	crease muscle glucose uptake and en-
		courage glycogenesis, high concentra-
		tion encourages glycogenolysis and
		gluconeogenesis and increases rate of
		absorption from the gut

(Cerny and Burton, 2001). The role of fat as an energy source varies with exercise, as discussed in section 2.2.4.

FFAs and glucose compete for oxidation in muscles, so increased FFA concentration inhibits muscular glucose uptake; this is known as the FFA-glucose cycle. Insulin has an anti-lypolytic effect, instead encouraging glucose uptake in order to bind fatty acids and form TGs.

# 2.1.9 Role of Glucose Transporters

The transport of glucose through membranes in the body relies on a number of proteins known as glucose transporters (GLUTs); these are summarised in Table 2.4. Other membrane proteins exist but their roles are less well-established or relate to substances other than glucose.

Table 2.4: Function of glucose transporters.

Transporter	Site of Expression	Purpose
GLUT-1	Red blood cells, barrier tissues, var-	Basal glucose uptake
	ious organs	
GLUT-2	Liver, small intestines, kidneys	Glucose transport from intes-
		tine, kidneys and liver
GLUT-3	Brain, kidneys, and other organs	Basal glucose uptake
GLUT-4	Muscle, adipose tissue	Insulin- and exercise-
		stimulated glucose uptake

GLUT-4 is of particular interest due to its role during physical activity. Exercise

encourages the translocation of GLUT-4, which helps enhance glucose uptake in muscles independently of insulin (Coderre et al., 1995; Goodyear and Kahn, 1998). Thorell et al. (1999) also hypothesise that the redistribution of GLUT-4 accounts for increased glucose uptake post-exercise (discussed in section 2.2).

Sodium-dependent glucose transporters (SGLT) aid the function of the GLUTs in the kidneys (SGLT1 and SGLT2) and intestines (SGLT1). In particular, the transporters in the kidney help reclaim filtered glucose. The amount of glucose that can be reclaimed is limited by the renal glucose threshold (RGT; discussed further in section 2.3.1).

#### 2.1.10 Implication of Type 1 Diabetes

The lack of endogenous insulin production in people with type 1 diabetes means that blood glucose cannot be metabolised by the insulin-sensitive cells and tissues, and thus parts of the body are starved of their primary source of energy. The lack of insulin also means there is no inhibition of glucagon secretion (and hence hepatic glucose release), and no regulation of the breakdown of TGs to FFAs. This results in extreme and prolonged hyperglycaemia and increased FFA circulation. The liver converts excess FFA into ketones, resulting in life-threatening DKA.

Exogenous insulin delivery, as part of diabetes treatment regimes, is designed to replace the lost function of the pancreas. However, the body's inability to regulate injected insulin means various physiological processes are sub-optimal. Insulin injections also fail to faithfully recreate the conditions of pancreatic insulin release, in particular the ratio of peripheral insulin to hepatic insulin (Buse et al., 2002). This may explain the lower hepatic glycogen stores in people with diabetes observed by Petersen et al. (2005), as well as dysfunctional glucagon response to carbohydrate consumption, where glucagon suppression was not observed after meals (Dinneen et al., 1995).

# 2.2 Exercise Physiology

Describing the body's response to exercise, and how this affects BGC, is a primary aim of the current work. It is therefore important to understand the underlying physiology, the effect of different durations, intensities and types of exercise, and the impact of diabetes on the physiology. The remainder of this section focuses on the role of blood glucose in providing energy for activity.

# 2.2.1 Whole-Body Changes

The onset of exercise triggers a number of physiological responses. Blood flow is redistributed through vasodilation and vasoconstriction (widening and narrowing of blood

vessels, respectively), with increased flow to the exercising muscle(s), heart and lungs, and a decrease to the liver and kidneys. Increased heart rate and hyperventilation aids delivery and removal of substances involved in cellular respiration. Various metabolic processes are stimulated to power activity, with the aim of maintaining the supply of the energy-rich compound adenosine triphosphate.

#### 2.2.2 Adenosine Triphosphate

The breakdown of adenosine triphosphate (ATP) and the subsequent chemical reactions release free energy, which contracts skeletal muscle and thus powers exercise. Stores of ATP in the body are limited and it must be replenished continuously during exercise. Carbohydrate and lipid metabolism dominate ATP synthesis, while oxidation of protein (more precisely amino acids) generally provides <5% of energy (Riddell and Iscoe, 2006). Amino acids are, however, essential to production of phosphocreatine (PCr), another energy-rich compound. PCr is predominantly stored in muscle and is crucial for anaerobic ATP production during very short-term (less than 10 seconds) exercise. It is replenished through ingestion of the necessary amino acids.

The roles of carbohydrate and lipid metabolism in ATP replenishment depend on the duration and intensity of physical activity, and the behaviour of BGC depends on how the body uses these sources of energy.

#### 2.2.3 Carbohydrates as a Source of Energy

During exercise, muscle glycogen is broken down into glucose, and then into pyruvate (see Figure 2.2, section 2.1). With sufficient oxygen, the pyruvate is fed into the citric acid cycle (also known as Krebs' cycle). The citric acid cycle creates a small amount of energy, as well as producing important substrates for the electron transport chain. This chain produces the majority of energy in aerobic respiration (Pocock and Richards, 2006).

When there is insufficient oxygen, the body will be unable to oxidise all the pyruvate derived from the breakdown of glucose. Excess pyruvate is instead converted to lactate and released into the blood. Lactate may then be taken up by the liver to be converted to glucose (via gluconeogenesis; see section 2.2.5), which is then released into the blood. The gluconeogenic stage in the liver is energy consuming, and hence anaerobic respiration is suitable only for short periods of time.

As muscle glycogen stores become depleted, the muscle may take up glucose from the blood to be used as a source of energy. Glucose levels in the blood are maintained by hepatic glucose release. Furthermore, blood glucose is important in replenishing the muscle glycogen stores post-exercise. The liver replenishes its own glycogen stores via gluconeogenesis and increased glucose uptake after carbohydrate intake. During high-intensity exercise, carbohydrates are the main source of energy; under such high energy demand, the body seeks to extract the maximum amount of energy from the available oxygen, and the use of carbohydrates is marginally more efficient than using fats (Cerny and Burton, 2001). FUrthermore, glycogen stores local to the exercising muscle(s) are readily available for immediate use as an energy source.

#### 2.2.4 Fats (lipids) as a Source of Energy

During low- and medium-intensity exercise, fat is the main source of energy. Deriving energy from fat stores is not as immediate as from carbohydrate: TGs must be broken down and transported from their storage site (predominantly adipose tissue) to the required cells. Furthermore, lipolysis is aerobic and oxygen uptake does not always increase immediately at the onset of exercise, initially limiting the rate at which energy from fats can be provided. However, due to the large stores in the body, triglycerides can provide energy for long periods of physical activity.

The hormonal response to exercise (further discussed in section 2.2.6) helps to stimulate the breakdown of TGs and the release of the resulting fatty acids and glycerol into the blood. The increase of fatty acids in the bloodstream counters a corresponding decrease in BGC (Cerny and Burton, 2001). Fatty acids are broken down to feed the citric acid cycle and electron transport chain, while glycerol may be converted to glucose in the liver via gluconeogenesis.

# 2.2.5 Other Sources of Energy

Gluconeogenesis is the process of converting non-carbohydrate substrates into glucose. This takes place in the liver (predominantly), kidneys and intestines. As noted previously, lactate and glycerol - both gluconeogenic substrates - are created in the breakdown of other energy sources. Various amino acids may also be used as a source of energy, particularly during times of fasting. Fatty acid metabolism in the liver produces ketones, which may be used by the heart and brain as a source of energy. The brain is particularly dependent on ketones during periods of low BGC as it cannot derive energy from fatty acids.

# 2.2.6 Hormonal Response to Exercise

The hormonal response to exercise is complex, depending on type, intensity and duration. Generally, the secretion of certain hormones (e.g., cortisol, glucagon, growth hormone, epinephrine and norepinephrine) increases to stimulate gluconeogenesis and glycogenolysis, which help to increase BGC. Catecholamines become the primary controllers of BGC during high-intensity exercise, and the ratio of glucagon to insulin

becomes less important (Marliss and Vranic, 2002).

Insulin secretion does not increase during exercise despite increased glucose uptake and may instead be inhibited by raised catecholamine levels, thereby sensitising the liver to glucagon and encouraging lipolysis. Insulin delivery is instead aided by the increased blood flow to the exercising muscle(s); furthermore, glucose uptake into skeletal muscle is aided by relocation of the glucose transporter GLUT-4.

Mild hyperglycaemia has been observed in healthy subjects during high-intensity exercise, which increases post-exercise (Marliss and Vranic, 2002). High blood insulin concentration (hyperinsulinaemia) then ensues, creating favourable conditions for glycogen replenishment in the muscles and liver. Replenishment may also continue after the next carbohydrate-containing meal, so the effects of exercise can last much longer than the duration of the exercise.

#### 2.2.7 Implication of Type 1 Diabetes

Excess or deficiency of injected insulin - i.e., insulin unregulated by the body - can result in hypo- or hyperglycaemia. Hypoglycaemia may be caused by any of the following circumstances, alone or in combination:

- hyperinsulinaemia, which suppresses glucagon secretion (and hence hepatic glucose release) and lipolysis;
- attenuated epinephrine and cortisol secretion (reducing stimulus for glycogenolysis and gluconeogenesis) as reported in people with diabetes (Petersen et al., 2005; Riddell and Iscoe, 2006);
- over-reliance on gluconeogenesis for hepatic glucose release (a slower process of glucose production than glycogenolysis), as reported in people with diabetes (Petersen et al., 2005);
- decreased insulin diffusion path due to vasodilation, resulting in accelerated absorption and action of insulin.

Conversely, hypoinsulinaemia may cause hyperglycaemia, during or post-exercise, due to:

- failure to suppress glucagon secretion (and hence hepatic glucose release) and breakdown of fat stores;
- inability of muscles to uptake blood glucose, resulting in increased glucose demand (despite hyperglycaemia);
- prevention of glycogen-store repletion in muscles and the liver.

Insulin requirements must be considered carefully before and after exercise. Different intensities and durations of exercise result in different responses from the body, which affect BGC in different ways. Furthermore, the effects of exercise may last longer than its duration.

# 2.3 Other Factors Affecting BGC

#### 2.3.1 Renal Clearance

When BGC passes a threshold, the kidneys can no longer reclaim all filtered glucose due to saturation of the SGLT. Excess glucose is then passed in the urine (glucosuria). The threshold varies from person-to-person and over time within the individual, though a modal value seems to be around 9-10 mmol/l (Johansen et al., 1984). The presence of glucose in the urine is thus an indication of current or recent hyperglycaemia, and generally only occurs in those with diabetes. Renal clearance is a function of glomerular filtration rate (GFR), the flow of filtered fluid through the kidney.

#### 2.3.2 Temporal Effects

Van Cauter et al. (1997) note that there appears to be evidence that glucose tolerance changes during the day, and in particular that there is reduced insulin sensitivity and glucose metabolism later in the day. Van Cauter et al. also discuss the "dawn phenomenon", where hyperglycaemia occurs pre-breakfast due to increased insulin requirements. Why this occurs is not fully understood, though it appears to be related to growth hormone secretion. Hejlesen et al. (1996) suggest that a post-hypoglycaemia rebound effect exists in individuals with recently-diagnosed type 1 diabetes (<2 years), resulting in hyperglycaemia. As noted previously, glucagon secretion may become diminished over time, so this rebound effect may depend on the duration of diabetes.

#### 2.3.3 Miscellaneous

The diffusion and absorption of injected insulin may vary according to a number of factors. Temperatures at 35°C and 85°C (sauna) have been shown to increase absorption rates for certain types of insulin (Koivisto, 1980; Koivisto et al., 1981), as has local massage (Berger et al., 1982). Like exercise, heat and massage stimulate vasodilation in the affected muscle and tissue, and hence can decrease the insulin diffusion path.

There are significant differences between absorption rates for insulin injected into the leg, arm and lower torso (Henriksen et al., 1993; Bantle et al., 1993). Injections in the leg can result in slower absorption than in the arm, while injections in the lower torso display varied but increased absorption compared to other injection sites (Frid and Linde, 1993). Correct injection technique is also important to avoid unpredictable insulin absorption (Hicks et al., 2011).

When insulin therapy commences, the body may, for a short period of time (days or weeks), exhibit some self-regulation of BGC. This is known as the "honeymoon period" (Abdul-Rasoul et al., 2006; Akirav et al., 2008).

Quality of sleep can affect brain and tissue glucose metabolism (Scheen and van Cauter, 1998). Stress, caused by illness or lifestyle, and the corresponding hormonal response can lead to raised hepatic glucose release.

Smoking can lead to temporary vasoconstriction, which may affect insulin delivery. It has been reported that smokers' insulin requirements are greater than non-smokers' (Klemp et al., 1982). Alcohol has been observed to reduce blood glucose for up to 12 hours after evening intake (Ploughmann et al., 2003).

# 2.4 Physiological Review: Summary

This section described how the complex glucoregulatory system maintains BGC within strict limits, minimising deviation and effectively damping the effect of external impulses such as food and exercise. Understanding this system, and how diabetes affects it, informs the modelling approaches used in the current work and other diabetes literature.

BGC homeostasis depends on various organs, tissues, cells and hormones individually and collectively performing different roles in order to supply energy to all parts of the body, whether for cell repair, general function and maintenance, or for physical activity. Insulin plays a crucial role in blood glucose homeostasis, being the only hormone that is geared towards lowering BGC by encouraging uptake in insulin-sensitive cells and tissues. When insulin-producing mechanisms are destroyed, as in type 1 diabetes, the body's ability to regulate BGC is terminally impaired. Exogenous insulin is then required, but balancing the body's needs with meal and exercise disturbances is an inherently complex process. This balance is particularly difficult to achieve when considering the effects of physical activity.

# Modelling Review

The second section of this chapter reviews techniques and models used in diabetes research, including descriptions of glucose-insulin dynamics and exercise physiology. A number of these techniques and models provide a basis for work presented in later chapters. The section offers a critique of modelling approaches in the diabetes literature, suggesting where the current work can enhance the body of knowledge.

# 2.5 Modelling Techniques

The modelling review begins with a discussion of different practical and theoretical techniques that frequently appear in the diabetes literature. These form the basis of many of the modelling approaches discussed throughout this and later chapters.

#### 2.5.1 Compartmental Modelling

Compartmental modelling is a technique often used in modelling biological processes (e.g., Godfrey, 1983). The body is split into various compartments, between which material(s) or energy can be transmitted. The substance being modelled is assumed to reside homogeneously in each compartment. The rate of change in each compartment is the sum of the substance entering the compartment (from other compartments or from external sources) minus the sum of the substance leaving the compartment (to other compartments or to a sink).

#### 2.5.2 Glucose Tolerance Tests

Glucose tolerance tests (GTTs) involve administering a glucose load to the body, either orally (OGTT) or intravenously (IVGTT), to estimate insulin sensitivity, e.g., Bergman et al. (1979). Blood glucose and insulin concentrations are measured frequently for up to a few hours after the load to assess their response.

#### 2.5.3 Continuous Glucose Monitors

Continuous glucose monitors (CGMs) are devices designed to frequently measure and record BGC, and consist of a sensor, transmitter and receiver/display. The sensor (usually changed every few days) is placed under the skin and measures glucose concentration in the interstitial fluid (IF; see section 3.2). This is more practical than measuring BGC directly, and offers a useful proxy. CGMs allow frequent measurements of glucose to be taken, in contrast to finger-prick tests; often, measurements are reported every five minutes. However, glucose concentrations in the IF and blood do not equilibrate immediately under transient disturbances, such as post-prandial glucose absorption, due to the process of diffusion between compartments; thus, a lag is inpresent in sensor readings. CGMs also require calibration (using a finger-prick test) when BGC is steady to ensure the accuracy of the measurements.

Gough et al. (2003) investigated the frequency properties of BGC for the purpose of determining suitable sampling rates for CGMs, i.e., sampling rates able to pick up important periodicities in BGC; they found that samples at least every ten minutes were required to accurately represent BGC profiles. Breton et al. (2008) furthered this work by comparing uncalibrated CGMs with a posteriori recalibrated (using frequent

finger-prick tests) measurements, and highlighted the different frequency properties of blood and interstitial glucose, suggesting frequent calibrations were necessary to accurately determine BGC.

Klonoff (2005) discuss in detail the testing, problems and benefits of CGMs. In particular, they note the reluctance of insurance companies or governments to fund CGMs. However, Tamborlane et al. (2008) report improvements in HbA<sub>1c</sub> when using continuous monitors.

#### 2.5.4 Percentage of Maximal Oxygen Consumption

 $VO_2^{max}$  represents an individual's maximal oxygen consumption, usually determined in a clinical setting by incremental exercise on a treadmill or stationary bicycle.  $PVO_2^{max}$  represents relative intensity of exercise as a percentage of  $VO_2^{max}$ . Oxygen consumption is approximately proportional to the work done by the body, so  $PVO_2^{max}$  provides a measure of how hard the body is working and can be used as a method of quantifying exercise intensity.

# 2.6 Diabetes Modelling

Some of the earliest work in the diabetes modelling literature was dedicated to describing blood glucose-insulin dynamics using compartmental models. These models were generally used for estimating insulin sensitivity and glucose effectiveness (the ability of blood glucose to suppress endogenous glucose production and encourage blood glucose uptake). More recently, advances in technology have presented the opportunity for an artificial pancreas (section 2.6.5), and contemporary literature has focused on designing the control algorithm component. Many control algorithms rely on whole-body models describing glucose-insulin dynamics; such models have built on the early compartmental models to include the effect of digestion, insulin injection and physical activity.

# 2.6.1 Glucose-Insulin Dynamics: Bergman's Minimal Model

One of the earliest models of glucose-insulin dynamics was developed in a series of papers by Bergman and colleagues (Bergman et al., 1979; Toffolo et al., 1980; Bergman et al., 1981). They proposed the minimal model (MM) based on results from IVGTTs. The model was tailored for clinical use by providing a non-invasive method for estimating insulin sensitivity. The MM consists of compartments for blood glucose, blood insulin and "remote" (or active) insulin, with concentrations denoted by G,  $I_p$  and  $I_a$ , respectively, and compartments representing the liver and the periphery; the model structure is given in Figure 2.4. The remote insulin compartment distinguished the

MM from previous models, e.g., Bolie, 1961, by removing the assumption that glucose metabolism was dependent on blood insulin. Instead, blood insulin must first enter the remote compartment before effecting its action on blood glucose, hence representing the process of blood insulin binding to insulin-sensitive cells.

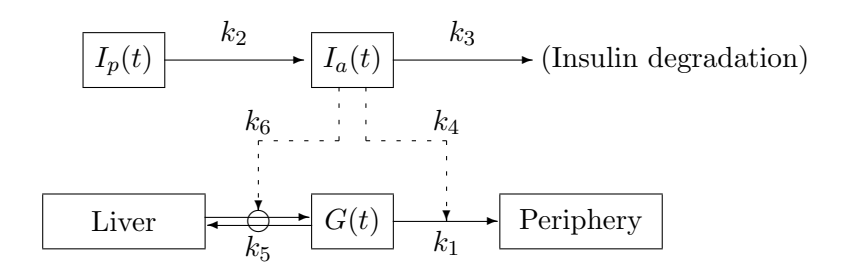


Figure 2.4: Minimal model of blood glucose metabolism; G represents BGC,  $I_p$  is plasma insulin concentration,  $I_a$  is active insulin concentration and parameters  $k_1, \ldots, k_6$  represent rates of exchange between compartments. Reproduced from Bergman et al. (1979).

The MM was chosen from a number of contenders posited by Bergman et al. (1979), based on its parsimonious nature and the identifiability and physiological meaning of parameters. The model describes the relationship between blood glucose, blood insulin and insulin action. Insulin action is given by  $X(t) = (k_4 + k_6)I_a(t)$ , and represents the effect of insulin in the remote compartment on blood glucose uptake. The model is described by a pair of differential equations:

$$\dot{G}(t) = [p_1 - X(t)]G(t) + p_4 
\dot{X}(t) = p_2 X(t) + p_3 I_p(t),$$
(2.6.1)

where model parameters  $p_1, \ldots, p_4$  are described in Table 2.5. Glucose effectiveness is given by  $p_1$ , and insulin sensitivity is given by  $-p_3/p_2$ .

Table 2.5: Parameters of the minimal model.

Relationship	Description
$p_1 = -(k_1 + k_5)$	Rate constant of insulin-independent glucose uptake
$p_2 = -k_3$	Rate of decreasing ability to uptake glucose
$p_3 = k_2(k_4 + k_6)$	Rate constant of insulin-dependent glucose uptake
$p_4 = H_0$	Hepatic balance extrapolated to zero BGC

The rate of change of glucose is derived from the difference between hepatic glucose balance, H, and peripheral uptake, U:

$$\dot{G} = H - U$$
.

where hepatic balance is determined by

$$H = H_0 - (k_5 + k_6 I_a)G$$

and peripheral glucose uptake is determined by insulin-dependent and -independent rates of uptake,

$$U = (k_1 + k_4 I_a)G.$$

The model was later appended (Toffolo et al., 1980; Bergman et al., 1981) with a third differential equation describing blood insulin:

$$\dot{I}(t) = p_5(G(t) - p_6)t - p_7I(t), \tag{2.6.2}$$

where  $p_5$  is the rate of insulin release by  $\beta$ -cells,  $p_6$  is the threshold of glucose above which this release begins, and  $p_7$  is the rate constant of insulin degradation.

Parameter estimation of the MM requires two stages: first, a known insulin time course is supplied to (2.6.1) to estimate the parameters  $p_1, \ldots, p_4$ , and second, a glucose time course is supplied to estimate parameters in (2.6.2). De Gaetano and Arino (2000) note that considering the MM as a complete system results in unrealistic behaviour. The authors instead propose a "dynamic model", which retains most features of the minimal model but allows simultaneous estimation of all parameters. Andersen and Højbjerre (2005) presented a Bayesian approach to overcome issues with full model parameter estimation. They extended their Bayesian network to a population-based model.

Various works (e.g. Regittnig et al., 1999; Cobelli et al., 1998, 1999) argue the minimal model is too simplistic, leading to poor estimates of insulin sensitivity. A second glucose compartment was suggested to account for differences in glucose concentration between blood and slowly-equilibrating tissue during glucose disturbances. An example of such a model, proposed by Dalla Man et al. (2007), is shown in Figure 2.5; the two glucose compartments represent glucose masses in the blood and quickly-equilibrating tissue  $(G_p)$  and slowly-equilibrating tissue  $(G_t)$ , with exchange between glucose compartments determined by rates  $k_1$  and  $k_2$ . The extended model of Dalla Man et al. also represents well the additional considerations needed to tailor the MM for use in type 1 diabetes and enhance its theoretical plausibility. The model includes glucose uptake separated into insulin-independent uptake from the plasma  $(U_{ii})$  and insulindependent uptake from tissue  $(U_{id})$ , appearance of glucose from meals (CHO), and renal clearance of excess glucose (R).

The original MM is further limited by providing only whole body measures of insulin sensitivity. Hovorka et al. (2001) used an IVGTT to separate the effects of insulin on glucose, establishing its action on distribution, disposal and production.

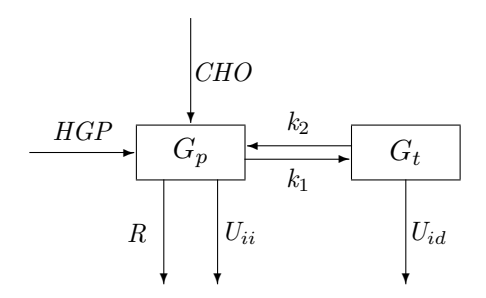


Figure 2.5: Two-compartment glucose subsystem of Dalla Man et al. (2007). Variables and parameters as described in text.

# 2.6.2 Glucose-Insulin Dynamics: Other Compartmental Models

There have been numerous other attempts to model glucose-insulin dynamics, many building on the work of Bergman and colleagues. As glucose-insulin models have developed, there has been interest in accounting for external influences, such as meals, and generalising to the wider diabetes population, by accounting for insulin injections. Hovorka (2005a) presents a comprehensive review of models that rely on either infrequent or continuous blood glucose measurements. It is worth noting that few of the models reviewed account for physical activity; predominantly, inputs are BGC measurements, meal intake and insulin type and dose.

Compartmental glucose-insulin models form the foundation of various computer packages designed for clinicians and patients. Generally these are designed for scenario analysis, where different insulin regimes may be tested *in silico* to see the effect on BGC. The Karlsburger Diabetes Management System (KADIS; Salzsieder et al., 1990; Salzsieder and Rutscher, 1998) involves subsystems for glucose and insulin linked by four state variables, blood glucose and insulin concentration, net endogenous glucose balance, and insulin action equivalent of exercise.

The Automated Insulin Dosage Advisor (AIDA) package (Lehmann and Deutsch, 1991), freely available online<sup>2</sup>, offers a number of case studies for educational purposes. The model takes into account meal intake, insulin absorption and action, insulin-independent glucose uptake, net hepatic balance and renal clearance, but fails to explicitly account for the effects of physical activity.

The Diabetes Advisory System (DIAS; Hejlesen et al., 1997) is structurally similar to AIDA, but instead models the liver's uptake and release separately. Again, there is no description of the effect of exercise. The model has, however, shown some success in providing advice on insulin dose in modest studies (Cavan et al., 1999). DIAS has been modified by Arleth et al. (2000) to account for the role of glucose transporters.

<sup>&</sup>lt;sup>2</sup>http://www.2aida.net/welcome/, last accessed 17/08/12

The revised model differentiates between glucose uptake by muscles and other organs, which may allow a further extension to account for physical activity.

GlucoSim (Agar et al., 2005) uses the compartmental model developed by Puckett (1992) as part of an educational simulator. The software allows input for food and insulin, as well as very limited options for input of physical activity. The simulator uses the data to produce profiles of blood glucose and insulin for up to 24 hours.

Sorensen (1985) developed a physiological, compartmental model to simulate glucose metabolism in "normal" man, i.e., no diabetes. The model is more comprehensive than most, comprising lung/heart, brain, gut and kidney compartments in addition to the liver and periphery, with 19 differential equations describing the model. The model pancreas was removed in order to simulate type 1 diabetes, allowing development of a control algorithm for use in closed-loop control. However, removing the pancreas entirely not only eliminates endogenous insulin secretion but also glucagon secretion, which is unrealistic. Hepatic glycogen stores are also not considered.

None of the above models account for the role of other hormones (except the Sorensen model which accounts for glucagon), fatty acids (unlike Roy and Parker (2006), a model based on the MM) or amino acids. Many models also fail to consider inter- and intra-patient variability.

#### 2.6.3 Glucose-Insulin Dynamics and Physical Activity

Attempts to include physical activity as an input to a glucose-insulin model are generally presented as extensions of existing glucose-insulin models. Derouich and Boutayeb (2002) extended Bergman's minimal model by adding parameters to each of the three differential equations governing the glucose-insulin system. However, the parameters do not relate to the intensity and duration of exercise. Roy and Parker (2007) also extended the minimal model by including terms relating to the changes in insulin removal, glucose uptake and hepatic release during activity (measured using PVO<sub>2</sub><sup>max</sup>). Parameter estimates are based on fitting the model against data from healthy volunteers. The DIAS computer package models exercise as insulin action equivalent (Salzsieder and Rutscher, 1998), but this is physiologically inaccurate as exercise can increase BGC.

Lenart and Parker (2002) and Hernandez-Ordonez and Campos-Delgado (2008) extended Sorensen's physiological model to account for physical activity. Energy expenditure was measured using PVO<sub>2</sub><sup>max</sup> as well as percentage of active muscle mass. The model of Lenart and Parker (2002) showed good agreement with BGC data (from healthy volunteers) for up to 90 minutes of low- and medium-intensity exercise (30% and 60% PVO<sub>2</sub><sup>max</sup> respectively). However, due to unrealistic assumptions, such as infinite hepatic glycogen stores, the model performed poorly after 90 minutes. Hernandez-Ordonez and Campos-Delgado (2008) extended the Lenart and Parker framework by

incorporating glycogen depletion and subsequent replenishment during the next absorptive stage.

Breton (2008) presented an alternative method for incorporating exercise into the minimal model. The intensity and duration of exercise is estimated by heart rate, which is correlated with oxygen uptake, itself correlated with energy expenditure. Thus, heart rate presents a surrogate measure for energy expenditure that may more realistically be measured in free-living conditions. The model includes terms for increased glucose uptake due to physical activity and longer-term changes in insulin action. Dalla Man et al. (2009) adopt the approach of Breton, testing three models (differing through the effect of physical activity on insulin-independent glucose uptake and insulin sensitivity) via simulation. A lack of data hinders the assumptions and conclusions of the model.

An alternative approach to measuring and quantifying physical activity is the use of recently-developed devices such as the BodyMedia® armband, which allow activity data to be collected from free-living conditions with minimal impact on the individual. Such armbands are able to measure and record a number of different variables, such as directional accelerations (movement) and skin temperature, and use these to estimate METs, a measure of energy expenditure relative to resting metabolic rate (discussed further in chapter 3). Rollins et al. (2008) used such a device to record the activity of an individual with type 2 diabetes. Data from several variables measured by the armband were used as inputs in a Wiener model of BGC. Valletta et al. (2009) used data from a continuous glucose monitor and the armband in a Gaussian process model. It was found that the assumption of stationarity (constant mean and variance) of BGC was not correct, hence limiting the accuracy of model predictions.

# 2.6.4 Empirical Modelling of BGC

Empirical models in diabetes are less prevalent given the problems in collecting relevant, sufficiently detailed data. Empirical models are particularly restricted by the difficulty in collecting data relating to internal processes in the body, e.g., the liver is a very inaccessible organ for the purposes of frequent testing, and hence processes such as glycogenolysis and gluconeogenesis are difficult or impossible to measure. Empirical models have thus been reliant on those variables that can be easily and safely measured, which itself has been limited until recent technological advances in CGMs.

One of the few data-true approaches to investigating insulin sensitivity was proposed by Marmarelis (2004). The methods are based on Volterra models, using principal dynamic mode (PDM) formulation; two PDMs were obtained to represent glucolepsis and glucogenesis (Marmarelis, 2004, section 6.4), where glucolepsis is defined as the insulin-assisted glucose uptake and glucogenesis as the production of glucose due to increased insulin.

Empirical models based on BGC measurements in standard treatment regimes are restricted due to the infrequent nature of testing. Bellazzi et al. (1999) used Bayesian analysis to determine trends and daily patterns for BGC measured only a few times per day. The model is a burden computationally, meaning real-time analysis is not possible. Yamaguchi et al. (2006) used data mining to predict fasting BGC and trend fluctuations for morning BGC.

The development of CGMs allows for more frequent measurements of BGC. Bremer and Gough (1999) investigated the behaviour of BGC from a number of studies using frequent sampling. BGC data from individuals with type 1 diabetes was seen to be nonstationary (non-constant mean and variance). Nonstationarity implies some form of temporal dependency between observations and presents problems for many conventional time series analysis. Differencing the data (subtracting successive observations) removed much of the nonstationarity in the mean, and the newly-created variable was used to construct autoregressive models; the linear models were unable to accurately predict over even relatively short time periods (30 minutes). Sparacino et al. (2007), however, showed that even a simple first-order polynomial or first-order autoregressive model could predict hypoglycaemic episodes 30 minutes in advance using a CGM. Model parameters were allowed to vary in time to compensate for the nonstationarity of BGC.

#### 2.6.5 Artificial Pancreas

The artificial pancreas (AP) represents the end goal of much diabetes research, as it can automate the process of maintaining euglycaemia. Figure 2.6 shows the conceptual basis of an AP, where a CGM relays information to a control algorithm that subsequently determines the release of insulin from a pump.

Much work has been dedicated to developing a control algorithm to be used as part of an AP. The control algorithm aims to minimise the difference between measured and reference (or target) BGC. Control algorithms are designed only for short-term prediction, often employing receding horizon control. Many control algorithms also rely on dynamic models of the process(es) to be controlled, hence the continued interest in models of blood glucose dynamics such as those described in the previous sections.

Various control methods have been proposed, and what follows is a very brief overview of more recent approaches:

- proportional-derivative-integral control (PID), e.g., Gantt et al. (2007) use a PI controller with asymmetric cost function to punish hypoglycaemia more than hyperglycaemia; Marchetti et al. (2008) use a PID controller with feed-forward component to announce meals and help limit post-prandial peaks in BGC;
- model predictive control (MPC), e.g., Abu-Rimleh and Garcia-Gabin (2010)

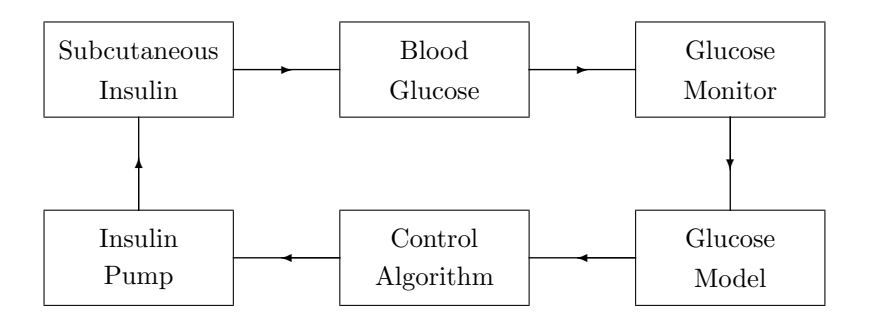


Figure 2.6: Basic structure of artificial pancreas

use multiple MPCs to deal with the nonlinearities of the glucoregulatory system; Lee and Bequette (2009) use meal detection and meal size estimation algorithms to deal with unannounced meals; Hovorka et al. (2004) use nonlinear MPC; Soru et al. (2012) use MPC with a focus on an individualised control algorithm;

- adaptive control, e.g., Eren-Oruklu et al. (2009) use an empirical approach using an autoregressive moving average (ARMA) model. Linear, low-order models are fitted as it is assumed that nonlinearities are rendered less significant by frequent glucose measurements;
- pseudo self-evolving cerebellar model algorithm controller (PSECMAC), e.g., Teddy et al. (2010) use the PSECMAC network, a computational model of the human cerebellum (part of the brain), to capture the dynamics of a healthy insulin secretion profile;
- H<sub>∞</sub> control, e.g., Parker et al. (2000) suggest the method is particularly robust by accounting for intra-patient variability and meal disturbances; Quiroz and Femat (2010) use H<sub>∞</sub> theory to design a controller with biosignals to indicate exercise disturbance (via the relationship between glucose and lactate) and hypoglycaemia (via the relationship between glucose and adrenaline);
- run-to-run strategy, e.g., Palerm et al. (2008) suggest a variable basal insulin infusion rate to account for changes in insulin sensitivity, with emphasis on clinical heuristics to design the strategy.

More detailed explanation of these methods may be found in the respective references. Further discussion may also be found in the various reviews of approaches to the AP in the literature, e.g., Naylor et al. (1995) on the risks and challenges of an artificial pancreas, El Youssef et al. (2009) on the history of closed-loop control algorithms, Bellazzi et al. (2001) on closed- and partially closed-loop strategies for subcutaneous insulin delivery, Parker et al. (2001) on closed-loop, intravenous insulin delivery, Kameth et al. (2006) on open- and closed-loop, feed-forward and feed-back approaches, and Hovorka (2005b) on approaches for frequent and infrequent BGC measurements.

The main problem regarding an AP is safety; any algorithm must be able to maintain euglycaemia during disturbances such as meals and exercise, which has yet to be demonstrated in free-living individuals. The majority of control algorithms have only been tested on data derived from the compartmental models previously described, predominantly the Hovorka et al. (2001) model (and the extension of Wilinska et al., 2005), and hence remain untested on the stimuli individuals experience in a free-living environment.

# 2.7 Modelling Review: Summary

The section presented a review of literature relevant to the current work. The review has highlighted a gap in the literature regarding modelling BGC using free-living data; in particular, compartmental models have not been tested using data that better reflects the real experiences of people in day-to-day life. Furthermore, empirical models that do not require simplified compartmental models of the human body are limited in number, due to the practical difficulties in collecting relevant data.

# Chapter 3

# Data Collection and Exploratory Analysis

The previous chapter highlighted the complex physiological processes by which the body maintains euglycaemia, and those which are disrupted by diabetes. To understand and describe these processes requires reliable, frequently sampled data. In some cases this is not possible, e.g., the liver is very inaccessible for the purposes of measurement, and processes such as gluconeogenesis are difficult or impossible to measure precisely. In other cases, collecting such data may be unethical, e.g., the effect of either food intake or insulin injections in T1D cannot be safely assessed in the other's absence. In the case of physical activity, measurement is not necessarily obvious in terms of how and what to quantify. Generally, physical activity data has been collected in a clinical environment under unrealistic protocols, and often from healthy volunteers. Such data can only be of limited use in understanding the behaviour of blood glucose concentration (BGC) in response to free-living stimuli in people with type 1 diabetes.

The following chapter begins by discussing the collection and nature of free-living data collected as part of a Diabetes UK study. This represents an important step in understanding the behaviour of BGC outside the clinical setting. The chapter also highlights important features of the physical activity, food and insulin data collected in the study. Exploratory analysis of the BGC data is carried out to inform modelling strategies to be used in this and following chapters.

# 3.1 Diabetes UK Study

Diabetes UK<sup>1</sup> (DUK), a diabetes charity, funded a three-year study (grant BDA: RD06/0003306; referred to as the DUK study from here on) to investigate the effect

<sup>&</sup>lt;sup>1</sup>http://www.diabetes.org.uk, last accessed 10/12/2012

of physical activity on capillary BGC<sup>2</sup>. Volunteers with type 1 diabetes were recruited through Southampton Diabetes Clinics, having previously expressed an interest in taking part in a research project. On recruitment, baseline characteristics were recorded at the Wellcome Clinical Research Facility at Southampton General Hospital. Variables measured included  $VO_2^{max}$ , fat distribution, and relative quantity to lean tissue, as well as standard diabetes screens, such as  $HbA_{1c}$ . Further details of the study may be found in Valletta (2011).

Of particular interest to the current work are the free-living data collected in the DUK study, discussed in the following sections: BGC measurements from the MiniMed Guardian real-time continuous glucose monitor (section 3.2), metabolic equivalent task of unit measurements from the BodyMedia SenseWear® armband (section 3.3), and the food and insulin diaries (sections 3.4 and 3.5, respectively). For every individual in the study (n=23), data was collected almost continuously over two weeks.

#### 3.2 Blood Glucose Concentration Data

The MiniMed Guardian device<sup>3</sup> (Medtronic MiniMed Inc., CA, USA) estimates BGC every 5 minutes by measuring glucose concentration in the interstitial fluid (IF). This fluid surrounds cells in tissues throughout the body. A sensor is inserted into the IF (typically in the lower torso or leg) to measure the current generated by glucose oxidation, proportional to glucose concentration in the tissue. A regression equation is then used to estimate BGC from the sensor readings. Full details of the equation and the design of the device may be found in Shin et al. (2006). The sensor, replaced every three days, is connected to the monitoring device via a wireless radio link, and must stay within a few metres of the sensor. An example of MiniMed output from one day's measurements is given in Figure 3.1; the profile of BGC highlights rapid fluxes that would not be captured with less frequent measurements.

Errors and time delays are introduced to estimates of BGC by signal processing in the device. Breton and Kovatchev (2008) report that the measurement error of sensors such as the MiniMed device is non-Gaussian, exhibits autocorrelation, and depends nonlinearly on the rate of change of BGC. Further errors are introduced by the differences between blood and interstitial glucose concentrations. These differences are most prominent during transient changes in glucose concentrations, and are attributed to the push-pull phenomenon; the theory argues that equilibration of blood and interstitial glucose concentrations after changes in one is not immediately reflected in the other. In one respect, BGC is raised by hepatic release or intestinal absorption of glucose

 $<sup>^2</sup>$ The study conformed to the principles of the Declaration of Helsinki and was approved by the Southampton and South West Hampshire Research Ethics Committee (REC reference number 07/H0502/134)

<sup>&</sup>lt;sup>3</sup>http://www.minimed.com/products/guardiancgm, last accessed 10/12/12

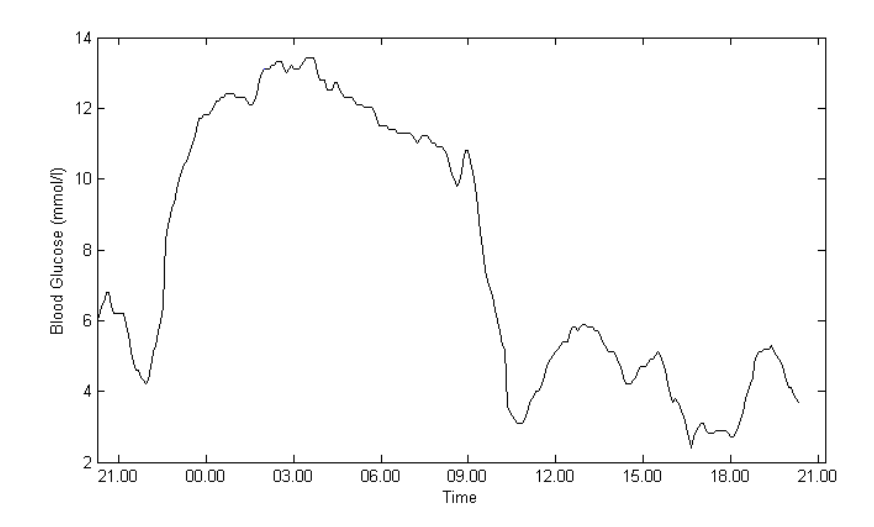


Figure 3.1: Example of Guardian BGC measurements over 24 hours.

into the blood, but the corresponding increase in interstitial glucose lags behind due to the diffusion process between capillaries and tissue. Conversely, when cells within the interstitial fluid uptake glucose, the decrease in BGC lags behind that of interstitial glucose, again due to diffusion. The transient disequilibrium between blood and interstitial glucose concentration depends primarily on the magnitude of change and rate of diffusion (Cengiz and Tamborlane, 2009). However, the extent of the push-pull phenomenon is disputed (Wentholt et al., 2007).

Despite the potential errors, the monitors provide a sufficiently accurate measurement of BGC for use with an insulin pump. Furthermore, the frequency of measurements is much higher than that provided by other means of blood testing.

#### 3.2.1 MiniMed Calibration

The MiniMed Guardian device requires frequent calibration with a capillary BGC measurement (usually a finger-prick test) due to measurement drift. The reliability of the MiniMed device decreases in time after calibration, so at least two calibrations per day is recommended. Calibrations should ideally be at times when BGC is at its most stable, i.e., not during or immediately after meals or exercise. Calibration may result in an immediate and rapid change in output as the device corrects itself towards the calibration value; an example of such occurrences is given in Figure 3.2, a plot of one-step changes in BGC from one individual in the DUK study. The largest absolute changes in BGC (between 1.3 and 1.9 mmol/l over five minutes) for this particular data set all occur within ten minutes of calibration.

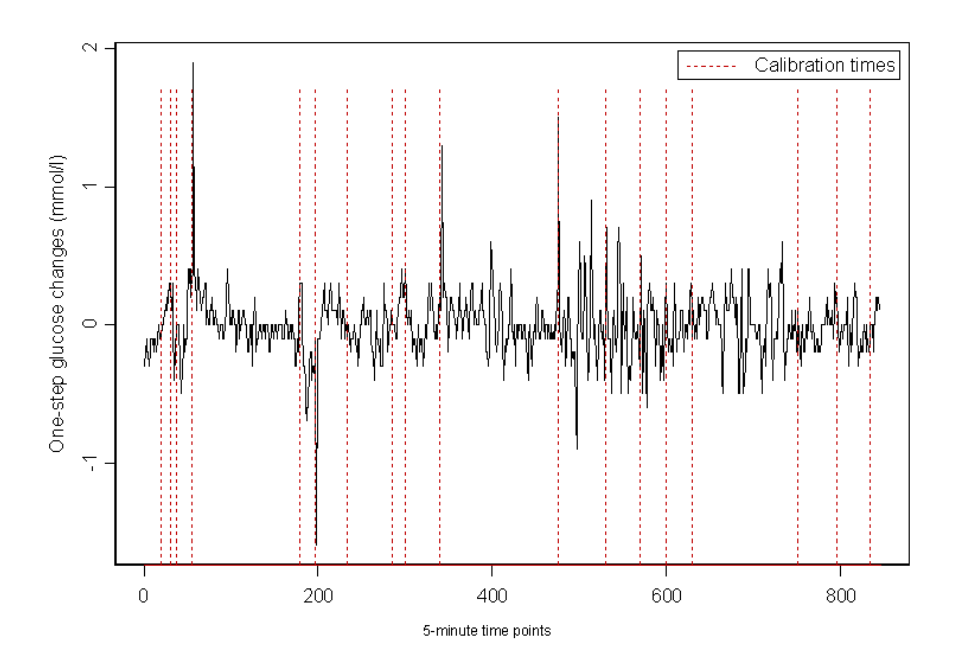


Figure 3.2: Example of the one-step change in BGC time series, with times of calibration, for an individual in the DUK study.

# 3.3 Physical Activity Data

The SenseWear® armband (BodyMedia Inc., PA, USA) measures a number of physiological variables, listed in Table 3.1, and uses these to estimate metabolic equivalent of task (METs, kcal/kg/hr). METs provide a person-specific measure of energy expenditure as a multiple of resting metabolic rate (RMR). RMR is the energy expenditure at rest (at room temperature and in a post-absorptive state), and represents the energy required to maintain function of the vital organs. The armband estimates METs using a proprietary algorithm that has been validated in numerous studies<sup>4</sup> against the gold-standard of indirect calorimetry (which uses oxygen uptake as a surrogate for calories burnt). Measurements from the armband are recorded every minute in the DUK study. Examples of METs for different activities are given in Table 3.2.

A series of papers (Liden et al., 2002, 2001; Sunseri et al.) detail the components of the device and their respective functions. The papers demonstrate the device's reliability and repeatability, as well as the practical advantages of the device compared to other methods for determining energy expenditure. In particular, the design of the device allows it to be worn continuously (except in wet conditions) with minimal impact on the mobility of the individual, meaning free-living data can be measured. This is particularly important for the applicability of the results from this study to

 $<sup>^4</sup>$ review available from http://www.bodymedia.com/Professionals/Whitepapers/The-Development-of-the-SenseWear-armband, last accessed 06/08/12

Table 3.1: Variables recorded by the SenseWear armband.

Variable	Description
Metabolic equivalent of task (METs)	Measure of energy expenditure
Transverse acceleration average (TAA)	Measured by two-axis accelerometer and provides information on body position and movement (av- erage over time interval)
Transverse acceleration mean absolute deviation (TAM)	As above but records mean absolute deviation
Transverse acceleration peaks (TAP)	As above but records peak during time interval
Longitudinal acceleration average	Measurement perpendicular to TAA
Longitudinal acceleration mean absolute deviation	As above but for TAM
Longitudinal acceleration peaks	As above but for TAP
Near body temperature	Average ambient temperature
Skin temperature	Average temperature of the skin
Heat flux	Heat dissipated by the body (average) along a conductive path between skin and vent in the armband
Galvanic skin resistance	Measures conductivity of the skin using two sensors; relates to physical and emotional stimuli

Table 3.2: Examples of approximate METs for various activities; values taken from Ainsworth et al. (2000).

Activity	$\mathbf{METs}$
Sleeping	0.9
Lying down	1
Walking (2mph)	2.5
Bicycling (general)	8
Running (6-10mph)	10-16

the wider population. Older versions of the device have been shown to underestimate certain types of exercise (Crawford, 2004), though this limitation has been overcome to a great extent by the use of exercise-specific algorithms.

Examples of armband data captured from a volunteer are given in Figures 3.3 and 3.4. The first figure shows skin temperature over a 24-hour period, with drops after activity due to sweating, and longitudinal acceleration, which is relatively stable during the night when the individual is asleep. The second figure shows the highly variable nature of METs, which fluctuates rapidly during the day but is relatively stable during the night. Such behaviour is relatively typical of other individuals in the DUK study; patterns and magnitudes vary, but METs is always highly variable during waking hours.

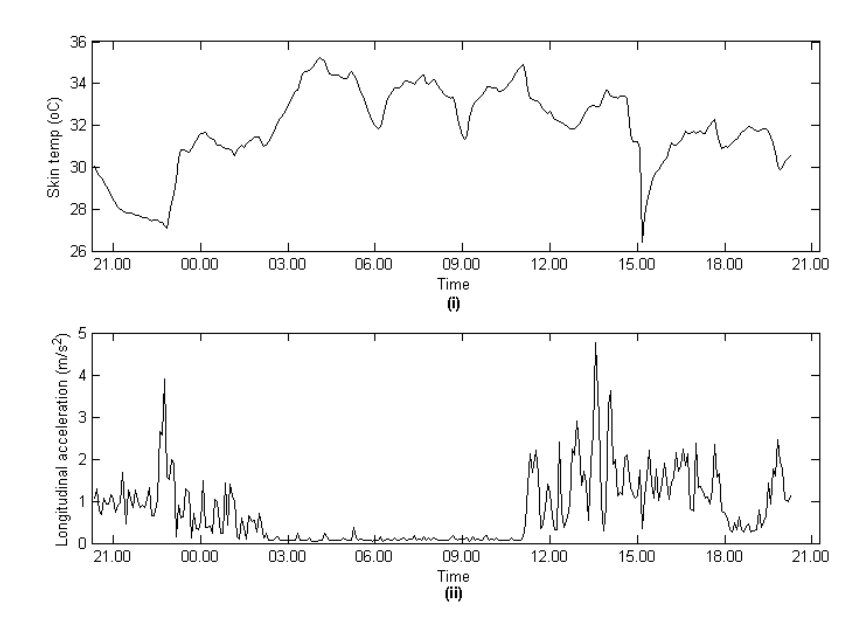


Figure 3.3: Activity armband output over a 24-hour period for an individual in the DUK study: (i) skin temperature; (ii) longitudinal acceleration.

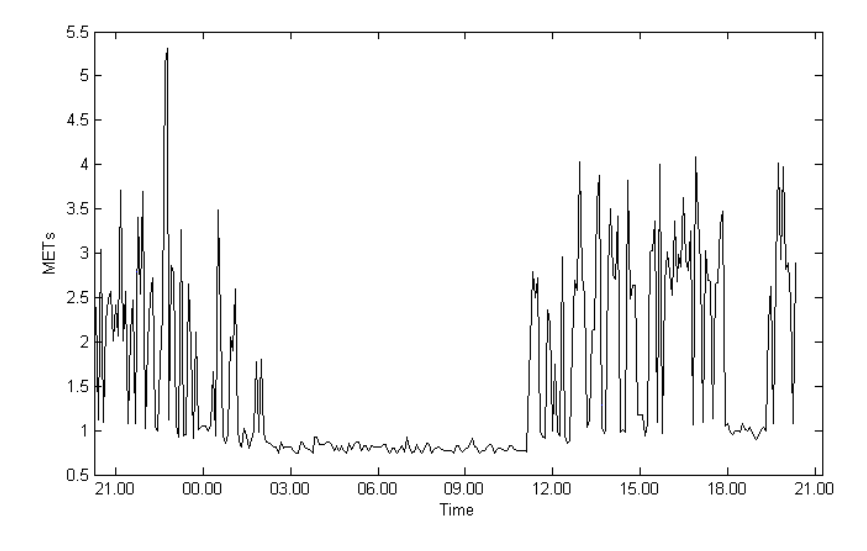


Figure 3.4: Metabolic equivalent units (METs) over a 24-hour period for an individual in the DUK study.

# 3.4 Food Diary

Food intake was recorded in a diary by each participant in the DUK study. The type and amount of food was recorded, as well as time of consumption, and subsequently the nutritional content was estimated using either reported nutritional information or food databases (Kellow et al., 2007). The process is subject to intra- and interpatient variable errors with regard to potential non-reporting of food consumption and estimating portion size; however, many individuals with type 1 diabetes have had training for carbohydrate counting, and are thus experienced in such matters. The method of data collection is appropriate in terms of the applicability of this study's outcomes to the wider type 1 diabetes population, who generally use carbohydrate counting as part of the MDI regime.

The food intake data from the DUK study offer no dynamical description of how food intake affects BGC. A model of the digestive process may be used to better represent how food intake effects BGC.

#### 3.4.1 Modelling the Digestive System

The breakdown of food begins in the mouth and continues via the oesophagus and stomach until the food is in a suitable form (i.e., relatively small molecules such as glucose) to be absorbed from the intestines into the blood. Jenkins et al. (1981) described the concept of the glycaemic index, which is used to group foods that display similar effects on BGC (depending on rate of absorption). However, Worthington (1997) argues that there are several fundamental flaws, in particular that the index offers no dynamical description of the rate of appearance of glucose in the blood after food intake. As such, a simple one-compartmental model was proposed, albeit one validated against a single individual and for only two foods. The model involves two parameters specific to food, the glycaemic value (ratio of glucose weight to total food weight) and fractional turnover rate (related to rate-limiting metabolic processes).

Lehmann and Deutsch (1992) proposed a more comprehensive model for the digestive system, which will be used in the current work. The model converts carbohydrate consumed into a profile of glucose absorption from the gut. The rate of change of glucose in the gut is described by

$$\frac{d(G_{\text{gut}})}{dt} = G_{\text{empt}} - k_{\text{abs}}G_{\text{gut}}$$
(3.4.1)

where  $G_{\text{empt}}$  is the rate of gastric emptying and  $k_{\text{abs}}$  is the rate constant of glucose absorption into the blood. Gastric emptying is modelled as a trapezoidal function:

$$G_{\text{empt}} = \begin{cases} \frac{k_{\text{max}}}{T_{\text{asc}}}t, & \text{for } t < T_{\text{asc}} \\ k_{\text{max}}, & T_{\text{asc}} < t \le T_{\text{asc}} + T_{\text{max}} \\ k_{\text{max}} - \frac{k_{\text{max}}}{T_{\text{des}}}(t - T_{\text{asc}} - T_{\text{max}}), & T_{\text{asc}} + T_{\text{max}} \le t < T_{\text{max}} \\ & + T_{\text{asc}} + T_{\text{des}} \\ 0, & \text{otherwise,} \end{cases}$$
(3.4.2)

with

$$k_{\text{max}} = \frac{2D}{T_{\text{asc}} + 2T_{\text{max}} + T_{\text{des}}}.$$
 (3.4.3)

Parameter values, units and descriptions are given in Table 3.3. The duration of the maximal gastric emptying  $(T_{\text{max}})$  is defined as a function of the carbohydrate ingested, but is zero when the amount of carbohydrate is small (emptying is a triangular function in this case). The rate of gastric emptying increases in proportion to the amount of carbohydrate consumed, before reaching the maximal (and constant) rate of emptying. Once almost all of the carbohydrate has been consumed, the rate begins to slow. Glucose absorption through the intestinal tract,  $G_{\text{in}}$ , is assumed to be linear and is given by

$$G_{\rm in} = k_{\rm abs}G_{\rm gut}. (3.4.4)$$

Further description of these parameters and their relationships is given in Lehmann and Deutsch (1992).

Table 3.3: Parameters of the Lehmann and Deutsch (1992) digestion model.

Parameter	Value	Description
k <sub>abs</sub>	$1 \; { m h}^{-1}$	Rate constant of glucose absorption from the gut
$k_{max}$	120  mmol/h	Maximal rate of gastric emptying
$T_{asc}$	0.5  h	Duration of ascending gastric emptying
$T_{ m des}$	0.5  h	Duration of descending gastric emptying
$T_{max}$	h	Duration of maximal gastric emptying
t	h	Time since start of meal

The estimated carbohydrate intake from the food diaries in the DUK study may be input to the model (as D) to estimate profiles of post-prandial glucose absorption in to the blood; Figure 3.5 shows recorded carbohydrate consumption and estimated glucose absorption every five minutes over a 24-hour period for one individual as an example of the digestion model's function. The large peaks correspond to meals, and smaller peaks to snacks.

The Lehmann and Deutsch (1992) digestion model is physiologically incorrect as it treats the digestive process as a single stage process, when it is really biphasic (Siegel

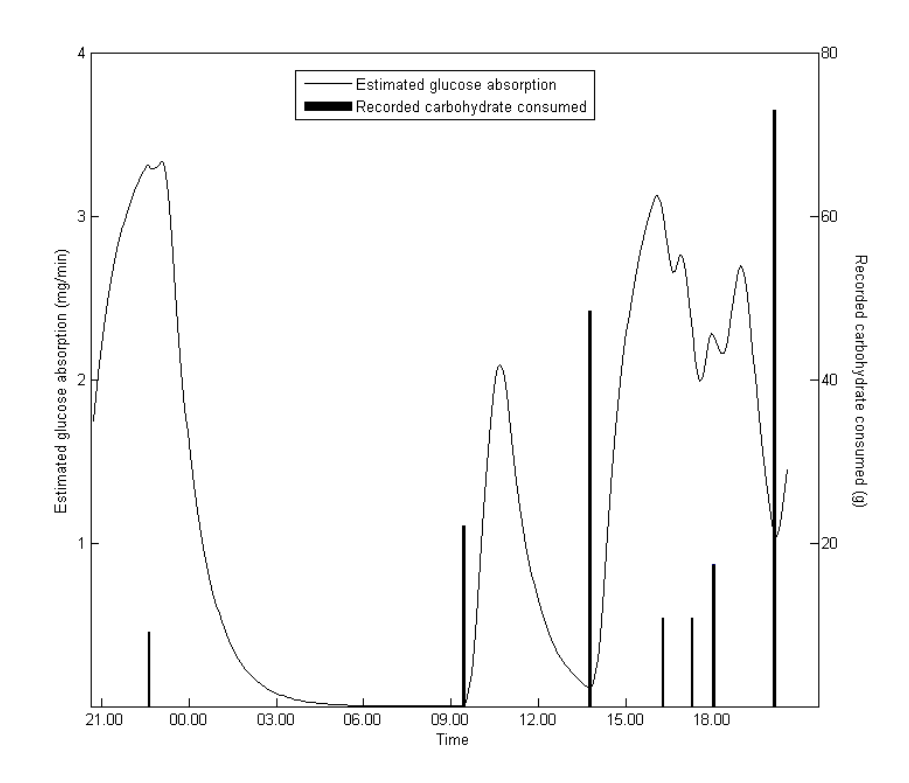


Figure 3.5: Estimated glucose absorption over a 24-hour period for one individual in the DUK study using the Lehmann and Deutsch model.

et al., 1988). Dalla Man et al. (2006) tested the above model against a newly-proposed nonlinear model, and found their model better described data from OGTT and mixed meals in volunteers with varying glucose tolerance; however, differences between model estimations were not substantial. The Lehmann and Deutsch (1992) model has been used in various other models in the literature, e.g., Wong et al. (2009), due to its parsimonious nature and ease of use.

# 3.5 Insulin Diary

Volunteers in the DUK study also recorded information regarding each insulin injection, specifically time of injection, dose, and type of insulin. As with the food diaries, these records offer no dynamical description of the effect of insulin on BGC. Understanding the behaviour of blood insulin concentration requires frequent blood samples and specialist equipment, and is hence not feasible in free-living conditions. A model describing the process of insulin absorption can provide an alternative to invasive blood samples, by offering important information on the appearance of insulin in the blood.

#### 3.5.1 Modelling Insulin Injection

A model of insulin absorption must be able to capture the differing absorption profiles for the various types of insulin used in diabetes care. Short/rapid-acting insulin, usually taken with food, is absorbed quickly after injection but may only act for up to four hours, while longer-lasting insulin may last beyond 24 hours to provide basal release of insulin throughout the day. Nucci and Cobelli (2000) provide a critical review of a number of proposed models for insulin kinetics; generally, compartmental models are favoured, often with two compartments corresponding to subcutaneous tissue and blood. The review pinpointed two models that performed well, notably the model described by Trajanoski et al. (1993). This model is an extension of that by Mosekilde et al. (1989), and has itself been extended by Tarin et al. (2005). The latter presents a generic model that is able to describe insulin absorption for a number of different insulin types, in particular glargine, whose long-lasting, peakless action has not been well described by other models; hence, this model is used in the current work.

Mosekilde et al. (1989), and their modelling descendants, assume that insulin resides in the subcutaneous tissue in dimeric, hexameric (according to molecular weight) and immobile, bound states. The model divides tissue into rings around the point of injection, into which the insulin diffuses. Tarin et al. (2005) changed the role of the bound state, allowing insulin in this state to break up into the hexameric form at a rate proportional to the concentration of the bound state.

The relationships between the three states of insulin in Tarin et al. (2005) are described by a series of coupled differential equations, which account for diffusion, hexameric-dimeric dissociation, bound-hexameric conversion and absorption of dimeric insulin:

$$\frac{\delta c_d(t,r)}{\delta t} = P(c_h(t,r) - Qc_r(t,r)^3) - B_d c_d(t,r) + D\Delta^2 c_d(t,r) 
\frac{\delta c_h(t,r)}{\delta t} = -P(c_h(t,r) - Qc_d(t,r)^3) + \kappa c_b(t,r)(c_{h,\max} - c_h(t,r)) 
+ D\Delta^2 c_h(t,r) 
\frac{\delta c_b(t,r)}{\delta t} = -\kappa c_b(t,r)(c_{h,\max} - c_h(t,r)) + d_b D\Delta^2 c_b(t,r),$$
(3.5.1)

where parameters are described in Table 3.4. Exogenous insulin flow in to the blood,  $I_{ex}(t)$ , is then given by

$$I_{ex}(t) = B_d \int_{V_{sc}} c_d(t, r) \ dV,$$
 (3.5.2)

where  $V_{sc}$  is the volume of the subcutaneous tissue. The integrand involves only the  $c_d$  term, as only insulin in the dimeric state is assumed to pass into the blood. The equations given in (3.5.1) have no closed-form solution, so they must be discretised in time and space (the full equations are given in Tarin et al., 2005). The Tarin et al.

model has been used throughout the diabetes literature, e.g., by the computer package AIDA (Lehmann et al., 2007).

Table 3.4: Parameters of the Tarin et al. (2005) insulin model.

Parameter	Description
$c_{\mathrm{d}}$	dimeric insulin concentration
$c_{ m h}$	hexameric insulin concentration
$c_{ m b}$	bound insulin concentration
P	dimeric production rate
Q	hexameric-dimeric equilibrium constant
$\mathrm{B_{d}}$	absorption rate of dimeric insulin
D	diffusion constant
$\kappa$	bound-hexameric conversion factor
$c_{ m h,max}$	bound-hexameric saturation constant
$\mathrm{d}_b$	reduction factor for diffusion constant of bound state

The insulin records of volunteers in the DUK study may be input to the model to estimate the profile of insulin absorption in to the blood. An example using one individual's insulin records is given in Figure 3.6, with estimates found every five minutes. The plot shows the profiles of two types of insulin: that of long-lasting insulin glargine, whose peakless action can last up to 26 hours to provide a basal release of insulin for low-level glucose metabolism, and that of short-acting insulin Novorapid, whose relatively quick action lasts only a few hours to compensate for post-prandial glucose absorption.

The profiles of estimated glucose and insulin absorption, for one individual over a 24-hour period, are given together in Figure 3.7. The plot shows peaks for the absorption of short-acting insulin just before peaks of glucose absorption. This highlights the delayed effect of blood insulin on BGC, as insulin must first bind to receptors on cells before effecting their action. The plot also shows the action of long-lasting insulin overnight when no food is consumed.

# 3.6 Modelling Limitations

The Lehmann and Deutsch (1992) digestion model and Tarin et al. (2005) insulin absorption model (referred to as the digestion model and insulin model, respectively, from here on) are approximations to complex biological processes and introduce errors due to various simplifications:

- i) neither model is subject-specific. They therefore do not differentiate between individuals who may have different physiological responses to the food and insulin inputs;
- ii) the digestion model does not account for any protein and/or fat consumed, nor the

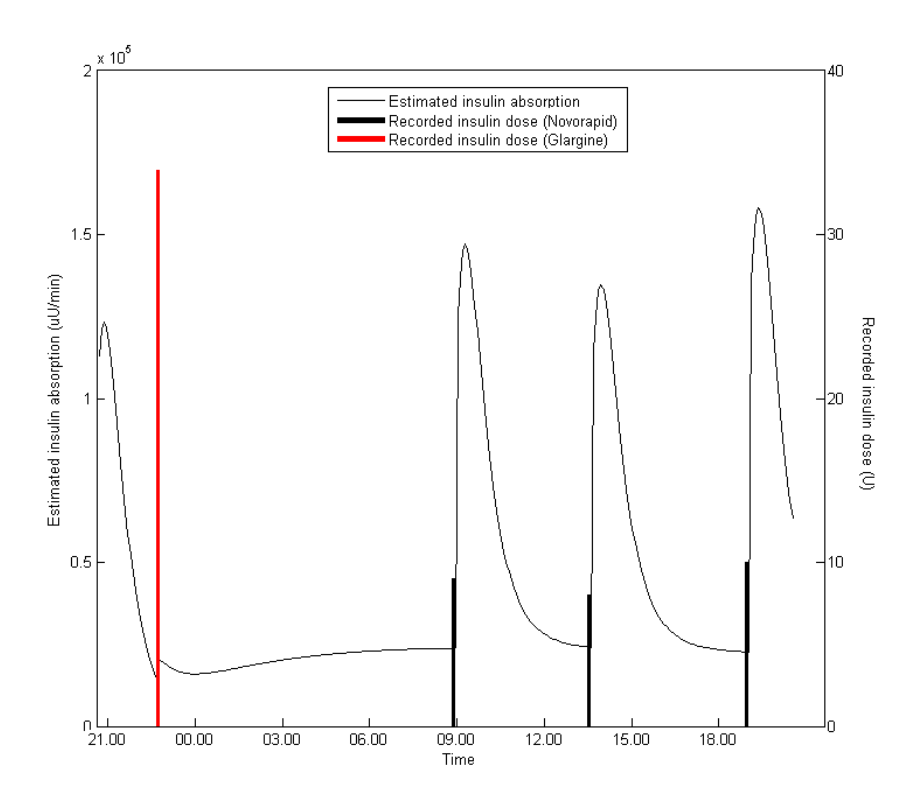


Figure 3.6: Estimated insulin absorption over a 24-hour period for one individual in the DUK study using the Tarin et al. model.

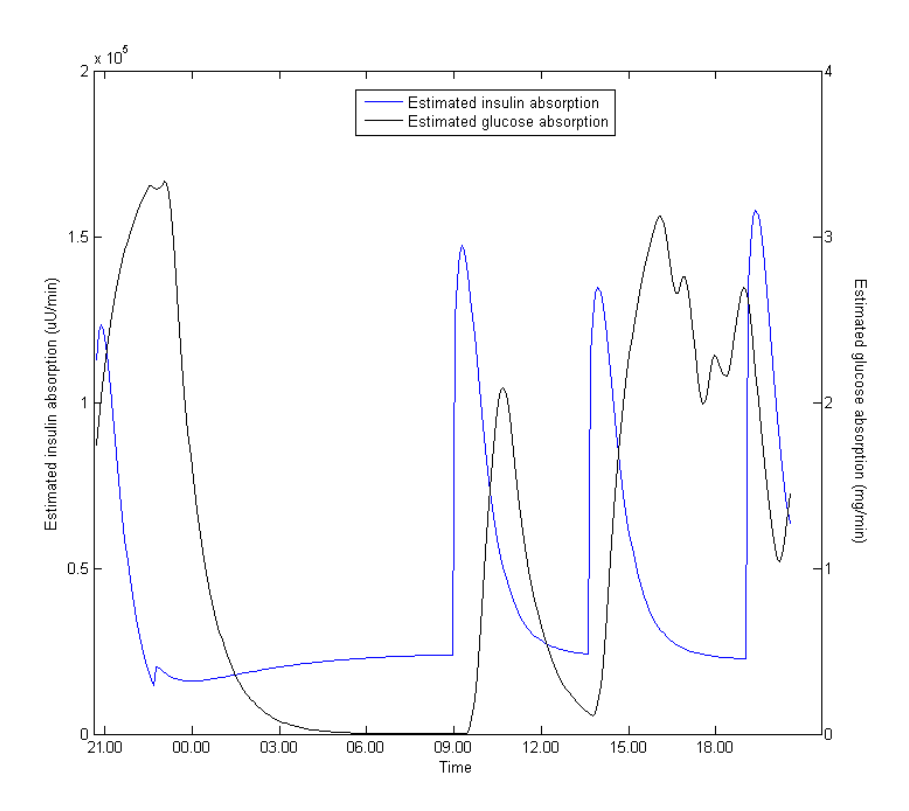


Figure 3.7: Glucose and insulin absorption over a 24-hour period for one individual in the DUK study using the Lehmann and Deutsch and Tarin et al. models, respectively.

GI of the food. This may lead to under- or over-estimation of the rate of glucose appearance;

- iii) the digestion model does not account for the biphasic nature of the digestive process. This may lead to poor estimation for the non-linear gastric emptying of liquids;
- iv) the insulin model does not take into account injection site (position or quality). Hence it may under- or over-estimate the appearance and amount of insulin in the blood.

Despite these limitations, it is believed that the models provide important information on how ingested carbohydrate and injected insulin appear in the blood, and hence affect BGC. Such information is beyond that provided by the raw data recorded in the food and insulin diaries.

# 3.7 Data Collection: Summary

The data collected in the DUK study drive the current project and its objectives. Food intake, insulin and physical activity represent the three major external factors affecting BGC, and the data and modelling approaches presented here allow analysis of uninterrupted time series over several days, on a range of individuals. The data can be used to build the most detailed empirical model of BGC yet, for descriptive and predictive purposes. This would ideally be able to provide accurate BGC profiles given the inputs of food, insulin and activity, and thus be appropriate for use within the MDI treatment regime. Furthermore, many of the more complex, compartmental models that claim to account for physical activity are based on only very simplified descriptions of physical activity. The current work aims to test how such models perform when supplied with free-living data.

The remainder of the chapter uses simple time series methods to explore the DUK data, with the aim of better understanding the behaviour of blood glucose and soliciting useful information that may inform or supplement more complex models.

# 3.8 Time Series Methods

The nature of BGC is such that neighbouring observations are highly correlated, and may not be considered independent (Bremer and Gough, 1999). In such cases, time series methods are preferred to standard statistical regression. In the following section, basic descriptive techniques for time series data are described. The remainder of the chapter uses such techniques to explore BGC data from the DUK study. Understanding

the nature of BGC can aid the modelling process, e.g., BGC may exhibit circadian behaviour (naturally occurring oscillations), or short- and/or long-term correlation that can be accounted for in a more comprehensive model. Given the limited amount of free-living data in the diabetes literature, the exploratory analysis offers an insight to the behaviour of BGC outside the clinical environment.

#### 3.8.1 Stochastic Processes

A stochastic, or random, process is the collective name for time series which involve some non-deterministic form. An observed time series,  $y_1, ..., y_n = \{y_t\}$ , can be considered to be one realisation of a series of random variables,  $Y_1, ..., Y_n = \{Y_t\}$  (the notation here applies to a series considered at discrete time intervals only). The series  $\{y_t\}$  is therefore considered to be a sample from the population of all possible observable time series, known as the ensemble. Rather than using sample properties to make inferences upon the population, it is the properties of the probabilistic model underlying the process that are of interest.

A stochastic process is said to be strictly stationary when the joint distribution of a time series does not change in time. This is often formally expressed in terms of the joint cumulative distribution,  $F_Y$  (Tong, 1993):

for any  $t_1, ..., t_n$ , with  $n \in \mathbb{N}$ , and any  $k \in \mathbb{Z}$ 

$$F_{Y_{t_1},Y_{t_2},\ldots,Y_{t_n}}(y_1,y_2,\ldots,y_n) = F_{Y_{t_1+k},Y_{t_2+k},\ldots,Y_{t_n+k}}(y_1,y_2,\ldots,y_n).$$

A process is weakly stationary if the first two moments of the joint distribution (described in section 3.8.2.1) are constant in time. This less restrictive definition is generally sufficient to study other properties of a process. Analysis of stationary time series is well-established (e.g., Chatfield, 1992; Priestley, 1981). Often, where possible, non-stationary time series are subject to certain techniques to make the series stationary, e.g., see section 3.8.2.4.

#### 3.8.2 Stochastic Processes in the Time Domain

Analysis in the time domain relates to studying functions with respect to time, as opposed to the frequency domain (as described in section 3.8.4). The joint distribution of  $\{Y_t\}$  is one method of describing a process over time, but will generally be too complex to handle. An alternative is to instead consider only the first two moments of the distribution. This is generally sufficient to explore the properties of a time series.

#### 3.8.2.1 Autocovariance and Autocorrelation

The mean, variance and autocovariance describe the first two moments of a time series, where the mean and variance are the standard functions relating to expectations. Autocovariance is the covariance of a time series with itself at different time lags, and is given by

$$\gamma_k = \gamma(Y_t, Y_{t+k}) = \mathbb{E}\left[ (Y_t - \mathbb{E}[Y_t])(Y_{t+k} - \mathbb{E}[Y_{t+k}]) \right]. \tag{3.8.1}$$

This may be used to determine the autocorrelation coefficient at lag k:

$$\rho_k = \gamma_k / \gamma_0, \tag{3.8.2}$$

where  $\gamma_0$  is the variance of the time series. The autocorrelation is a measure of the linear association between  $Y_t$  and  $Y_{t+k}$ , and has similar properties to the standard correlation function, e.g.,  $|\rho_k| \leq 1$ . The correlogram is a plot of the autocorrelation coefficients as a function of lag k, and can highlight a number of important features of a time series such as short- and long-term dependence between observations. For a stationary process, the mean and variance are constant and the autocovariance depends only on the absolute time difference.

Methods for estimating these functions rely on ergodic theorems. The theorems show that (in most cases) the sample estimates of the moments converge in mean square error to the ensemble moments as  $n \to \infty$ . The theorems are discussed with regards to the mean and autocovariance in Priestley (1981), with further references within, and are not considered further here.

#### 3.8.2.2 Simple Stochastic Models

The simplest stochastic model is the purely random series, made up of a sequence of independent and identically distributed (iid) variables. A process,  $Y_t$ , is a random walk if it can be written as  $Y_t = Y_{t-1} + Z_t$ , where  $Z_t$  is an iid process. This simple model forms the basis for the more sophisticated stochastic models described in the following sections, throughout which it is assumed  $Z_t$  is an iid process.

#### 3.8.2.3 Autoregressive Moving-Average Models

An autoregressive process of order j, represented by AR(j), is based on a linear combination of the j previous values of the time series:

$$Y_t = \alpha_1 Y_{t-1} + \alpha_2 Y_{t-2} + \ldots + \alpha_i Y_{t-i} + Z_t. \tag{3.8.3}$$

Fitting an AR process involves determining a suitable order, j, and estimating the parameters,  $\{\alpha_i\}$ . The estimated coefficient of an AR(j) process at lag i,  $\hat{\alpha}_i$ , is known as

the partial autocorrelation, and represents the sample correlation between the variable and itself at lag i that is not accounted for by lags 1 to i-1; the plot of i against  $\hat{\alpha}_i$  is the partial autocorrelation function.

A moving average process of order k, represented by MA(k), is based on a linear combination of a purely random process:

$$Y_t = Z_t + \beta_1 Z_{t-1} + \ldots + \beta_k Z_{t-k}. \tag{3.8.4}$$

Again, fitting such a model requires estimating the order, k, and the parameters,  $\{\beta_i\}$ . The combination of AR and MA models is an ARMA(j, k) model.

### 3.8.2.4 Extensions of ARMA models

In some cases, non-stationary series can be made stationary by differencing, represented by the difference operator,  $\nabla$ :

$$x_t = \nabla y_t = y_t - y_{t-1}, \tag{3.8.5}$$

and taking d differences gives:

$$x_t = \nabla^d y_t = \sum_{i=0}^d (-1)^i \binom{d}{i} y_{t-i}.$$
 (3.8.6)

An ARMA model applied to data such as  $x_t$  is an autoregressive integrated moving average model, represented by ARIMA(j, d, k).

### 3.8.3 Estimation in the Time Domain

Analysis of the autocorrelation function is referred to as analysis in the time domain. The sample autocovariance at lag k may be constructed in a similar way to estimating a population variance from a sample:

$$\hat{\gamma}_k = c_k = \frac{1}{n} \sum_{t=1}^{n-k} (y_t - \bar{y})(y_{t+k} - \bar{y}). \tag{3.8.7}$$

The divisor n gives this estimator a larger bias compared to n-k (though is asymptotically unbiased), but tends to result in a lower mean square error (Jenkins and Watts, 1968). The sample autocorrelation coefficient at lag k is then given by:

$$\hat{\rho}_k = r_k = c_k / c_0, \tag{3.8.8}$$

where  $c_0$  is the (biased) estimator of the variance. One could use the estimator of  $\gamma_k$  with smaller bias (i.e., use divisor n-k) but again the estimator with larger bias has preferable properties, e.g., it ensures that  $|r_k| \leq 1$  (Priestley, 1981).

Theoretically, for a purely random process,  $\rho_k = 0$ , except at lag zero. It can be shown that asymptotically and under weak conditions (Kendall et al., 1983):

$$r_k \sim N(-1/n, 1/n),$$
 (3.8.9)

with approximate 95% confidence intervals given by:

$$-\frac{1}{n} \pm \frac{2}{\sqrt{n}}. (3.8.10)$$

For large n, this may be further approximated by  $\pm 2/\sqrt{n}$ . Autocorrelation coefficients outside this range suggest non-randomness.

The sample partial autocorrelation coefficients may be determined by fitting AR models of increasing order. The estimated coefficients can be plotted against order, with values outside  $\pm 2/\sqrt{n}$  suggesting statistically significant correlation at the 5% level. A purely AR(j) process will show significant partial correlation up to lag j. The coefficients of an AR model can be determined using the Yule-Walker equations (Chatfield, 1992, chapter 3), which use the relationship between the parameters and autocorrelation function. The equations are given by

$$\rho_k = \alpha_1 \rho_{k-1} + \ldots + \alpha_i \rho_{k-i}, \quad \text{for } k \in \mathbb{N}.$$

Models of successively higher order may also be compared on some suitable measure; a general method for aiding model selection is Akaike's Information Criterion (AIC), which allows comparison of models using the maximised likelihood (L) and a penalty for including more parameters (p):

$$AIC(p) = -2\ln(L) + 2p. (3.8.11)$$

Lower values indicate a preferable model.

# 3.8.4 Stochastic Processes in the Frequency Domain

To complement analysis in the time domain, the frequency properties of a series may be analysed. This is called analysis in the frequency domain (or spectral analysis, or harmonic analysis) and is based on techniques estimating the spectral density function. The spectral density function represents the contribution of different frequencies to the variation in a series. Spectral analysis is based on Fourier analysis, extending its use on deterministic functions of time to stochastic functions. Much theory exists regarding Fourier and spectral analysis which will not be discussed here; the reader is directed to Chatfield (1992), Bloomfield (1976), and Priestley (1981) for increasingly detailed discussions of these techniques.

A key tool in frequency domain analysis is the Fourier transform (FT). This converts a given function of time, f(t),  $t \in \mathbb{R}$ , in to a function of frequency,  $F(\omega)$ :

$$F(\omega) = \int_{-\infty}^{\infty} f(t) \exp(-i\omega t) dt, \qquad (3.8.12)$$

where  $\omega$  is frequency in radians per unit time. The integral can be considered as a summation when a time series is observed only at discrete points.

The spectral density function is the Fourier transform of the autocovariance coefficients (Chatfield, 1992, chapter 7). The autocovariance function is an even function, so the FT may be simplified to:

$$F(\omega) = \frac{1}{\pi} \left[ \gamma_0 + 2 \sum_{k=1}^{\infty} \gamma_k \cos(\omega k) \right]. \tag{3.8.13}$$

The spectral density function uses the same information as the autocovariance function, but summarises the second-order properties in a different form. By comparing the behaviour of a function to sinusoidal curves of different frequencies, important structural behaviour regarding periodicities may be highlighted. It is worth noting that spectral analysis should be performed on stationary series, as any trends in the data tend to dominate estimation and may obscure important periodicities.

# 3.8.5 Estimation in the Frequency Domain

Fourier analysis involves reconstructing a function as the sum of sine and cosine terms, known as the Fourier series representation. This representation may be thought of as repeatedly fitting a simple sinusoidal model,

$$Y_t = \mu + a\cos(\omega t) + b\sin(\omega t) + Z_t$$

for t = 1, ..., n, across the range of Fourier frequencies,  $\omega$ . Parameter estimation is simplified by considering frequencies that are multiples of  $2\pi/n$ , i.e.,  $\omega_k = 2k\pi/n$ , in the range [0,n/2]; frequencies outside this range are aliased due to the periodic nature of sinusoids (Bloomfield, 1976). The Fourier series representation is given by:

for 
$$t = 1, \dots, n$$
,
$$y_t = \sum_{k=0}^{n/2} \left[ a_k \cos(\omega_k t) + b_k \sin(\omega_k t) \right], \tag{3.8.14}$$

with parameter estimates (Chatfield, 1992, chapter 7)

$$a_0 = \bar{y}$$

$$a_{n/2} = \frac{1}{n} \sum_{t=1}^{n} (-1)^t y_t$$

$$a_k = \frac{2}{n} \sum_{t=1}^{n} y_t \cos(\omega_k t)$$

$$b_k = \frac{2}{n} \sum_{t=1}^{n} y_t \sin(\omega_k t),$$

for k = 1, ..., n/2 - 1, where  $b_0 = b_{n/2} = 0$  (as  $\sin(\omega_0) = \sin(\omega_{n/2}) = 0$ ). There are n parameters to estimate, and so a series may be completely represented by its Fourier representation (i.e., no error term). The variability of a time series at a given Fourier frequency, k, is called the  $k^{th}$  harmonic, with associated amplitude  $v_k^2 = a_k^2 + b_k^2$ . The contribution of a frequency to the variability may be found by considering the breakdown of the total sum of squares. It can be shown that the contribution to the sum of squares for the  $k^{th}$  harmonic is given by (Chatfield, 1992, chapter 7):

$$\frac{n}{2}v_k^2$$
, for  $k \neq n/2$ ,  
 $a_k^2 n$ , for  $k = n/2$ .

The sum of squares may then be written as:

$$\sum_{t=1}^{n} (y_t - \bar{y})^2 = \frac{n}{2} \sum_{k=1}^{\frac{n}{2} - 1} v_k^2 + n a_{n/2}^2$$

$$\Rightarrow \frac{1}{n} \sum_{t=1}^{n} (y_t - \bar{y})^2 = \frac{1}{2} \sum_{k=1}^{\frac{n}{2} - 1} v_k^2 + a_{n/2}^2,$$

and so the  $k^{th}$  harmonic contributes  $v_k^2/2$  to the overall variance (except for k=n/2 when the contribution is  $a_{n/2}^2$ ). Rather than plot  $v_k^2/2$  against frequency to obtain a spectrum, it is more appropriate to consider  $v_k^2/2$  as the contribution to the variance in the range  $\omega_k \pm \pi/n$ . This gives a more realistic estimation of the spectral density function which is usually continuous (recall that the range  $[0,\pi]$  was discretised to multiples of  $2\pi/n$ ). This gives a histogram where the variance contribution is centred on  $\omega_k$ , with width  $2\pi/n$ . The heights of the histogram bars,  $I(\omega)$ , are found by dividing

the variance contribution by the width:

$$I(\omega_k) = nv_k^2/4\pi$$
, for  $k = 1, ..., n/2 - 1$   
 $I(\omega_{n/2}) = na_{n/2}^2/\pi$ ,  $k = n/2$ .

The plot of  $I(\omega)$  against  $\omega$  is called the periodogram. Often  $I(\omega)$  is instead plotted against  $f_r = \omega/2\pi$ , where  $f_r$  corresponds to the number of cycles completed per unit time, a more natural definition of frequency than the Fourier frequencies,  $\omega_k$  (sometimes referred to as angular frequencies to distinguish them from  $f_r$ ).

## 3.8.6 Analysis of the Periodogram

As noted previously, the spectral density function is the FT of the autocovariance coefficients. Given that  $I(\omega)$  is the FT of the sample autocovariance coefficients, it would seem to be the natural estimator of  $f(\omega)$ . However, there are a number of problems with using the periodogram to estimate the spectral density function:

- i)  $I(\omega)$  is not a consistent estimator of  $f(\omega)$  as it can be shown that  $Var[I] \rightarrow 0$  as  $n \rightarrow \infty$  (Diggle, 1990);
- ii) the sample autocovariance coefficients may only be calculated up to n. The spectral density is a Fourier transform of the infinite sequence of autocovariance coefficients, so the estimator  $I(\omega)$  suffers from an abrupt truncation at lag n;
- iii) the estimated autocorrelations  $r_k$  become less reliable as k increases due to the lack of data to calculate higher lags;
- iv) periodogram ordinates are only estimated at the discrete Fourier frequencies. Periods that exist at non-Fourier frequencies are ignored, and so the variance explained by such periods may "leak" into neighbouring Fourier frequencies. This may result in spurious peaks in the periodogram;
- v) periodogram ordinates  $I(\omega)$  are asymptotically uncorrelated and so the periodogram may fluctuate rapidly.

Problem iv) may be partially countered by ensuring a suitable sampling rate. For a given time span, a higher sampling rate will result in more frequencies that can be explored, equivalent to improving resolution. The following sections give a brief overview of methods that can help to overcome some of these issues; full theory and discussion may be sought in the respective references.

### 3.8.6.1 Smoothing the Periodogram

Problems i) and v) can be overcome by smoothing the periodogram ordinates. Perhaps the simplest smoothing technique is the Daniell smoother (Daniell, 1946), a moving average applied to the periodogram ordinates. The modified Daniell smoother applies a halved weight to the end-points of the moving average:

for 
$$j \in \mathbb{N}$$
,

$$\hat{f}(\omega_k) = \sum_{i=k-j}^{k+j} \kappa_i I(\omega_i),$$

where

$$\kappa_{i} = \begin{cases} \frac{1}{2(j-1)}, & \text{for } i = k \pm j \\ \frac{1}{j}, & \text{for } i \in [k-j+1, k+j-1], \end{cases}$$
(3.8.15)

with adjustments made for the end frequencies 0 and  $\pi$  by considering the periodogram to be symmetric about these frequencies. The choice of the span, 2j, decides the number of periodogram ordinates used in weighting and hence the degree of smoothing; it is recommended to try values around j = n/80 (Chatfield, 1992, chapter 7). The Daniell smoother introduces bias to the estimator if the spectrum is not linear over the interval (k-j,k+j), but this is not so important if the spectrum is smooth or if  $2j \ll n$ . The smoother may be applied several times. Note that after smoothing, the area under the periodogram no longer directly represents the variance of the time series.

### 3.8.6.2 Tapering

Tapering is a method used primarily to reduce bias in the periodogram and resolve the issue of leakage, by smoothing the ends of the data toward zero. The theory behind it is discussed thoroughly in Bloomfield (1976) and Priestley (1981). The use of tapering has been labelled "controversial" (Chatfield, 1992, p. 120), and it has been noted there is little to be gained from tapering if using a smoothing window (Priestley, 1981). Furthermore, by tapering the data, the effective data is reduced and hence variance of the estimated spectrum will increase. However, if a smoothing window with discontinuities is used (such as the Daniell smoother), tapering can give a better-behaved Fourier transform (Priestley, 1981).

A split cosine bell is suggested as a convenient taper (Bloomfield, 1976). This taper is smooth, and the majority of data can be left unaffected. The weights,  $\lambda_t$ , are applied

to the raw data before the Fourier transform, and are given by:

$$\lambda_{t} = \begin{cases} \frac{1}{2} \left( 1 - \cos\left[\frac{\pi}{m} (t - \frac{1}{2})\right] \right), & t = 1, \dots, m \\ 1, & t = m + 1, \dots, n - m \\ \frac{1}{2} \left( 1 - \cos\left[\frac{\pi}{m} (n - t + \frac{1}{2})\right] \right), & t = n - m + 1, \dots, n. \end{cases}$$
(3.8.16)

The value of m is chosen so that the proportion of tapered data, p = 2m/n, is some appropriate value; a value of p = 0.1 is suggested (Bloomfield, 1976).

## 3.8.7 Autoregressive Spectral Estimation

An alternative to the spectral estimates in the preceding sections is autoregressive spectral estimation (ASE). This is of use when the data may be adequately explained by an AR model of the form given in equation 3.8.3, section 3.8.2.4. An AR model describes the entire process and is not limited to sample data, nor certain frequencies. However, by imposing global assumptions, some errors may be incurred. ASE is based on the fact that the spectral density function for an AR(j) process can be calculated by (Priestley, 1981):

$$f(\omega) = \frac{\sigma_Z^2}{2\pi} |1 - \alpha_1 e^{i\omega} - \dots - \alpha_j e^{ij\omega}|^{-2}.$$

# 3.9 BGC Variation in the Time Domain

The methods described in sections 3.8.2 and 3.8.3 are now applied to an individual's (Subject A) BGC measurements,  $\{g_t\}$ , and may be seen as being relatively representative (unless stated otherwise) of BGC time series from other individuals in the DUK study. The data recorded spans almost three days (n=845) without interruption, as shown in Figure 3.8.

The autocorrelation coefficients for BGC were calculated using equation 3.8.8, section 3.8.5. The maximum lag was chosen to be 432, which corresponds to one-and-a-half days. The plot suggests non-stationary behaviour as the autocorrelation coefficients do not come down to zero except at very high lags (Figure 3.9). Thus, observations above (or below) the mean are followed by a large number of other observations above (or below) the mean. The data are consistent with that presented elsewhere, e.g., Bremer and Gough (1999); Sparacino et al. (2007). Data for other individuals in the DUK study also suggest high autocorrelation, but in varying patterns; Figure 3.10 shows the difference between two other individuals.

Trends in BGC dominate the correlogram so it is useful to consider methods for making the data stationary. One common method is differencing, as described in

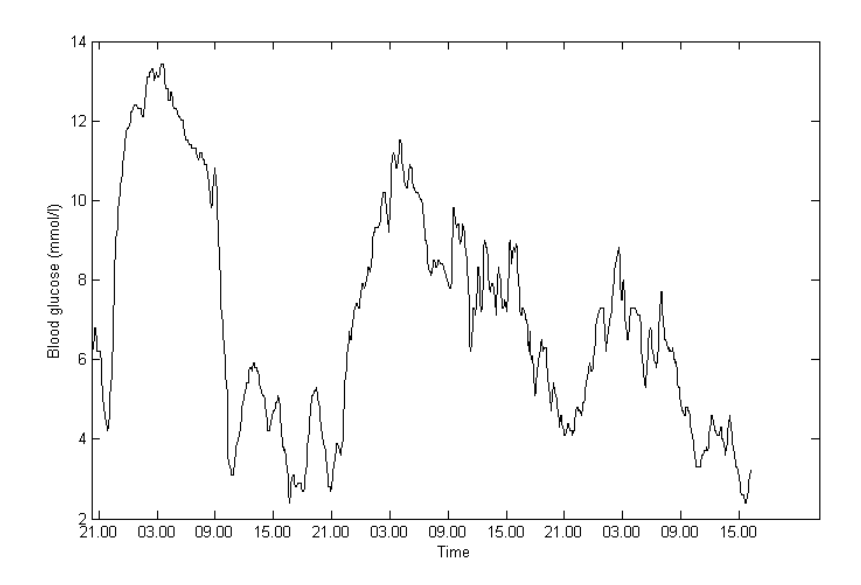


Figure 3.8: Subject A's measured BGC time series.

equation 3.8.6, section 3.8.2.4. One-step changes in BGC,  $g_t^*$ , is thus defined by:

$$g_t^* = \nabla g_t = g_t - g_{t-1}. \tag{3.9.1}$$

The resulting time series can be seen in Figure 3.11. The correlogram for  $g_t^*$  shows sharply decreasing short-term dependence between values, suggesting an AR process (Figure 3.12). The plot shows strong coherence to the theoretical autocovariance function for an AR(1) model.

Further guidance for determining the order of an AR model can be gained from the partial autocorrelation function, as described in section 3.8.2.3. The sample partial autocorrelation plot for  $g_t^*$  supports the case for an AR(1) process, as the function approaches zero after the first lag (Figure 3.13). Again there appear to be some peaks outside the 95% confidence interval, though not large enough to suggest strong correlation. Of possible interest in the current data set is the moderate peak that occurs at lag 279. This peak is close to the 24-hour mark, suggesting some similarity in the behaviour of BGC from day-to-day; however, this feature is not replicated in other data sets.

The Yule-Walker equations were used to fit successively higher order models and suggest that an AR(1) model is appropriate for change in BGC; Table 3.5 shows (for a small selection of models) AIC is minimised for the first-order AR model.

Changes in BGC for other individuals suggest a range of orders for AR models. Variation in order was found both between and within individuals, and were found to be as high as 15 in some cases; however, in all cases the first lag (and occasionally second lag) were found to be the most influential, with relatively little gained by including

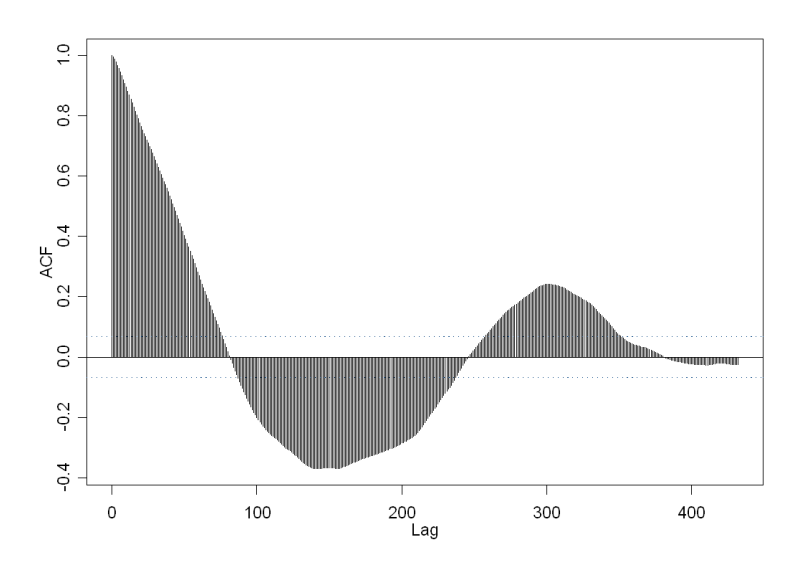


Figure 3.9: Autocorrelation coefficient against respective lag for BGC of Subject A. Dotted lines represent theoretical 95% confidence intervals given by  $\pm \frac{2}{\sqrt{n}}$ .

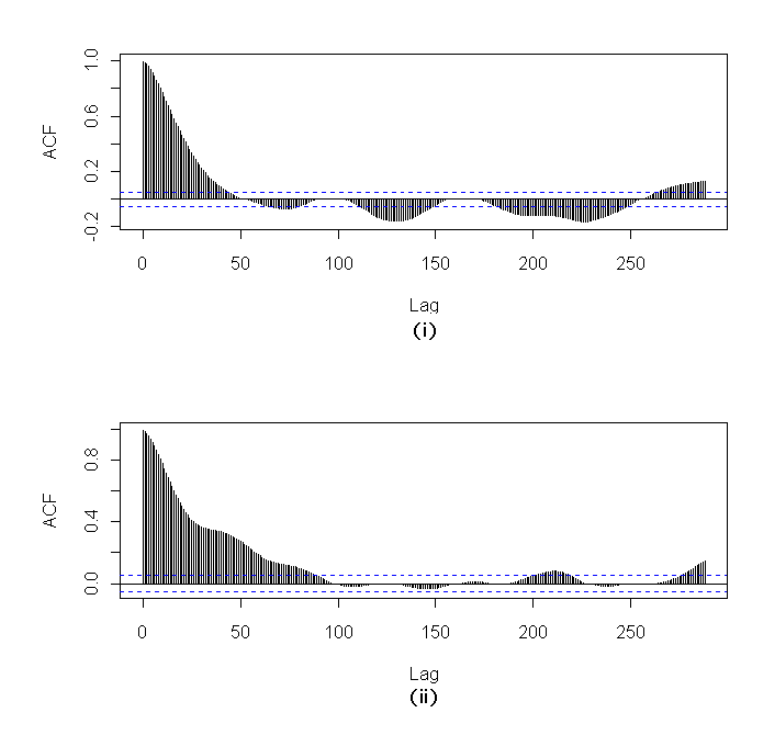


Figure 3.10: Autocorrelation coefficient against respective lag for BGC for two different individuals in the DUK study. Dotted lines represent theoretical 95% confidence intervals given by  $\pm \frac{2}{\sqrt{n}}$ .

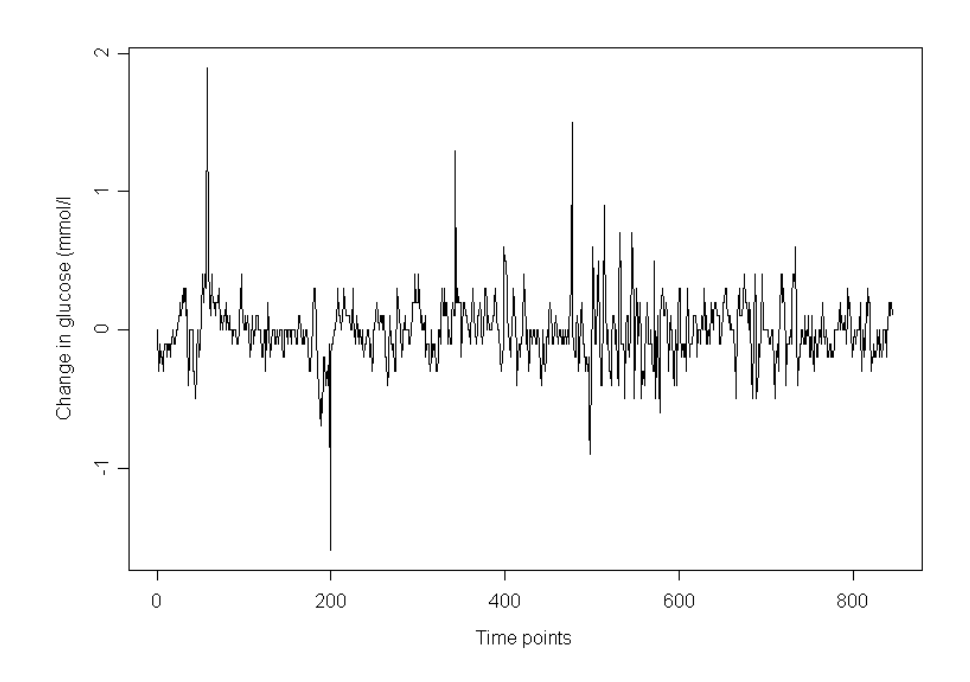


Figure 3.11: One-step changes in BGC time series for Subject A.

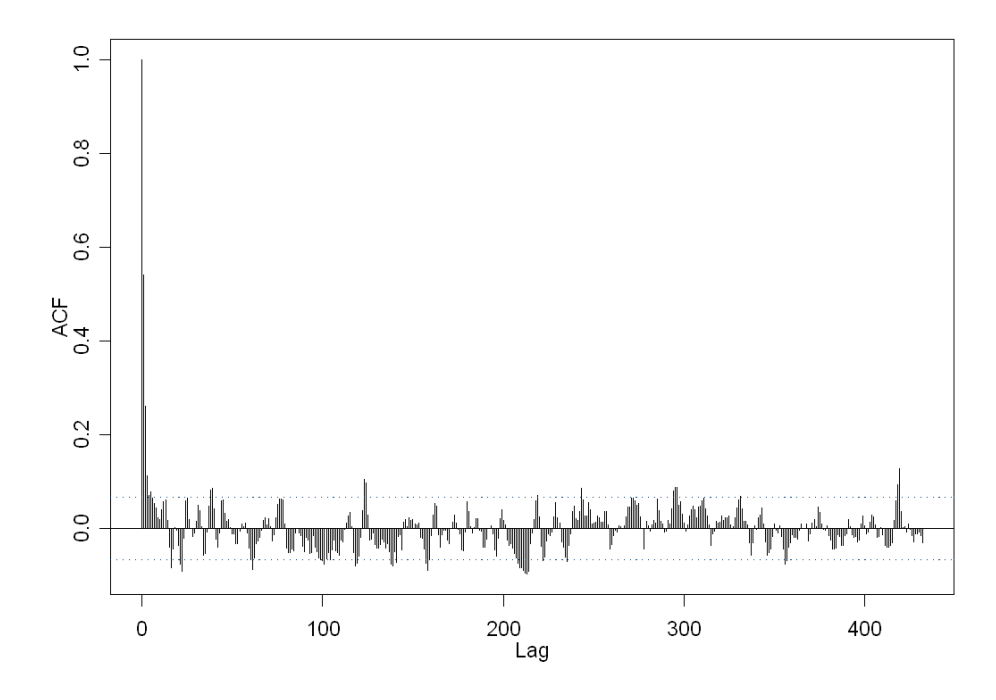


Figure 3.12: Sample autocorrelation function for change in BGC of Subject A. Dotted lines represent theoretical 95% confidence intervals given by  $\pm \frac{2}{\sqrt{n}}$ .

further lags.

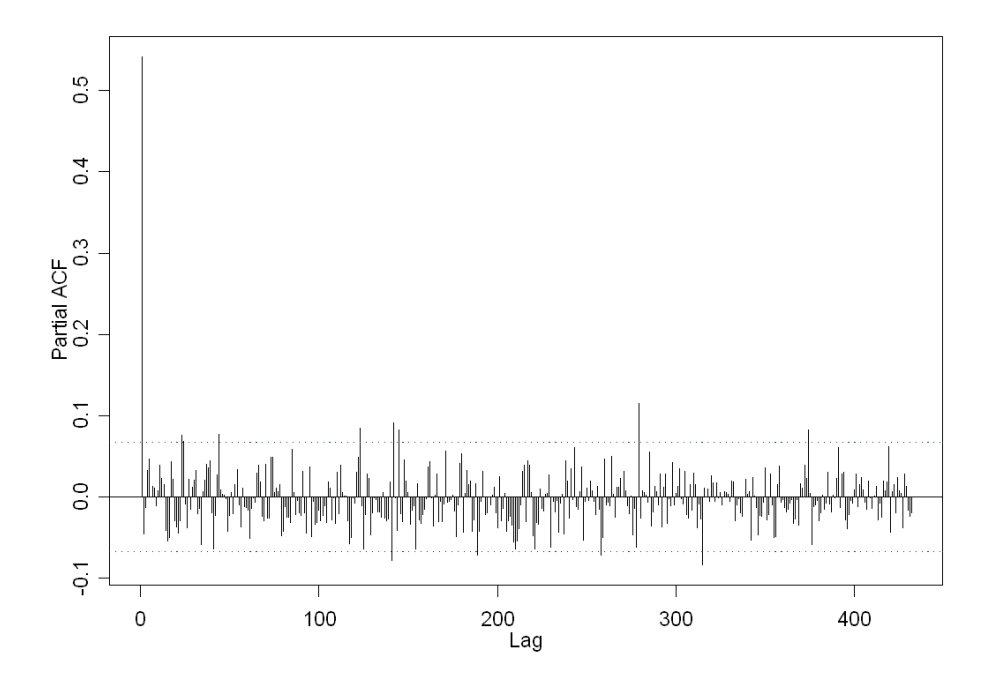


Figure 3.13: Sample partial autocorrelation function for change in BGC of Subject A. Dotted lines represent theoretical 95% confidence intervals given by  $\pm \frac{2}{\sqrt{n}}$ .

Table 3.5: AIC of autoregressive models for change in BGC.

Order	$\overline{\mathrm{AIC}}$ - $\overline{\mathrm{min}}(\overline{\mathrm{AIC}})$
0	290.9
1	0
2	0.2197
3	2.070
4	3.150

### 3.9.1 BGC AR Model

Given the above analysis for Subject A, an autoregressive model of order 1 was fitted to change in BGC (equivalent to fitting an ARIMA(1,1,0) model to BGC), with the parameters of the model estimated using the Yule-Walker equations. For this individual, the  $\alpha$  parameter is the correlation between  $g_t^*$  and  $g_{t-1}^*$ :

$$g_t^* = 0.541g_{t-1}^* + \epsilon_t$$

$$\Rightarrow E[g_t^*] = 0.541g_{t-1}^*,$$
(3.9.2)

where it is assumed that the residuals,  $\epsilon_t$ , are independent, and independent of  $g_t^*$ . From the fitted model, the residuals,  $\{e_t = \hat{g}_t^* - g_t^*\}$ , have sample standard deviation  $s_e^2 = 0.0371$  and approximately zero mean. Residual analysis does not suggest any temporal dependence, except perhaps the tendency for pairs of large positive-negative values, e.g., around time point 200 (Figure 3.14).

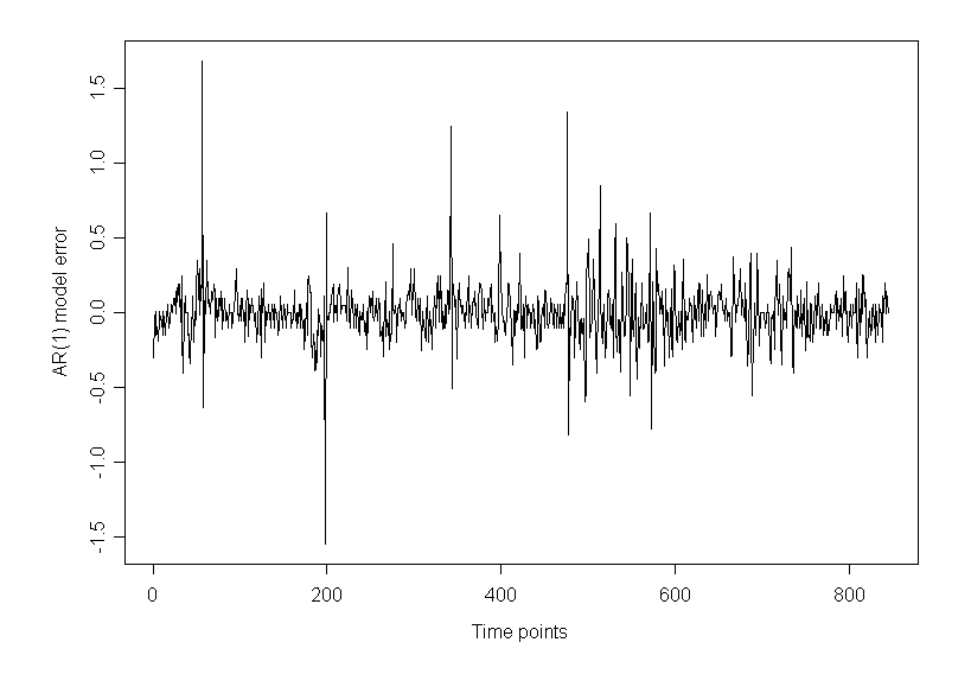


Figure 3.14: AR(1) model residuals for change in BGC of Subject A.

The residual correlogram also does not suggest any temporal dependence of the residuals; Figure 3.15 shows most autocorrelation coefficients are within the 95% intervals. In addition the partial autocorrelation function (not shown) does not suggest any violation of the assumptions.

### 3.9.2 BGC AR Prediction

Using the above model of  $g_t^*$ , it is of interest to assess predictive performance. The conditional expectation is given by

$$\mathbb{E}[g_{t+1}^*|g_t^*,...,g_0^*] = \mathbb{E}[g_{t+1}^*|g_t^*]$$
$$= 0.541q_t^*,$$

so the one-step ahead forecast at time t is

$$\hat{g}_{t+1}^* = 0.541 g_t^*. \tag{3.9.3}$$

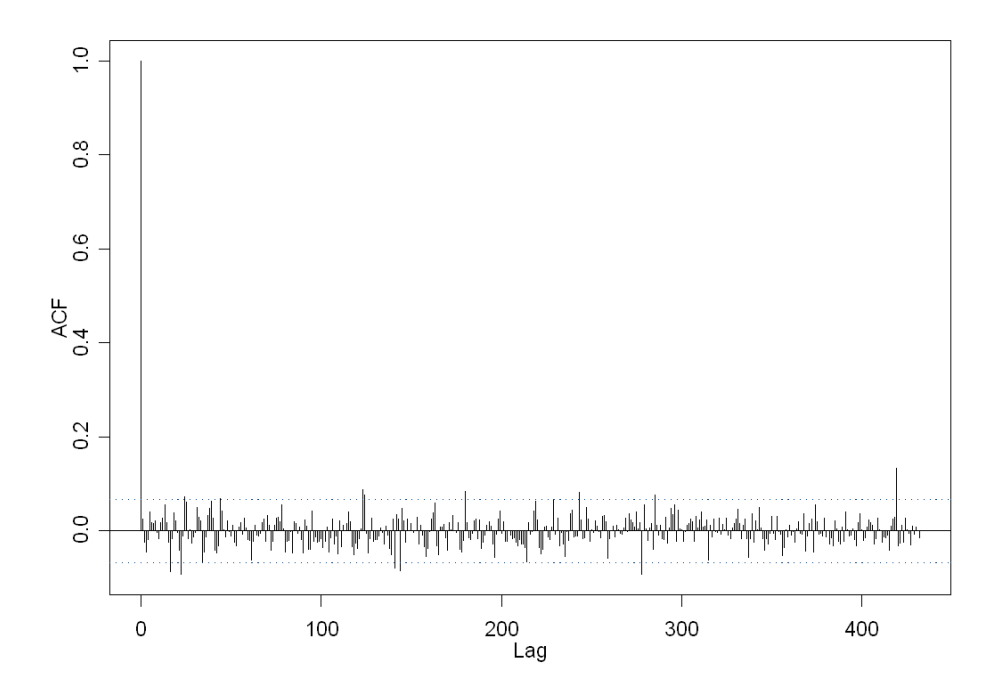


Figure 3.15: Correlogram of the AR(1) model residuals for change in BGC of Subject A.

Similarly, for the k-step ahead forecast:

$$\mathbb{E}[g_{t+k}^*|g_t^*, ..., g_0^*]$$

$$= \mathbb{E}[g_{t+k}^*|g_t^*]$$

$$= 0.541\hat{g}_{t+k-1}^*$$

$$= 0.541^2\hat{g}_{t+k-2}^*$$

$$\vdots$$

$$= 0.541^kg_t^*.$$

Given a positive (negative) reading at time n all future estimates  $g_{n+k}^*$  will also be positive (negative) and will decay to zero as k increases; this suggests the AR model will be poor for long-term prediction.

The data used to build the AR model may be considered as a training set, and the model may be tested on a second set to assess its predictive ability. The test set measurements were taken from the same individual starting on the same day as the training set finished. The model was set to predict one and 48 time steps ahead, equivalent to five minutes and four hours respectively, where four hours represents a reasonable time between finger-prick tests as part of the MDI treatment regime. In each case, the predictions for change in BGC were used to then predict actual BGC.

### 3.9.2.1 Results

The one-step AR(1) model shows good predictive capability; Figure 3.16 shows predictions follow the peaks and troughs of measured BGC well. However, five-minute ahead predictions are of little or no relevance to a clinician or individual looking to make longer-term predictions for BGC.

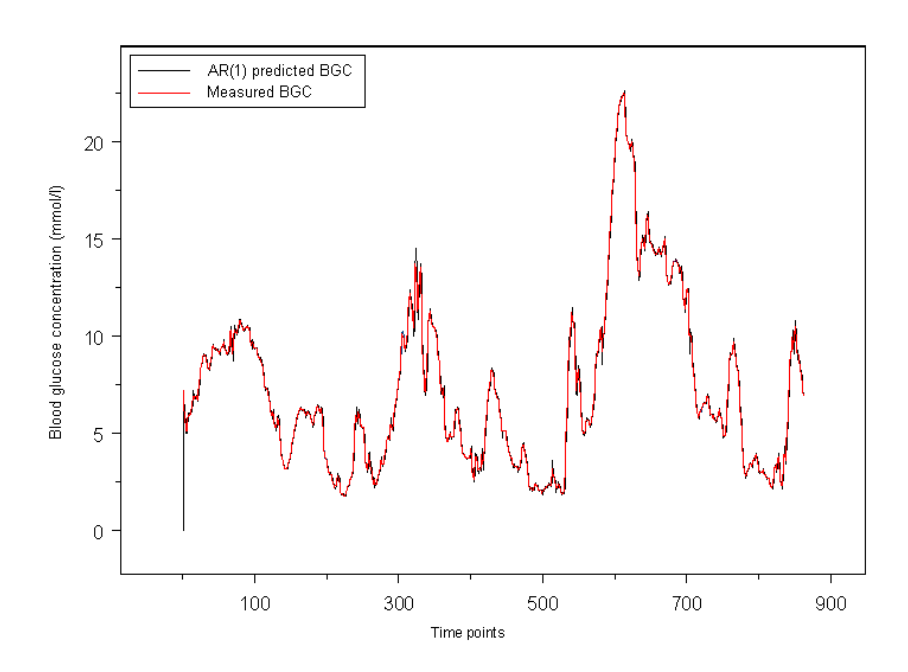


Figure 3.16: Measured BGC and one-step (five minutes) ahead prediction for BGC using ARIMA(1,1,0) model for Subject A.

The 48-step AR(1) model highlights the limited predictive capabilities of AR models. Predicted change in BGC quickly tends to zero the more steps ahead the prediction is made, and so misses the peaks and troughs in the data; Figure 3.17 shows the 48-step model predictions are essentially the original BGC time series shifted. Similar results were seen for other individuals in the DUK study, regardless of AR model order. AR models are thus inadequate for long-term prediction, and more sophisticated methods are required to model BGC over several hours.

### 3.9.3 Conclusions

Changes in BGC appear to behave like an AR process, and hence exhibits short-term trend; this is certainly noticeable in the case of Subject A, whose BGC rapidly increases at night and experiences other short-term peaks and troughs. Although consecutive changes in BGC are highly correlated, there is little scope for using this information to predict the behaviour of BGC over several hours. Long-term predictive models of

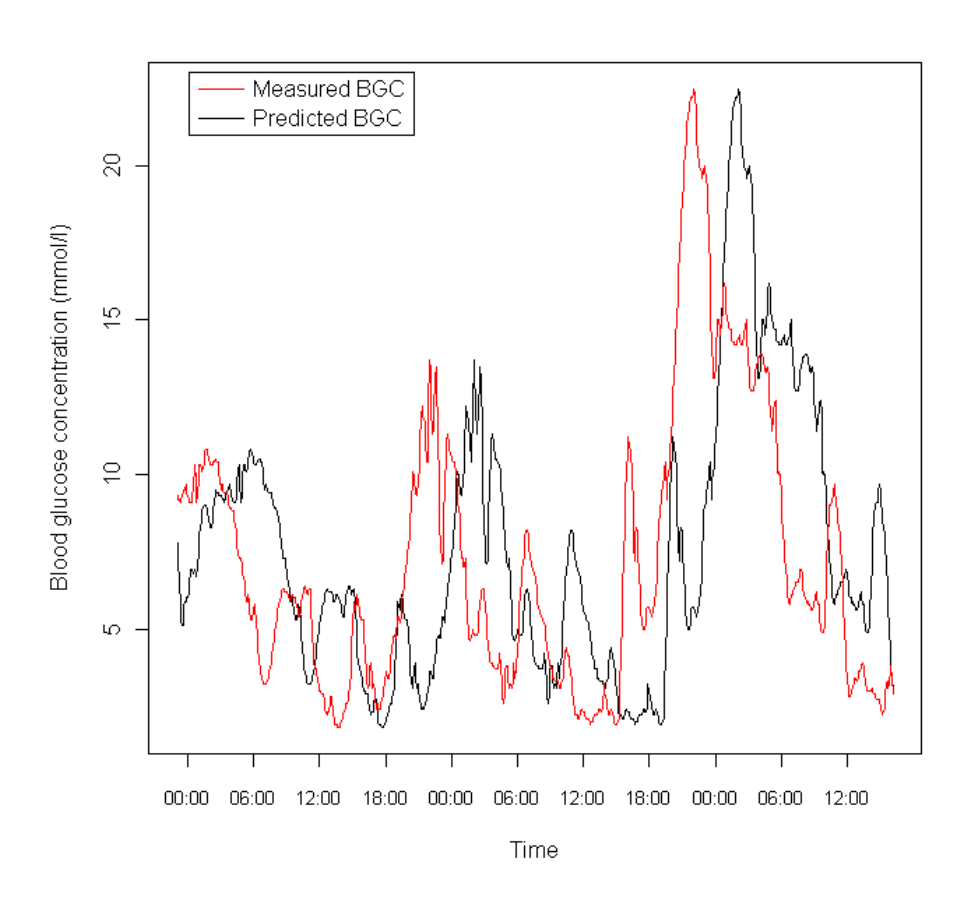


Figure 3.17: Measured BGC and 48-step (four hours) ahead prediction for BGC using ARIMA(1,1,0) model for Subject A.

BGC require more sophisticated methods, and may be improved by including relevant data on factors affecting BGC, such as meals, insulin and physical activity.

# 3.10 BGC Variation in the Frequency Domain

The methods described in section 3.8.5, regarding periodogram estimation, were applied to Subject A's BGC time series. Periodogram analysis should be performed on stationary processes so the change in BGC,  $g_t^*$ , remains the variable of interest. Given the sampling interval of five minutes and the time span of almost three days, the amount of leakage should be small. The periodogram will be able to investigate periods occurring at a minimum of every ten minutes, which should be enough to pick up important periodicities (Gough et al., 2003).

The periodogram for  $g_t^*$  was calculated using the discrete Fourier transform. A split-cosine bell taper was applied to 10% of the data (5% at either end). The periodogram was then smoothed twice using the Daniell smoother of spans of 7 and 11. This choice of span was judged to smooth the periodogram adequately enough to remove spurious peaks, without losing too much resolution. The periodogram was plotted using a  $10 \log_{10} I(\omega)$  scale for the estimated spectrum. This ensures clarity for higher frequencies (Bloomfield, 1976). The estimated spectrum was plotted against frequency, f, as a line plot rather than histogram (for clarity).

### 3.10.1 Results

The periodogram shows peaks at low frequencies (<0.05) and also notable peaks at around f = 0.07 and f = 0.16 (Figure 3.18). The peaks at low frequencies are potentially a result of leakage, due to the relative sparseness of the low frequencies (the first ten frequencies correspond to cycles completed between eight hours and 70 hours, while the last ten frequencies correspond to cycles completed over ten minutes and ten minutes and 13 seconds). The other notable frequencies highlighted correspond to cycles completed over approximately 31 and 66 minutes. Patterns for other individuals in the DUK study were very similar, with most variation concentrated at low frequencies but no particular periodicities standing out.

The alternative methods for spectral estimation described in section 3.8.7 were also applied to Subject A's data set. The AR(1) model described in (3.9.2) is used. This approach gives a smoother spectrum but with a similar trend to that of the previous, non-parametric estimate (Figure 3.19). The periodogram again highlights that power is concentrated at low frequencies.

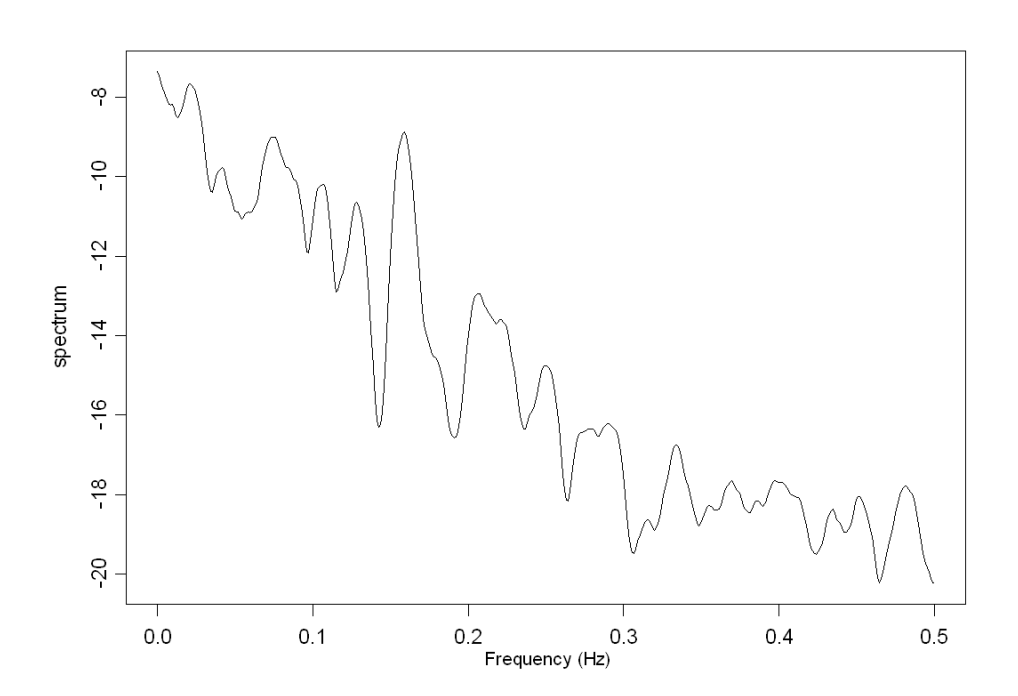


Figure 3.18: Periodogram for change in BGC of Subject A with taper proportion 0.1 and Daniell smoothers of spans 7 and 11.

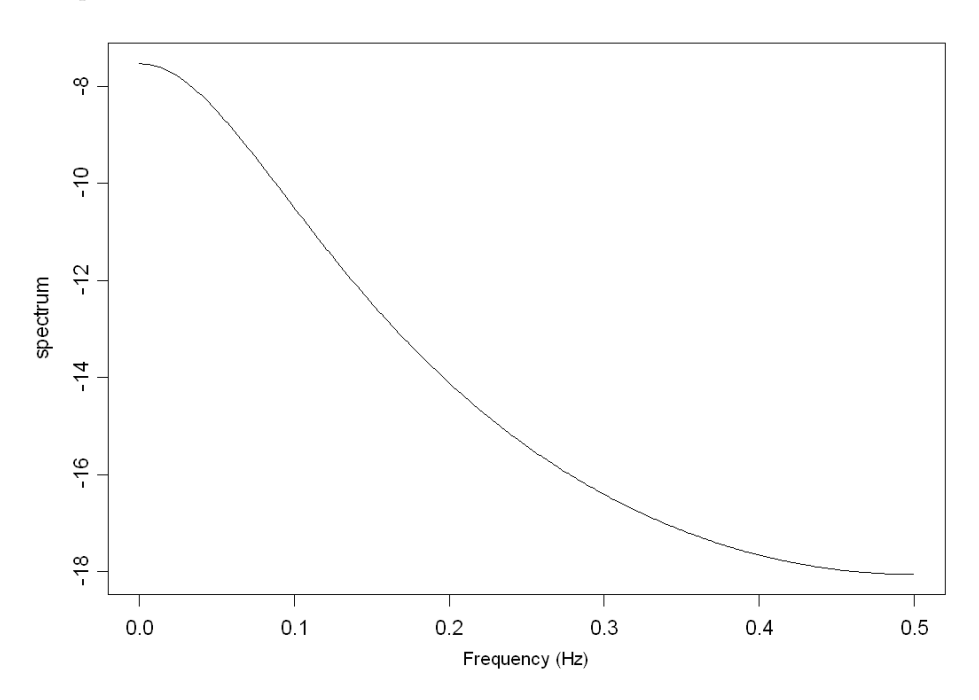


Figure 3.19: Periodogram for change in BGC of Subject A using ASE.

### 3.10.2 Conclusions

It appears that change in BGC exhibits some indistinct oscillations over periods of several hours, and potentially days. This is most likely to be due to lifestyle factors, e.g., timing of meals and sleep, rather than naturally occurring biological rhythms, which may be indistinguishable under the greater influence of food and insulin.

The BGC plot of Subject A shows repeated cases of mild, night-time hypergly-caemia, and compensatory decreases in the morning. It is possible that the insulin-carbohydrate ratio, used by the individual to calculate insulin dose with meals, is not appropriate for the evening meal, resulting in an underestimation of the required insulin. This may be due to changes in insulin sensitivity or other physiological changes, but may also be explained by miscounting of carbohydrate content in the meal, inappropriate insulin profile with respect to the glycaemic index of the food, or other external influences, e.g., stress.

# 3.11 Summary

Free-living data from the Diabetes UK study, relating to BGC, physical activity, food and insulin, have been presented, and practical modelling issues regarding these data have been highlighted. The information from the food and insulin diaries has been converted from discrete inputs to continuous processes using models in the literature, to describe the appearance of glucose and insulin in the blood and hence better understand their effect on BGC. It was also found that physical activity data fluctuates greatly during the day, creating new challenges for models in the literature trained and/or validated on simplified representations of activity.

Exploratory analysis of the DUK data showed that BGC is non-stationary. Simple time series analysis suggests temporal dependence between changes in BGC, but simple models could not use this information to predict over long periods of time. Frequency analysis did not highlight any important periodicities in changes in BGC. Thus, BGC alone does not itself offer useful information on future behaviour of blood glucose over periods of several hours. The inclusion of explanatory variables such as food intake, insulin, and METs in more complex models may help to improve predictive performance of BGC.

# Chapter 4

# Dynamic Modelling of Blood Glucose Concentration

The previous chapter highlighted the need for more sophisticated methods to predict the behaviour of blood glucose concentration (BGC), which account for food, insulin and physical activity. This chapter introduces dynamic linear models (DLMs) and applies them to the DUK study data. DLMs are empirical models not previously used in the diabetes literature. It is hypothesised they can be a useful tool for investigating the role of physical activity in the behaviour of BGC by assessing their relationship over time, in the presence of food and insulin injection disturbances, using dynamic regression models. Understanding the effects of physical activity on BGC can help those with diabetes incorporate physical activity safely into their daily routine. DLMs may also be used to predict BGC over several hours, based on future profiles of glucose and insulin absorption, and physical activity. A suitable predictive model could be incorporated in the current treatment regime of MDI by guiding the insulin therapy decision process, and hence help limit hypo- and hyperglycaemia and associated complications. The chapter begins by describing the structure of DLMs and features relevant to the current work. A simple DLM is used as a starting point to build more complex DLMs that account for explanatory variables and other features of the data.

# 4.1 Dynamic Linear Models

Linear models are used to determine the dependence of an  $(n \times 1)$  response vector,  $\boldsymbol{y}$ , on a linear combination of explanatory variables,  $\boldsymbol{x}_i$ , for i = 1, ..., p, using a  $(p \times 1)$  vector of regression parameters,  $\boldsymbol{\theta}$ . Dynamic linear models (DLMs) add flexibility by allowing the values of the parameters to vary in time, and are hence able to track changes in mean and variance inherent in non-stationary time series. DLMs as presented in this chapter were originally proposed by Harrison and Stevens (1976), using the work of

Kalman (1963).

DLMs are a general class of models that apply the Bayesian paradigm to time series, making use of the convenient features of Bayesian methods for descriptive and predictive purposes. Bayesian methods provide a structure for updating statistical inference as data becomes available, and are described further in appendix A for those unfamiliar with this approach.

DLMs have been used in a number of areas, including biology, e.g., modelling growth hormone levels (Bolstad, 1988), but not in diabetes modelling. The advantages of DLMs in the context of the current work will be highlighted throughout the following sections, which discuss their theory and structure.

### 4.1.1 Structure of a DLM

The basic regression DLM structure consists of the observation and system equations, and initial information on the parameters. The observation equation relates the time series of interest (the response,  $Y_t$ , for t = 1, ..., T, assumed univariate here) to a set of p known explanatory variables,  $X_t$ :

$$Y_t = \boldsymbol{X}_t^{\mathrm{T}} \boldsymbol{\theta}_t + \epsilon_t, \qquad \epsilon_t \sim N(0, \sigma_t^2),$$
 (4.1.1)

where  $\theta_t$  is the  $(p \times 1)$  vector of regression parameters,  $\epsilon_t$  is the scalar observation error, and  $\sigma_t^2$  is the scalar observation error variance. Successive  $Y_t$  are assumed to be conditionally independent given  $\theta$ . The observation errors are assumed to be independent and normally distributed with zero mean. The variance of the error distribution may vary across time to account for changes in measurement accuracy.

The system equation describes the dependence of parameter values on their previous values:

$$\boldsymbol{\theta}_t = \boldsymbol{G}_t \boldsymbol{\theta}_{t-1} + \boldsymbol{\omega}_t, \qquad \boldsymbol{\omega}_t \sim N(\mathbf{0}, \boldsymbol{\Omega}_t),$$
 (4.1.2)

where  $G_t$  is the  $(p \times p)$  system matrix,  $\omega_t$  is the  $(p \times 1)$  vector of system errors, and  $\Omega_t$  is the  $(p \times p)$  variance-covariance matrix of system errors. Parameters are allowed to change in time to account for possible changing conditions in the system. The system errors are again assumed to be independent and normally distributed with zero mean. Furthermore, the system errors are assumed to be independent of the observation errors and the initial information. Finally, the two equations are augmented by initial information of the form:

$$(\boldsymbol{\theta}_0|D_0) \sim N(\boldsymbol{m}_0, \boldsymbol{C}_0),$$

where  $(\boldsymbol{\theta}_0|D_0)$  represents the conditional distribution of the parameters given all known prior information,  $D_0$ ; more generally,  $D_t$  represents all known information up to and including time t. The initial information is characterised by some appropriate mean,

 $m_0$ , and variance,  $C_0$ , which must be specified to initialise the model.

# 4.1.2 Updating Procedure

Based on the structure of the initial information and the observation and system equations, predictions and parameter inference may be updated as new data is collected. The updating procedure is in closed-form due to conjugacy of the prior distribution, and DLMs thus provide a structure for rapid, non-computationally intensive time series analysis. If  $X_t$ ,  $G_t$ , and the error variances,  $\sigma_t^2$  and  $\Omega_t$ , are assumed known, then the DLM updating procedure is as follows:

Assume the posterior distribution for the parameters at time t-1 is:

$$(\boldsymbol{\theta}_{t-1}|D_{t-1}) \sim N(\boldsymbol{m}_{t-1}, \boldsymbol{C}_{t-1}).$$

By (4.1.2),  $\theta_t$  is a linear combination of normal variables, so the prior distribution for the parameters at time t is given by

$$(\boldsymbol{\theta}_t | D_{t-1}) \sim N(\boldsymbol{a}_t, \boldsymbol{R}_t),$$
 (4.1.3)

where

$$\boldsymbol{a}_t = \boldsymbol{G}_t \boldsymbol{m}_{t-1},$$

and

$$oldsymbol{R}_t = oldsymbol{G}_t oldsymbol{C}_{t-1} oldsymbol{G}_t^{\mathrm{T}} + \Omega_t.$$

The marginal distribution for  $Y_t$  defines the probability function assigned to the onestep forecast at time t. By (4.1.1),  $Y_t$  is a linear combination of normal variables, so the one-step ahead forecast distribution is given by

$$(Y_t|D_{t-1}) \sim N(f_t, Q_t),$$

where

$$f_t = \boldsymbol{X}_t^{\mathrm{T}} \boldsymbol{a}_t,$$

and

$$Q_t = \boldsymbol{X}_t^{\mathrm{T}} \boldsymbol{R}_t \boldsymbol{X}_t + \sigma_t^2.$$

The one-step ahead point forecast is given by the mean of the distribution,  $f_t$ , with associated uncertainty given by the variance,  $Q_t$ . A credible interval for the mean may be calculated from the forecast distribution. Upon observing  $y_t$ , the forecast error is determined by the difference between the observed value and the forecast:  $e_t = y_t - f_t$ . The prior distribution for the parameters may then be updated by applying Bayes'

Theorem to  $\boldsymbol{\theta}_t$ :

$$p(\boldsymbol{\theta}_t|D_t) = p(\boldsymbol{\theta}_t|Y_t = y_t, D_{t-1}) \propto p(\boldsymbol{\theta}_t|D_{t-1})p(Y_t|\boldsymbol{\theta}_t, D_{t-1}),$$

and by (4.1.1) and (4.1.3),

$$p(\boldsymbol{\theta}_t|D_{t-1}) \propto \exp[-1/2(\boldsymbol{\theta}_t - \boldsymbol{a}_t)^T \boldsymbol{R}^{-1}(\boldsymbol{\theta}_t - \boldsymbol{a}_t)]$$

and

$$p(Y_t|\boldsymbol{\theta}_t, D_{t-1}) \propto \exp[-1/2(Y_t - f_t)^2/Q_t].$$

Rearranging these exponentials it can be shown that

$$p(\boldsymbol{\theta}_t|D_t) \propto \exp[-(\boldsymbol{\theta}_t - \boldsymbol{m}_t)^{\mathrm{T}} \boldsymbol{C}_t^{-1} (\boldsymbol{\theta}_t - \boldsymbol{m}_t)/2],$$

where

$$\boldsymbol{m}_t = \boldsymbol{a}_t + \boldsymbol{A}_t e_t,$$

and

$$\boldsymbol{C}_t = \boldsymbol{R}_t - \boldsymbol{A}_t \boldsymbol{A}_t^{\mathrm{T}} \boldsymbol{Q}_t,$$

with the adaptive vector,  $A_t$ , given by

$$\boldsymbol{A}_t = \boldsymbol{R}_t \boldsymbol{X}_t / Q_t.$$

The posterior distribution of the parameters a time t may then be written as

$$(\boldsymbol{\theta}_t|D_t) \sim N(\boldsymbol{m}_t, \boldsymbol{C}_t).$$

The posterior mean,  $m_t$ , is a combination of the prior mean and the forecast error, weighted by  $A_t$ . The weight assigned to the error depends on the size of the prior variance,  $R_t$ , relative to the forecast error,  $Q_t$ .

# 4.1.3 Unknown System Error Variance

In the above, it is assumed that the error variances,  $\sigma_t^2$  and  $\Omega_t$ , are known; this may be unrealistic without any prior knowledge of the system. While the observation error variance,  $\sigma^2$ , may be incorporated into the updating process of the DLM (as discussed in section 4.1.4), including the system error variance matrix,  $\Omega_t$ , in the process can lead to problems (Pole et al., 1994). Furthermore, specifying this matrix can be difficult for a number of reasons:

i) it is not invariant to the scale of measurement of the covariates, X;

ii) it can lead to ambiguities, as an uncountable number of different models with the same forecast distribution may be specified that differ only in  $\Omega_t$  (West and Harrison, 1997, chapter 5).

A solution is to use a method known as discounting. Consider a process which at a given time, t, has precision  $C_{t-1}^{-1}$  associated with  $\theta_{t-1}$ . The precision associated with  $G_t\theta_{t-1}$  is  $(G_tC_{t-1}G_t^{\mathrm{T}})^{-1} \doteq P_t^{-1}$ . If  $\Omega_t = 0$  then  $P_t$  also describes the precision associated with  $\theta_t$ . However, the uncertainty in the system equation means that  $R_t^{-1}$ , the actual precision associated with  $\theta_t$ , is reduced by the term  $\Omega_t$  relative to  $P_t^{-1}$ . This loss of precision may be applied directly to  $P_t$  using a multiplicative factor,  $\lambda$ , known as the discount factor. The variance of  $\theta_t$  is now given by  $R_t = \frac{1}{\lambda}P_t$ . From this it can be seen that  $\Omega_t = \frac{1-\lambda}{\lambda}P_t$ . The system equation in (4.1.2) is thus amended to

$$\boldsymbol{\theta}_t = \boldsymbol{G}_t \boldsymbol{\theta}_{t-1} + \boldsymbol{\omega}_t, \qquad \boldsymbol{\omega}_t \sim N(\boldsymbol{0}, \frac{1-\lambda}{\lambda} \boldsymbol{P}_t).$$
 (4.1.4)

For most practical purposes,  $\lambda$  will lie in the range (0.9, 1] with unity representing  $\Omega_t = \mathbf{0}$  (West and Harrison, 1997, chapter 6).

The discount factor may be determined by comparing model performance for a suitable range of values of the discount factor. Model performance may be measured in a number of ways, often based on measures of the forecast errors; two common measures are MSE and MAD (section C.3.2, Appendix C):

MSE = 
$$\frac{1}{T} \sum_{t=1}^{T} e_t^2$$
; MAD =  $\frac{1}{T} \sum_{t=1}^{T} |e_t|$ .

Small values of each are preferred. A likelihood function for  $\lambda$  may also be constructed from the forecast distributions evaluated at each observation:

$$L(\lambda | \mathbf{Y}, D_0) = p(\mathbf{Y} | \lambda, D_0) = \prod_{t=1}^{T} p(Y_t | D_{t-1}),$$
 (4.1.5)

where  $\mathbf{Y} = (Y_1, \dots, Y_T)$ . The likelihood takes into account the forecast variance, unlike MSE or MAD. The likelihood is often used to form a log-likelihood ratio (LLR), where alternative models are compared to some baseline model.

### 4.1.4 Unknown Observation Error Variance

Assuming that the observation error variance is unknown but constant ( $\sigma_t^2 = \sigma^2$ ), the closed-form, conjugate updating procedure for the DLM may be retained by scaling the system error variance,  $\Omega_t$ , and the initial prior variance,  $C_0$ , by  $\sigma^2$ . Conjugacy is then achieved with an inverse gamma prior distribution on  $\sigma^2$ . This is equivalent

to a gamma distribution<sup>1</sup>,  $G(\cdot, \cdot)$ , on the precision,  $\phi = \sigma^{-2}$ . The gamma distribution is commonly used in Bayesian analysis for reflecting uncertainty on strictly positive values.

Prior information must be specified for the precision,  $\phi$ , so the initial information is appended by

$$(\phi|D_0) \sim G(n_0/2, d_0/2),$$

where the shape parameter,  $n_0$ , and the inverse scale,  $d_0$ , are to be specified. Note that  $\mathbb{E}[\phi|D_0] = n_0/d_0 \doteq 1/S_0$  is the prior point estimate of the observation error precision. At time t, the prior distribution of  $\phi$  is given by

$$(\phi|D_{t-1}) \sim G(n_{t-1}/2, d_{t-1}/2),$$
 (4.1.6)

with the point prior estimate of  $(\sigma^2|D_{t-1})$  given by  $S_{t-1} = d_{t-1}/n_{t-1}$ . After observing  $y_t$ , the prior distribution may be updated via Bayes' Theorem to

$$(\phi|D_t) \sim G(n_t/2, d_t/2),$$
 (4.1.7)

where  $n_t = n_{t-1} + 1$ ,  $d_t = d_{t-1} + e_t^2/Q_t^*$ , and  $Q_t^*$  represents the unscaled forecast variance, i.e.,  $Q_t/\sigma^2$ .

Ignoring the time subscript and dependence on D for convenience, the joint distribution of Y and  $\phi$  is the product of a normal and a gamma distribution:

$$\begin{split} p(Y,\phi) &= p(Y|\phi)p(\phi) \\ &\propto & \{\phi^{1/2}\exp(-\phi(Y-f)^2/2Q^*)\} \\ &\times & \{\phi^{n/2-1}\exp(-\phi d/2)\}. \end{split}$$

The marginal distribution for Y is given by  $p(Y,\phi)/p(\phi|Y)$ , where  $p(\phi|Y)$  represents the updated gamma distribution given by (4.1.7). Algebraic manipulation gives a T-distribution for p(Y), denoted by  $T_n(\cdot,\cdot)$  for n degrees of freedom. This argument extends to the multivariate normal case for  $p(\theta_t,\phi)$ , with  $\theta_t$  following a multivariate T-distribution.

Defining  $\Omega_t^*$  to be the part of the matrix  $\Omega_t$  that does not depend on  $\sigma^2$ , and likewise for  $C_t^*$ ,  $R_t^* \doteq G_t C_{t-1}^* G_t^{\mathrm{T}} + \Omega_t^*$  and  $Q_t^* \doteq X_t R_t^* X_t + 1$ , the updating procedure unconditional on  $\sigma^2$  is now as follows:

The gamma parameterisation used here and throughout specifies that if  $X \sim G(\alpha, \beta)$  then  $p(X; \alpha, \beta) \propto X^{\alpha-1} \exp(-X\beta)$ .

Assume the posterior distribution for the parameters at time t-1 is given by

$$(\boldsymbol{\theta}_{t-1}|D_{t-1}) \sim T_{n_{t-1}}(\boldsymbol{m}_{t-1}, \boldsymbol{C}_{t-1}),$$
 (4.1.8)

for some location,  $m_{t-1}$ , and scale matrix,  $C_{t-1}$ . This is updated to the prior distribution at time t,

$$(\boldsymbol{\theta}_t | D_{t-1}) \sim \mathbf{T}_{n_{t-1}}(\boldsymbol{a}_t, \boldsymbol{R}_t), \tag{4.1.9}$$

where  $\boldsymbol{a}_t = \boldsymbol{G}_t \boldsymbol{m}_{t-1}$  and  $\boldsymbol{R}_t = S_{t-1} (\boldsymbol{G}_t \boldsymbol{C}_{t-1}^* \boldsymbol{G}_t^{\mathrm{T}} + \boldsymbol{\Omega}_t^*) = S_{t-1} \boldsymbol{R}_t^*$ . The forecast distribution is given by

$$(Y_t|D_{t-1}) \sim T_{n_{t-1}}(f_t, Q_t),$$
 (4.1.10)

where  $f_t = \boldsymbol{X}_t^{\mathrm{T}} \boldsymbol{a}_t$  and  $Q_t = S_{t-1}(1 + \boldsymbol{X}_t^{\mathrm{T}} \boldsymbol{R}_t^* \boldsymbol{X}_t) = S_{t-1} Q_t^*$ . After observing  $y_t$ , the one-step forecast error is as defined previously, the prior distribution for  $\phi$  is updated to obtain the updated estimate,  $S_t$ , and the prior distribution for the parameters is updated to

$$(\boldsymbol{\theta}_t|D_t) \sim T_{n_t}(\boldsymbol{m}_t, \boldsymbol{C}_t),$$
 (4.1.11)

where  $\mathbf{m}_t = \mathbf{a}_t + \mathbf{A}_t e_t$ ,  $\mathbf{C}_t = S_t(\mathbf{R}_t^* - \mathbf{A}_t \mathbf{A}_t^T Q_t^*) = S_t \mathbf{C}_t^*$ , and  $n_t = n_{t-1} + 1$ . The adaptive vector,  $\mathbf{A}_t$ , is as defined previously.

### 4.1.4.1 Time-Varying Observation Error Variance

The above procedure can be extended to include temporal changes in observation variance. This is relevant if it is thought that the observation error is subject to change, e.g., due to variation in measurement accuracy. Changes in variance may be included in the conjugate, closed-form updating procedure using discounting (West and Harrison, 1997, chapter 10). This involves introducing a stage between (4.1.6) and (4.1.7), prior to observing  $y_t$ . Appending a time subscript to (4.1.6) so that

$$(\phi_{t-1}|D_{t-1}) \sim G(n_{t-1}/2, d_{t-1}/2)$$
 (4.1.12)

represents all information on  $\phi$  at time t-1, additional uncertainty may be introduced at time t as follows:

Define

$$\phi_t = \gamma_t \phi_{t-1} / \delta, \tag{4.1.13}$$

where  $\gamma_t$  follows a beta distribution, Beta $(\cdot,\cdot)$ , independent of  $\phi$ , given by

$$\gamma_t \sim \text{Beta}(\delta n_{t-1}/2, (1-\delta)n_{t-1}/2),$$
(4.1.14)

whose shape parameters are determined by the parameters in (4.1.12) and discount

factor,  $\delta$ . By (4.1.12) and (4.1.13), the variable  $\phi_t$  is a product of beta and gamma distributions and so follows a gamma distribution. The amended information on  $\phi$  is given by

$$(\phi_t|D_{t-1}) \sim G(\delta n_{t-1}, \delta d_{t-1}).$$
 (4.1.15)

The value of the discount factor,  $\delta$ , is restricted to the range (0,1]. Unity implies no loss of information, equivalent to the model described in section 4.1.4. Note that under (4.1.15):

$$\mathbb{E}(\phi_t|D_{t-1}) = n_{t-1}/d_{t-1}$$

$$= 1/S_{t-1}$$

$$= \mathbb{E}(\phi_{t-1}|D_{t-1}),$$

and

$$V(\phi_t|D_{t-1}) = n_{t-1}/\delta d_{t-1}^2$$
  
=  $(1/\delta)V(\phi_{t-1}|D_{t-1}),$ 

so the point estimate of  $(\sigma_t^2|D_{t-1})$  is the same but with increased uncertainty. The updating procedure in section 4.1.4 still applies, with only the following changes:

$$(\phi_t|D_{t-1}) \sim G(\delta n_{t-1}/2, \delta d_{t-1}/2)$$
  
 $(Y_t|D_{t-1}) \sim T_{\delta n_{t-1}}(f_t, Q_t)$   
 $n_t = \delta n_{t-1} + 1$   
 $d_t = \delta d_{t-1} + S_{t-1}e_t^2/Q_t.$ 

The degrees of freedom for the forecast distribution are thus reduced by a factor of  $\delta$ . Additional uncertainty can be supplied to the model at individual time-points by decreasing  $\delta$  momentarily. The introduction of a discount factor for the observation variance,  $\sigma^2$ , is relatively superficial; there is no change in the forecast, only a change in the estimate of  $\phi$ . Although the discount factor is designed to increase uncertainty in predictions, it may artificially reduce the prediction interval depending on the forecast error (see appendix B).

# 4.1.5 K-step Forecasting

The updating procedure as presented allows for one-step ahead prediction. Given observations up to time t, the distribution of the parameters for k steps ahead may be

determined by repeated application of the system equation, and is given by:

$$(\boldsymbol{\theta}_{t+k}|D_t) \sim N[\boldsymbol{a}_t(k), \boldsymbol{R}_t(k)],$$

where

$$\boldsymbol{a}_t(k) = \boldsymbol{G}_{t+k} \boldsymbol{a}_t(k-1)$$

and

$$\boldsymbol{R}_{t}(k) = \boldsymbol{G}_{t+k} \boldsymbol{R}_{t}(k-1) \boldsymbol{G}_{t+k}^{\mathrm{T}} + \boldsymbol{\Omega}_{t+k}$$

are calculated recursively.

The forecast distribution for k steps ahead is determined from the observation equation, and is given by:

$$(Y_{t+k}|D_t) \sim N[f_t(k), Q_t(k)],$$

where

$$f_t(k) = \boldsymbol{X}_{t+k}^{\mathrm{T}} \boldsymbol{a}_t(k)$$

and

$$Q_t(k) = \boldsymbol{X}_{t+k}^{\mathrm{T}} \boldsymbol{R}_t(k) \boldsymbol{X}_{t+k} + \sigma_{t+k}^2.$$

The starting values are defined at time t by:

$$\mathbf{a}_t(0) = \mathbf{m}_t$$

$$\mathbf{R}_t(0) = \mathbf{C}_t.$$

If  $\sigma_t^2$  is unknown, it is replaced by  $S_t$  in the above structure. For unknown  $\Omega_t$ , the discounting approach requires some care: if  $\mathbf{P}_{t+k} = \mathbf{G}_{t+k} \mathbf{R}_t (k-1) \mathbf{G}_{t+k}^{\mathrm{T}}$ , it can be shown that  $\mathbf{R}_t(k) \propto \mathbf{C}_t/\lambda^k$ , hence the information in  $\mathbf{C}_t$  has exponential decay rather than the arithmetic decay associated with the additive process of one-step forecasts. A suggested approach is to define

$$\Omega_t(k) = \Omega_{t+1} = \frac{1}{\lambda} \boldsymbol{P}_{t+1}, \tag{4.1.16}$$

so that  $\Omega_{t+1}$  is the forecast of the system error variance at all times until the next observation, when it can then be updated (West and Harrison, 1997, chapter 6).

# 4.1.6 Filtering and Smoothing

Interest in a system may not be solely in predictive performance. DLMs may also be used to monitor the behaviour of the parameters through time, where inferences on the parameters at time t may be revised in the wake of observed data after this time;

this process is known as filtering. Given observed data up to time T, the k-step filtered distribution,  $p(\boldsymbol{\theta}_{T-k}|D_T)$ , for  $k=1,\ldots,T-1$ , may be found by evaluating

$$p(\boldsymbol{\theta}_{T-k}|D_T) = \int p(\boldsymbol{\theta}_{T-k}|\boldsymbol{\theta}_{T-k+1}, D_T) p(\boldsymbol{\theta}_{T-k+1}|D_T) d\boldsymbol{\theta}_{T-k+1}.$$

Defining  $M_t = C_t G_{t+1}^T R_{t+1}^{-1}$ , the filtered distributions are given by

$$(\boldsymbol{\theta}_{T-k}|D_T) \sim N[\boldsymbol{a}_T(-k), \boldsymbol{R}_T(-k)],$$

where

$$a_T(-k) = m_{T-k} + M_{T-k}[a_T(-k+1) - a_{T-k+1}]$$

and

$$R_T(-k) = C_{T-k} + M_{T-k}[R_T(-k+1) - R_{T-k+1}]M_{T-k}^T.$$

The full proof by induction for the filtered distributions may be found in West and Harrison (1997, chapter 4). The proof makes use of the following important result, invoked later in this chapter:

$$(\boldsymbol{\theta}_{T-k}|\boldsymbol{\theta}_{T-k+1}, D_{T-k}) \sim N[\boldsymbol{h}_T(k), \boldsymbol{H}_T(k)],$$
 (4.1.17)

where

$$h_T(k) = m_{T-k} + M_{T-k}(\theta_{T-k+1} - a_{T-k+1})$$

and

$$\boldsymbol{H}_T(k) = \boldsymbol{C}_{T-k} - \boldsymbol{M}_{T-k} \boldsymbol{R}_{T-k+1} \boldsymbol{M}_{T-k}^{\mathrm{T}}.$$

The filtered distributions may also be used to retrospectively assess the behaviour of the mean of the time series,  $\mu_t = \boldsymbol{X}_t^{\mathrm{T}} \boldsymbol{\theta}_t$ , with the k-step smoothed distributions,  $p(\mu_{T-k}|D_T)$ . By simple extension from the above results, the k-step smoothed distribution is given by

$$(\mu_{T-k}|D_T) \sim N(f_T(-k), \mathbf{X}_{T-k}^T \mathbf{R}_T(-k)\mathbf{X}_{T-k}),$$
 (4.1.18)

where

$$f_T(-k) = \boldsymbol{X}_{T-k}^{\mathrm{T}} \boldsymbol{a}_T(-k).$$

For the case of unknown, constant observation variance,  $\sigma^2$ , the filtered distributions are adjusted to

$$\boldsymbol{\theta}_{T-k}|D_T \sim T_{n_T}[\boldsymbol{a}_T(-k), (S_T/S_{T-k})\boldsymbol{R}_T(-k)],$$

and the k-step smoothed distributions become

$$(\mu_{T-k}|D_T) \sim T_{n_T}(f_T(-k), (S_T/S_{T-k})\boldsymbol{X}_{T-k}^T\boldsymbol{R}_T(-k)\boldsymbol{X}_{T-k}).$$

## 4.1.7 Reference Analysis

A further concession to a lack of prior knowledge of the system may be achieved with the use of non-informative, improper prior distributions to initialise the model, where the prior distribution for the parameter set,  $p(\theta_1|D_0)$ , need not be specified in terms of the hyperparameters,  $m_0$  and  $C_0$ . For unknown observation error variance, the joint prior distribution of  $\theta_1$  and  $\phi$  may instead be defined by

$$p(\boldsymbol{\theta}_1, \phi | D_0) \propto \phi.$$

More generally, the prior distribution at time t may be expressed as

$$p(\boldsymbol{\theta}_t, \phi | D_{t-1}) \propto \phi^{1+(t-1)/2} \exp\{-\phi/2(\boldsymbol{\theta}_t^{\mathrm{T}} \boldsymbol{A}_t \boldsymbol{\theta}_t - 2\boldsymbol{\theta}_t^{\mathrm{T}} \boldsymbol{a}_t + \tau_{t-1})\},$$

with starting values  $A_1 = 0$ ,  $a_1 = 0$  and  $\tau_0 = 0$ . After observing  $y_t$ , this updates to

$$p(\boldsymbol{\theta}_t, \phi | D_t) \propto \phi^{1+t/2} \exp\{-\phi/2(\boldsymbol{\theta}_t^{\mathrm{T}} \boldsymbol{B}_t \boldsymbol{\theta}_t - 2\boldsymbol{\theta}_t^{\mathrm{T}} \boldsymbol{b}_t + \tau_t)\},$$

where  $\boldsymbol{b}_t = \boldsymbol{a}_t + \boldsymbol{X}_t Y_t$ ,  $\boldsymbol{B}_t = \boldsymbol{A}_t + \boldsymbol{X}_t \boldsymbol{X}_t^{\mathrm{T}}$  and  $\tau_t = \tau_{t-1} + Y_t^2$ . The prior distributions for the next time point are determined from the relationships

$$\boldsymbol{a}_t = (\boldsymbol{G}_t^{-1})^{\mathrm{T}} \boldsymbol{b}_{t-1}$$

and

$$A_t = (G_t^{-1})^{\mathrm{T}} B_{t-1} G_t^{-1}.$$

Posterior distributions will remain improper until at least (but generally not beyond) time  $t = t^* = p + 1$ , where p is the dimension of  $\theta$ . At time  $t^* + 1$  the analysis reverts to the usual updating procedure described previously, where the prior distribution of the parameters is given by

$$(\boldsymbol{\theta}_{t^*+1}|D_{t^*}) \sim N(\boldsymbol{m}_{t^*+1}, \boldsymbol{C}_{t^*+1}),$$

where  $m_{t^*+1} = B_{t^*+1}b_{t^*+1}$  and  $C_{t^*+1} = S_{t^*+1}B_{t^*+1}$ .

The above method is a simplified approach that assumes, for  $t \in [1, t^*]$ , the system error variance,  $\Omega$ , is equal to the zero matrix; this is justified by the fact that the amount of information collected during the reference period does not allow for the detection of changes in parameters. Full proof and discussion of the procedure may be

# 4.2 DLM of Blood Glucose Concentration

Although the glucose-insulin dynamical system is non-linear, it is hypothesised that DLMs are able to model BGC given the inputs of glucose and insulin absorption and physical activity. These inputs represent the biggest challenges to BGC regulation, and it is to be investigated whether the effect of these can be captured in an empirical model. Using a linear modelling approach is, at the very least, a useful basis for exploring non-linear systems; this is certainly true when, as with the glucoregulatory system, nonlinearities may be unknown, and potentially time- and subject-specific. Furthermore, linear models may be suitable in a non-linear system over limited time frames. The methods proposed have not previously been applied in diabetes modelling.

DLMs have a number of favourable properties for modelling BGC: time-varying parameters may capture effects such as changes in insulin sensitivity through the day, time-varying error variances account for changes in measurement accuracy of CGMs, the models can be individualised (hence taking into account inter-patient variability) and a rapid, computationally efficient updating procedure allows for on-line prediction.

DLMs also allow scope for modelling BGC with differing aims. The first is to assess the role of physical activity (using METs) and its effect on BGC. This may be achieved by monitoring the behaviour of the model parameters using filtering (as described in section 4.1.6). The second aim is to assess the capability of DLMs for long-term prediction (at least four hours). It has been established, e.g., chapter 3 and Sparacino et al. (2007), that BGC can be predicted in the short term purely from recent values of itself, using relatively simple time series methods. The current approach is aimed at longer-term prediction based on the major inputs of consumed carbohydrates, injected insulin and physical activity, with less reliance on frequent BGC measurements. This has the potential to enhance an individual's control of their BGC by predicting profiles for different insulin doses, and thus suggesting the most appropriate dose. Such an approach could improve the predominant current treatment regime of MDI.

The structure of DLMs assumes a normally distributed response variable. BGC does not necessarily satisfy this assumption given that it is a strictly positive value (and is likely to have some unknown physiological limit above this). In such a situation, it is common to transform the response, e.g., using natural logarithms. To maintain the desired linear structure, it is then required to take logarithms of the covariates also. However, carbohydrate intake and insulin absorption may be zero. Instead it is argued here that the natural restriction of BGC will have minimal impact on the assumptions of the DLM, and hence BGC will be not be transformed.

A number of variants of the basic DLM structure are now applied to an individual's

BGC measurements. Analysis will initially focus on one-step ahead prediction and parameter behaviour, before considering long-term forecasts.

# 4.2.1 First-order Polynomial Model

The first model fitted is the simplest DLM, the first-order polynomial (FOP) DLM, with  $\theta_t = \mu_t$  representing an overall level of the process, and  $G_t = X_t = 1$ :

$$Y_t = \mu_t + \epsilon_t, \quad \epsilon_t \sim N(0, \sigma^2)$$
  
$$\mu_t = \mu_{t-1} + \omega_t, \quad \omega_t \sim N(0, \Omega).$$

The error variances,  $\sigma^2$  and  $\Omega$ , are assumed constant but unknown. The methods described in sections 4.1.3 and 4.1.4, regarding a gamma prior distribution and discounting, are used for the respective variances. The prior information is given by:

$$(\mu_0|D_0) \sim T_1(Y_0, 10)$$
  
 $(\phi|D_0) \sim G(2, 1),$ 

where  $Y_0$  is the finger-prick measurement used to calibrate the CGM at the start of the measurement period. The values for  $(\phi|D_0)$  were chosen to give a weakly informative prior distribution; likewise, the variance of  $(\mu_0|D_0)$  is chosen to be deliberately large. This model was used for one-step (5 minutes) ahead predictions.

As noted in section 4.1.3, the discount factor for  $\Omega$  cannot be included in the updating procedure. Hence the model was fit repeatedly for  $\lambda \in (0,1]$  in increments of 0.01. For the LLR, the baseline model for comparison will be  $\lambda = 1$ , equivalent to  $\mathbf{W}_t = \mathbf{0}$ ; the LLR for an alternative discount factor,  $\lambda^*$ , is thus given by:

$$LLR(\lambda^*) = \log \left[ \frac{L(\lambda = 1 | \mathbf{Y})}{L(\lambda^* | \mathbf{Y})} \right]. \tag{4.2.1}$$

The results from the FOP model suggest that MSE and MAD are minimised, and LLR maximised, as  $\lambda \to 0$ , or equivalently,  $\Omega_t \to \infty$ ; selected results for MSE, MAD and LLR are shown in Table 4.1, and plots of one-step predictions for  $\lambda = 0.01$  and  $\lambda = 1$ , shown in Figure 4.1, highlight the difference in model performance. As  $\lambda \to 0$ , parameter estimates change greatly with each new observation, and the posterior mean for  $\mu$  is almost entirely decided by the most recent observation,  $Y_t$ . Despite good performance when predicting one step ahead, such a model is of little practical use for predicting many steps ahead, when correlation between observations far apart in time is much less. The model may be improved by the inclusion of covariates.

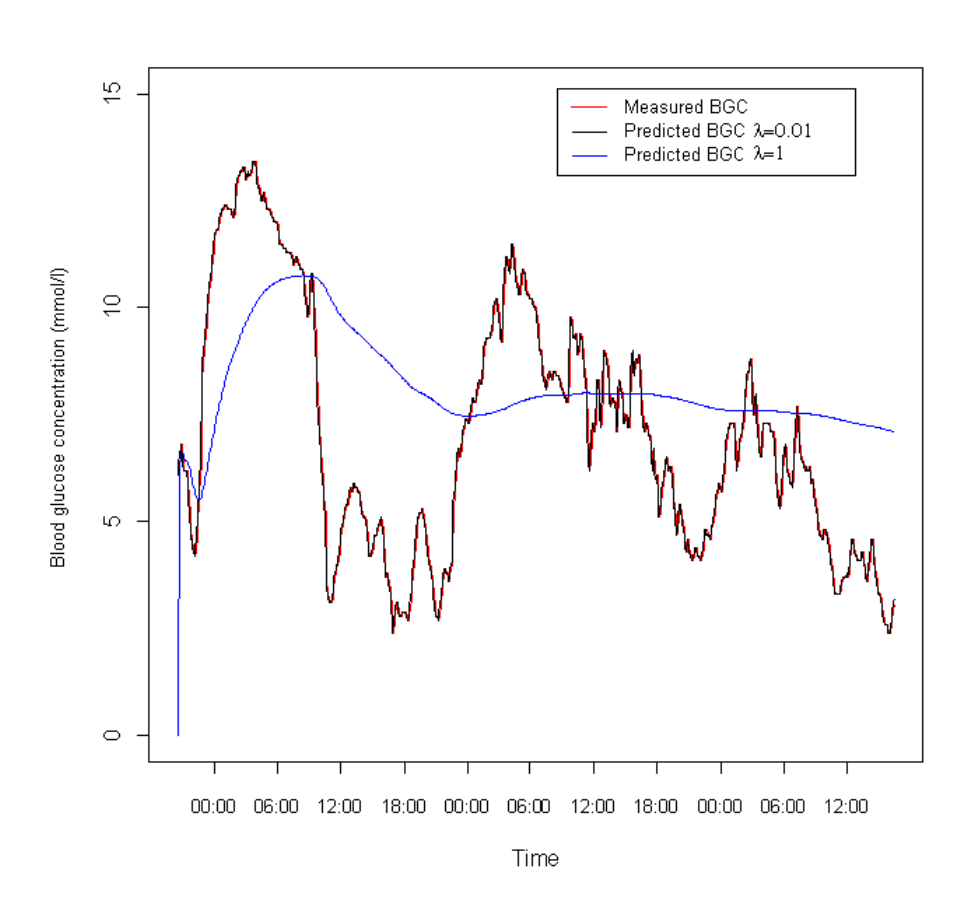


Figure 4.1: Measured BGC and FOP DLM predicted BGC for  $\lambda = 0.01$  and  $\lambda = 1$ .

Table 4.1: FOP model error properties for selected values of discount factor,  $\lambda$ ; all values rounded to 3sf. Mean squared error (MSE), mean absolute deviation (MAD) and log-likelihood ratio (LLR) as defined in section 4.1.3. Starred (\*) entries, where given, indicate minimum values for MAD and MSE, and the maximum value for LLR.

Discount factor	MSE	MAD	LLR
0.01	0.099*	0.161*	3,930*
0.02	0.100	0.163	3,920
0.03	0.101	0.164	3,920
0.25	0.120	0.199	3,910
0.5	0.167	0.261	3,890
0.75	0.326	0.400	3,830
1	8.38	2.36	0

## 4.2.2 One-Step Regression DLM

The FOP model can be extended to a regression DLM by setting  $\boldsymbol{\theta}_t = \{\mu_t, \boldsymbol{\beta}_{it}\}$  and  $\boldsymbol{X}_t = \{1, \boldsymbol{X}_{it}\}$ , for  $i = 1, \dots, p$ , so that

$$\mathbb{E}[Y_t] = \mu_t + \sum_{i=1}^p \beta_{it} X_{it}.$$
 (4.2.2)

Possible covariates include model-estimated glucose and insulin absorption, and METs, as presented in chapter 3. It is well established that each of these variables has an impact on BGC, so conventional model-building techniques, e.g., stepwise regression, will be overlooked. It is also of interest to determine if these variables can be used to predict BGC without using previous measurements of BGC.

Prior information for the regression DLM is chosen to be deliberately vague:

$$(\boldsymbol{\theta}_0|D_0) \sim T_1(\mathbf{0}, 10 \cdot \boldsymbol{I}_4)$$
  
 $(\phi|D_0) \sim G(2, 1),$ 

where  $I_4$  is the  $4 \times 4$  identity matrix. The most appropriate value of the discount factor,  $\lambda$ , is again chosen by comparing error properties through MAD, MSE and LLR. The discount factor is applied uniformly for all variables. The system matrix,  $G_t$ , is the identity matrix.

### 4.2.2.1 Results

MSE generally decreased as  $\lambda$  increased, up to a minimum at  $\lambda = 0.96$ . MAD is minimised for  $\lambda = 0.93$ , but the variation across models is far less than that for MSE. The LLR is maximised at  $\lambda = 0.95$ , with strong support for models with  $\lambda$  in the range [0.94,0.97]; selected results for the error measures are given in Table 4.2. The

model with  $\lambda = 0.96$  is preferred as the most suitable compromise between these error measures. This value of discount factor means the model places far less emphasis on new observations compared to the first-order polynomial model.

Table 4.2: One-step regression model error properties for selected values of discount factor,  $\lambda$ ; all values rounded to 3sf. Mean squared error (MSE), mean absolute deviation (MAD) and log-likelihood ratio (LLR) as defined in section 4.1.3. Starred (\*) entries, where given, indicate minimum values for MAD and MSE, and the maximum value for LLR.

Discount factor	MSE	MAD	LLR
0.5	$3.97 \times 10^4$	12.4	$-1.10 \times 10^8$
0.8	699	1.43	$-1.78 \times 10^5$
0.9	30.3	0.693	-1,290
0.95	1.95	0.726	1,540*
0.96	1.34*	0.800	1,500
0.97	1.46	0.927	1,360
0.98	2.02	1.11	1,110
0.99	3.05	1.37	697
1	5.55	1.88	0

The chosen model shows reasonable predictive capability, barring one or two considerable deviations from measured BGC (Figure 4.2). The larger deviations correspond to sudden increases in magnitude and variation of METs when the individual ceases to sleep/lie down. These sudden fluctuations also correspond to jumps in uncertainty about the forecast. Predicted BGC is far smoother when the individual is sleeping or lying down at night.

The 95% credible intervals contain the measured BGC almost entirely. In particular they are able to highlight the most extreme period of hyperglycaemia. However the intervals are not narrow enough to highlight periods of hypoglycaemia or mild hyperglycaemia with great certainty.

### 4.2.2.2 Double-Discount DLM

As noted in section 3.2, calibration of the CGM can lead to rapid changes in BGC readings. To compensate for this, the discounting procedure described in section 4.1.4.1 is applied to the one-step model, so that the observation error variance is no longer constant. At times immediately after calibration, the discount factor,  $\delta$ , is decreased to 0.9 before increasing uniformly to 1 over the next five time points, hence introducing added uncertainty into the model. This half-hour window was chosen to match the times when the largest changes in BGC occurred post-calibration. Use of the discount factor introduces added uncertainty into the model at times when rapid changes in BGC readings may be related to influences beyond those of the covariates. This is reflected in wider prediction credible intervals, but no change in BGC prediction; Figure 4.3 shows an example of the effect of introducing a second discount factor.

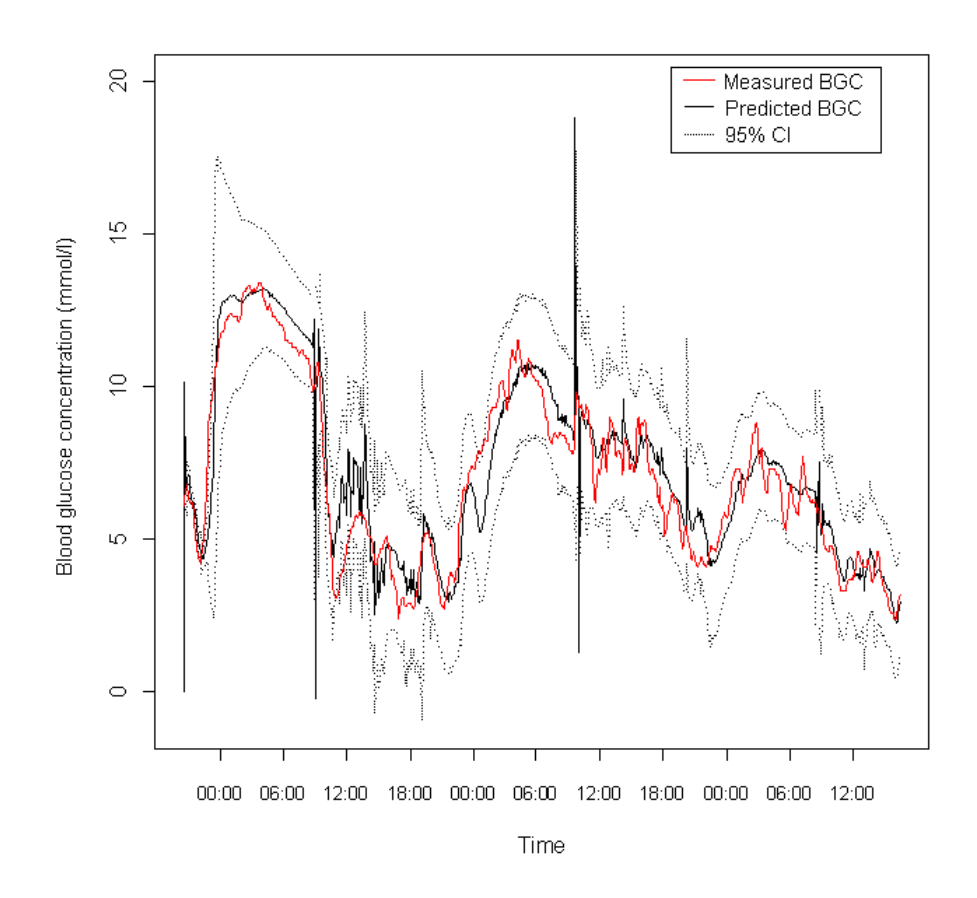


Figure 4.2: One-step (five minutes) ahead prediction of BGC and measured BGC, with 95% credible intervals. Extreme values of intervals omitted for clarity.

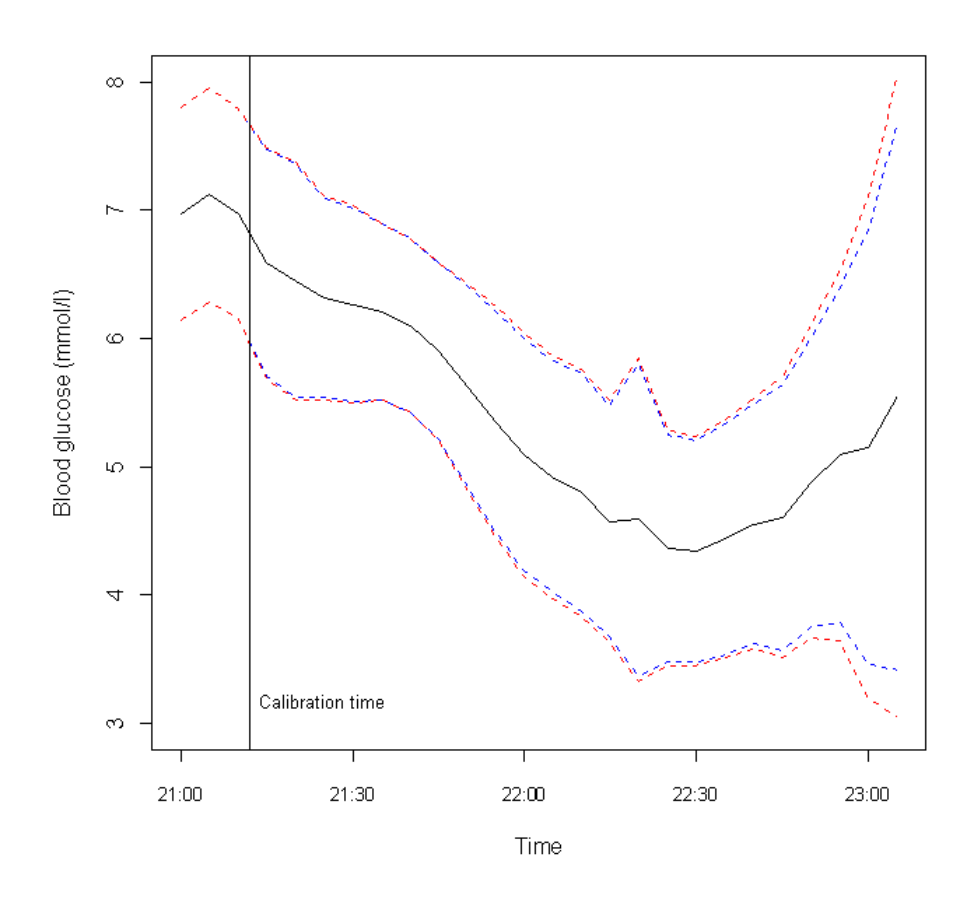


Figure 4.3: Predicted BGC (solid line) and 95% credible intervals for standard DLM ( $\delta = 1$ ; blue lines) and double discount model ( $\delta$  as described in the text, representing increased uncertainty at time 21.12; red lines).

### 4.2.2.3 Sensitivity Analysis

Sensitivity of the model to starting inputs must be assessed to test the model's ability to cope with misinformation. All initial inputs, and the discount factor, may be varied to assess how they affect model performance.

Altering the value of the discount factor affects the behaviour of parameter estimates, as the representative example in Figure 4.4 demonstrates; in particular, changing the discount factor effects the magnitude of estimates. Decreasing the discount factor is equivalent to increasing the variance of the prior distribution for  $\theta_t$ . This also results in greater uncertainty about the forecast values.

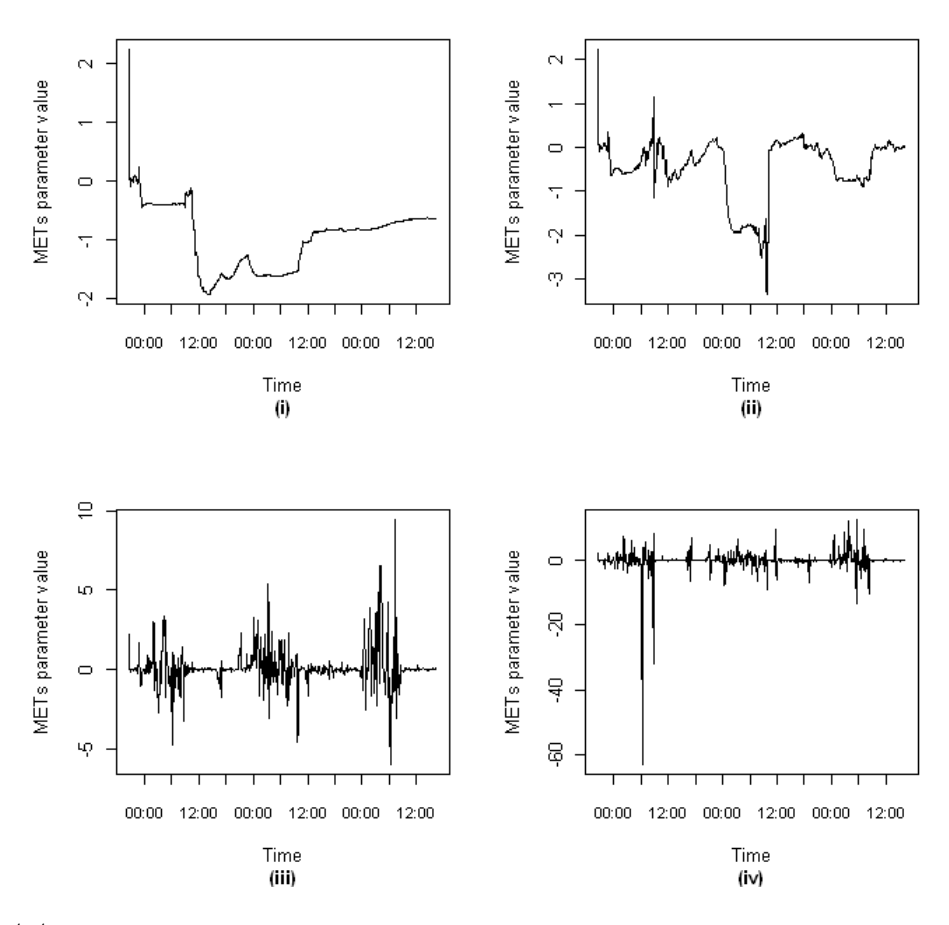


Figure 4.4: METs parameter estimates for varying discount factor: (i)  $\lambda = 1$ ; (ii)  $\lambda = 0.96$ ; (iii)  $\lambda = 0.5$ ; (iv)  $\lambda = 0.1$ .

Varying the starting values for parameters has very little effect on the one-step forecasts and parameter estimates; Figure 4.5 shows consistency of the METs parameter estimate for different values of  $m_0$ . Hence the model results are not unduly affected by the mean values used to initialise the model.

In contrast, model performance depends greatly on the matrix entries for  $C_0$ , suggesting user misspecification of the matrix can affect results adversely. The model copes well with diagonal matrices, but performance deteriorates when off-diagonal entries are

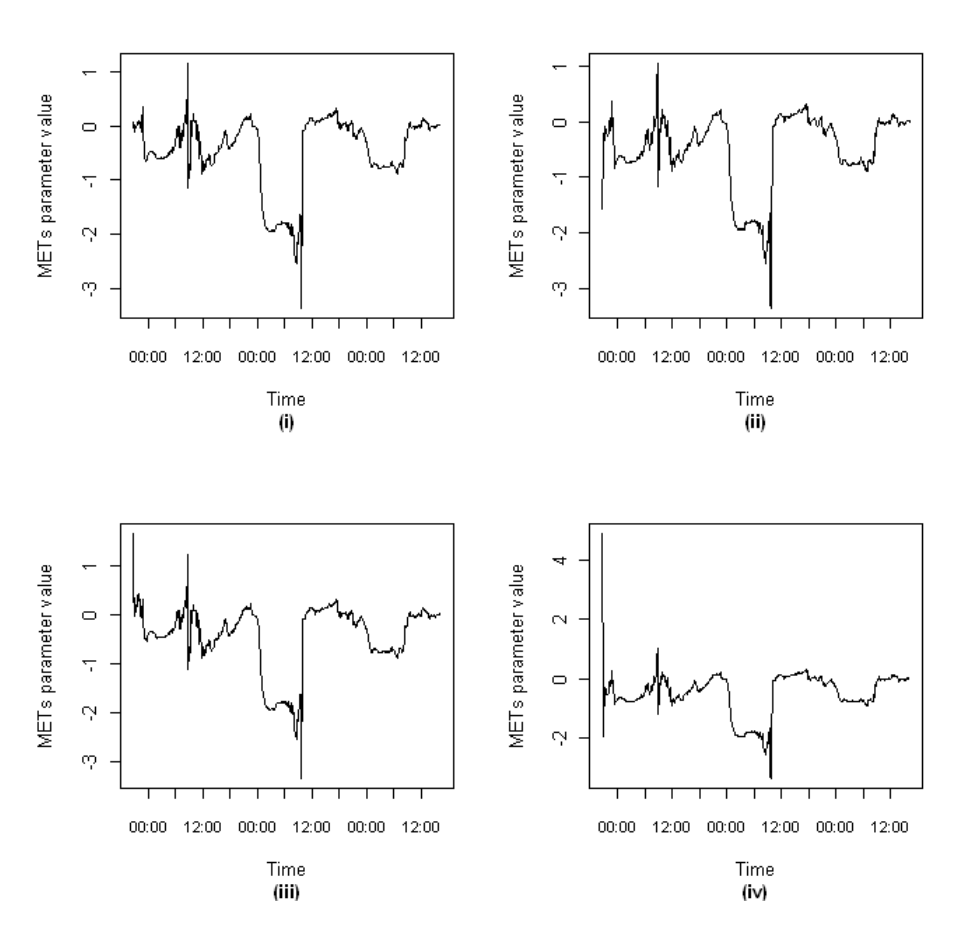


Figure 4.5: METs parameter estimates for varying initial values: (i)  $\theta = (0,0,0,0)$ ; (ii)  $\theta = (100,100,100,100)$ ; (iii)  $\theta = (-100,-100,-100,-100)$ ; (iv)  $\theta = (100,-100,100,-100)$ .

non-zero. To overcome this limitation the model was rerun using the reference analysis approach described in section 4.1.7. The model is therefore guided by the data rather than user input. However, model performance is still susceptible to change depending on when the model analysis (and hence reference period) begins.

Assessment of reference model errors for different values of the discount factor again suggests that  $\lambda = 0.96$  is appropriate; results are given in Table 4.3. Comparison of error measures suggest that the reference DLM performs slightly worse than the first-order polynomial model, but better than the standard DLM.

Table 4.3: Reference model error properties for selected values of discount factor,  $\lambda$ ; all values rounded to 3sf. Mean squared error (MSE), mean absolute deviation (MAD) and log-likelihood ratio (LLR) as defined in section 4.1.3. Starred (\*) entries, where given, indicate minimum values for MAD and MSE, and the maximum value for LLR.

Discount factor	MSE	MAD	LLR
0.5	$4.00 \times 10^4$	12.5	$-1.10 \times 10^8$
0.8	703	1.42	$-1.82 \times 10^5$
0.9	30.4	0.683	-1,260
0.95	1.92	0.716	1,550*
0.96	1.30*	0.789	1,510
0.97	1.40	0.917	1,380
0.98	1.96	1.11	1,120
0.99	3.00	1.36	705
1	5.52	1.88	0

The reference model is able to predict one-step ahead with accuracy, but is susceptible to sharp spikes in prediction upon waking (Figure 4.6). The prediction variance is generally relatively small and stable, except for occasional spikes corresponding with the sudden increase in METs upon waking (Figure 4.7).

#### 4.2.2.4 Model Diagnostics

Model assumptions may be assessed by determining the behaviour of the errors. Plots of the errors suggest some minor violations of the assumptions of temporal independence; the error time series in Figure 4.8 suggests some temporal dependence, with runs of consecutive positive or negative errors. The partial autocorrelation function of errors, as shown in Figure 4.9, also suggest some short-term dependence. The assumption of constant variance of the errors appears valid; Figure 4.10 suggests a random spread of errors about 0 across the range of BGC, though there is some evidence of consistent underestimation for larger values of BGC.

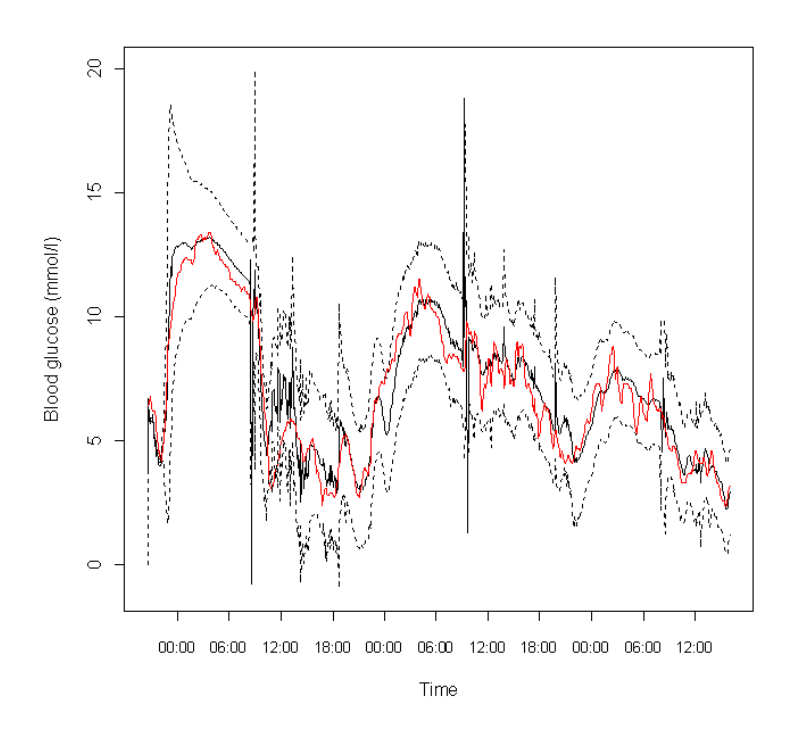


Figure 4.6: Measured BGC and predicted BGC for reference analysis approach, with 95% credible intervals.

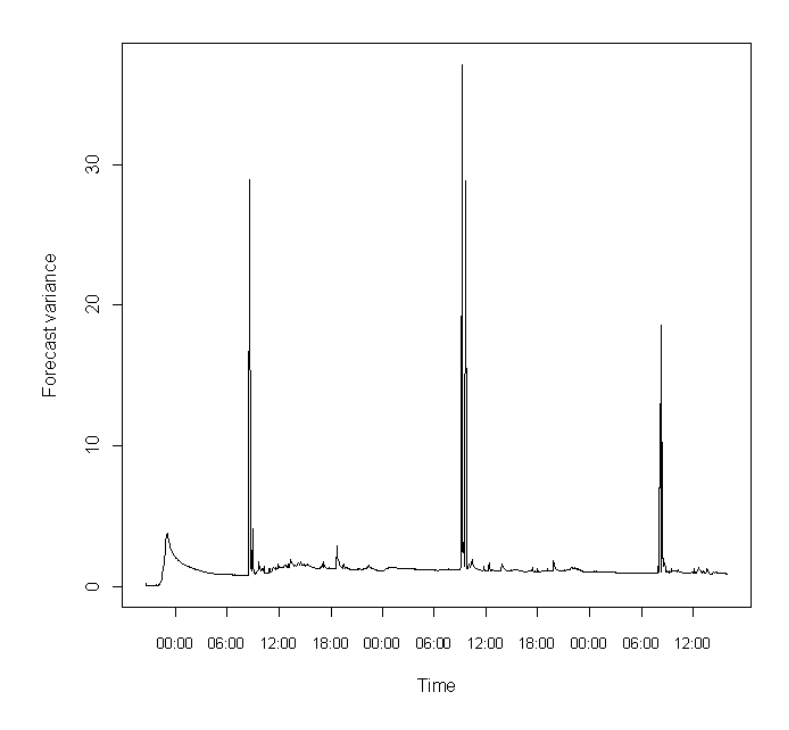


Figure 4.7: Time series of reference model forecast variance.

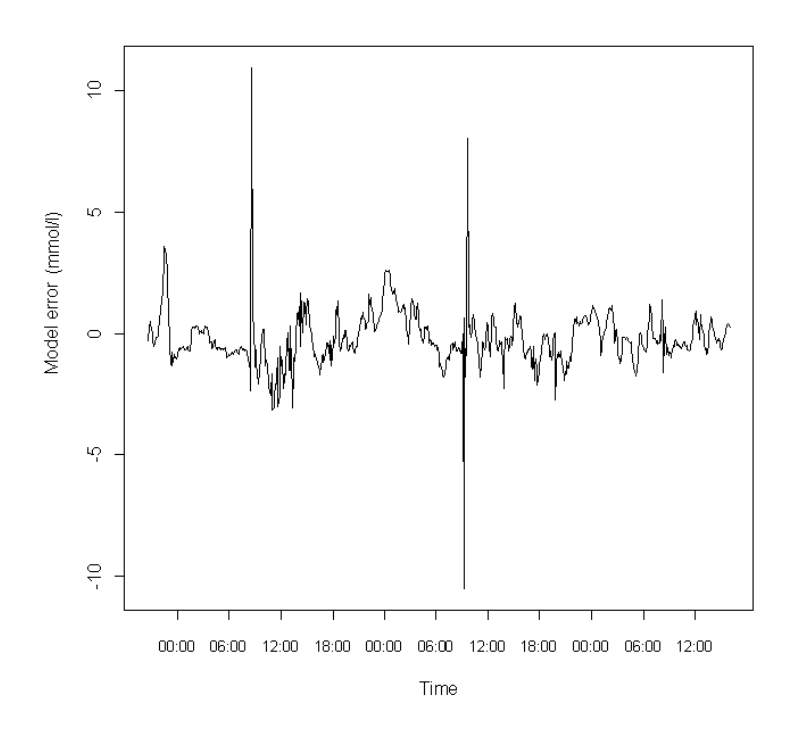


Figure 4.8: Time series of filter model one-step BGC prediction errors.

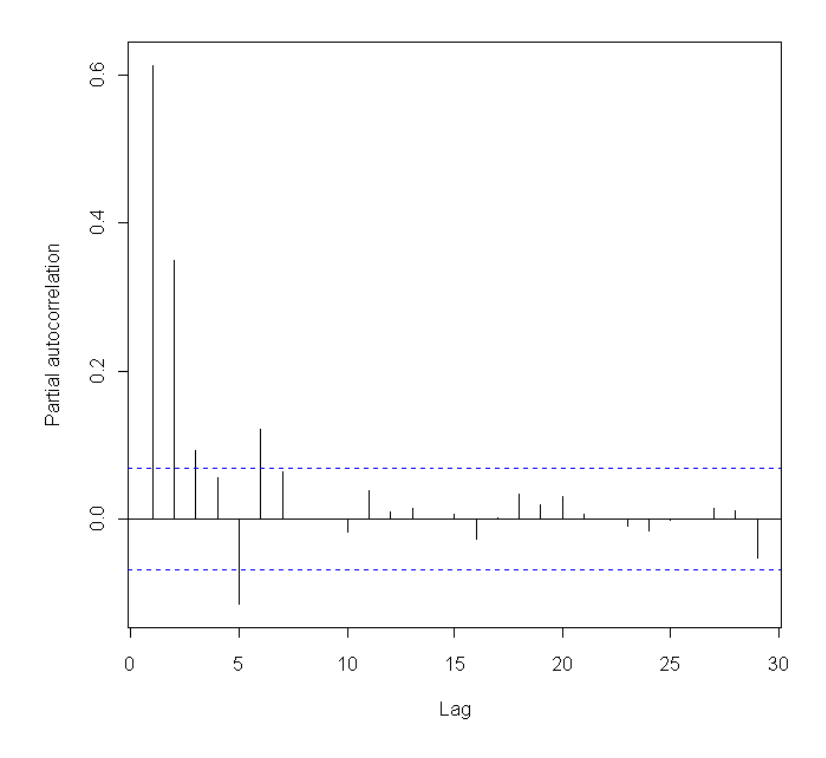


Figure 4.9: Partial autocorrelation function of filter model errors.

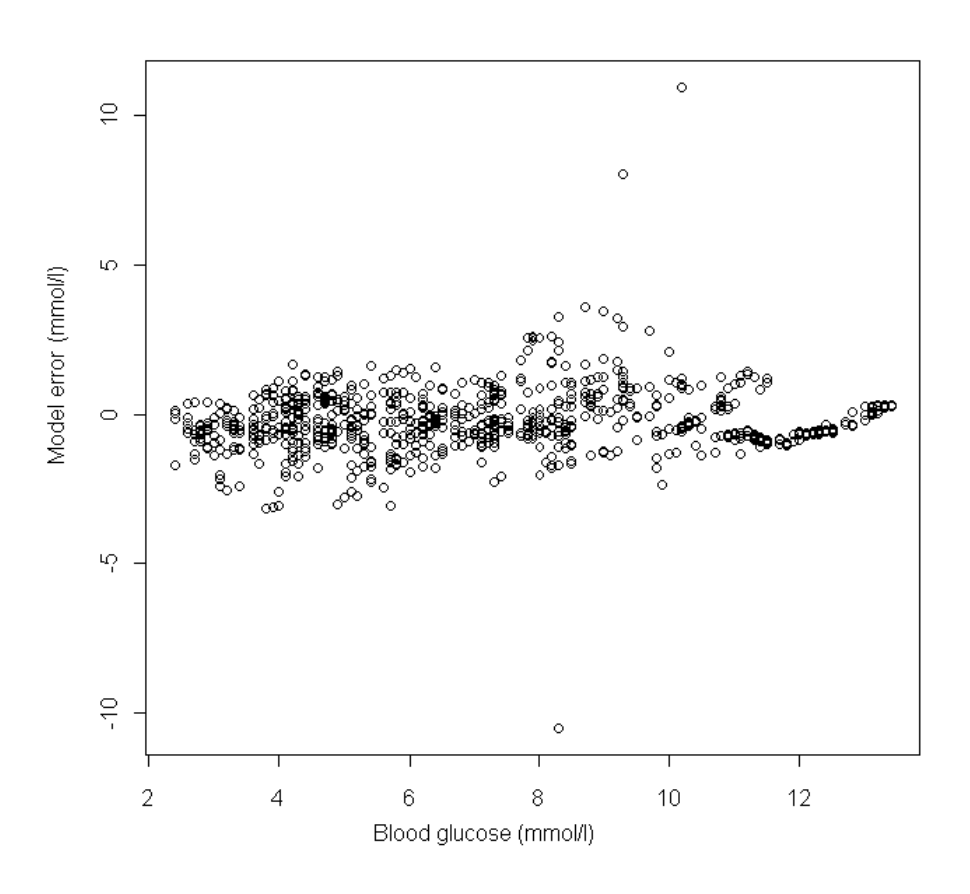


Figure 4.10: Reference model errors against measured BGC.

#### 4.2.2.5 Filtered DLM of BGC

Parameter inference may be improved by using all collected data for an individual. This is achieved by filtering the one-step DLM, as detailed in section 4.1.6. The reference model was used for filtering.

The filtered model shows good adherence to the measured BGC (Figure 4.11). However, the parameters show unrealistic behaviour; the insulin parameter is occasionally positive and the carbohydrate parameter occasionally negative (Figure 4.12). It is therefore difficult to draw reliable conclusions about the METs parameter.

The parameter for the constant term tracks measured BGC relatively closely, leaving little variation to be explained by the covariates. This lack of covariate influence may be highlighted in a "what if" analysis. For example, predicted BGC using the filtered model results barely alter if the insulin input is kept constant at zero (Figure 4.13). Given the carbohydrate input, it would be expected that a lack of insulin would result in extreme hyperglycaemia; the ingested carbohydrate would increase BGC, and the absence of insulin would fail to restrict hepatic glucose release, further increasing BGC.

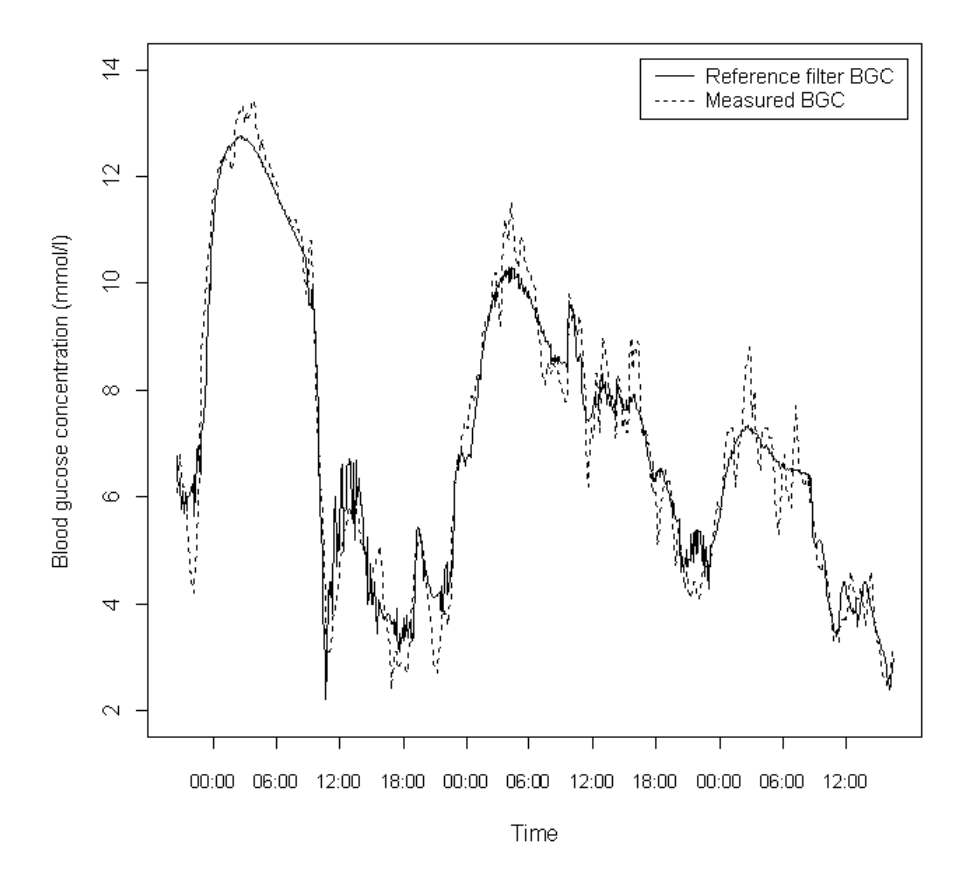


Figure 4.11: Reference filter model output for BGC and measured BGC.

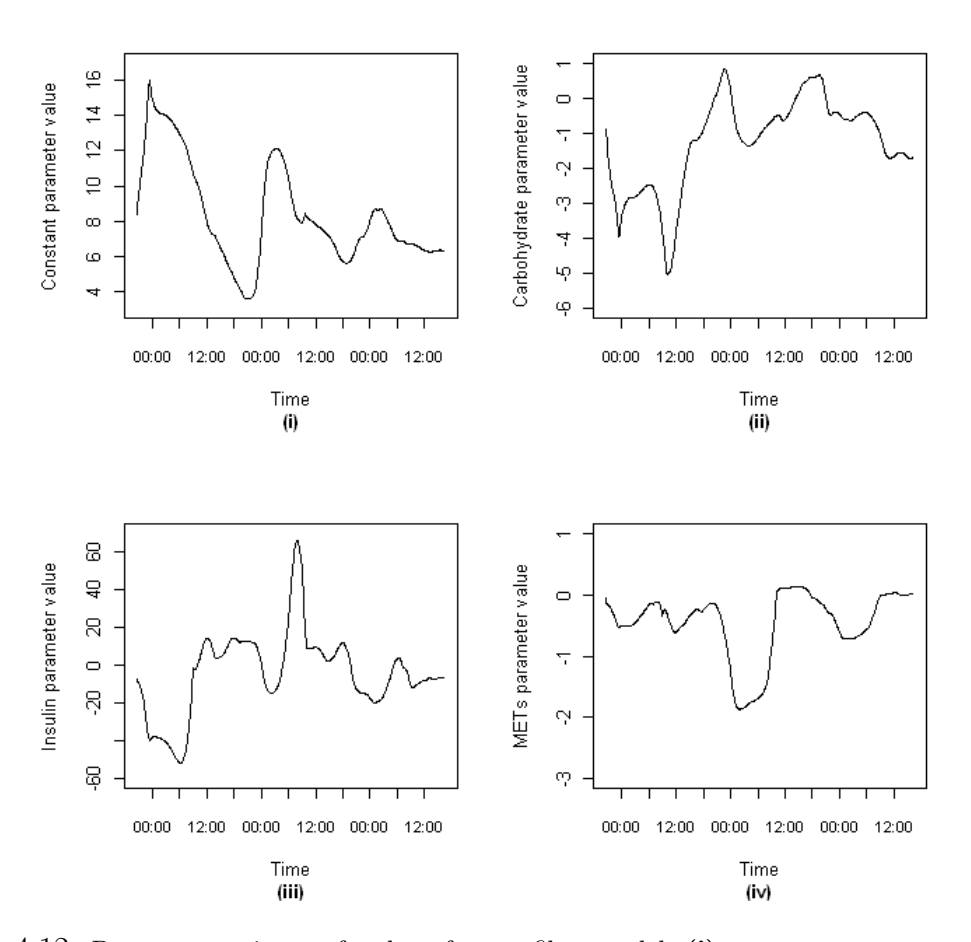


Figure 4.12: Parameter estimates for the reference filter model: (i) constant parameter; (ii) carbohydrate parameter; (iii) insulin parameter; (iv) METs parameter.

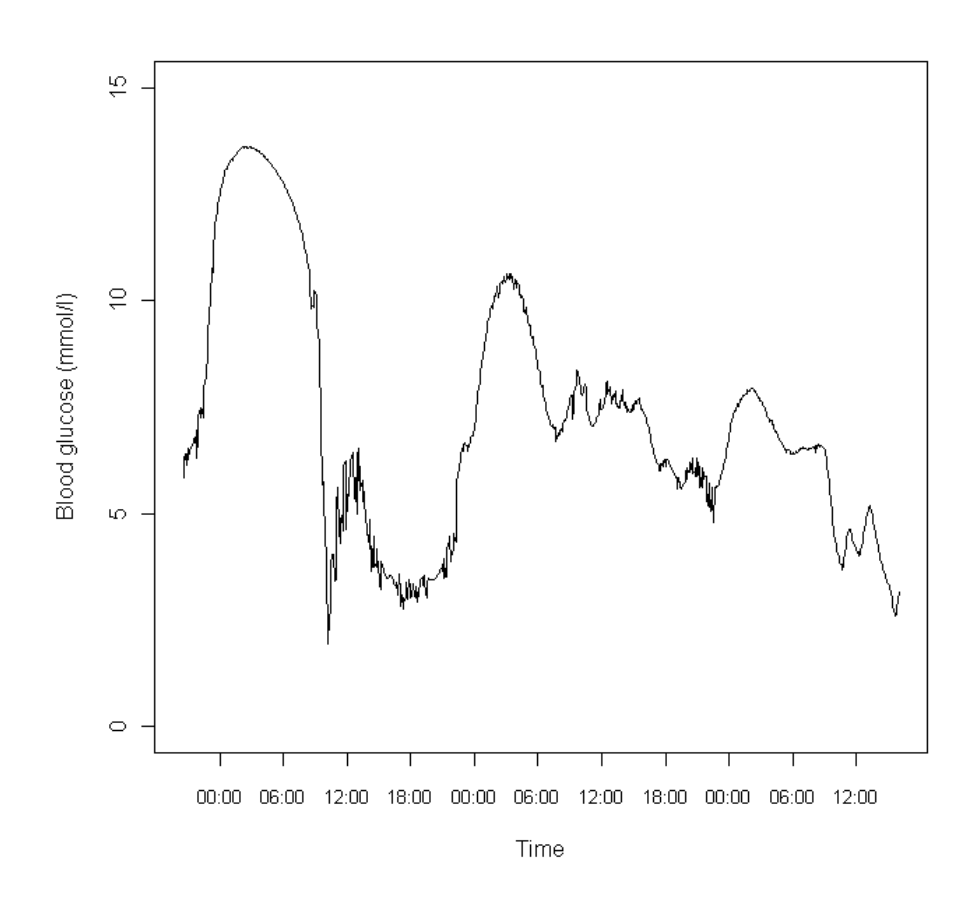


Figure 4.13: Predicted BGC in the absence of insulin based on filter model results.

Filtered results from a 24-hour period were used to predict BGC over a successive 24-hour period, whose food, insulin and METs inputs are assumed known. While the model is capable of predicting a period of hyperglycaemia, it also shows periods of consistent under- and over-prediction (Figure 4.14). There is also a period of time where negative BGC is predicted. The behaviour of the parameters will depend on the timing of food and insulin injections, as well as when the individual is active; hence, parameter values are unlikely to vary in the same way from day to day unless the individual follows a strict routine.

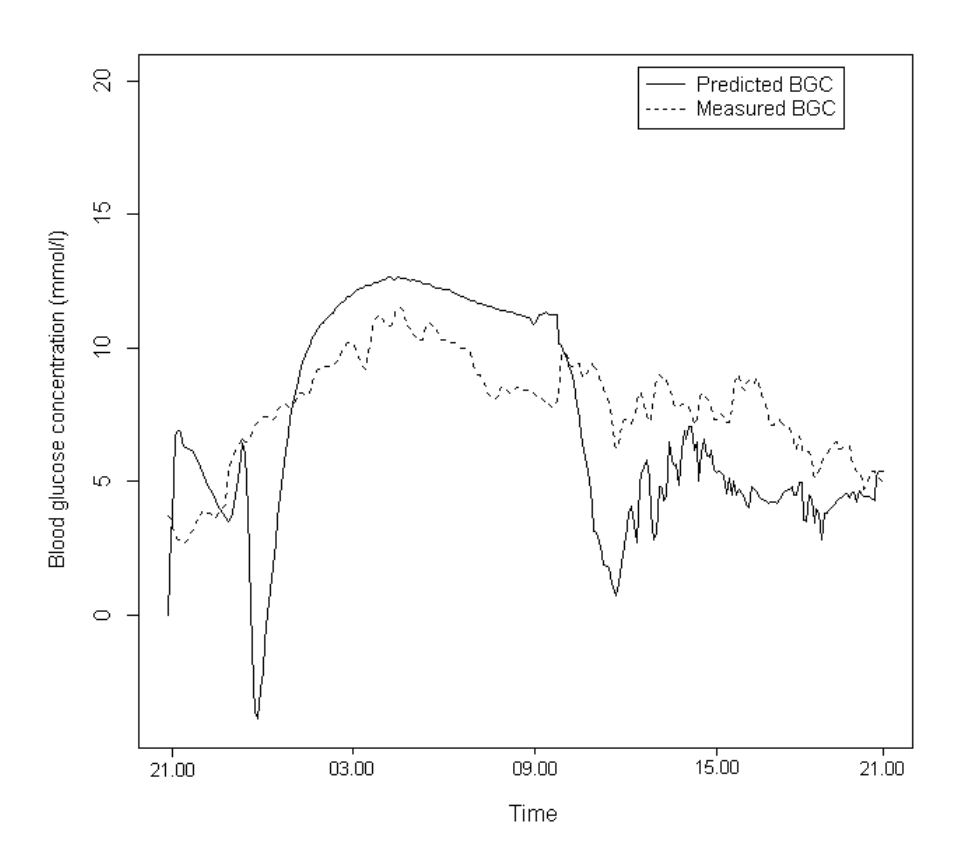


Figure 4.14: Predicted BGC and measured BGC using parameter predictions from previous 24-hour period.

#### 4.2.2.6 Conclusions

From a theoretical perspective, the DLMs showed many favourable properties when modelling BGC; one-step ahead predictions were accurate and were robust to misspecification of starting parameter values. However, the filtered DLM was unable to accurately reflect the established underlying physiology regarding glucose and insulin absorption, and hence it is not possible to draw conclusions regarding METs and the effect of physical activity on BGC. Parameter estimates from the DLMs for carbohy-

drate and insulin do not agree with established knowledge, suggesting the models would be unsuitable for a "what if" analysis and hence could not aid the MDI regime. The disparity between model estimates and established physiology may be due to issues with parameter identification. This is a particular problem in diabetes modelling; it is not possible to safely excite individual inputs (particularly food and insulin) while keeping others constant, thus the individual effects of simultaneously-excited inputs are obscured.

# 4.3 Sampling the DLM of Blood Glucose Concentration

Another approach to parameter learning is to sample the full posterior distribution of parameters,

$$p(\boldsymbol{\Theta}_T, \sigma^2, \boldsymbol{\Omega}) = \prod_{i=0}^T [p(\boldsymbol{\theta}_i) | \sigma^2, \boldsymbol{\Omega}] p(\sigma^2) p(\boldsymbol{\Omega}),$$

where  $\Theta_T = (\theta_0, \theta_1, \dots, \theta_T)$  is the full set of regression parameters. The posterior distribution is complex, making parameter learning difficult; in such situations, computationally-intensive methods such as Markov chain Monte Carlo (MCMC) are often used (Gilks et al., 1996). MCMC methods provide a general approach for sampling from probability distributions, and are discussed in appendix C for those unfamiliar with this approach. MCMC will be used here to simulate from the posterior distribution of the parameters.

## 4.3.1 Full, Individual Conditional Sampling

One method for sampling the parameter vector,  $\boldsymbol{\Theta}$ , is to sample from the full, individual conditional distribution,  $p(\boldsymbol{\theta}_i|\boldsymbol{Y}^T,\boldsymbol{\Theta}_{\cdot-i},\phi,\boldsymbol{\Omega}_t)$ , where  $\boldsymbol{\Theta}_{\cdot-i}=(\boldsymbol{\theta}_0,\ldots,\boldsymbol{\theta}_{i-1},\boldsymbol{\theta}_{i+1},\ldots,\boldsymbol{\theta}_T)$ . Given the structure of the DLM, neighbouring values of  $\boldsymbol{\theta}_i$  will be correlated; hence, sampling from these distributions will generally result in slower mixing compared to sampling from the joint distribution (Chib and Greenberg, 1996). However, this approach allows a little more flexibility in terms of defining the error variances, as there is no need to use a discount factor for  $\Omega_t$ . Assuming  $\Omega$ , a  $(p \times p)$  matrix, is constant, the conjugate prior distribution is given by an inverse Wishart distribution with parameters v and  $\Sigma$ , representing the degrees of freedom and an inverse scale matrix, respectively. The distribution is denoted by  $\Omega \sim IW_p(v, \Sigma)$ , where

$$p(\mathbf{\Omega}) = \frac{|\mathbf{\Sigma}|^{\upsilon/2} |\mathbf{\Omega}|^{-\upsilon+p+1} \exp[-\frac{1}{2} \mathrm{trace}(\mathbf{\Sigma} \mathbf{\Omega}^{-1})]}{2^{\upsilon p/2} \Gamma_p(\upsilon/2)},$$

with  $\Gamma_p(\cdot)$  representing the p-variate gamma function. The inverse Wishart is the multivariate generalisation of the inverse gamma distribution. The prior distribution for  $\phi = \sigma^{-2}$ , assumed constant, is a gamma distribution.

Setting  $\psi = \{\Theta, \sigma^2, \Omega\}$ , the full, joint posterior distribution for the parameter set is given by the product of the likelihood (the observation and system equations) and prior distributions:

$$p(\boldsymbol{\psi}|\boldsymbol{y}) \propto p(\boldsymbol{\psi}) \cdot p(\boldsymbol{y}|\boldsymbol{\psi})$$

$$\propto \prod_{t=1}^{T} \{\phi^{1/2} \exp[-\frac{\phi}{2}(y_{t} - \boldsymbol{x}_{t}^{\mathrm{T}}\boldsymbol{\theta}_{t})^{2}]\}$$

$$\times \prod_{t=1}^{T} \{|\boldsymbol{\Omega}|^{-1/2} \exp[-\frac{1}{2}(\boldsymbol{\theta}_{t} - \boldsymbol{\theta}_{t-1})^{\mathrm{T}}\boldsymbol{\Omega}^{-1}(\boldsymbol{\theta}_{t} - \boldsymbol{\theta}_{t-1})]\}$$

$$\times \exp[-\frac{1}{2}(\boldsymbol{\theta}_{0} - m_{0})^{\mathrm{T}}C_{0}^{-1}(\boldsymbol{\theta}_{0} - m_{0})]$$

$$\times (\phi)^{n-1} \exp(-d\phi)$$

$$\times |\boldsymbol{\Omega}|^{-(v+p+1)/2} \exp(-\operatorname{trace}(\boldsymbol{\Sigma}\boldsymbol{\Omega}^{-1})/2). \tag{4.3.1}$$

After observing the data, the conditional posterior distribution for  $\phi$  is updated to

$$\phi|(\boldsymbol{y},\boldsymbol{\theta}_0,\boldsymbol{\Theta},\boldsymbol{\Omega}) \sim G(n+T/2,d+\frac{1}{2}\sum_{t=1}^{T}(y_t-\boldsymbol{x}_t^{\mathrm{T}}\boldsymbol{\theta}_t)^2).$$
 (4.3.2)

The conditional posterior distribution for  $\Omega$  is

$$\Omega|(\boldsymbol{y}, \boldsymbol{\theta}_0, \boldsymbol{\Theta}, \phi) \sim \mathrm{IW}_p(\upsilon + T, \boldsymbol{\Sigma} + \sum_{t=1}^T (\boldsymbol{\theta}_t - \boldsymbol{\theta}_{t-1})^{\mathrm{T}} (\boldsymbol{\theta}_t - \boldsymbol{\theta}_{t-1})).$$

The initial regression parameters are updated to

$$\boldsymbol{\theta}_0 | (\boldsymbol{y}, \boldsymbol{\Theta}, \tau_t^2, \lambda_t^2) \sim \mathrm{N}(\boldsymbol{b}_0, \boldsymbol{B}_0)$$

where

$$egin{array}{lcl} m{B}_0^{-1} &=& \lambda_1^2 m{W}^{-1} + m{C}_0^{-1}, \ m{B}_0^{-1} m{b}_0 &=& \lambda_1^2 m{W}^{-1} m{ heta}_1 + m{C}_0^{-1} m{m}_0. \end{array}$$

For t = 1, ..., T - 1, the regression parameters have a posterior distribution given by

$$\boldsymbol{\theta}_t | (\boldsymbol{y}, \boldsymbol{\theta}_0, \boldsymbol{\Theta}_{-t}, \tau_t^2, \lambda_t^2) \sim \mathrm{N}(\boldsymbol{b}_t, \boldsymbol{B}_t)$$

where

$$m{B}_t^{-1} = au_t^2 m{x}_t m{x}_t^{\mathrm{T}} + \lambda_t^2 m{W}^{-1} + \lambda_{t+1}^2 m{W}^{-1}, \ m{B}_t^{-1} m{b}_t = au_t^2 y_t m{x}_t + \lambda_t^2 m{W}^{-1} m{ heta}_{t-1} + \lambda_{t+1}^2 m{W}^{-1} m{ heta}_{t+1}.$$

For t = T, the posterior distribution is

$$oldsymbol{ heta}_T | (oldsymbol{y}, oldsymbol{ heta}_0, oldsymbol{\Theta}_{-T}, au_t^2, \lambda_t^2) \sim \mathrm{N}(oldsymbol{b}_T, oldsymbol{B}_T)$$

where

$$oldsymbol{B}_T^{-1} = au_T^2 oldsymbol{x}_T oldsymbol{x}_T^{\mathrm{T}} + \lambda_T^2 oldsymbol{W}^{-1}, \ oldsymbol{B}_T^{-1} oldsymbol{b}_T = au_T^2 y_T oldsymbol{x}_T + \lambda_T^2 oldsymbol{W}^{-1} oldsymbol{ heta}_{T-1}.$$

The posterior distributions are all of standard form, hence Gibbs sampling may be used. Under Gibbs sampling methods, samples are drawn from the full conditional distribution,  $p(\psi|y)$ . For parameter  $\psi_i$  this involves considering only terms involving  $\psi_i$ . Defining  $\psi_{-i} = (\psi_1, \dots, \psi_{i-1}, \psi_{i+1}, \dots, \psi_k)$ , this is equivalent to sampling from  $p(\psi|y, \psi_{-i})$ . Conjugacy of the priors and the likelihood ensures closed distributions. Gibbs sampling also allows for component-wise updating, where components may be of differing dimensions. In this case the regression parameters will be considered as one component, and the variances,  $\sigma^2$  and  $\Omega$ , as individual components.

#### 4.3.1.1 Results

The output for the full, individual conditional approach shows varied results. Mixing is good for  $\Theta$  at early time points but becomes considerably worse as t increases, as seen in the trace plots in Figure 4.15. The poor mixing remains after 20,000 iterations. This is likely to be due to the correlation between the parameters. Mixing is, however, good for the error variances; Figure 4.16 shows the trace plot for the observation error variance.

## 4.3.2 Full, Joint Conditional Sampling

An alternative approach to sampling the regression parameters is proposed by Carter and Kohn (1994). This approach simulates the  $\boldsymbol{\theta}_i$ , for i = 0, ..., T, from their full, joint conditional distribution,  $p(\boldsymbol{\Theta}|\boldsymbol{y}, \sigma_t^2, \Omega_t)$ . Dropping the dependence on the error variances for convenience, the joint distribution may be written as

$$p(\boldsymbol{\Theta}|\boldsymbol{Y}^T) = p(\boldsymbol{\theta}_T|\boldsymbol{Y}^T) \prod_{i=0}^{T-1} p(\boldsymbol{\theta}_i|\boldsymbol{Y}^i, \boldsymbol{\theta}_{i+1}),$$

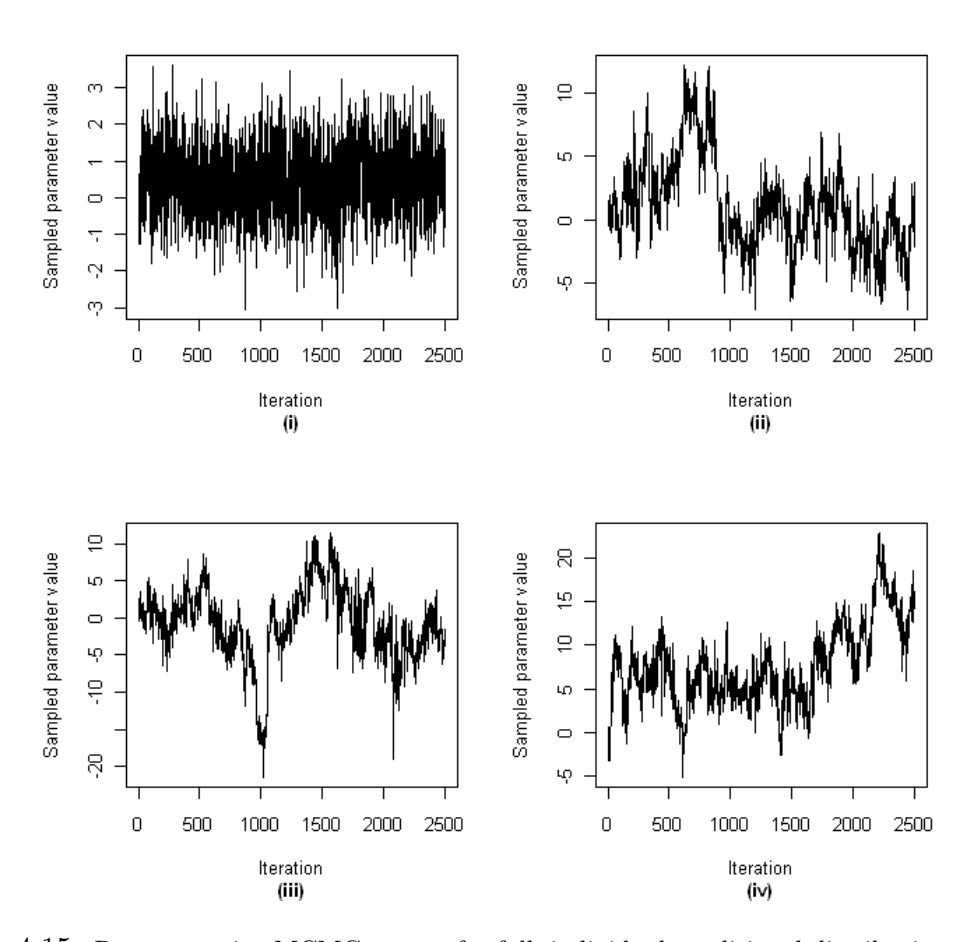


Figure 4.15: Representative MCMC output for full, individual conditional distribution sampling of DLM parameters: (i) the constant parameter at time t = 1 and (ii) t = 800; (iii) the carbohydrate parameter at t = 100; (iv) the insulin parameter at time t = 500.

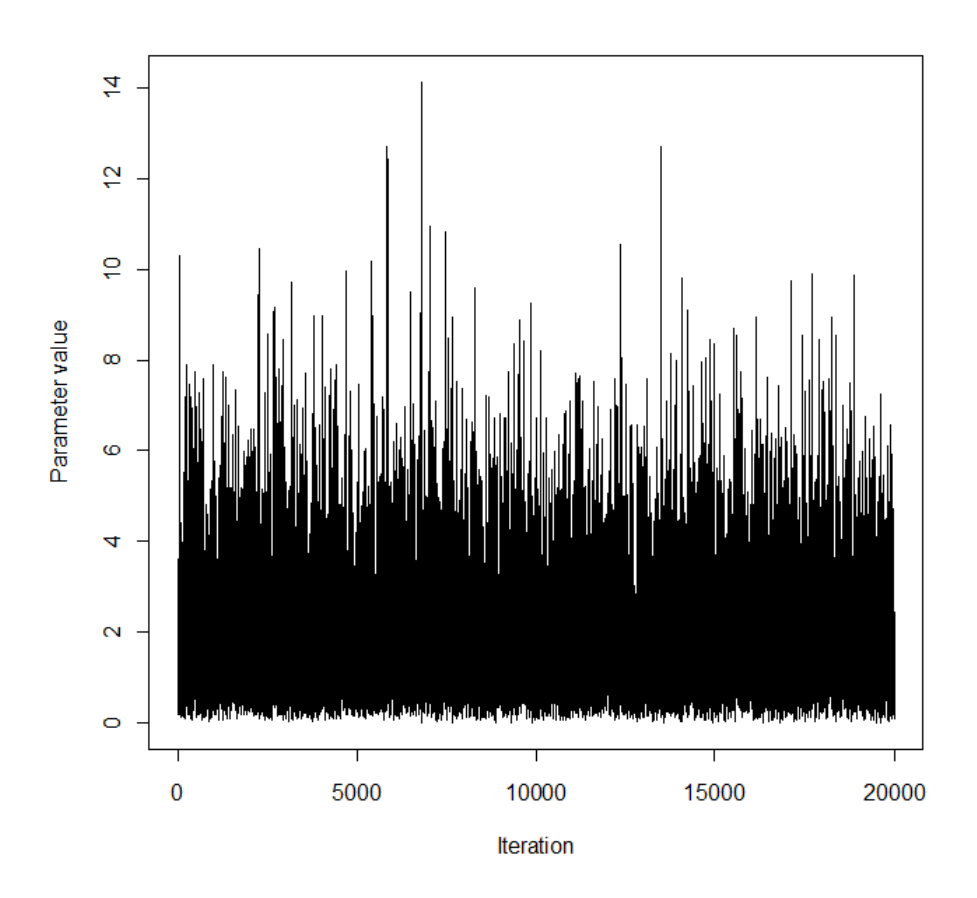


Figure 4.16: MCMC output for observation error precision,  $\phi$ , under full, individual conditional distribution sampling of DLM parameters.

where  $\mathbf{Y}^i = (y_1, \dots, y_i)$ . The process of sampling from the joint distribution begins by generating a value from  $p(\boldsymbol{\theta}_T | \mathbf{Y}^T)$ , and then successively generating from  $p(\boldsymbol{\theta}_i | \mathbf{Y}^i, \boldsymbol{\theta}_{i+1})$  through times  $t = T - 1, \dots, 0$ . The structure of the DLM implies that

$$(\boldsymbol{\theta}_T | \boldsymbol{Y}^T) \sim N(\boldsymbol{m}_T, \boldsymbol{C}_T),$$

and the remaining samples also come from normal distributions. The means and variances of these distributions are as given in equation 4.1.17, section 4.1.6. The process therefore requires running a form of the DLM analysis described in section 4.1.1, and storing the appropriate values.

The full joint distribution of the DLM will also contain contributions from the error variances. To run the DLM, the system error variance,  $\Omega$ , is replaced by a discount factor. The observation error precision,  $\phi$ , is again modelled using a gamma prior distribution, with associated posterior distribution given by (4.3.2).

#### 4.3.2.1 Results

The output suggests mixing occurs quickly for each parameter across all time points (Figure 4.17). This is also the case for the observation error precision,  $\phi$  (Figure 4.18). Given the rapid mixing, MCMC was run for 2,500 iterations with an arbitrary burnin of 500. The means of each of the remaining 2,000 sampled values were used to estimate all parameters at each time point, and empirical 95% credible bounds were derived by determining the 2.5<sup>th</sup> and 97.5<sup>th</sup> percentiles of the sorted sampled values. The results are similar to those for the filtered DLM, again suggesting unrealistic parameter estimates (Figure 4.19).

#### 4.3.2.2 Conclusions

The MCMC approach to parameter learning was also unable to accurately reflect established physiological behaviour regarding glucose and insulin absorption. The results did not differ greatly from the basic DLM learning procedure, suggesting no advantage to this method in this case despite increased computational cost.

## 4.4 Many-Step Regression DLM

Predictions from a regression DLM are now calculated for 12, 24 and 48 steps ahead (equivalently one, two and four hours), and are discussed in the following sections. Four hour predictions are of particular interest, as this represents a reasonable amount of time between finger-prick tests as part of the MDI treatment regime. A predictive model could improve insulin therapy by offering guidance when choosing insulin dose,

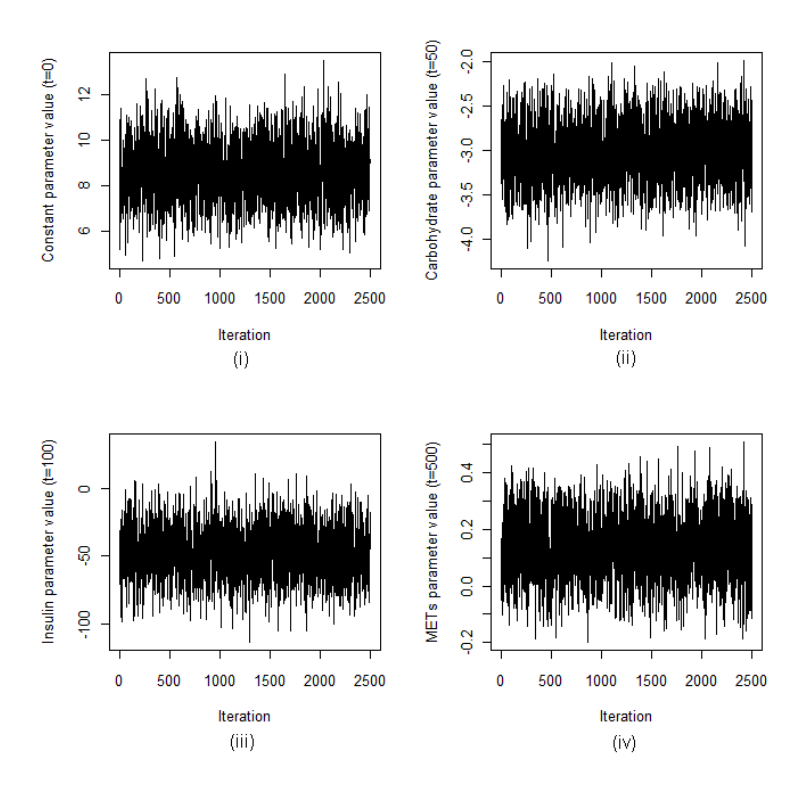


Figure 4.17: Representative MCMC trace plots, sampled values for: (i) constant parameter at time t=0; (ii) carbohydrate parameter at time t=50; (iii) insulin parameter at time t=100; (iv) METs parameter at time t=500.

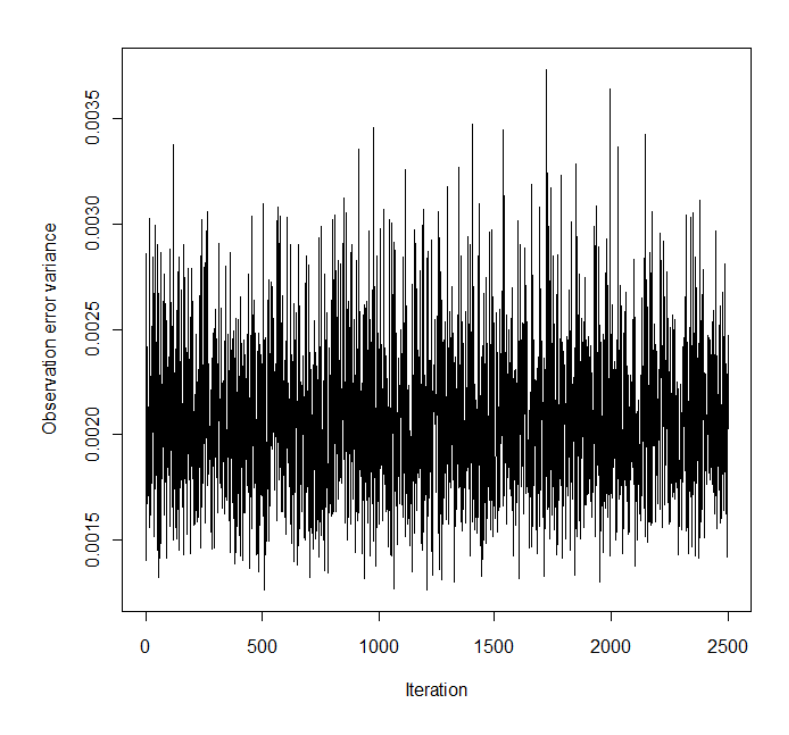


Figure 4.18: MCMC trace plot for observation error precision,  $\phi$ .

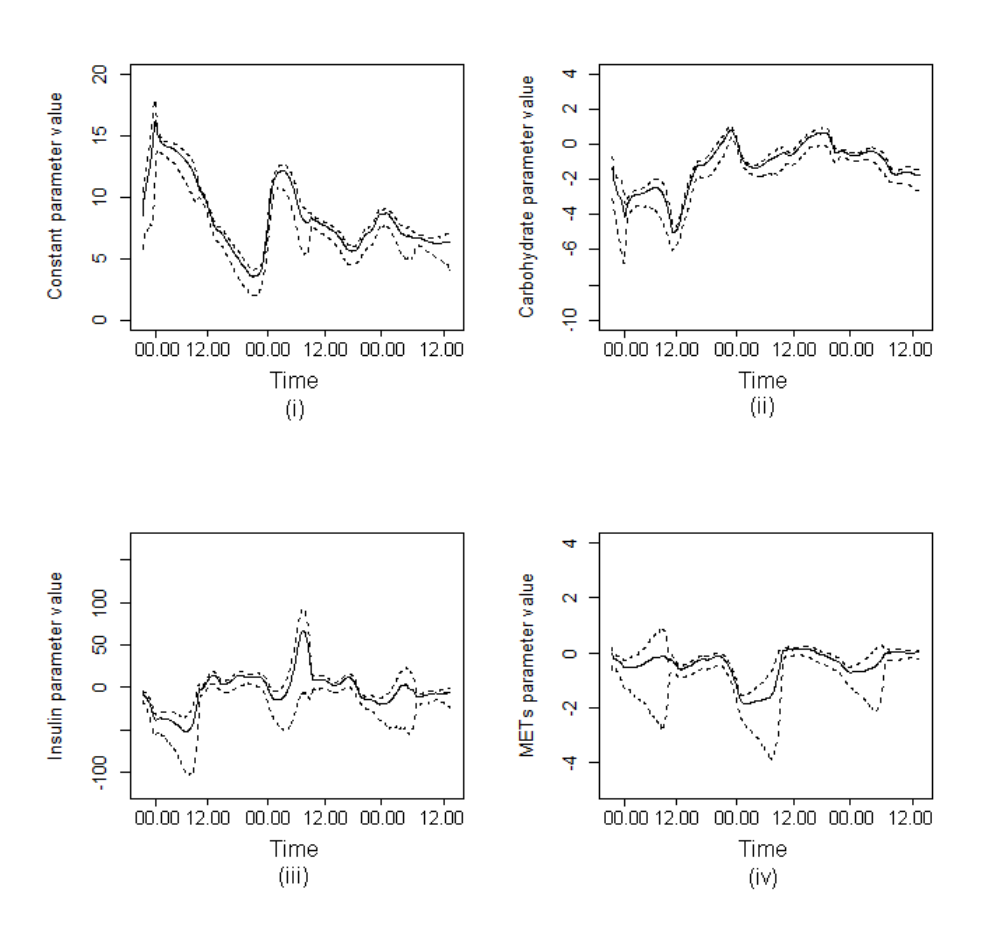


Figure 4.19: Means (solid lines) and 95% quantiles (dotted lines) from MCMC output for: (i) constant parameter; (ii) carbohydrate parameter; (iii) insulin parameter; (iv) METs parameter.

and help avoid hypo- or hyperglycaemia.

For  $k = \{12, 24, 48\}$ -step ahead predictions, the full set of BGC measurements (the ensemble; t = 1, ..., T) is split into k time series, whose BGC measurements are k steps (5k minutes) apart:

for 
$$n = 1, ..., k$$
,  

$$g_{[n]} = \{g_n, g_{n+k}, ..., g_{n+t_k k}\}, \tag{4.4.1}$$

where  $t_k$  is such that  $t_k k \leq T < (t_k + 1)k$ . For each time series,  $g_{[n]}$ , a one-step single-discount DLM (as in section 4.2.2) is run (note that these DLMs will be referred to as many-step DLMs in reference to the fact they are forecasting 5k minutes ahead). To initiate each time series, a one-step single-discount DLM is applied to the ensemble, from time t = 1 to t = k; these results are filtered (as in section 4.2.2.5), and the filtered distributions are used as the initial distributions,  $p(\theta_{[n]}|D_0)$ , for the associated time series,  $g_{[n]}$ .

Forecast performance may be assessed by comparing measured and forecast BGC both within each time series and by considering forecasts from each time series concurrently. Two new indices are also presented to assess forecast performance; these are introduced to determine a model's ability to predict hypo- and hyperglycaemia. Though a model may not be able to accurately predict the future profile of BGC, it would still be of value if it can accurately determine periods of hypo- or hyperglycaemic (collectively referred to from here on as glycaemic excursions). Index 1 is defined as

$$I_t^{(1)}(g_t) = \begin{cases} -1, & \text{for } g_t < 4 \text{ mmol/l} \\ 0, & \text{for } 4 \text{ mmol/l} \le g_t \le 8 \text{ mmol/l} \\ +1, & \text{for } g_t > 8 \text{ mmol/l}, \end{cases}$$
(4.4.2)

and thus separates BGC into ranges for hypoglycaemia, euglycaemia and hyperglycaemia, respectively. The ability of the model to predict glycaemic excursions may be assessed by comparing  $I_t^{(1)}(g_t)$  (measured BGC) with  $I_t^{(1)}(f_t)$  (model forecasts of BGC). The predictive ability of the model may be further assessed by Index 2, defined as

$$I_{t}^{(2)}(g_{t}) = \begin{cases} 0, & \text{if } I_{t}^{(1)}(g_{t}) = I_{t}^{(1)}(f_{t}) \\ 1, & \text{if } |I_{t}^{(1)}(g_{t}) - I_{t}^{(1)}(f_{t})| = 1 \\ 2, & \text{if } |I_{t}^{(1)}(g_{t}) - I_{t}^{(1)}(f_{t})| = 2, \end{cases}$$

$$(4.4.3)$$

and so highlights agreement and large discrepancies between measured and predicted BGC.

## 4.4.1 12-Step BGC Prediction

The discount factor for the 12-step (one hour) predictive model is chosen to be 0.66 based on the error measures MAD, MSE and LLR (results not shown). Figure 4.20 shows predictions for time series  $g_{[1]}$  and  $g_{[12]}$ , and suggests the model is generally able to match the profile of measured BGC; however, there are some large discrepancies between predictions and measurements, caused by the increase in METs upon waking. Considered as a single time series, the 12-step predictions generally matches the profile of measured BGC, albeit with consistent under- or overestimation across consecutive time points. Early in the day, predictions become unstable due to the sudden increase in METs upon waking. Indices 1 and 2 suggest the model is generally able to distinguish between euglycaemia and glycaemic excursions; Figure 4.22, plot (i) suggests the model is able to determine glycaemic excursions, albeit with a lag when predicting hyperglycaemia, and Figure 4.22, plot (ii) suggests predicted and measured BGC are in the same glycaemic range for the majority of the time series.

Parameter estimates for the 12-step model appear to vary between time series; Figure 4.23 shows oscillations for each parameter, suggesting marked differences between estimates depending on when the time series begins. Parameter estimates do not comply with established physiological knowledge, as the insulin parameter is predominantly positive and the carbohydrate parameter predominantly negative. This suggests the model is unable to adequately describe the effect food and insulin has on BGC, perhaps due to the inputs' simultaneous excitations; hence, the model would not be suitable for guiding insulin dosing.

## 4.4.2 24-Step BGC Prediction

The discount factor for the 24-step (two hours) predictive model is chosen to be 0.98 based on the error measures (results not shown). Figure 4.24 shows predicted and measured BGC for time series  $g_{[1]}$  and  $g_{[24]}$ , which suggests mixed predictive results across time series; plot (i) shows  $g_{[1]}$  fails to recreate the profile of measured BGC, in particular the predictions miss the hyperglycaemia during the first night, while plot (ii) shows better predictive performance, albeit with evidence of a lag in the predictions with regard to the hyperglycaemia during the first night. Figure 4.25 shows the compiled time series, and suggests there are particular problems with time series  $g_{[1]}$  through the night as it consistently underestimates measured BGC; it is unclear why this problem appears to affect only this time series. Predictions during the day fluctuate due to the influence of METs, and are generally unable to reflect the profile of measured BGC. Index 1 suggests that 24-step predictions are able to determine periods of hyperglycaemia, but fail to pick up periods of hypoglycaemia (Figure 4.26, plot (i)). Index 2 suggests there is moderate agreement between predictions and measurements

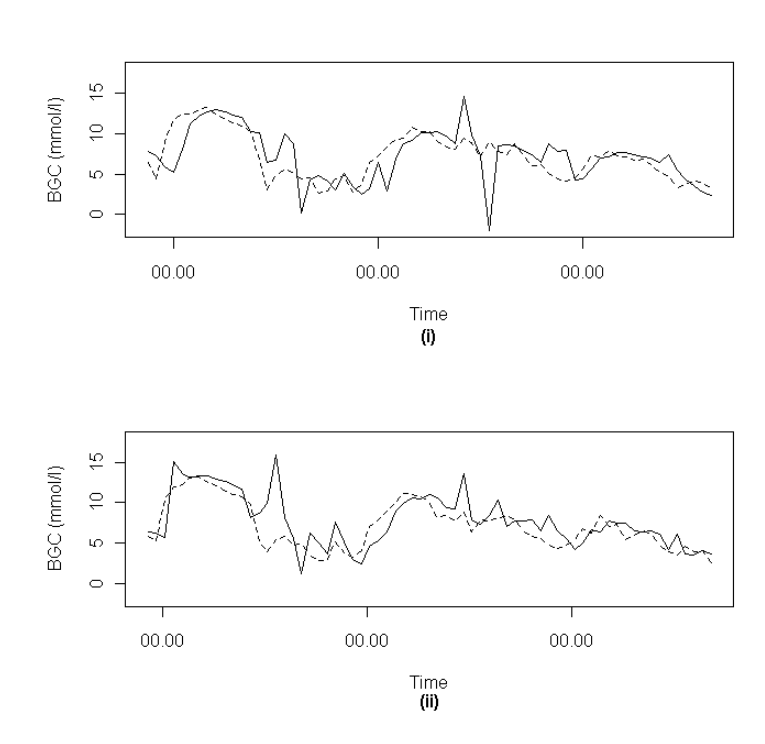


Figure 4.20: 12-steps (one hour) ahead predicted BGC (solid line) and measured BGC (dotted line): (i) time series  $g_{[1]}$ , as given in (4.4.1); (ii) time series  $g_{[12]}$ .

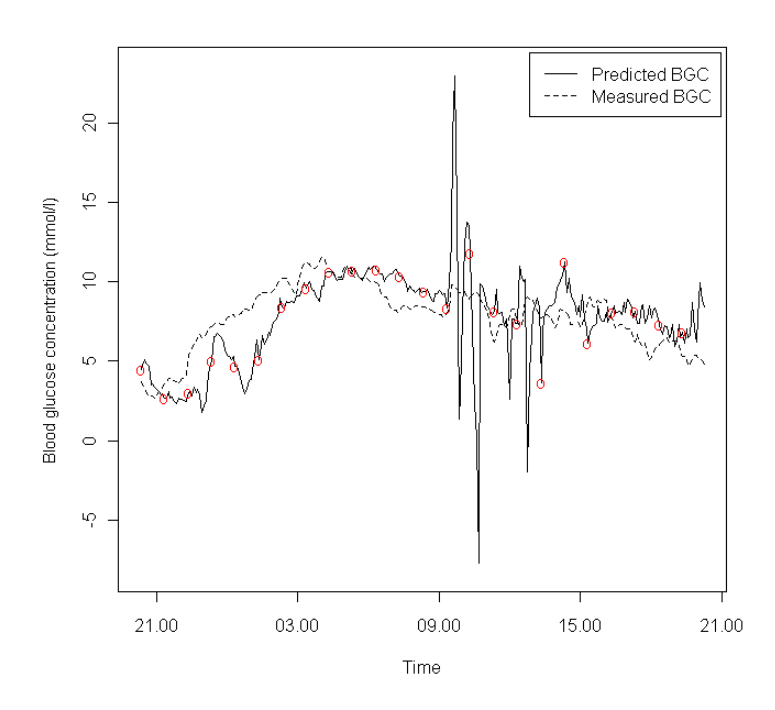


Figure 4.21: 24-hour window of compiled 12-step predicted BGC from all time series,  $g_{[n]}$ , and measured BGC. Red circles indicate points in time series  $g_{[1]}$ .

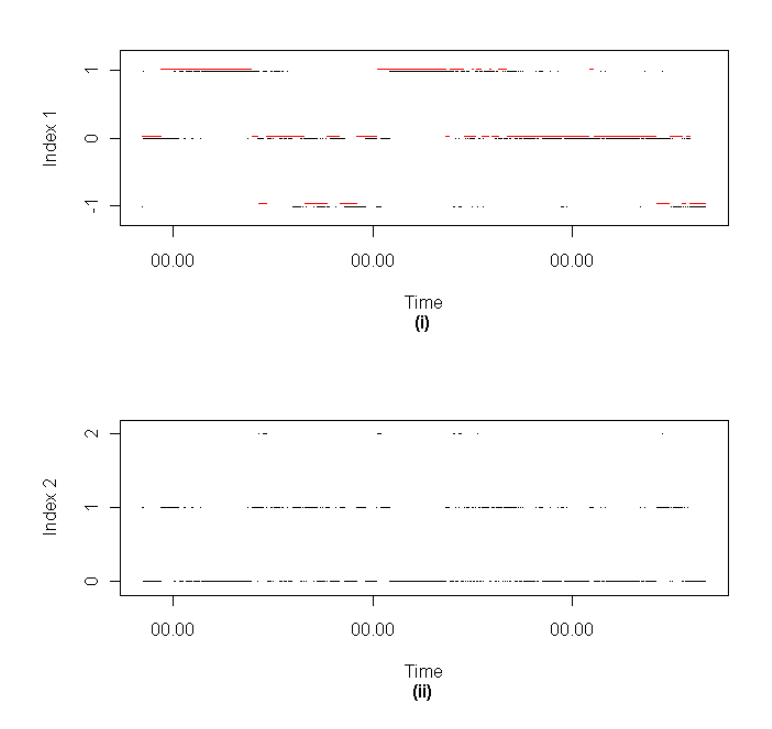


Figure 4.22: (i) Function  $I_t^{(1)}(\cdot)$  (4.4.2) applied to 12-step predicted BGC (black dots) and measured BGC (red dots); (ii) function  $I_t^{(2)}(\cdot)$  applied to 12-step predicted and measured BGC.

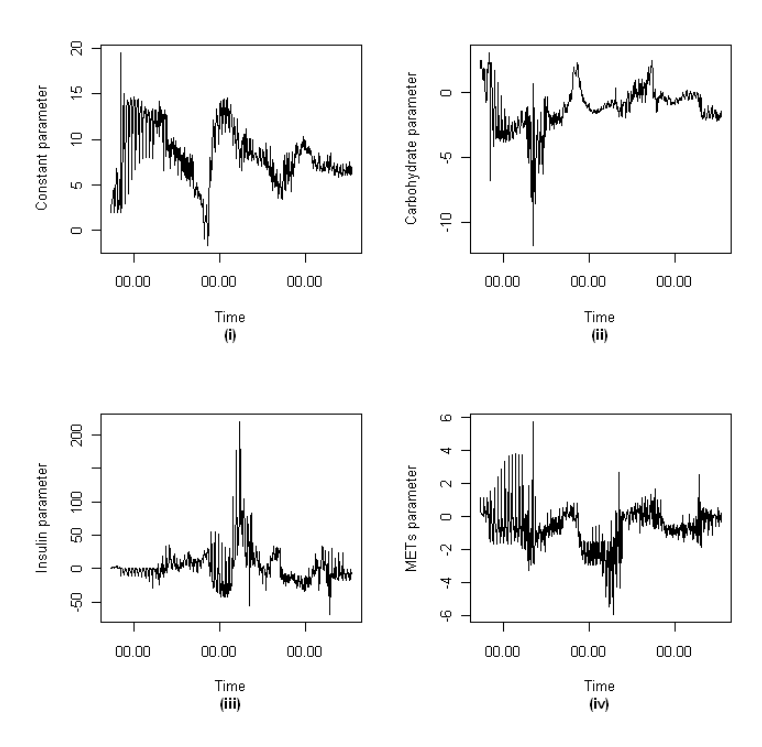


Figure 4.23: Parameter estimates for 12-step predictive model: (i) constant parameter; (ii) carbohydrate parameter; (iii) insulin parameter; (iv) METs parameter.

in terms of the range of BGC, with small discrepancies in prediction also fairly common and large discrepancies relatively rare (Figure 4.26, plot (ii)). Parameter estimates oscillate, as with the 12-step model, suggesting estimates are dependent on when the time series begins. Furthermore, parameter estimates again fail to comply with established knowledge, as the carbohydrate parameter is predominantly negative (Figure 4.27).

## 4.4.3 48-Step BGC Prediction

The discount factor for this model is chosen to be 0.85 based on the error measures (results not shown). Figure 4.28 shows predictions and measurements for time series  $g_{[1]}$  and  $g_{[48]}$ , which suggest a lag between predictions and measurements. Predictions appear to be unable to determine the larger changes in BGC and consistently overestimate BGC during the first day. For  $g_{[48]}$ , there is a negative prediction which is physiologically non-viable. Figure 4.29 shows reasonable predictive performance during the night, again with the exception of  $g_{[1]}$ . During the day, predicted BGC is occasionally greatly below measured BGC, most likely due to the nature of METs. Index 1 suggests the fluctuating nature of the predictions leads to an overestimation of glycaemic events (Figure 4.30, plot (i)); however, the model is able to determine periods of hyperglycaemia, albeit for longer durations than the measured BGC. Index 2 suggests moderate agreement between predictions and measurements with regard to the glycaemic ranges of BGC (Figure 4.30, plot (ii)). As with the previous many-step predictive models, parameter estimates oscillate and the carbohydrate parameter is negative (Figure 4.31).

#### 4.4.4 Conclusions

Many-step DLMs were unable to accurately reflect the profile of measured BGC. The 12-step model suggested reasonable predictive performance, particularly when predictions and measurements of BGC were compared using the indices; however, predictions were unstable in the mornings due to the sudden increase in METs upon waking. Parameter estimates also failed to comply with established knowledge, suggesting the model is unable to offer appropriate guidance for insulin dosage. The 24-step and 48-step models were generally unable to predict the profile of measured BGC, and the indices suggested that the models were also unable to accurately predict the range of measured BGC for any length of time.

## 4.5 Summary

DLMs were used to predict BGC using food intake, insulin, and physical activity as explanatory variables, with two aims: firstly, to understand the effect of physical ac-

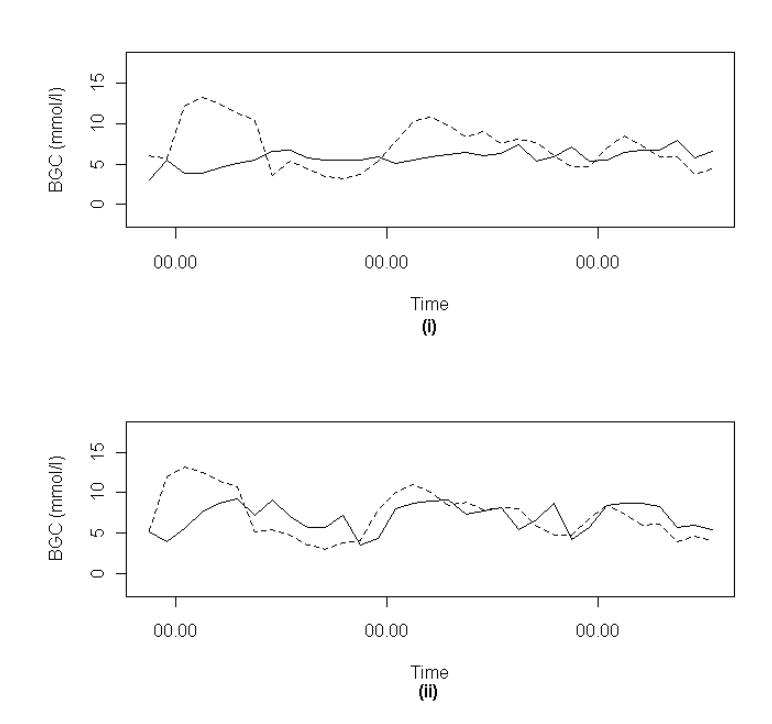


Figure 4.24: 24-steps (two hours) ahead predicted BGC (solid line) and measured BGC (dotted line): (i) time series  $g_{[1]}$ , as given in (4.4.1); (ii) time series  $g_{[24]}$ .

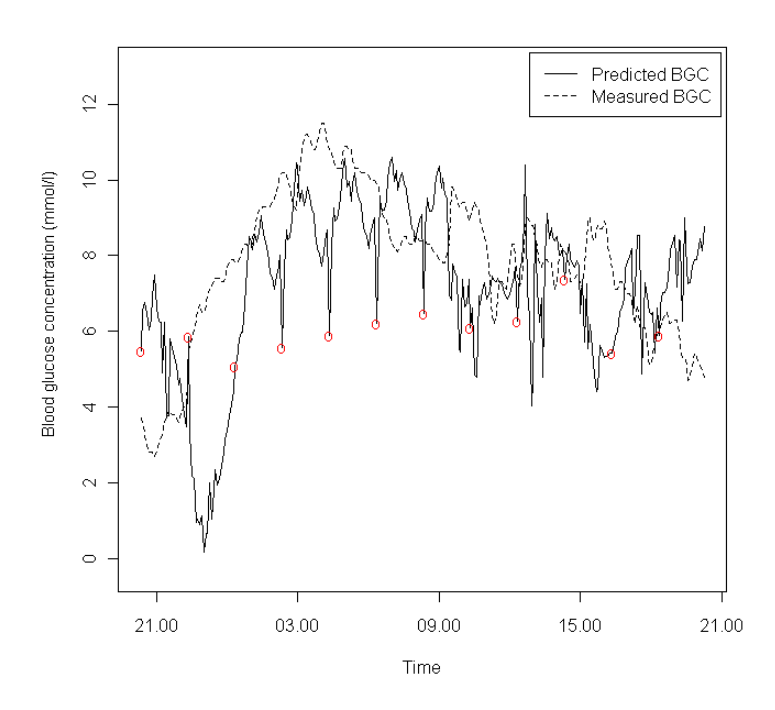


Figure 4.25: 24-hour window of compiled 24-step predicted BGC from all time series,  $g_{[n]}$ , and measured BGC. Red circles indicate points in time series  $g_{[1]}$ .

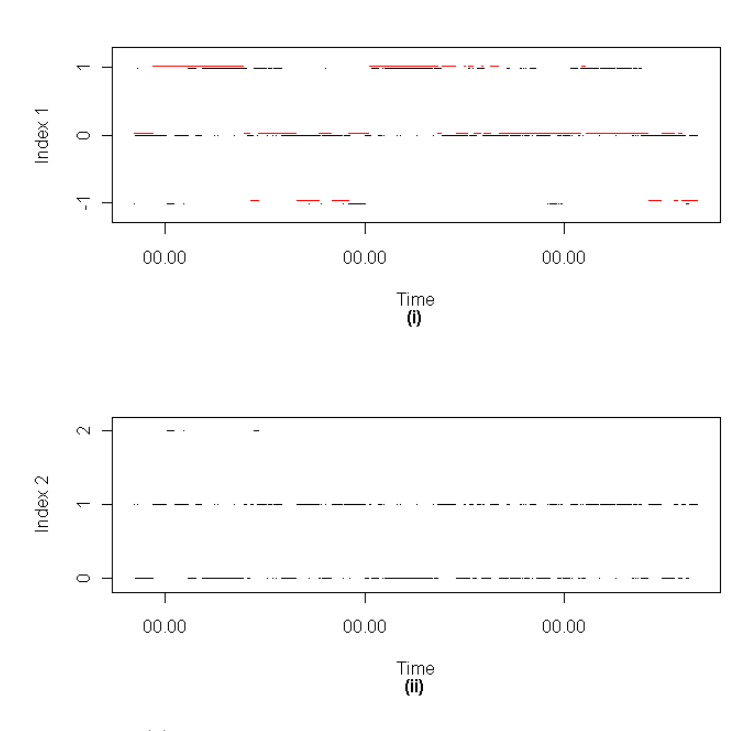


Figure 4.26: (i) Function  $I_t^{(1)}(\cdot)$  (4.4.2) applied to 24-step predicted BGC (black dots) and measured BGC (red dots): (ii) function  $I_t^{(2)}(\cdot)$  applied to 24-step predicted and measured BGC.

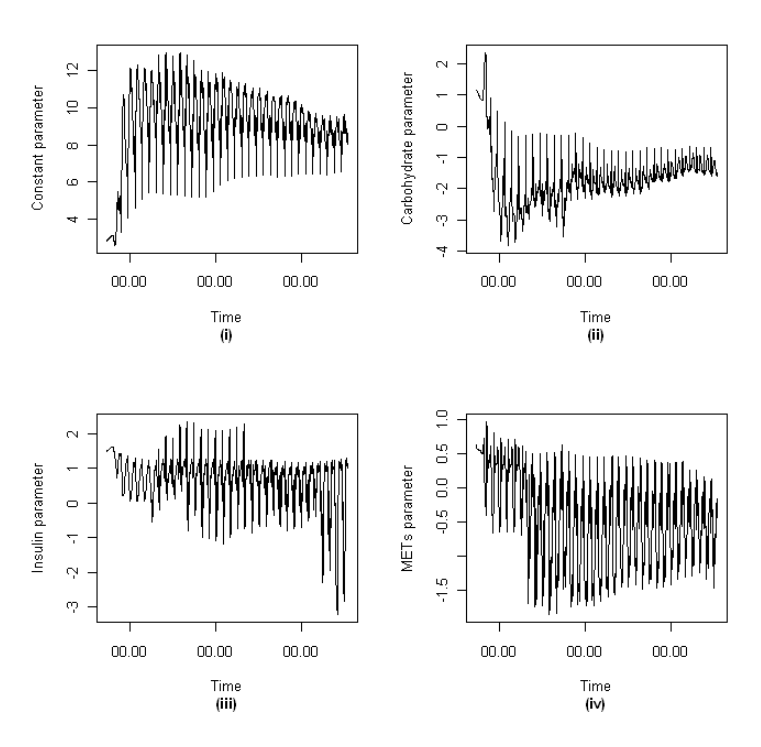


Figure 4.27: Parameter estimates for 24-step predictive model: (i) constant parameter; (ii) carbohydrate parameter; (iii) insulin parameter; (iv) METs parameter.

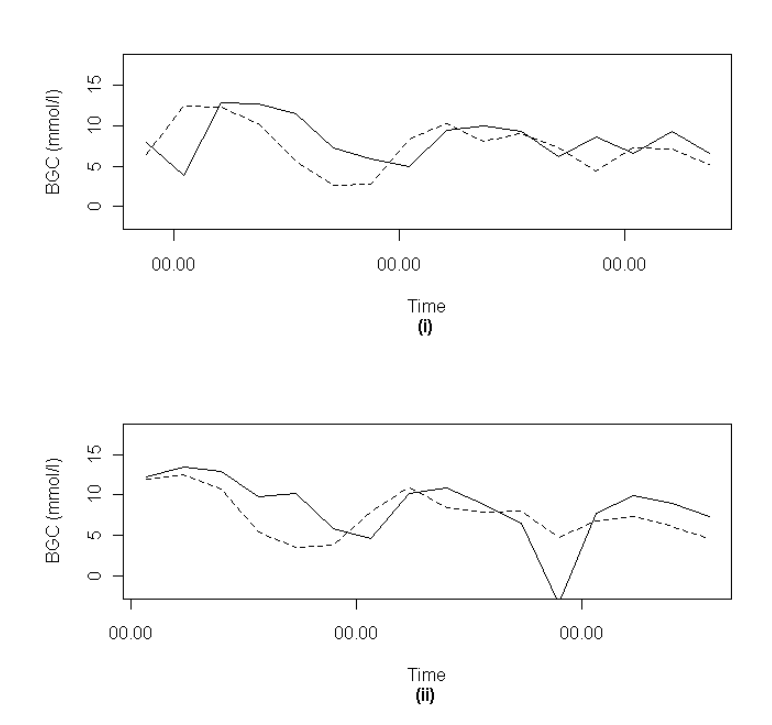


Figure 4.28: 48-steps (four hours) ahead predicted BGC (solid line) and measured BGC (dotted line): (i) time series  $g_{[1]}$ , as given in (4.4.1); (ii) time series  $g_{[48]}$ .

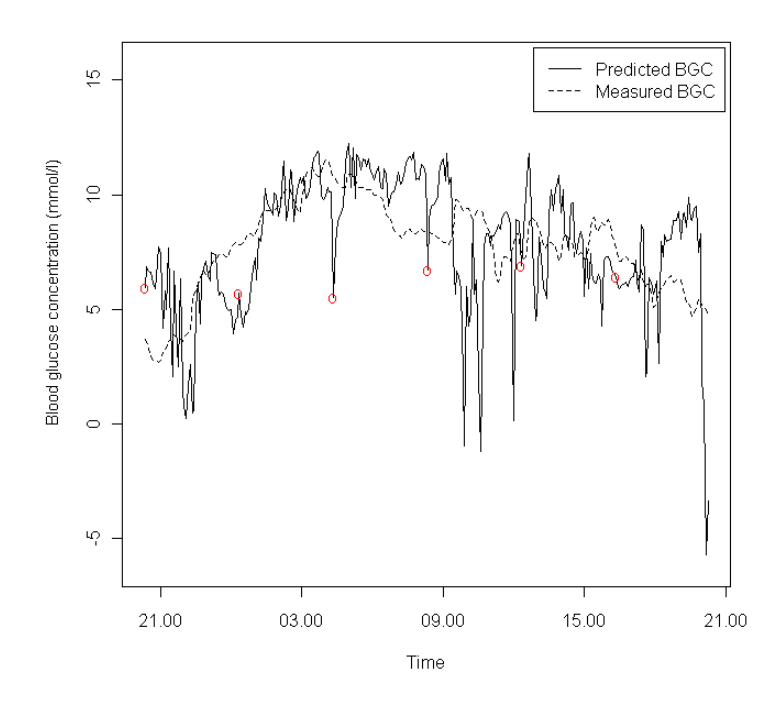


Figure 4.29: 24-hour window of compiled 48-step predicted BGC from all time series,  $g_{[n]}$ , and measured BGC. Red circles indicate points in time series  $g_{[1]}$ .

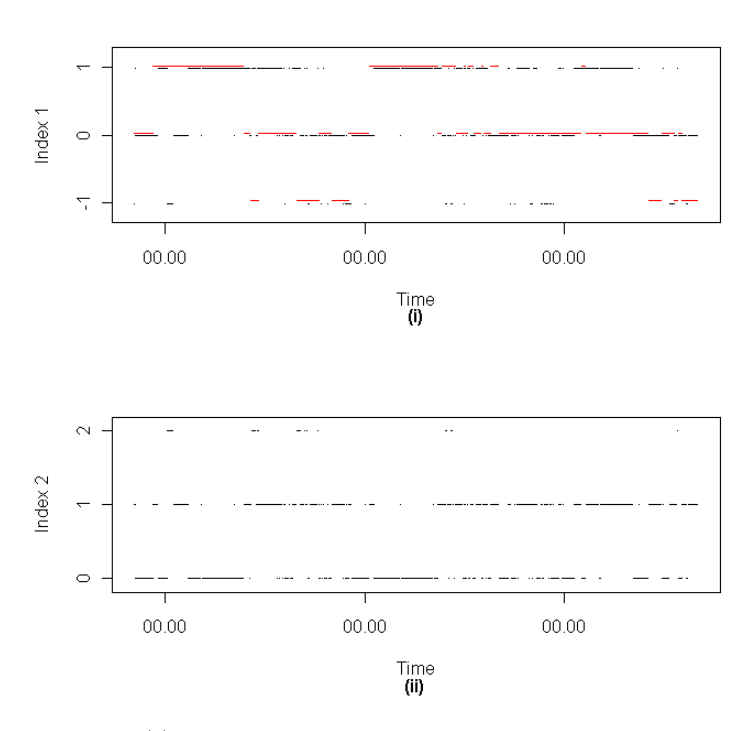


Figure 4.30: (i) Function  $I_t^{(1)}(\cdot)$  (4.4.2) applied to 48-step predicted BGC (black dots) and measured BGC (red dots); (ii) function  $I_t^{(2)}(\cdot)$  applied to 48-step predicted and measured BGC.

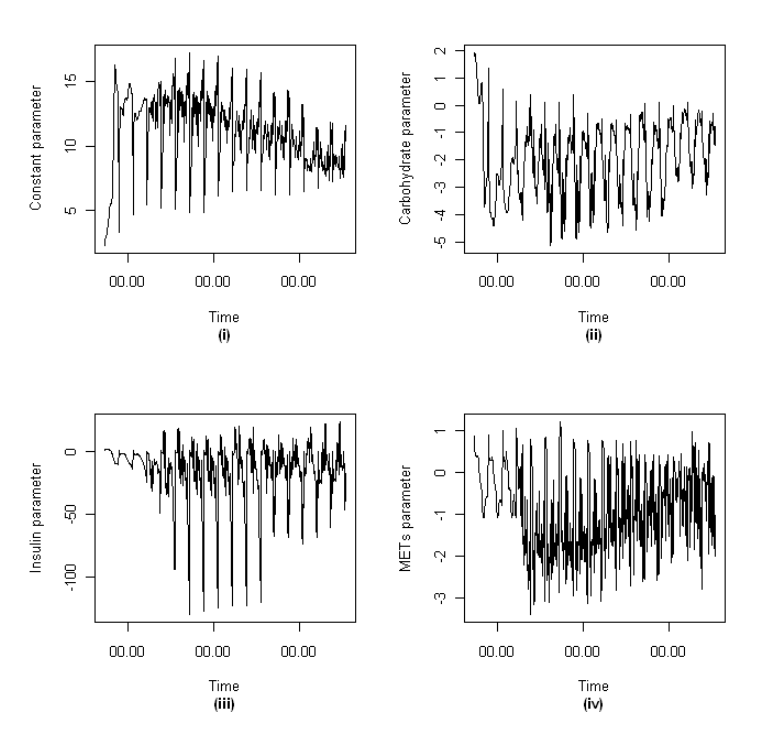


Figure 4.31: Parameter estimates for 48-step predictive model: (i) constant parameter; (ii) carbohydrate parameter; (iii) insulin parameter; (iv) METs parameter.

tivity on BGC, and secondly to assess the ability of DLMs to predict BGC over fours. Understanding the role of physical activity in the behaviour of BGC is vital in helping individuals with type 1 diabetes safely incorporate exercise in their daily routine, and enjoy the benefits without the risk of hypo- or hyperglycaemia. Accurate four-hour predictions can also aid an individual's BGC control by helping determine appropriate insulin dosage and highlighting potential periods of hypo- or hyperglycaemia, hence reducing the risk of the short- and long-term complications associated with type 1 diabetes. The DLMs proposed here are the use of such an empirical modelling approach for BGC, and one of few that use free-living data from non-invasive and readily accessible sources.

Predictions over five minutes were able to recreate the profile of measured BGC, though such short-term forecasts are of relatively little use to clinicians or individuals with type 1 diabetes. Parameter estimates from the filtered DLM did not comply with established physiological knowledge, as the insulin parameter was often positive and carbohydrate was often negative; MCMC methods did not provide any new information. In this context, it is inappropriate to draw conclusions on the role of physical activity in the behaviour of BGC.

The proposed many-step DLMs were able to predict BGC for up to an hour - at least with regard to highlighting glycaemic events - but were unable to accurately predict BGC over four hours. This may be due to imposing a linear structure on the non-linear glucoregulatory system, overlooking important internal processes, or problems with the data and its handling.

#### 4.5.1 Discussion

Empirical models such as those used in the current work are limited by the accuracy of the data and the digestion and insulin absorption models. The quantity of food intake may be under- or overestimated by individuals when recording meals in the food diary, and there may also be inconsistency in recording timing of food and insulin injections. The digestion and insulin models also each introduce various errors due to their simplified nature. The digestion model does not take into account the GI of food nor the presence of other nutrients, and hence may under- or over-estimate postprandial glucose absorption; there is also no consideration of the effect of digestion on physiological processes (immediate or delayed). The insulin model does not take into account injection site, and offers no indication of insulin action; as noted in section 2.6, compartmental models include separate compartments for plasma and active insulin, which represent the delay in the effect plasma insulin has on BGC. Lags or moving averages of glucose and insulin absorption may be more appropriate model inputs; however, the issue then becomes one of determining suitable lengths and weightings of

lags for these inputs.

Physical activity presents an even greater modelling challenge, as the effect of activity may be immediate and/or last several hours, depending on the type, duration and intensity of activity. The use of lags or moving averages may represent the effects of activity in a more physiologically-appropriate manner, but requires choice of appropriate time intervals, which are likely to vary depending on type, duration and intensity of activity. It is also apparent that the high variability of METs during the day resulted in highly fluctuating predictions. This problem could be overcome by smoothing METs; however, this requires finding suitable weights and time windows for smoothing, and risks losing important information.

Modelling BGC during the night with the proposed form of DLMs also presents its own problems. The food, insulin and METs inputs are generally very stable at night (and close to zero in the case of carbohydrate) and effects that are unaccounted for, such as hepatic glucose release, become much more prominent, and may be erroneously attributed to one or more of the inputs.

Empirical models based only on easily measurable inputs may be improved by more accurate representations of glucose and insulin absorption after meals and injections, respectively, and better understanding of the physiological processes affected by these disturbances. Furthermore, METs requires better handling, whether through smoothing, lags or otherwise, in order to better represent the effect of physical activity on BGC. Non-linear dynamic models would be more physiologically representative, but would be difficult to construct given that non-linearities in the glucoregulatory system are not well understood, and potentially time- and subject-specific.

The roles of food, insulin and physical activity may be better captured in a model with a physiological basis. The semi-empirical compartmental models discussed in sections 2.6.1 and 2.6.2 are more physiologically representative of the glucoregulatory system than a DLM, albeit at the cost of greater complexity. However, such models may be able to better reflect the role of food, insulin and physical activity in the behaviour of BGC.

## Chapter 5

## Stochastic Modelling of Glucose-Insulin Dynamics in Free-Living Conditions for People with Type 1 Diabetes

The previous chapter highlighted the difficulties in building empirical models of blood glucose concentration (BGC). The focus of this chapter remains on investigating the role of physical activity, now through semi-empirical compartmental models. The work draws on the decades of research stimulated by the minimal model proposed by Bergman et al. (1979, 1981).

This chapter begins with a description of the minimal model and its various extensions, in particular the work of Andersen and Højbjerre (2005) and the physical activity minimal model of Roy and Parker (2007) (referred to as the PA model from here). The focus then moves onto testing the viability of combining the PA model with free-living data. The PA model, like the vast majority of models in the diabetes literature, is tested only on clinical or simulated data that do not accurately reflect the daily experience of individuals. Using the DUK study data (as discussed in chapter 3), the first aim is to explore the practical issues of using frequently-sampled, highly-variable free-living data on the PA model; this is the first attempt to combine free-living data on BGC, food intake, insulin and physical activity with such models.

New methods for analysing compartmental models are then presented as a more realistic representation of the underlying physiology. Markov chain Monte Carlo methods are tested as a tool for estimating all model parameters using a simulation study.

## 5.1 Development of the Minimal Model

The minimal model (MM) was discussed in section 2.6.1; to recap, the MM is a compartmental model used to describe blood glucose-insulin kinetics, whose structure is given in Figure 5.1. The variables G(t) [mg/dl],  $I_p(t)$  [ $\mu$ U/ml], and  $I_a(t)$  [ $\mu$ U/ml] represent the concentrations of blood glucose, blood insulin, and remote (or active) insulin, respectively. The equations used to describe glucose-insulin kinetics are

$$\frac{dG(t)}{dt} = \dot{G} = [p_1 - X(t)]G(t) + p_4$$

$$\dot{X} = p_2 X(t) + p_3 I_p(t)$$

$$\dot{I}_p = p_5 (G(t) - p_6)t - p_7 I_p(t),$$
(5.1.1)

where  $X = (k_4 + k_6)I_a(t)$  [min<sup>-1</sup>] describes the insulin action in the remote compartment. The relationships between model and equation parameters ( $k_i$  and  $p_i$ , respectively) are described in Table 5.1.

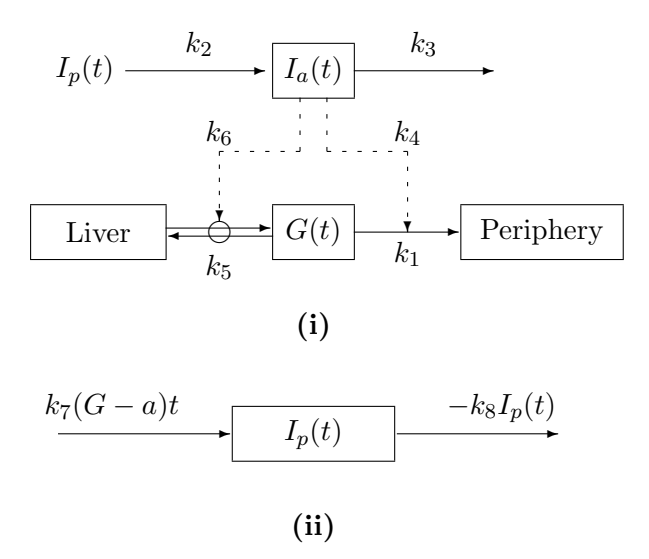


Figure 5.1: Minimal model of glucose-insulin kinetics: (i), model of glucose metabolism; (ii), model of insulin kinetics. Reproduced from Bergman et al. (1979, 1981).

Table 5.1: Relationship of model and equation parameters for the minimal model.

Parameter	Units	Description
$p_1 = -(k_1 + k_5)$	$\min^{-1}$	Rate of insulin-independent glucose uptake
$p_2 = -k_3$	$\min^{-1}$	Rate of decreasing ability to uptake glucose
$p_3 = k_2(k_4 + k_6)$	$\mathrm{ml}/\mu\mathrm{U}/\mathrm{min}^2$	Rate constant of insulin-dependent glucose uptake
$p_4 = H_0$	mg/dl/min	Hepatic balance extrapolated to zero BGC
$p_5 = k_7$	$\mu \mathrm{U/mg/min^2}$	Rate of insulin release by $\beta$ -cells
$p_6 = a$	m mg/dl	Threshold for insulin release
$p_7 = k_8$	$\min^{-1}$	Rate of insulin clearance

Originally, the MM was used to determine insulin sensitivity in people with type 2 diabetes. Analysis involves two stages: firstly, a known insulin time course is supplied to the glucose model (Figure 5.1 (i)) for parameter estimation; secondly, a glucose time course is supplied to estimate parameters in the insulin model (Figure 5.1 (ii)). Considering the model as one unified system can lead to unrealistic behaviour (De Gaetano and Arino, 2000). Various generalisations and improvements have been posited in the literature to extend the MM and/or overcome its limitations; of particular interest here is the extension proposed by Roy and Parker (2007) to include the physical activity of exercise, and the stochastic, population model proposed by Andersen and Højbjerre (2005), discussed in the following sections.

#### 5.1.1 Stochastic Minimal Model

It is argued here that a stochastic model of blood glucose-insulin dynamics would better reflect the uncertainty inherent in complex biological systems, and hence would be a more physiologically-viable representation of the glucoregulatory system when compared to a set of deterministic differential equations. Andersen and Højbjerre (2005) approached the minimal model with a similar perspective; their reformulation of the MM converts the deterministic differential equations (DEs) into a Bayesian network, where modern sampling techniques may then be used for parameter estimation based on an IVGTT and subsequent blood samples. The reformulation uses vague prior distributions, based on previous studies, to allow unified analysis of the model, and proceeds as follows:

- i) rewrite (5.1.1) in terms of the natural logarithms of the (positive) latent processes:  $g(t) = \ln[G(t)], x(t) = \ln[X(t)]$  and  $i(t) = \ln[I_p(t)]$  (note that  $I_p$  will be represented by I from here on, and  $I_a$  from the original MM is only considered in terms of X);
- ii) add a stochastic term to each equation to account for measurement and process variability: stochastic terms are Wiener processes representing the integral of Gaussian white noise;
- iii) convert the DEs to integral equations by integration over a small time frame;
- iv) approximate integrals to determine an iterative set of equations;
- v) determine conditional distributions for the log-transformed latent processes: the means of the distributions are determined by the MM, and the precisions by the Wiener process;
- vi) model observations as Gaussian to account for measurement errors: the means of the distribution are given by the underlying latent process.

Using blood glucose as an example, the reformulation converts the DEs into the form:

$$(g_{t_k}|g_{t_{k-1}}, x_{t_{k-1}}, \tau_g) \sim N(f_{g,t}(g_{t_{k-1}}, x_{t_{k-1}}), (\nabla t)\tau_q^{-1}),$$

where

$$f_{g,t}(g_{t_{k-1}}, x_{t_{k-1}}) = g_{t_{k-1}} - \nabla t \{ p_1[1 - G_b \exp(-g_{t_{k-1}})] + \exp(x_{t_{k-1}}) \};$$

note that  $p_1$  has changed sign from the original MM,  $G_b = p_4/p_1$  is basal glucose,  $\tau_g$  is the precision associated with the Wiener process, and  $\nabla t = t_k - t_{k-1}$  represents the time span over which the approximations are made.

Parameters  $\{p_1, \ldots, p_6\}$  are assumed to have log-normal prior distributions, and precisions are assumed to have gamma prior distributions. The parameters of these distributions may also be assigned prior distributions to extend the reformulation to a population model. A directed acyclic graph (DAG) is used to represent the relationships between variables,  $\{g, x, i\}$ , and blood glucose and insulin observations,  $\{g^o, i^o\}$  (Figure 5.2); vertices represent variables at given time points (here square boxes are the unobserved, latent processes and the circles represent observed processes), while directed edges describe the dependencies between variables. The posterior distribution of all unknown parameters is analysed using MCMC methods, allowing for simultaneous, model-wide parameter estimation.

The approach presented by Andersen and Højbjerre is aimed at improving analysis of the minimal model, and hence is concerned only with type 2 diabetes. The methods are geared specifically toward estimating the insulin sensitivity and glucose effectiveness parameters based on intermittent blood samples collected for up to four hours. The approach has therefore only been tested on data collected in a clinical setting over a limited time frame, with no attempt to extend the model to include the influence of digestion, insulin injection or physical activity.

## 5.1.2 Physical Activity Minimal Model

Roy and Parker (2007) generalised and adapted the original minimal model for use in type 1 diabetes by including terms for exogenous insulin, meals and physical activity. Six DEs were included to account for the effects of physical activity: one accounting for  $\text{PVO}_2^{\text{max}}$  (E; see section 2.5.4), one for integrated activity intensity (A), and one each for the activity-induced effects on hepatic glucose production (H; mg/kg/min), glucose uptake (U; mg/kg/min), insulin clearance (Z;  $\mu \text{U/ml/min}$ ), and decline in rate of glycogenolysis (K; mg/kg/min).

The blood glucose DE of the MM is modified by including the influence of the

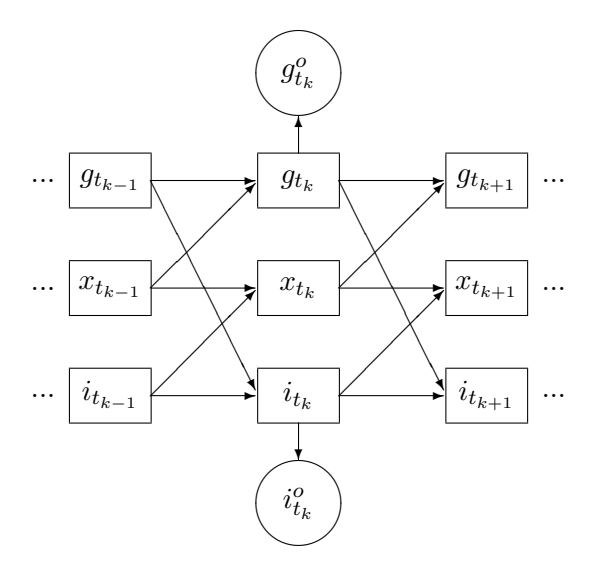


Figure 5.2: Directed acyclic graph of the Andersen and Højbjerre (2005) model.

processes H, K and U, and glucose absorption from food ( $M_G$ ; mg/min):

$$\dot{G}(t) = -p_1(G(t) - G_b) - X(t)G(t) + (W/V_G)[H(t) - K(t) - U(t)] + M_G(t)/V_G,$$
(5.1.2)

where W is weight (kg), and  $V_G$  is the glucose distribution space (dl). The blood insulin DE is modified by the influence of Z and insulin absorption after injection ( $M_I$ ;  $\mu \text{U/min}$ ):

$$\dot{I}(t) = -p_2 I(t) + p_3 M_I(t) - Z(t). \tag{5.1.3}$$

Insulin action is given by

$$\dot{X}(t) = -p_4 X(t) + p_5 (I(t) - I_b), \tag{5.1.4}$$

where  $I_b$  is basal insulin. Physical activity intensity, measured by  $PVO_2^{max}$ , is modelled by a DE to describe the delay in reaching a steady state value at the onset of activity (therefore mimicking the delay in increased oxygen uptake and heart rate):

$$\dot{E}(t) = -p_6 E(t) + p_7 M_E(t), \qquad (5.1.5)$$

where  $M_E$  is the actual intensity of activity above basal level (8% VO<sub>2</sub><sup>max</sup>). Parameter values of  $p_6 = p_7 = 0.8$  were chosen to acheive an appropriate settling time of five minutes. The DEs representing the new processes H, U and Z are given by

$$\dot{H}(t) = p_8 E(t) - p_9 H(t), 
\dot{U}(t) = p_{10} E(t) - p_{11} U(t), 
\dot{Z}(t) = p_{12} E(t) - p_{13} Z(t).$$
(5.1.6)

The rate of change of each process thus increases with increasing activity intensity. The decline of glycogenolysis rate, which occurs when hepatic glycogen stores are depleted during prolonged physical activity, is modelled by

$$\dot{K}(t) = \begin{cases}
0, & A(t) < A_{\text{th}} \\
p_{14}, & A(t) \ge A_{\text{th}} \\
-p_{15}K(t), & M_E(t) = 0,
\end{cases}$$
(5.1.7)

where A is the integrated activity intensity given by

$$\dot{A}(t) = \begin{cases} M_E(t), & \text{for } M_E(t) > 0\\ -p_{16}A(t), & M_E(t) = 0, \end{cases}$$
 (5.1.8)

and  $A_{\rm th}$  is the threshold for the decline in glycogenolysis rate, given by

$$A_{\text{th}} = M_E(t)[-1.152M_E(t) + 87.471].$$

The term H(t) - K(t) in (5.1.2) may be thought of as representing the overall contribution of the liver to BGC during activity. At the onset of activity, H increases until integrated activity intensity passes the threshold,  $A_{\rm th}$ . The process K then becomes active, and reduces the net hepatic release. Post-activity, the decline in glycogenolysis returns toward zero as the liver replenishes glycogen stores via gluconeogenesis; likewise, integrated activity intensity also quickly returns to zero. Parameter estimates and initial values presented in Roy and Parker (2007) are given in Table 5.2.

The vast majority of parameter fitting and validation in the PA model is carried out using data collected from healthy volunteers. As discussed in chapter 2, the response to physical activity of an individual with type 1 diabetes is markedly different to that of healthy individuals. Furthermore, the activity data is assumed to be non-fluctuating throughout the data collection period. When compared to the free-living data, it is clear this is an over-simplification. It remains to be seen how the model performs given free-living inputs.

## 5.2 PA Model and Free-Living Data

The performance of the PA model was tested using the free-living data from the DUK study. The results presented and discussed here relate to one individual (Subject A) chosen as being relatively representative of the model results seen across other individuals. The estimated glucose and insulin absorption and measured activity for this individual are given in Figure 5.3, with the data collection period covering almost

Table 5.2: Parameters for the Roy and Parker (2007) model. Parameters  $p_i$  are assumed known and taken from the original Bergman et al. (1979) model. The set of parameters  $a_i$  are fitted using various studies; see Roy and Parker (2007) and references within.

Parameter	Value	Units	Initial values
$\overline{p_1}$	0.035	$\min^{-1}$	$G(0)=G_b$
$p_2$	0.142	$\min^{-1}$	$I(0)=I_b$
$p_3$	0.098	$\mathrm{ml}^{-1}$	X(0)=0
$p_4$	0.05	$\min^{-1}$	E(0) = 0
$p_5$	0.000028	$\mathrm{ml}/\mu\mathrm{U}/\mathrm{min}^2$	H(0) = 0
$p_6$	0.8	$\min^{-1}$	U(0)=0
$p_7$	0.8	$\min^{-1}$	Z(0) = 0
$p_8$	0.00158	$mg/kg/min^2$	K(0) = 0
$p_9$	0.056	$\min^{-1}$	A(0) = 0
$p_{10}$	0.00195	$mg/kg/min^2$	
$p_{11}$	0.0485	$\min^{-1}$	
$p_{12}$	0.00125	$\mu \mathrm{U/ml/min}$	
$p_{13}$	0.075	$\min^{-1}$	
$p_{14}$	0.0108	$mg/kg/min^2$	
$p_{15}$	0.1667	min	
$p_{16}$	1000	$PVO_2^{max}$	
$G_b$	80	mg/dl	
$V_G$	117	dl	
$I_b$	[not defined]	$\mu \mathrm{U/ml}$	

three days.

Measured physical activity was converted from METs to relative  $PVO_2^{max}$  (rPVO<sub>2</sub><sup>max</sup>) by

$$rPVO_2^{max} = max \left(0, \frac{METs}{METs_{max}} \times 100 - 8\right),$$

where METs<sub>max</sub> is the maximum METs achievable by the individual (equivalent to  $VO_2^{max}$ ), and basal activity ( $\sim 8\% VO_2^{max}$ , equivalently  $\sim 1$  METs) is adjusted to zero. The DEs were solved numerically using the Dormand-Prince (DP) method (Dormand and Prince, 1980) implemented in Simulink<sup>1</sup>. DP is a fourth/fifth-order solver which achieves an appropriate balance between speed and accuracy.

#### 5.2.1 Results

The model was unable to accurately reflect the behaviour of BGC, even predicting negative concentration (Figure 5.4). A number of other unfavourable results were also found, due, in particular, to the differences between artificial and free-living physical activity. Free-living physical activity data are far more variable than the data used to build the PA model, and rarely return to basal level for an extended period of time during the day. This results in the integrated exercise, A, increasing throughout the day (Figure 5.5), and a great over-estimation of the decline in rate of glycogenolysis.

 $<sup>^{1} \</sup>rm http://www.mathworks.co.uk/products/simulink/, \, last \, accessed \, 29/11/2012$ 

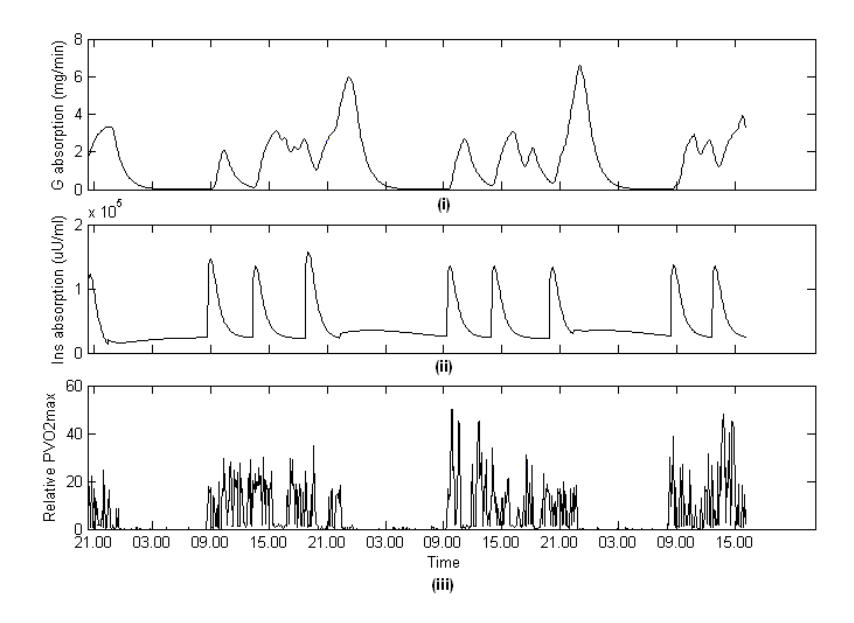


Figure 5.3: Glucose (i) and insulin absorption (ii) (from the digestion and insulin models) and relative PVO<sub>2</sub><sup>max</sup> (iii) for Subject A.

Subsequently, the model estimates frequent negative contribution from the liver (Figure 5.6), when instead the process K was originally intended to merely dampen the effect of process H. Such excessive hepatic glucose uptake contradicts what would reasonably be expected given that the individual did not pass 50%  $VO_2^{max}$ , and did not maintain an activity level far above basal level for any extended period of time.

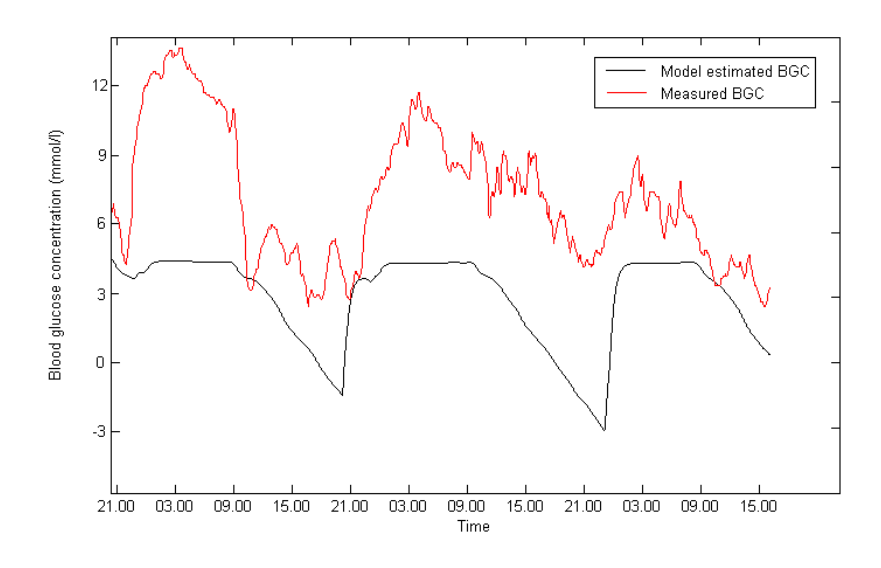


Figure 5.4: PA model predicted of BGC and measured BGC for Subject A.

The model also returned negative values for blood insulin concentration (Figure 5.7) and insulin action. This is predominantly due to the activity-stimulated insulin clearance rate, Z. Insulin clearance increases above the insulin absorbed after injection, resulting in negative blood insulin; negative insulin action then follows.

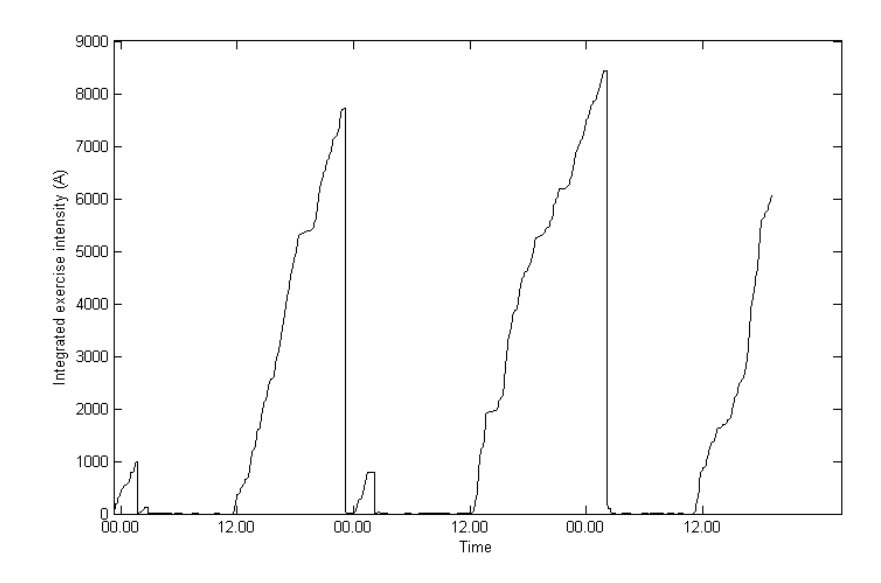


Figure 5.5: Integrated exercise intensity from the PA model for Subject A.

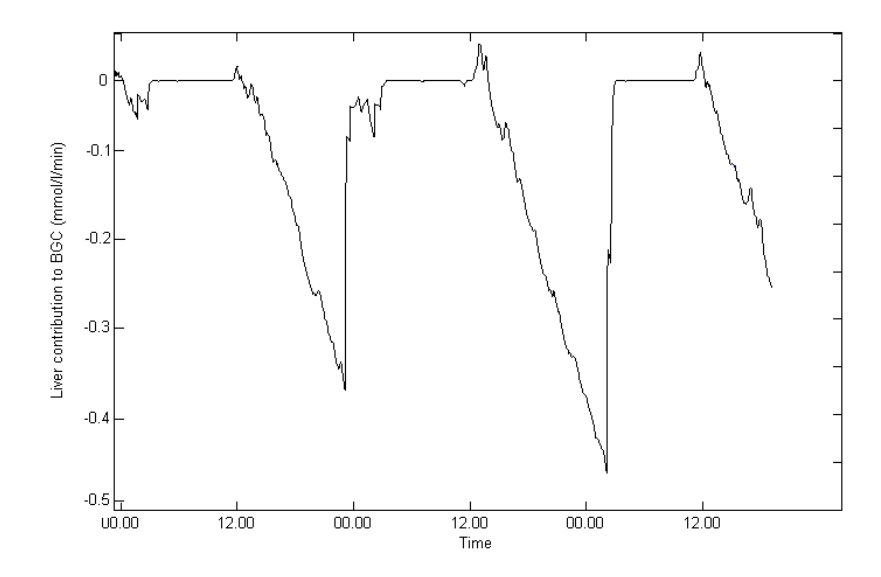


Figure 5.6: Hepatic contribution to BGC from the PA model for Subject A.

Poor model performance may be due to poor parameter estimates as a result of using data based on healthy subjects. The model is sensitive to small changes in parameter estimates; Figure 5.8 illustrates this with two different BGC profiles based on basal glucose values differing by less than 7%. It is clear, however, that the structure of the model needs revising in light of free-living data characteristics.

#### 5.2.2 Modified PA Model

The process Z was originally introduced by Roy and Parker (2007) to model the effect of physical activity on blood insulin concentration seen in two separate studies (Wolfe et al., 1986; Ahlborg et al., 1986), against which the parameters of the equations

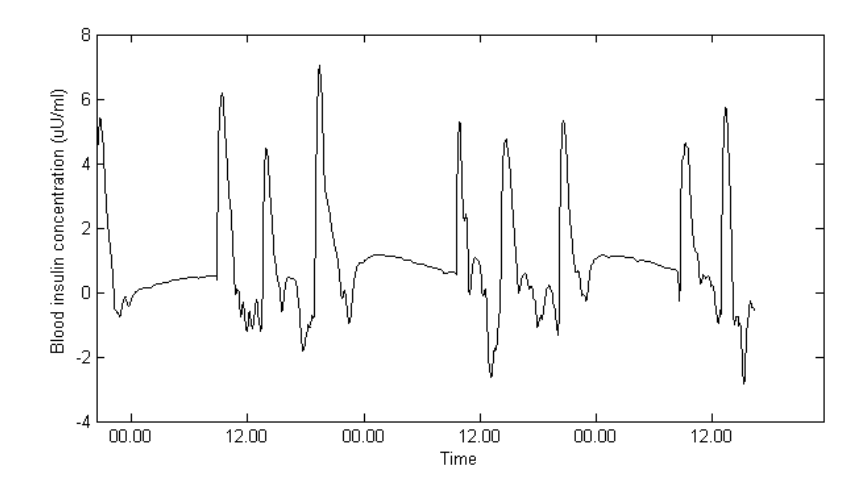


Figure 5.7: Blood insulin concentration from the PA model for Subject A.

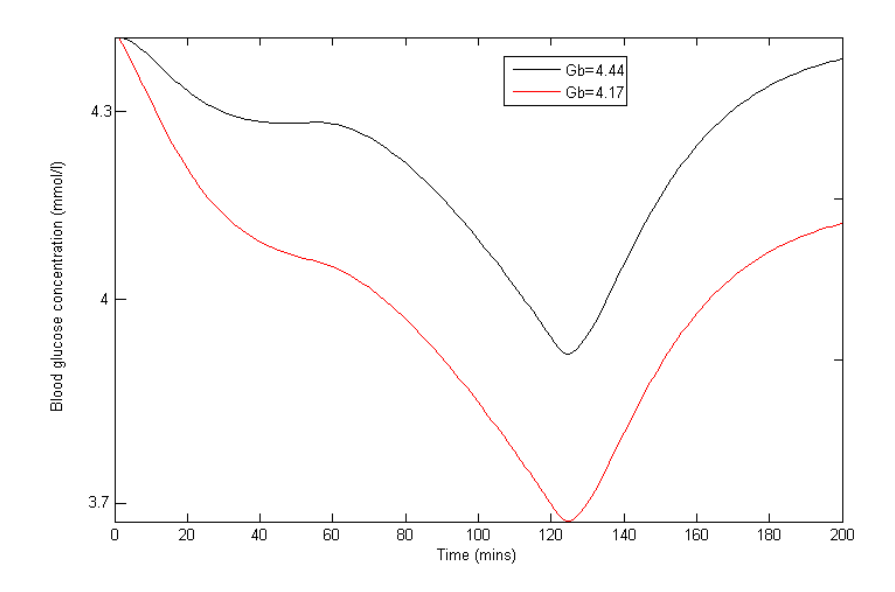


Figure 5.8: BGC profiles for two different basal glucose values,  $G_b=4.44$ mmol/l and  $G_b=4.17$ mmol/l.

in (5.1.6) were fitted and validated. The two studies were both based on healthy subjects, where the observed decrease in blood insulin concentration may be explained by decreased insulin secretion rather than increased clearance. Indeed, Zajadacz et al. (2009) reported no change in insulin clearance during activity, and Petersen et al. (2005) reported no decrease in blood insulin in subjects with diabetes during medium intensity exercise. Hence, the process Z may be modelling a non-existent phenomenon in type 1 diabetes and is therefore removed from the model.

The basal insulin term,  $I_b$ , is also removed from the insulin action DE. In the context of an individual with type 1 diabetes, the notion of a basal insulin level is not physiologically accurate. The model implies that, should blood insulin concentration drop below basal level, the flow of blood insulin into the remote compartment will decrease; however, the body can not regulate exogenous insulin. In addition, the basal

insulin term means that, in hypoinsulinaemic conditions, the insulin action can become negative.

Absorbed insulin  $(M_I)$  in the blood insulin DE is scaled by insulin distribution space, given by  $V_I$  (ml), as presented by Roy (2008, chapter 2). Absorbed insulin is therefore assumed to dissipate throughout the bloodstream, in a similar manner to that of absorbed glucose  $(M_G)$  in the blood glucose DE.

To account for the effect of renal glucose clearance, a new term is added to the blood glucose differential equation. Renal clearance, as discussed in section 2.3.1, may have significant impact on BGC during hyperglycaemia (a common occurrence in type 1 diabetes), when BGC exceeds the threshold for glucose reabsorption. A term describing renal clearance, taken from Arleth et al. (2000), is therefore added to the blood glucose DE. Renal clearance, R, is given by a moving average (MA) of a function of glomerular filtration rate, f, and blood glucose:

$$R = MA[\max(0, f \cdot G - r)],$$

where r is the maximum glucose transport rate above which reabsorption of glucose is no longer total. The moving average is of width 7 mmol/l to match literature values of the renal clearance threshold. This smooths the transition from no clearance to full clearance. The values r = 125 mmol/h and f = 7.5 l/h are also both taken from the literature. Figure 5.9 shows the renal clearance across a range of BGC according to this model.

Finally, due to the disproportionate and physiologically unrealistic influence of the process K, the decline of glycogenolysis rate will not be considered further. The model thus only represents short- to medium-term physical activity at mild to moderate intensity, where the depletion of hepatic glycogen stores has little or no effect on hepatic glucose release. The full modified model, shown in Figure 5.10, is believed to be a better reflection of the underlying physiology under these conditions. The model now comprises six DEs:

$$\dot{G}(t) = -p_1[G(t) - G_b] + (W/V_G)[H(t) - U(t) - R(t)] 
- X(t)G(t) + M_G(t)/V_G 
\dot{I}(t) = -p_2I(t) + p_3M_I(t)/V_I 
\dot{X}(t) = -p_4X(t) + p_5I(t) 
\dot{E}(t) = p_6M_E(t) - p_7E(t) 
\dot{H}(t) = p_8E(t) - p_9H(t) 
\dot{U}(t) = p_{10}E(t) - p_{11}U(t)$$
(5.2.1)

The modified PA model is still unable to accurately recreate measured BGC profiles,

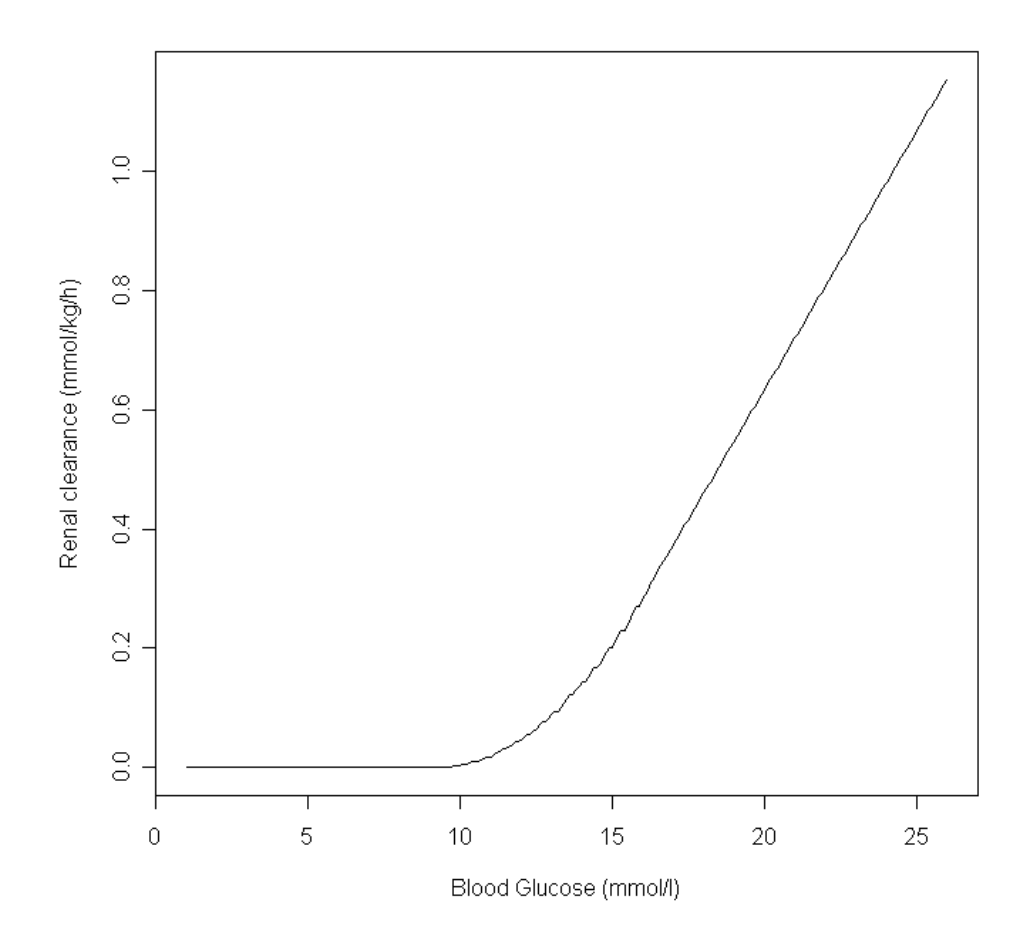


Figure 5.9: Renal clearance for a range of BGC. Recreated from Arleth et al. (2000).

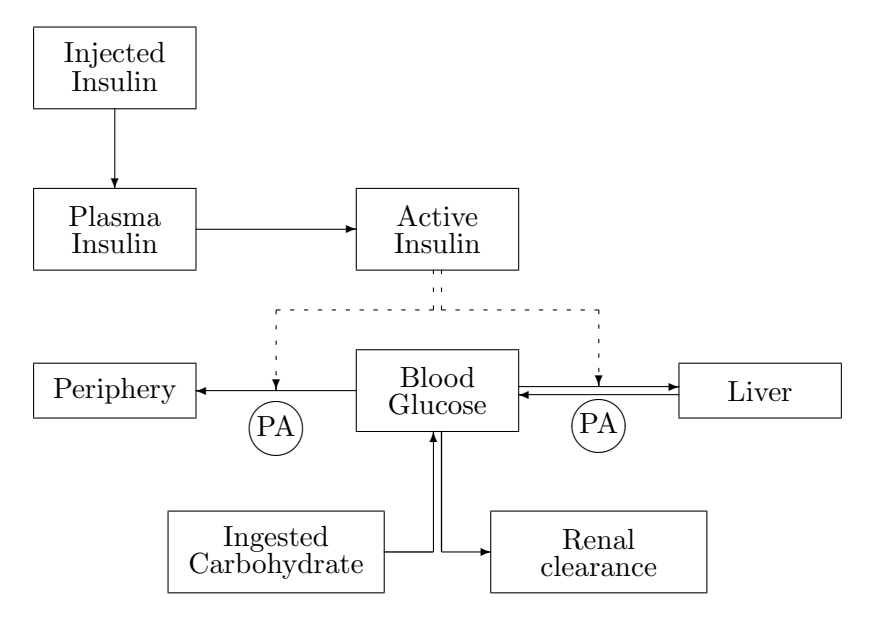


Figure 5.10: The modified physical activity model for glucose-insulin kinetics, where PA indicates the relationships affected by physical activity.

but does now return physiologically viable estimates (Figure 5.11). There remains the issue of re-estimating all model parameters, and quantifying uncertainty of the estimates. The stochastic model approach presented by Andersen and Højbjerre (2005)

allows for simultaneous estimation of all model parameters in a Bayesian framework. A stochastic model is advocated here as it is more physiologically representative of the body.

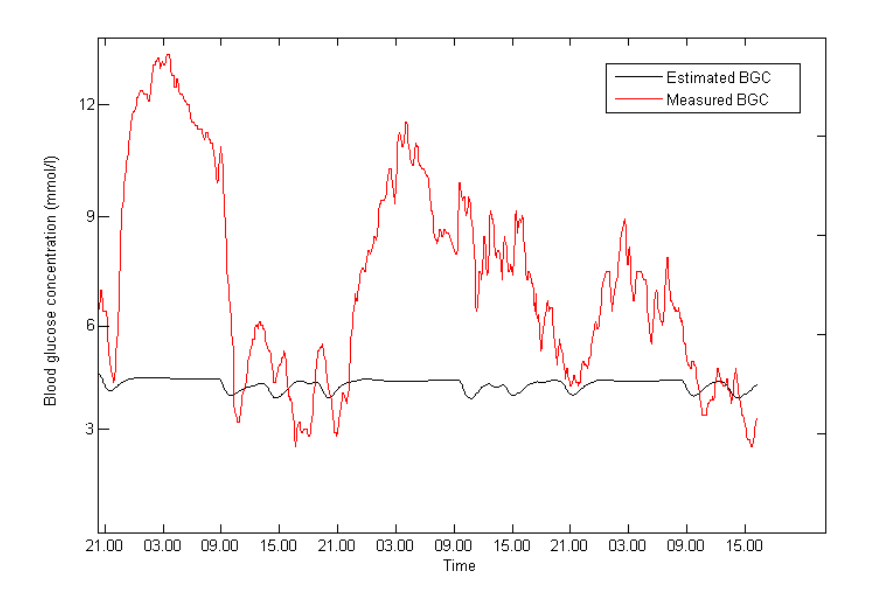


Figure 5.11: Measured BGC and modified PA model results for BGC.

### 5.3 Stochastic Modified PA Model

A stochastic version of the modified PA model is now presented (SPA model); the methods are applied here using the blood glucose DE as an example. The latent processes are first converted on to the log scale<sup>2</sup>; setting  $g(t) = \ln[G(t)], \ldots, u(t) = \ln[U(t)]$ , gives

$$\dot{g}(t) = \dot{G}(t)/G(t) = \dot{G}(t) \exp[-g(t)]$$

$$= -p_1\{1 - G_b \exp[-g(t)]\} - \exp[x(t)] + M_G(t) \exp[-g(t)]/V_G$$

$$+ (W \exp[-g(t)]/V_G)\{\exp[h(t)] - \exp[u(t)] - R(t)\}.$$

The DE is appended with a stochastic term, represented by a Wiener process,  $w_g(t)$ , with associated precision,  $\tau_g$ , to model possible deviations. By convention, such a

<sup>&</sup>lt;sup>2</sup>Theoretically, the processes H and U can be zero, where the logarithm is undefined. However, the form of the differential equations mean these processes cannot return to zero, only become so small as to be practically zero.

stochastic DE is written as:

$$dg(t) = \left\{ -p_1 \{ 1 - G_b \exp[-g(t)] \} - \exp[x(t)] + (W \exp[-g(t)]/V_G) \{ \exp[h(t)] - \exp[u(t)] - R(t) \} + M_G(t) \exp[-g(t)]/V_G \} dt + (\tau_g^{-1/2}) dw_g(t).$$

This is converted to an integral equation by integrating over a small time frame, t to  $t + \delta$ , for small  $\delta > 0$ , assumed constant here:

$$g(t+\delta) - g(t) = \int_{t}^{t+\delta} \left\{ -p_1 \{1 - G_b \exp[-g(t)]\} - \exp[x(t)] + \{W \exp[-g(t)]/V_G\} \{\exp[h(t)] - \exp[u(t)] - R(t)\} + M_G(t) \exp[-g(t)]/V_G \right\} dt + \epsilon_g(t),$$

where  $\epsilon_g(t) = \tau_g^{-1/2}[w_g(t+\delta) - w_g(t)]$ . The integral is approximated by the product of the width and the integrand evaluated at the lower limit (Euler approximation; Butcher, 2008). The model is now concerned with discrete time rather than continuous, hence a change in notation of the form  $g(t) = g_t$  and  $\epsilon_g(t) = \epsilon_{g,t}$ . The change in BGC over the time span  $\delta$  is now given by

$$g_{t+1} - g_t = \delta\{-p_1[1 - G_b \exp(-g_t)] - \exp(x_t) + [W \exp(-g_t)/V_G][\exp(h_t) - \exp(u_t) - R_t] + M_{G,t} \exp(-g_t)/V_G\} + \epsilon_{g,t+1}.$$
(5.3.1)

Standard results for a Wiener process gives  $\epsilon_{g,t+1} \sim N(0, \delta \tau_q^{-1})$ . Setting

$$f_{g,t+1} = g_t + \delta \{-p_1[1 - G_b \exp(-g_t)] - \exp(x_t) + [W \exp(-g_t)/V_G][\exp(h_t) - \exp(u_t) - R_t] + M_{G,t} \exp(-g_t)/V_G\}$$
(5.3.2)

gives  $g_{t+1} = f_{g,t+1} + \epsilon_{g,t+1}$ , and hence

$$(g_{t+1}|g_t, x_t, h_t, u_t) \sim N(f_{g,t+1}, \delta \tau_g^{-1}),$$
 (5.3.3)

ignoring for convenience the dependence of latent processes on the equation parameters. Following the same procedure for each DE in (5.2.1) gives

$$(i_{t+1}|i_t) \sim N(f_{i,t+1}, \delta \tau_i^{-1})$$

$$(x_{t+1}|x_t, i_t) \sim N(f_{x,t+1}, \delta \tau_x^{-1})$$

$$(e_{t+1}|e_t) \sim N(f_{e,t+1}, \delta \tau_e^{-1})$$

$$(h_{t+1}|h_t, e_t) \sim N(f_{h,t+1}, \delta \tau_h^{-1})$$

$$(u_{t+1}|u_t, e_t) \sim N(f_{u,t+1}, \delta \tau_u^{-1}),$$

$$(5.3.4)$$

where

$$f_{i,t+1} = i_t + \delta[-p_2 + p_3 M_{I,t} \exp(-i_t)/V_I]$$

$$f_{x,t+1} = x_t + \delta[-p_4 + p_5 \exp(-x_t) \exp(i_t)]$$

$$f_{e,t+1} = z_t + \delta[p_6 M_{E,t} \exp(-e_t) - p_7]$$

$$f_{h,t+1} = h_t + \delta[p_8 \exp e_t \exp(-h_t) - p_9]$$

$$f_{u,t+1} = u_t + \delta[p_{10} \exp e_t \exp(-u_t) - p_{11}].$$
(5.3.5)

The log of BGC measurements,  $\{g_t^*\}$ , are assumed to have measurement error modelled by white noise, with expectation equal to the underlying latent process:

$$g_t^*|(g_t, \tau_{g^*}) \sim N(g_t, \tau_{g^*}^{-1}).$$
 (5.3.6)

The DAG of the SPA model is given in Figure 5.12, and shows the conditional relationships between the latent processes.

The final stage of the process requires setting prior distributions for the equation parameters and precisions. The positive equation parameters,  $\{p_1, \ldots, p_{11}, G_b, V_G, V_I\}$ , are assumed to have a log-normal prior distribution, e.g.,

$$p_1 \sim \ln N(\mu_{p_1}, \tau_{p_1}^{-1}),$$
 (5.3.7)

where if  $X \sim \ln N(\mu, \tau^{-1})$  then

$$f(x) = \frac{\tau^{1/2}}{x\sqrt{2\pi}} \exp\left[\frac{-\tau(\ln x - \mu)^2}{2}\right],$$

with  $\mathbb{E}[X] = \exp[\mu + 1/(2\tau)]$  and  $V[X] = [\exp(\tau^{-1}) - 1] \exp(2\mu + \tau^{-1})$ . The precisions,  $\{\tau_{g^*}, \tau_g, \dots, \tau_u\}$ , are assumed to have a conditionally conjugate gamma prior distribution (for modelling convenience), e.g.,

$$\tau_g \sim G(\alpha_{\tau_g}, \beta_{\tau_g}). \tag{5.3.8}$$

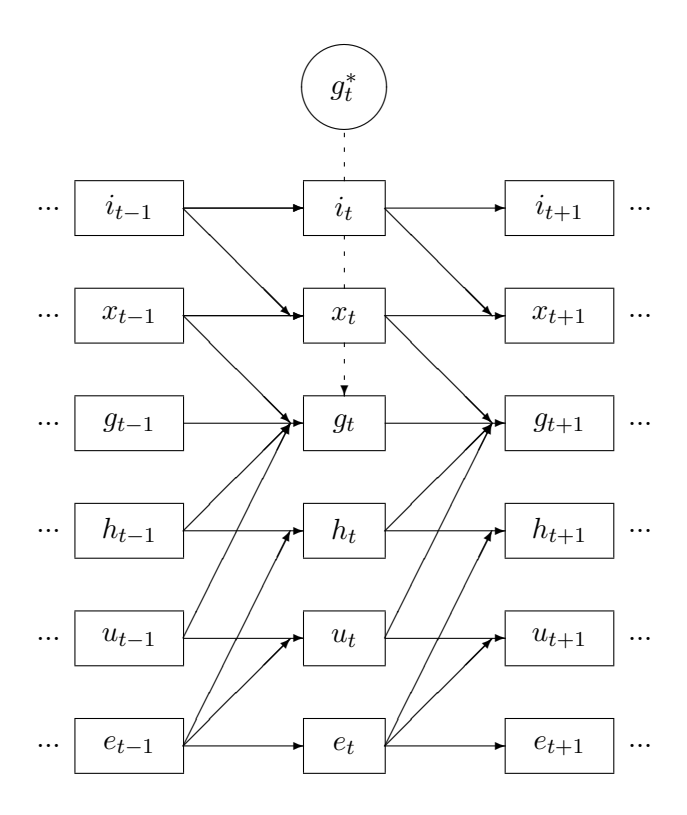


Figure 5.12: Directed acyclic graph of the extended model.

#### 5.3.1 Posterior Distribution of the SPA model

For convenience, the equation parameters, precisions and latent processes are split into three groups:

$$\begin{split} &\Omega_{1} = &\{p_{1}, p_{2}, p_{3}, p_{4}, p_{5}, p_{6}, p_{7}, p_{8}, p_{9}, p_{10}, p_{11}, G_{b}, V_{G}, V_{I}\}, \\ &\Omega_{2} = &\{\tau_{g}, \tau_{i}, \tau_{x}, \tau_{h}, \tau_{u}, \tau_{e}, \tau_{g^{*}}\}, \\ &\Phi = &\{g, i, x, h, u, e\}, \end{split}$$

with the full collection denoted by  $\boldsymbol{\theta} = \{\Omega_1, \Omega_2, \Phi\}$ . By Bayes' Theorem the full, joint posterior distribution of all unobserved quantities is given by

$$p(\boldsymbol{\theta}|\boldsymbol{g}^*) \propto p(\boldsymbol{g}^*|\boldsymbol{\theta})p(\boldsymbol{\theta})$$
$$\propto p(\boldsymbol{g}^*|\boldsymbol{\theta})p(\boldsymbol{\Phi}|\Omega_1, \Omega_2)p(\Omega_1)p(\Omega_2), \tag{5.3.9}$$

where  $\mathbf{g}^* = \{g_1^*, \dots, g_T^*\}$ . The first part of the likelihood,  $p(\mathbf{g}^*|\mathbf{\theta})$ , is determined by (5.3.6):

$$p(\boldsymbol{g}^*|\boldsymbol{\theta}) = \prod_{t=1}^T p(g_t^*|g_t, \tau_{g^*}) \propto (\tau_{g^*})^{T/2} \exp[(-\tau_{g^*}/2) \sum_{t=1}^T (g_t^* - g_t)^2].$$

The joint distribution of the latent processes (the second part of the likelihood) is:

$$p(\Phi|\Omega_1, \Omega_2) = \prod_{t=1}^{T} p(g_t|\cdot)p(i_t|\cdot)p(x_t|\cdot)p(e_t|\cdot)p(h_t|\cdot)p(u_t|\cdot)$$

where, e.g.,  $p(g_t|\cdot)$  implies the conditional distribution of  $g_t$  given all other parameters in  $\Omega_1$ ,  $\Omega_2$  and  $\phi$ . This joint distribution is determined by (5.3.2)–(5.3.5):

$$p(\Phi|\Omega_1, \Omega_2) \propto (\tau_g \tau_i \tau_x \tau_e \tau_h \tau_u \tau_y \tau_k)^{T/2} \exp\left\{-\frac{1}{2\delta} \sum_{t=1}^{T} \left[\tau_g (g_t - f_{g,t})^2 + \tau_i (i_t - f_{i,t})^2 + \tau_x (x_t - f_{x,t})^2 + \tau_e (e_t - f_{e,t})^2 + \tau_h (h_t - f_{h,t})^2 + \tau_u (u_t - f_{u,t})^2\right]\right\}$$

The final terms in the full posterior distribution are determined by (5.3.7) and (5.3.8), where

$$p(\Omega_1) = p(p_1)p(p_2)p(p_3)p(p_4)p(p_5)p(p_6)p(p_7)p(p_8)p(p_9)p(p_{10})$$

$$\times p(p_{11})p(G_b)p(V_G)p(V_I)$$

and

$$p(\Omega_2) = p(\tau_{a^*})p(\tau_a)p(\tau_i)p(\tau_x)p(\tau_e)p(\tau_h)p(\tau_u),$$

assuming independence of the parameters and precisions.

The posterior distributions for each parameter, precision and latent process may then be found. The posterior distributions for the precisions are of standard form, e.g.,

$$p(\tau_g|\cdot) \sim \text{Gamma}[\alpha_{\tau_g} + T/2, \beta_{\tau_g} + \frac{1}{2\delta} \sum_{t=1}^{T} (g_t - f_{g,t})^2],$$

and

$$p(\tau_{g^*}|\cdot) \sim \text{Gamma}[\alpha_{\tau_{g^*}} + T/2, \beta_{\tau_{g^*}} + \frac{1}{2} \sum_{t=1}^{T} (g_t^* - g_t)^2].$$

The posterior distributions of parameters in  $\Omega_1$  are not of standard form, e.g.,

$$p(p_1|\cdot) \propto p_1^{-1} \exp(-1/2\{\tau_{p_1}(\ln p_1 - \mu_{p_1}) + \frac{\tau_g}{\delta} \sum_{t=1}^T [g_t - f_{g,t}(p_1)]^2\}),$$

where  $f_{g,t}(p_1)$  highlights the fact that  $f_{g,t}$  depends on  $p_1$ . The posterior distributions of the latent processes are also not of standard form, e.g.,

for time t=0,

$$p(i_0|\cdot) \propto \exp(-\frac{1}{2\delta} \{\tau_i [i_1 - f_{i,1}(i_0)]^2 + \tau_x [x_1 - f_{x,1}(i_0)]^2 \});$$

for time  $t=1,\ldots,T-1$ ,

$$p(i_t|\cdot) \propto \exp(-\frac{1}{2\delta} \{ \tau_i (i_t - f_{i,t})^2 + \tau_i [i_{t+1} - f_{i,t+1}(i_t)]^2 + \tau_x [x_{t+1} - f_{x,t+1}(i_t)]^2 \});$$

except at time t=T,

$$p(i_T|\cdot) \propto \exp\{-\frac{1}{2\delta}[\tau_i(i_T - f_{i,T})^2]\}.$$

## 5.4 Simulation Study of MCMC and the SPA Model

Markov chain Monte Carlo (MCMC) methods (discussed in appendix C) are a well-established approach for analysing highly complex distributions (Gilks et al., 1996), such as the posterior distribution of the SPA model. A simulation study was run to test the viability of using MCMC methods to estimate the parameters of the SPA model. Parameters in  $\Omega_1$  were fixed to the values reported by Roy and Parker (2007)<sup>3</sup>, and the precisions in  $\Omega_2$  were also fixed; values are given in Table 5.3. Glucose and insulin absorption, as estimated by the digestion and insulin models, from one day of Subject A's records were used as the inputs  $M_G$  and  $M_I$ , respectively, and the same day's physical activity (METs) measurements were used as the input  $M_E$ ; these inputs are given in Figure 5.13. The conditional distributions presented in (5.3.3) and (5.3.4) were used to simulate values of the latent processes,  $\{g, i, x, e, h, u\}$ , every five minutes for one day (288 time points). Blood glucose "observations" were then simulated using (5.3.6). Given this series of observations, MCMC methods were used to estimate the parameters in  $\Omega_1$  and  $\Omega_2$ .

#### 5.4.1 Practical MCMC Considerations

Given the complexity of the model, with regard to the number of processes and parameters, the computational burden is large; to reduce this burden, the process E, and associated parameters,  $p_6$  and  $p_7$ , were treated as known. The process E describes the body's delayed response to physical activity, i.e., the delayed increase in heart rate and oxygen uptake, and introduces a lag on the impact of activity on other processes; its

 $<sup>^{3}</sup>$ The value of parameter  $p_{3}$  was altered as the value presented in Roy and Parker (2007) led to an unstable blood insulin time series.

Table 5.3: Parameter values used to generate BGC time series for simulation study.

Parameter	Value	Parameter	Value
$p_1$	0.035	$G_b$	80
$p_2$	0.142	$V_G$	117
$p_3$	0.0001	$V_{I}$	1760
$p_4$	0.05	$ au_g$	5
$p_5$	0.000028	$ au_i$	5
$p_6$	0.8	$ au_x$	5
$p_7$	0.8	$ au_h$	5
$p_8$	0.00158	$ au_u$	5
$p_9$	0.056	$ au_{g^*}$	5
$p_{10}$	0.00195		
$p_{11}$	0.0485		

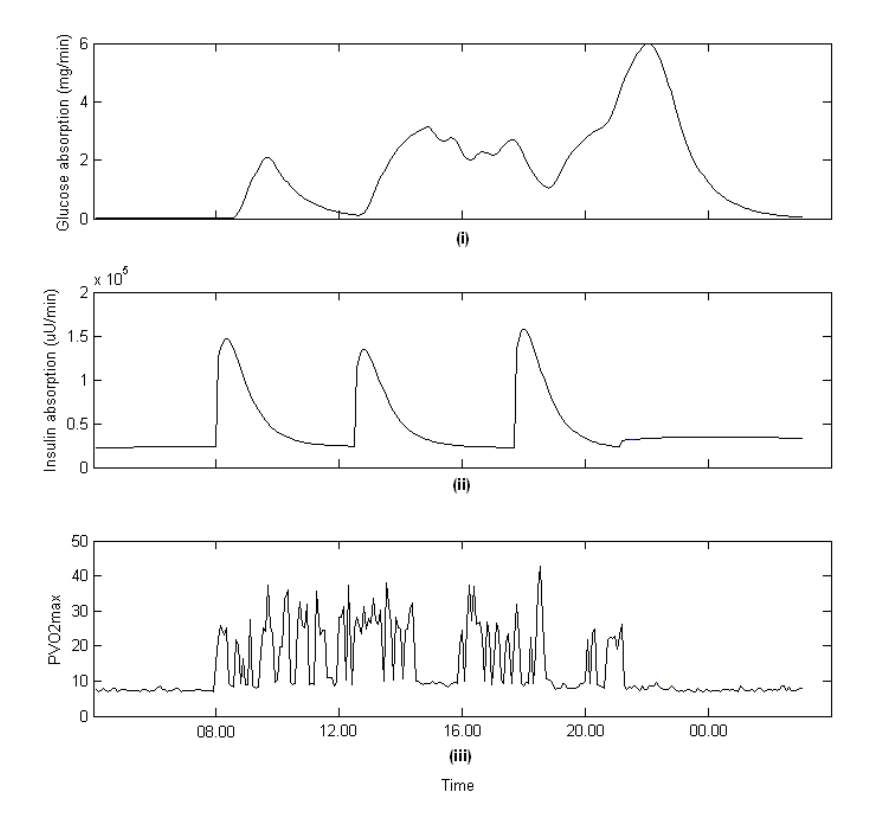


Figure 5.13: (i) Estimated glucose and (ii) insulin absorption (from the digestion and insulin models) and (iii) relative PVO<sub>2</sub><sup>max</sup> for one day of Subject A's records.

intended behaviour is therefore well understood, and it is dependent only on armband measurements. The parameters  $p_6$  and  $p_7$  were set to 0.8, as in Roy and Parker (2007), and the DE for E was solved using Simulink. Solutions at each time point were treated as known in the rest of the model.

The remaining latent processes and parameters in  $\Omega_1$  were updated using the single-component Metropolis-Hastings algorithm, while precisions were updated using Gibbs sampling. The normal distribution was chosen to be the proposal density for each

parameter in  $\Omega_1$ ,  $\Omega_2$  and  $\Phi$ , with the mean determined by the current state of the chain, i.e., for parameter  $\theta_i$ , the proposal distribution at iteration j,  $q(\cdot|\theta_i^{(j-1)})$ , is  $N(\theta_i^{(j-1)}, \lambda_i)$ , for given variance,  $\lambda_i$ , which may be tuned appropriately to return desirable acceptance rates. For sampling convenience, the equation parameters in  $\Omega_1 = \{\omega_i^{(1)}\}$ , for  $i = 1, \ldots, 12$ , were transformed using natural logarithms. This brings the scale of the parameters on to the whole real line, and ensures that a normal proposal distribution will give realistic candidates. The transformed parameters follow a normal distribution:

$$\alpha_i = \ln(\omega_i^{(1)}) \Rightarrow p(\alpha_i) = p_{\omega_i}(\alpha_i) |d\omega_i/d\alpha_i|$$
  
 $\Rightarrow \alpha_i \sim N(\mu_{\alpha_i}, \tau_{\alpha_i}^{-1}),$ 

The relationships in (5.3.2) and (5.3.5) are altered accordingly, e.g.,

$$f_{i,t+1} = i_t + \delta[-\exp(\alpha_2) + \exp(\alpha_3)M_{I,t}\exp(-i_t)].$$

The posterior distributions of the unknown parameters are not of standard form, e.g.,

$$p(\alpha_1|\cdot) \propto \exp(-\frac{1}{2} \{ \tau_{\alpha_1} (\alpha_1 - \mu_{\alpha_1})^2 + \sum_{t=1}^T \tau_g [g_t - f_{g,t}(\exp{\{\alpha_1\}})]^2 \}).$$

Generally, visual inspection of MCMC output will be used here as a guide to performance. Convergence to the stationary distribution, and hence burn-in length, is often identifiable from a trace plot of the output. Mixing can also be determined from a trace plot, as the properties of a well-mixing chain are generally well established, e.g., see Gilks et al. (1996, p. 6) for a simple demonstration. Comparison between trace plots of chains with different starting points can give further indication of mixing and convergence.

#### 5.4.1.1 Initialisation

To run MCMC, prior distributions for parameters in  $\Omega_1$  and  $\Omega_2$  must be specified, as well as starting values for the chain (which constitute iteration zero). The means of the prior distributions for the equation parameters were chosen to be the values reported by Roy and Parker (2007), and the variances were chosen to be relatively large, e.g.,

$$\alpha_1 = \ln(p_1) \sim N(\ln(0.035), 1).$$

The prior distributions of the precisions are given by

$$\tau_q \sim G(2,1),$$

a weakly-informative prior distribution without the problems associated with a gamma distribution of the form  $G(\epsilon, \epsilon)$  as  $\epsilon \to 0$  (Gelman, 2006).

Starting values for the equation parameters and precisions were chosen to be the means of their respective priors, e.g.,  $\alpha_1^{(0)} = \ln(0.035)$  and  $\tau_g^{(0)} = 2$ . The latent processes were given arbitrary starting values across all time points:  $\forall t, g_t = \ln(G_b) = \ln(80)$ ,  $i_t = -5, x_t = -5, h_t = -5,$  and  $u_t = -5.$ 

#### 5.4.1.2 Tuning

A series of pilot studies, using chains of length 5,000–10,000, were run to determine suitable variances of the proposal distributions. Variances were repeatedly tuned in order to return acceptance rates of between 0.15 and 0.5. It was found that the high correlation between successive time points in the latent processes led to occasional poor mixing; blocking of correlated parameters can help overcome this limitation, though blocking whole latent processes led to very slow convergence in this case and so was not pursued.

The pilot studies highlighted the difficulty of estimating all processes and parameters. In particular, a number of parameter estimates were highly negative, suggesting the parameters are zero on the original scale. This feature remained in a long chain; Figure 5.14 shows the trace plot for  $p_5$  from a chain of length 50,000 with burn-in 20,000. It was later established that the poor parameter estimates appeared to bias estimates of other parameters. To account for this, three parameters in  $\Omega_1$  with highly negative estimates were not included in the MCMC estimation procedure. These parameters,  $G_b$ ,  $V_G$  and  $V_I$ , represent basal glucose, glucose distribution space, and insulin distribution space, respectively, and are physical attributes that may be estimated using other methods, e.g., Hirota et al. (1999). Further pilot studies also suggested that parameters  $p_3$ ,  $p_5$ ,  $a_2$  and  $a_4$  were also highly negative. These were also omitted from the MCMC estimation procedure. For the remaining parameters, trace plots suggested a burn-in of 5,000 was acceptable for estimation; Figure 5.15 shows trace plots for  $p_1$ using three over-dispersed starting values. Chains of length 10,000 suggested posterior estimation of BGC agreed well with simulated BGC; Figure 5.16 shows estimated BGC closely matches the profile of simulated BGC.

#### 5.4.2 Results

Fifty data sets were simulated, and for each set a Markov chain, of size 10,000 with burn-in of 5,000, was run. The delayed average (equation C.1, section C.2, Appendix C) was calculated for each chain to estimate parameters in  $\Omega_1$  and  $\Omega_2$ . Corresponding 95% credible intervals were found by determining the 2.5<sup>th</sup> and 97.5<sup>th</sup> precentiles according to ascending order of the sampled values. Coverage was assessed by comparison of

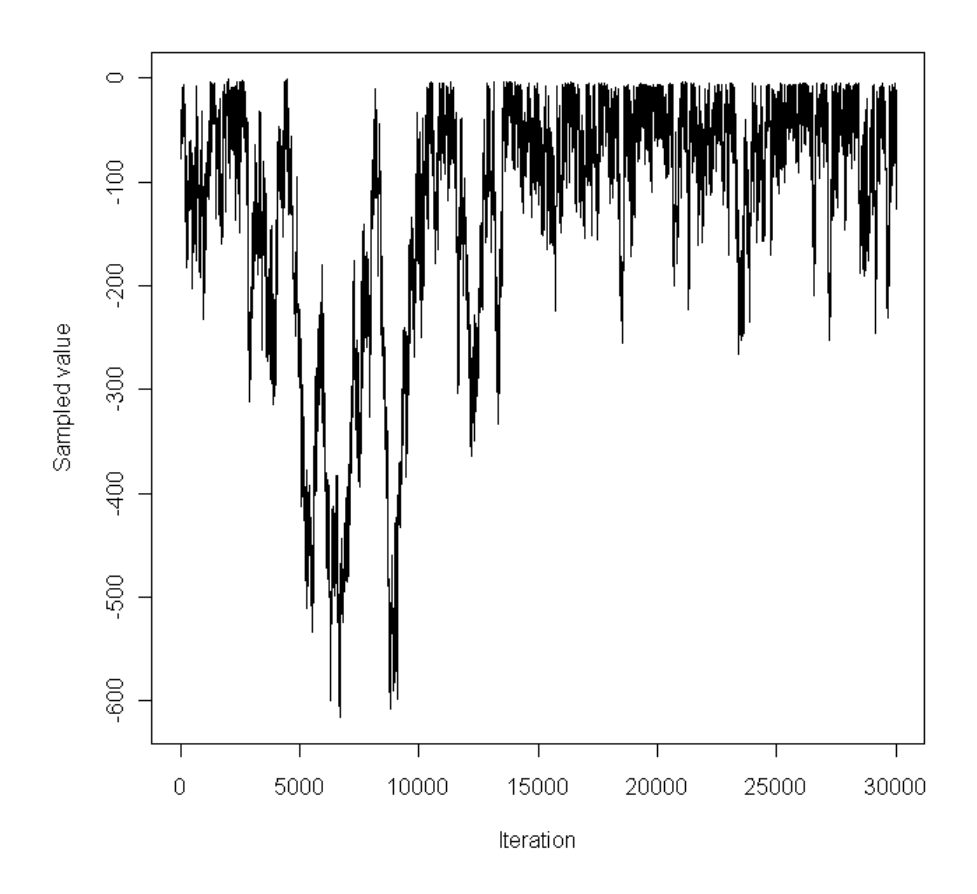


Figure 5.14: MCMC trace plot for  $p_5$  from a long chain.

credible intervals from all chains against the true parameter value (expressed as a percentage of intervals containing the true value). Comparison of the true parameter value against its respective MCMC sample means (across all chains) was used to identify bias in parameter estimates, where consistent under- or overestimation of a parameter suggests downward or upward bias, respectively.

Figures 5.17–5.19 show means and credible intervals for parameters  $p_1$ ,  $p_2$  and  $p_{10}$ , respectively, ordered by lower bound of the credible interval. Figure 5.17 suggests very good coverage of parameter  $p_1$  with the majority (90%) of credible intervals containing the parameter value used to generate the simulated BGC. Coverage for  $p_2$  is 0%, with consistent underestimation (Figure 5.18); this implies there may be issues with parameter identification, where different values of  $p_2$  can give rise to the same distribution of observations. Coverage for  $p_{10}$  is far better, though still short of ideal (Figure 5.19); this may be due to an inadequate burn-in period, where non-convergence of the chain leads to poor parameter estimation. However, time restrictions meant a larger simulation study could not be conducted to thoroughly investigate this. Results similar to those of  $p_{10}$  were seen for parameters  $p_4$  and  $p_8$ .

Figures 5.20 and 5.21 show means and credible intervals for precisions  $\tau_i$  and  $\tau_{q^*}$ ,

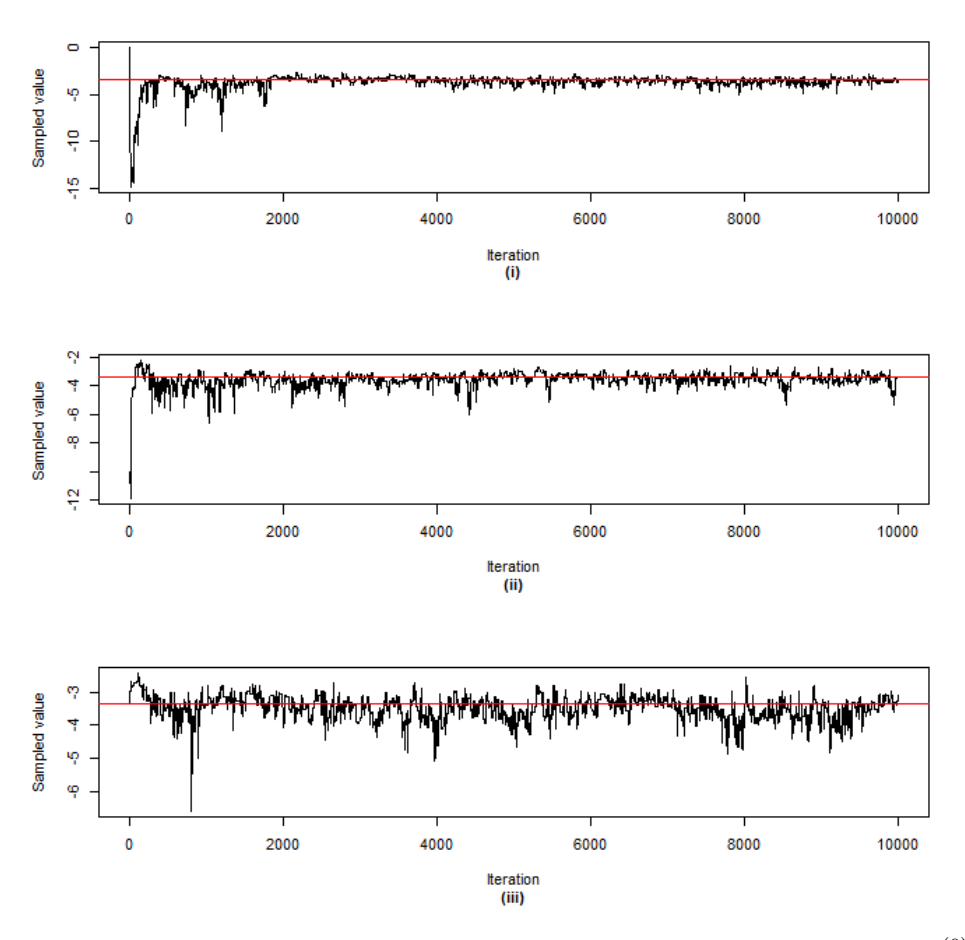


Figure 5.15: MCMC trace plots for  $p_1$  based on three different starting values: (i)  $p_1^{(0)} = 0$ , (ii)  $p_1^{(0)} = -10$  (iii)  $p_1^{(0)} = -3.35$  (the true value, as indicated by the red line in each plot).

respectively, ordered by lower bound of the credible interval. The results for  $\tau_i$  are typical of those seen for  $\tau_x$ ,  $\tau_h$  and  $\tau_u$ , with 100% coverage but a tendency for overestimation (Figure 5.20). The results for  $\tau_{g^*}$  show equally good coverage but with no obvious bias (Figure 5.21), and is similar to the results seen for  $\tau_g$ .

#### 5.4.3 Model Verification

MCMC methods may be further assessed by monitoring performance in the predictive space; this was achieved by removing a selection of BGC measurements (to be used as verification values) according to a number of scenarios:

- scenario A 25 randomly-selected measurements;
- scenario B one-hour block during early morning (when asleep);
- scenario C one-hour block after breakfast, and three-hour block after an evening meal and into the night.

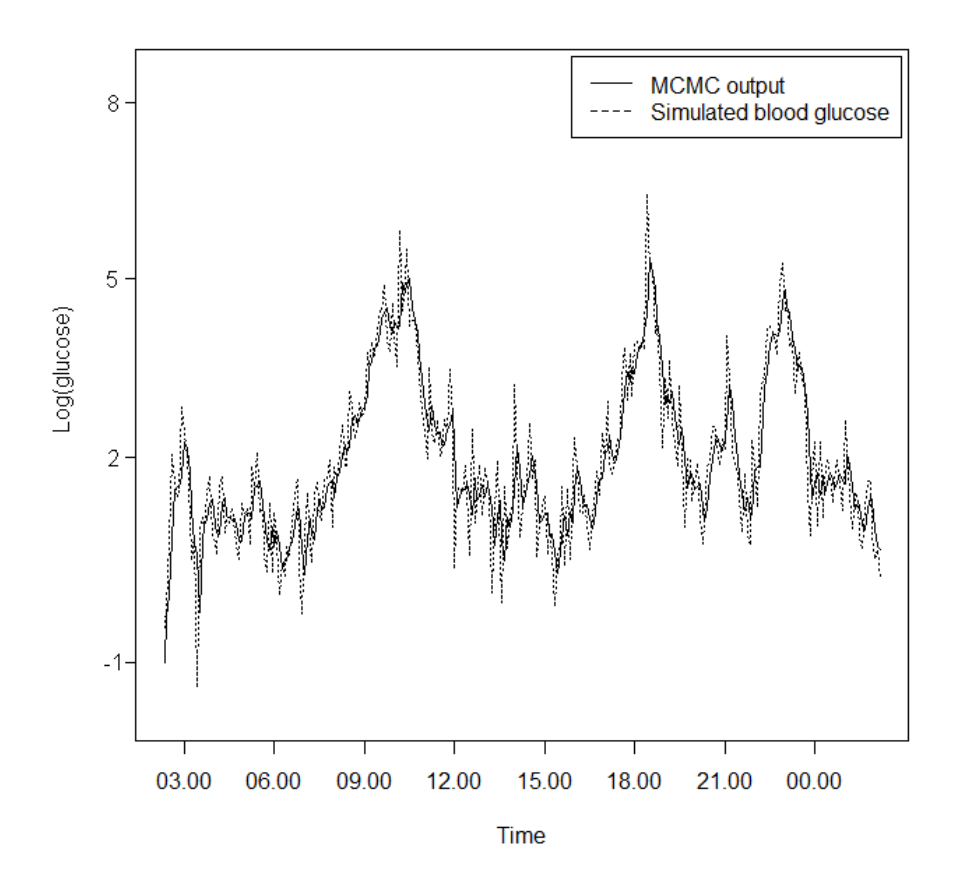


Figure 5.16: Measured BGC and MCMC output.

The MCMC methods used in the previous section were extended to sample from the distribution of BGC measurements (equation 5.3.6); Gibbs sampling was used as the conditional posterior distribution of BGC measurements is a normal distribution. Chains of size 20,000, including burn-in of 5,000, were run to determine the ability of MCMC to predict measured BGC. Starting values of the missing observations were chosen to be  $G_b = 4.44$ mmol/l.

#### **5.4.3.1** Results

For each scenario, MCMC sample means and 95% credible intervals were calculated for each missing BGC measurement. Figure 5.22 suggests good predictive performance under scenario A (random missing measurements), with the credible intervals all containing the true value, and no obvious prediction bias. Figure 5.23 shows the result for scenario B, with the credible intervals again containing the simulated BGC entirely. However, the intervals are so wide as to be of limited use in practical terms; for example an interval of (2,6) is equivalent to BGC in the range  $\sim (0.5,22)$ mmol/l, which spans much of the hypo- and hyperglycaemic range. The MCMC sample means also

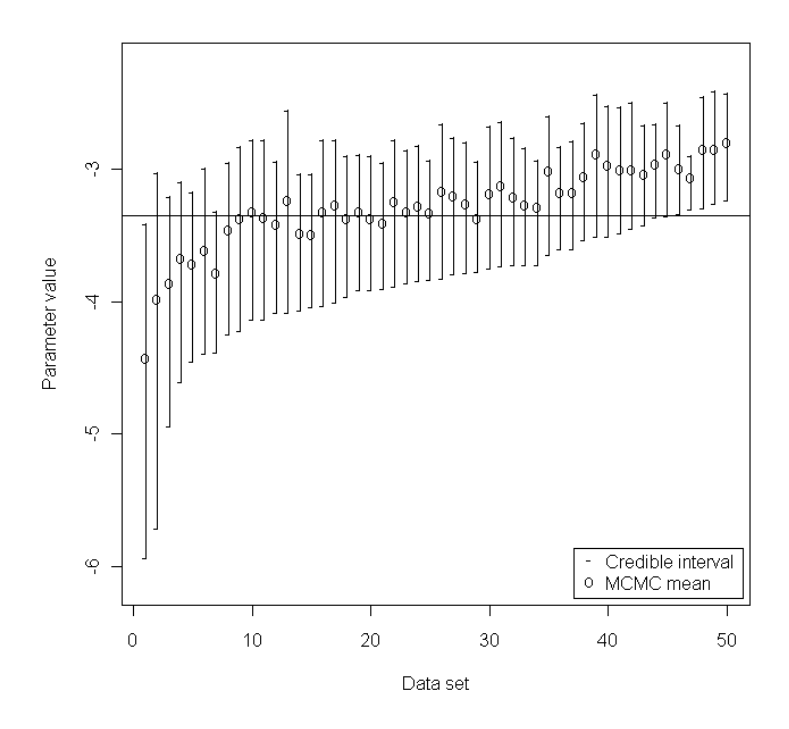


Figure 5.17: Means and 95% credible intervals for  $p_1$  from each Markov chain in the simulation study; the horizontal line represents the value of  $p_1$  used to generate the simulations.

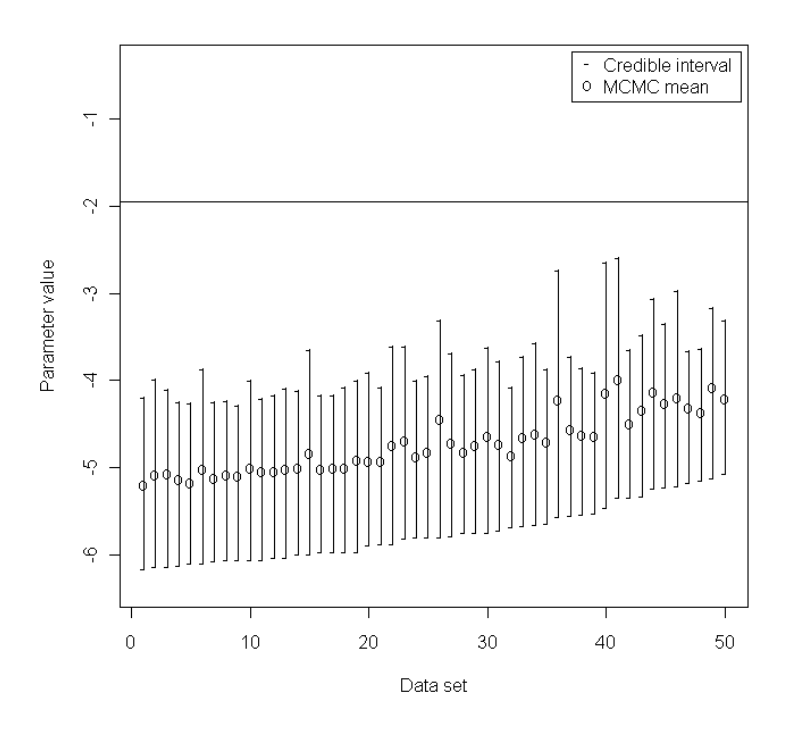


Figure 5.18: Means and 95% credible intervals for  $p_2$  from each Markov chain in the simulation study; the horizontal line represents the value of  $p_2$  used to generate the simulations.

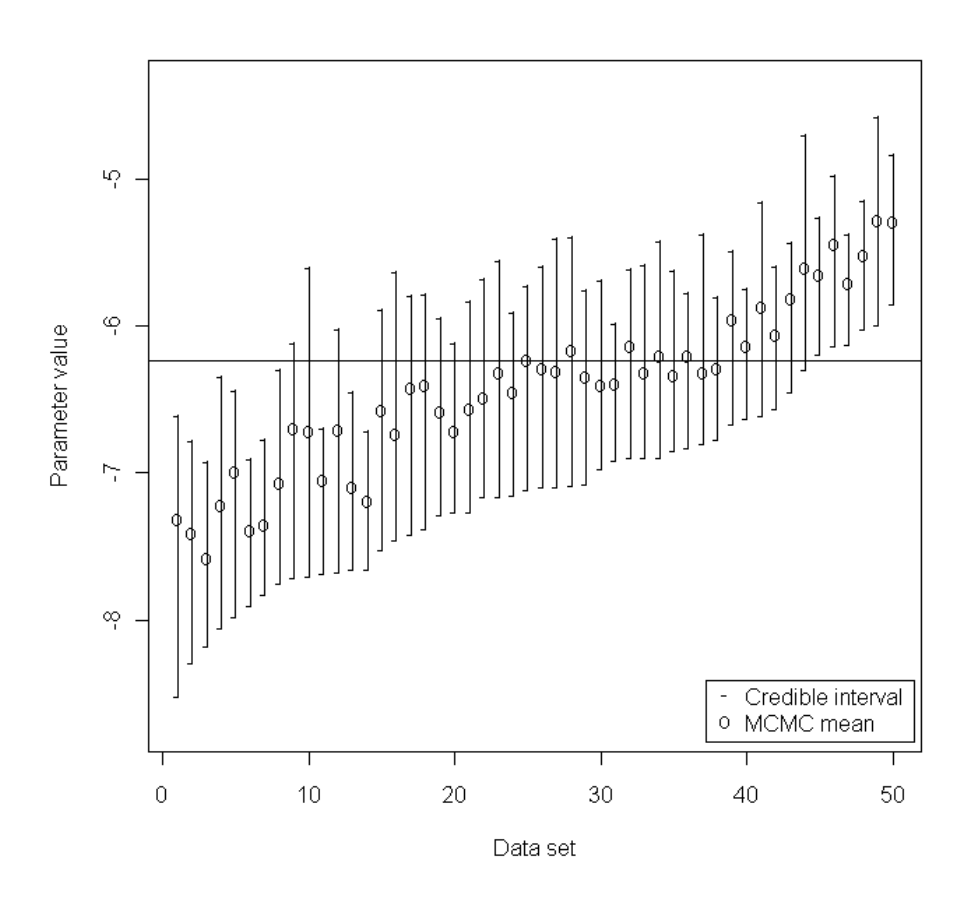


Figure 5.19: Means and 95% credible intervals for  $p_{10}$  from each Markov chain in the simulation study; the horizontal line represents the value of  $p_{10}$  used to generate the simulations.

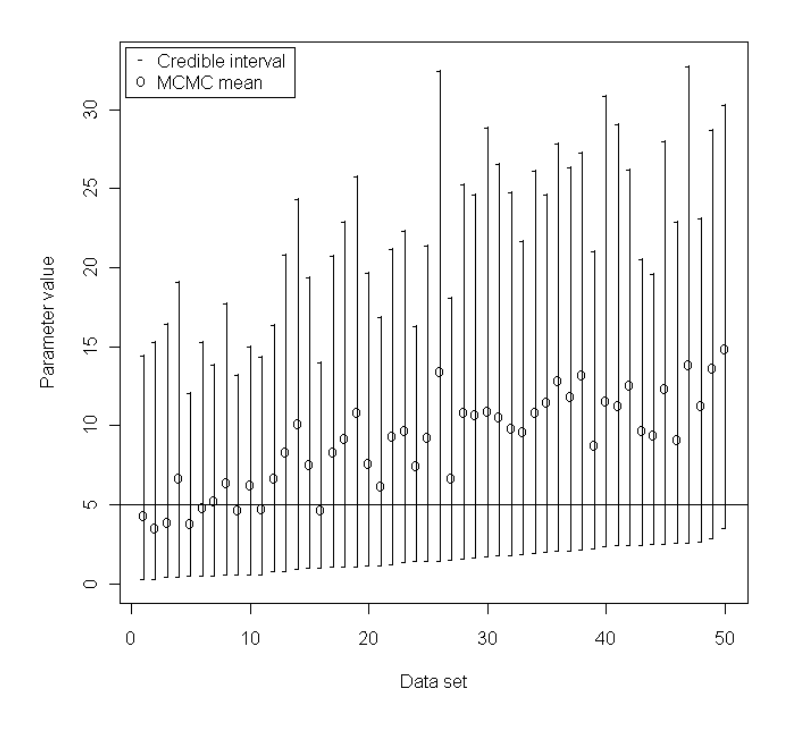


Figure 5.20: Means and 95% credible intervals for  $\tau_i$  from each Markov chain in the simulation study; the horizontal line represents the value of  $\tau_i$  used to generate the simulations.

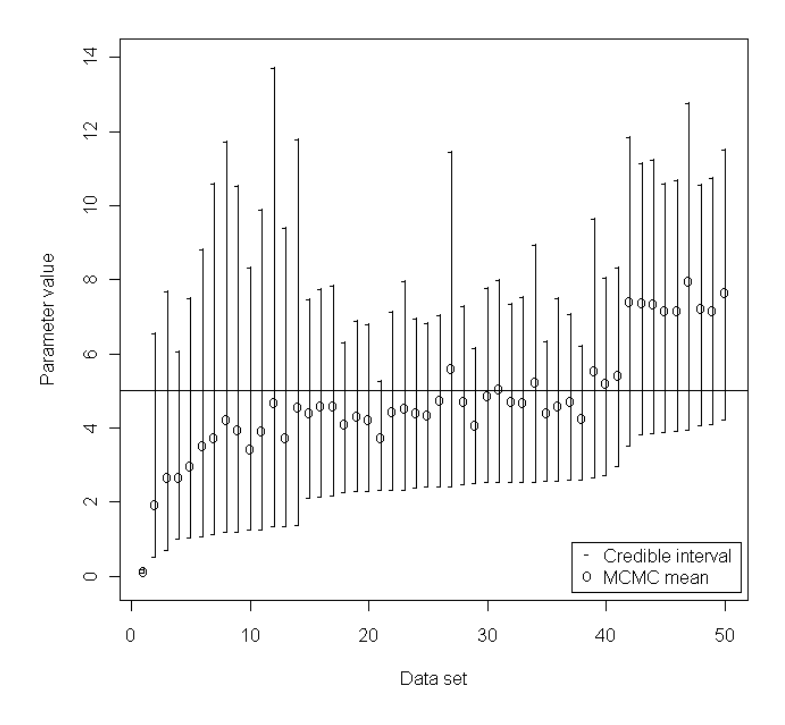


Figure 5.21: Means and 95% credible intervals for  $\tau_{g^*}$  from each Markov chain in the simulation study; the horizontal line represents the value of  $\tau_{g^*}$  used to generate the simulations.

do not appear to pick up the fluctuating nature of the simulated BGC. Figure 5.24 and 5.25 show the results for scenario C, split into blocks of verification values; these suggest that the credible intervals contain the simulated BGC almost entirely (one interval does not) but are again relatively wide. There are large discrepancies between simulated BGC and MCMC predictions at the start of both blocks of missing values, but improved performance later in the blocks.

#### 5.4.4 Robustness

Predictive performance may also be assessed by testing robustness to specification of prior distributions or misspecification of parameters. Misleading prior distributions may affect MCMC output by directing posterior distribution estimates away from the true value and toward subjective information supplied by the prior distribution; hence, MCMC estimates could be inaccurate without some form of reliable prior knowledge. Furthermore, model performance must also be robust to parameter misspecification to ensure MCMC estimates are reliable; parameters that are fixed during the MCMC estimation procedure may have been estimated using other methods, and hence contain error that could bias MCMC estimates. Predictive performance was assessed over 25 randomly-selected BGC simulated values across a number of arbitrarily-determined scenarios, involving either (misleading) informative prior distributions, parameter misspecification, or a combination:

- scenario 1 (baseline scenario) all fixed parameters kept at simulation values, prior distributions as specified in section 5.4.1.1. Other scenarios are as scenario 1 except where specified;
- scenario 2 overestimation of basal glucose (simulation value of 4.44mmol/l; fixed value of 5mmol/l);
- scenario 3 ten-fold overestimation of  $a_2$  (0.056; 0.56) and underestimation of insulin distribution space (1760ml; 1500ml);
- scenario 4 ten-fold underestimation of  $p_{11}$  (0.0485; 0.00485), prior distribution for  $p_{10}$  given by N(1,0.1);
- scenario 5 all fixed parameters kept at simulation values, with prior distributions  $\tau_g \sim G(10, 10)$  and  $\tau_i \sim G(0.1, 0.1)$ ;
- scenario 6 prior distribution  $p_1 \sim N(0.35, 3)$ ;
- scenario 7 all equation parameter prior distributions set to N(5,0.01), 100-fold overestimation of  $p_5$  (0.000028; 0.0028), ten-fold underestimation of  $p_9$  (0.056; 0.0056) and overestimation of glucose distribution space (117dl; 140dl).

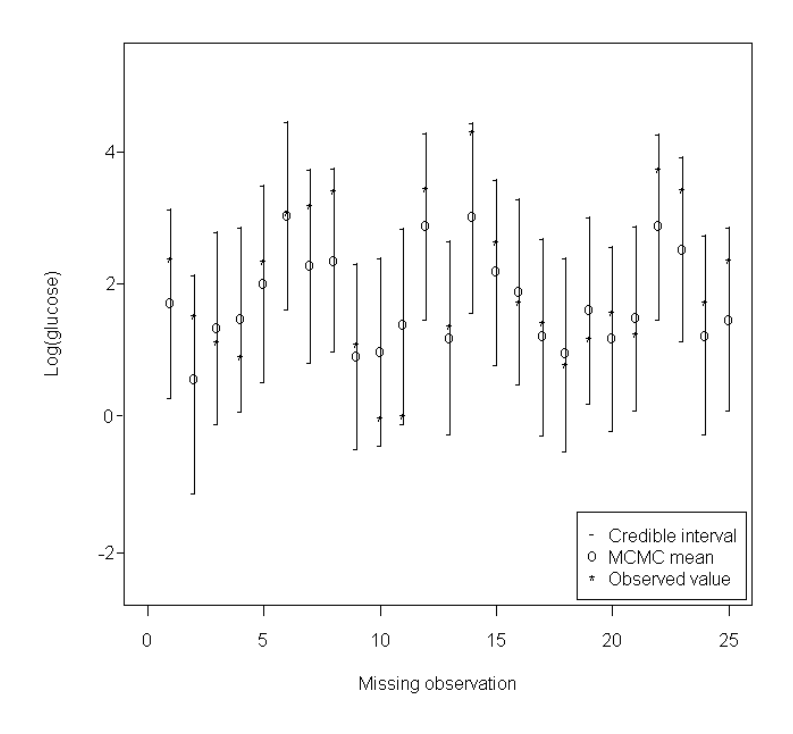


Figure 5.22: Means and 95% credible intervals for each missing observation under scenario A.

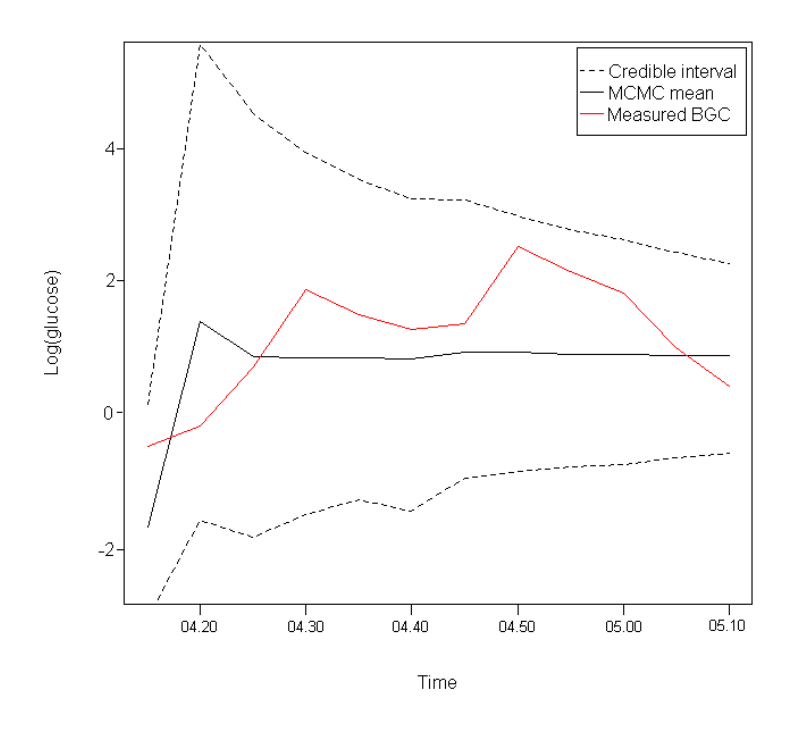


Figure 5.23: Means and 95% credible intervals for each missing observation under scenario B.

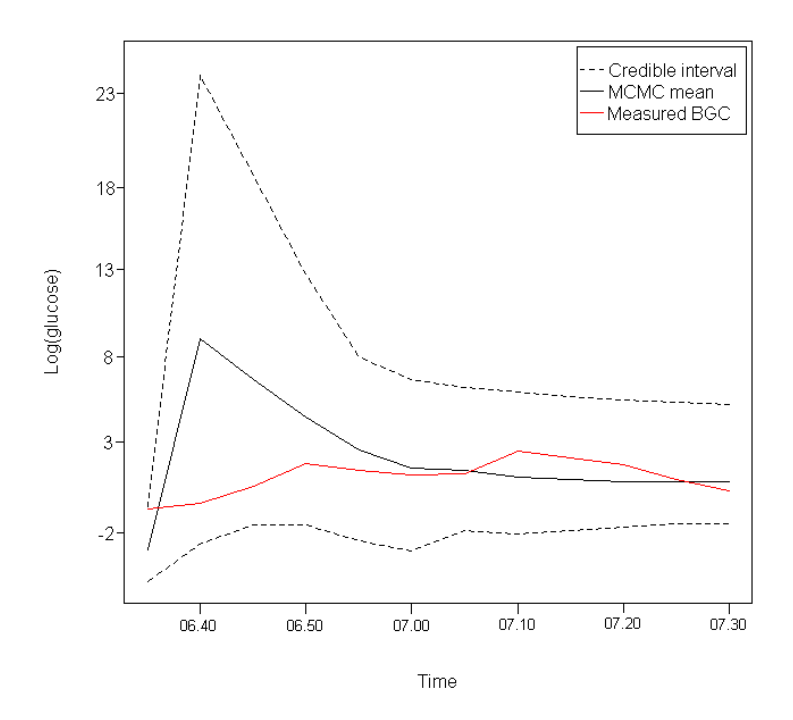


Figure 5.24: Means and 95% credible intervals for each missing observation under scenario C (first block).

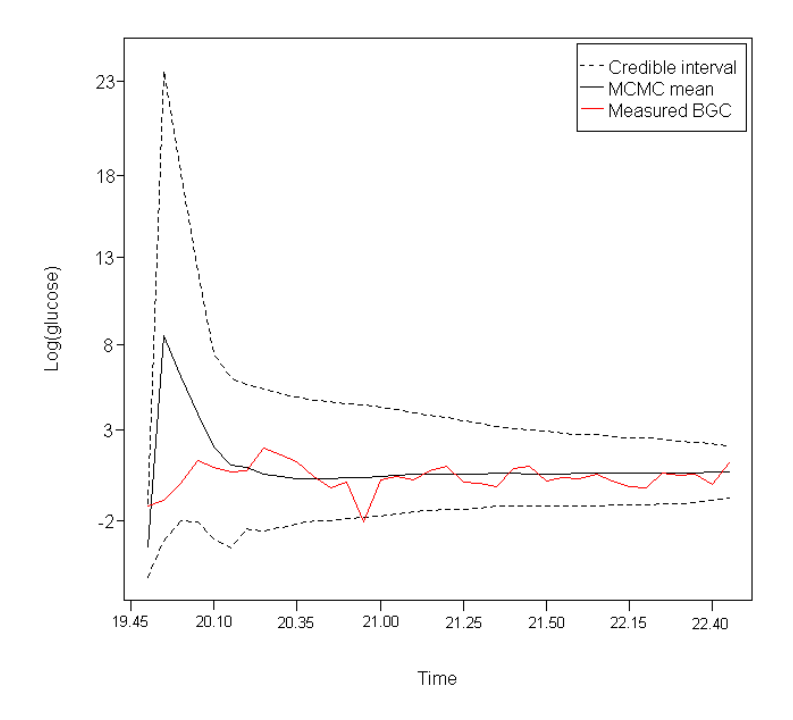


Figure 5.25: Means and 95% credible intervals for each missing observation under scenario C (second block).

The continuous ranked probability score (CRPS; section C.3.2, Appendix C) was used to compare the MCMC samples under each scenario.

#### **5.4.4.1** Results

Estimated CRPS for each of the scenarios is given in Table 5.4. CRPS is relatively consistent across the scenarios, suggesting the model is robust to misspecification of parameters and/or different specification of prior distributions. In particular, all scenarios performed at a similar level to scenario 1, suggesting, at worst, only a minor loss of predictive performance compared to the standard set-up.

Table 5.4: CRPS values under scenarios given in section 5.4.4.

Scenario	CRPS
1	0.395
2	0.397
3	0.410
4	0.393
5	0.393
6	0.400
7	0.412

#### 5.4.5 Conclusions

The feasibility of using MCMC methods to analyse the proposed Bayesian network has been demonstrated. MCMC was unable to identify all parameters simultaneously, but was able to estimate most parameters with good coverage. Precisions had 100% coverage, but there was evidence of upward bias for the precisions of processes i, x, hand u. The parameter  $p_1$  was generally well estimated by MCMC with good coverage and no obvious bias; parameters  $p_4$ ,  $p_8$  and  $p_{10}$  had lower coverage, though MCMC sample means were for the most part within 10% of the true value. Again, there was no obvious bias in estimates. MCMC estimates of parameter  $p_2$  were, in contrast, downwardly biased, with consistent underestimation of the parameter. This may be due to the complex form of the posterior distribution causing issues with parameter identification, where different values of  $p_2$  can give rise to the same observation distributions. Parameter  $p_2$  relates to clearance of blood insulin, and affects the distribution of BGC observations via the active insulin and blood glucose equations. It is possible that the effect of  $p_2$  is attributed to other parameters in this pathway, so its role is attenuated and hence underestimated by MCMC. It is interesting to note that only one parameter from  $\Omega_1$  in each of the original DEs (5.2.1) could be adequately estimated. Again, this may be due to issues with parameter identification.

MCMC methods were verified by testing performance in the predictive space under a number of scenarios with missing BGC values; credible intervals almost entirely contained the simulated BGC, although MCMC means did not always reproduce the fluctuating nature of the simulated BGC. MCMC methods also appeared to be robust to specification of prior distributions and parameter misspecification, suggesting the methods can produce reliable estimates even if misleading information is included in the estimation procedure.

### 5.5 Summary

In this chapter, modern, computationally-intensive statistical methods for analysis of a glucose-insulin compartmental model were presented. The methods were proposed as a new approach to analysing compartmental models in the diabetes literature, which play an important role in the development of the artificial pancreas. A new compartmental model was derived from the physical activity minimal model presented by Roy and Parker (2007), with modifications to enhance the physiological plausibility and to ensure the model was valid for data collected in free-living conditions. The modified model was converted to a Bayesian network (the SPA model), which expresses the relationship of a number of physiological processes via conditional probability distributions, to better reflect the uncertainty inherent in the glucoregulatory system. The network was analysed using MCMC methods, a well-established approach for analysing highly complex distributions.

A simulation study was run to determine the ability of the proposed approach to estimate parameters of the SPA model and predict missing BGC observations, where fifty data sets were generated to test MCMC coverage across parameter estimates. MCMC was implemented using both Gibbs sampling (where conditional posterior distributions were of standard form) and the Metropolis algorithm. It was found that MCMC was unable to accurately determine estimates for all parameters, perhaps due to issues with parameter identification (which may be caused by model formulation). Parameters whose estimates were far removed from their true value were removed from the MCMC estimation procedure; for the remaining parameters, MCMC was generally able to produce good estimates. Precisions were generally overestimated but had total coverage, while coverage for other parameters was lower but with no obvious bias in most cases. MCMC performance in the predictive space was tested under a number of scenarios, involving parameter misspecification and misleading informative prior distributions; variation in performance was relatively small (as measured by CRPS) suggesting robustness to situations where incorrect information is supplied to the estimation procedure.

## Chapter 6

## Conclusions and Future Work

#### 6.1 Conclusions

This thesis investigated the use of free-living data and new modelling techniques to improve current and potential treatment regimes for type 1 diabetes. The disease is associated with increased morbidity and mortality due to the imperfections of insulin therapy; better understanding of blood glucose concentration (BGC) under typical daily stimuli can improve BGC control by either providing support and education for individuals or helping realise the goal of an artificial pancreas. The current work presented a unique, free-living data set from a Diabetes UK study, and used mathematical and statistical methods for the purpose of building generic and personalised models capable of describing and/or predicting BGC. Time series of BGC were analysed to determine any short- or long-term structure that might be exploited for predictive purposes. Predictive models of BGC, based on food, insulin and physical activity, were tested over four hours to determine their suitability for inclusion in the MDI regime, as a tool for describing the profile of BGC between finger-prick tests. Finally, a descriptive model derived from the literature was tested using free-living data, raising important practical and theoretical modelling issues for an artificial pancreas, and new methods were proposed for parameter estimation and analysis of semi-empirical compartmental models.

#### 6.1.1 Contributions

Chapter 2 presented a review of diabetes literature, highlighting the lack of free-living data and empirical modelling approaches. In this context, the data from the Diabetes UK study, as presented in chapter 3, offered a unique opportunity to explore the behaviour of BGC under the influence of food intake, insulin injections and physical activity in free-living conditions. Analysis of BGC in the time domain confirmed results presented previously in the literature, with regard to the non-stationarity and

short-term dependence of BGC measurements. Short-term dependence was found to vary between and within individuals. An AR model was used to describe BGC, with predictions based only on previous measurements of BGC. The model was able to predict accurately over five minutes, but failed to capture BGC dynamics over several hours. Analysis in the frequency domain investigated for the first time the possibility of exploiting periodicities in BGC for predictive purposes. The spectral densities of BGC time series were approximated using a periodogram; variation in BGC was found to be concentrated at lower frequencies, but no notable periodicities were evident.

Chapter 4 introduced DLMs as a new method for modelling BGC, due to their ability to describe non-stationary time series, and account for time-varying parameters and varying measurement accuracy. Food and insulin diary records were used to estimate glucose and insulin absorption profiles, respectively, using physiological models in the literature, and used as inputs to the DLMs, along with physical activity armband measurements. DLMs were used to predict the profile of BGC for up to four hours ahead. They were found to be suitable for short-term prediction, and able to detect periods of hypo- and hyperglycaemia. However, predictions over four hours were inaccurate, due to the linear structure of the models and/or the inability of the model to account for the effect of other physiological processes. Furthermore, it was found that parameter estimates did not comply with established physiological behaviour. This may be due to modelling the effect of glucose and insulin absorption on BGC as immediate, with no longer-term influence on stimulating/suppressing metabolic processes. In this context, it was not appropriate to make inference regarding the role of physical activity.

Chapter 5 considered a more physiologically-representative compartmental model as a tool for descriptive modelling of BGC. A glucose-insulin model (PA model) composed of differential equations (DEs) was taken from the literature and tested using the free-living data, and was found to return physiologically-unrealistic results. This highlights potential flaws in compartmental models based on data from healthy subjects, whose performance has not been tested with free-living data. This suggests that control algorithms (designed to be included in an artificial pancreas) developed and tested using simulations from other compartmental models are not realistically challenged with such data. A modified version of the PA model was presented for further use; the new model included inputs for food, insulin and physical activity, as well as a term for renal clearance. The set of DEs was converted to a Bayesian network (SPA model) to better represent the underlying physiology, with the relationships between physiological processes determined by conditional distributions. MCMC was then proposed as a method for analysing the complex posterior distribution of the SPA model. A simulation study found that MCMC methods were able to estimate most parameters in the SPA model with good coverage. MCMC performance in the predictive space was found to be robust to the specification of prior distributions and misspecification

#### 6.2 Future Work

The role of physical activity in the behaviour of BGC is highly complex; this is particularly true for individuals with type 1 diabetes, whose response is complicated by unregulated insulin. Under- or overdosing of insulin compromises the entire glucoregulatory system, and the level of impairment depends on the discrepancy between the current and ideal plasma insulin concentrations. Thus, the response to physical activity will vary depending on plasma insulin concentration as well as the characteristics (type, intensity, duration) of physical activity. The role of blood insulin concentration for different activity characteristics, both immediate and longer-lasting, needs to be established to better represent the role of physical activity in the behaviour BGC.

Empirical models of BGC, such as those used in the current work, require accurate descriptions of post-prandial glucose absorption, insulin absorption and physical activity. However, taking into account all the effects of these external influences detracts from the advantage of DLMs, given their rapid computation, and simple and easily-understood nature. It is possible the performance of DLMs (from both a predictive and descriptive perspective) may be improved by the introduction of lags to better reflect the physiology; this is certainly true in the case of insulin, where absorption into the blood is a precursor to its actual effect on BGC. The Tarin et al. (2005) model may also be used to describe plasma, hepatic and interstitial insulin concentrations (albeit without consideration of the effects of exercise), which may offer more relevant information to a DLM.

The current work highlighted a number of practical and theoretical issues related to free-living data. In particular, the physical activity data was found to be highly fluctuating. It is yet to be understood which features of such data must be captured in order to better understand the behaviour of BGC. For example, highly fluctuating data may be smoothed, but this may lose peaks (and troughs) which have physiological importance.

The SPA model presented in chapter 5 does not take into account the decline in rate of glycogenolysis during prolonged activity; the process was removed from the original PA model as it caused physiologically unrealistic results with free-living data. Further work may investigate new approaches for including this process in the model, and hence extend the model's practical use to long periods of exercise where the effect of depleting the liver's glycogen stores becomes more apparent. The decline in glycogenolysis rate, as modelled by Roy and Parker (2007), is dependent on integrated activity passing a certain threshold, whereas it may be more realistic to have this threshold depend on both energy expenditure and energy intake from food. The processes H and U,

representing hepatic glucose release and muscular glucose uptake due to activity, may be better represented by a mixture model, where the processes take a value of zero with probability p or follow a log-normal distribution with probability 1-p.

Sequential Monte Carlo (SMC) methods are an alternative method to MCMC for analysing the posterior distribution of the SPA model. Doucet et al. (2001) suggest that SMC is better suited to estimation of recursive problems, as it considers the sequence of conditional distributions rather than the entire posterior distribution. Once a suitable estimation procedure is found, the SPA model, as presented in (chapter 5), may be applied to individuals from the DUK study. The behaviour of latent variables may be explored and compared to expected behaviour according to established physiology.

The stochastic approach advocated in chapter 5 may also be extended to a population model. The relationship of parameter estimates and physical characteristics may also be explored, using the all the data collected in the DUK study; e.g., the proportion or distribution of fat in the body may be related to certain parameters. With longer-term assessment, the effects of changes in lifestyle could be related to changes in parameter estimates.

### 6.3 Summary

The contributions of the current work to the body of knowledge may be summarised as:

- a unique free-living data set was presented, highlighting the highly fluctuating nature of physical activity data;
- frequency analysis of BGC data did not present any exploitable periodicities for the purposes of predicting BGC;
- DLMs were presented as an empirical approach to modelling BGC, using glucose and insulin absorption (estimated by models in the literature), and physical activity data as explanatory variables. The results suggest that predicting BGC over periods of several hours is not possible using the current inputs;
- compartmental models based on simulated data, or data from healthy volunteers, may not be able to handle free-living data, and can return physiologically non-viable estimates. This suggests that proposed control algorithms, as part of an artificial pancreas, are not being realistically challenged by current models;
- a new compartmental model of the body was presented, bringing together models of digestion, insulin absorption, and renal clearance;

- a stochastic version of the new compartmental model was also presented, to better reflect the underlying physiology. Bayesian methods were used to simultaneously estimate model parameters and define person-specific models;
- MCMC methods for parameter estimation and BGC prediction were tested in a simulation study. The methods were suitable for a subset of parameters, and predictions of BGC were robust to misleadingly informative prior distributions and parameter misspecification.

# Appendix A

# Bayesian Methods

Bayesian methodology differs to classical statistical approaches by treating unknown parameters as random variables, with appropriate probability distributions used to represent uncertainty. The methods make use of Bayes' Theorem, which states that, for a given set of data,  $\mathbf{y} = (y_1, \dots, y_n)$ , with a probability density function,  $p_Y(\mathbf{y}; \boldsymbol{\theta})$ , described by an unknown parameter set,  $\boldsymbol{\theta} = (\theta_1, \dots, \theta_p)$ :

$$p_{\boldsymbol{\theta}}(\boldsymbol{\theta}|\boldsymbol{Y}=\boldsymbol{y}) = \frac{p_{Y}(\boldsymbol{y}|\boldsymbol{\theta})p_{\boldsymbol{\theta}}(\boldsymbol{\theta})}{\int_{\boldsymbol{\theta}} p_{Y}(\boldsymbol{y}|\boldsymbol{\theta})p_{\boldsymbol{\theta}}(\boldsymbol{\theta})d\boldsymbol{\theta}}.$$

The normalising constant in the denominator is the marginal distribution,  $p_Y(y)$ . It does not involve  $\theta$  and so is not of particular interest compared to the form of the numerator. Instead, the above is often presented as

$$p_{\theta}(\theta|Y=y) \propto p_Y(y|\theta)p_{\theta}(\theta).$$
 (A.1)

The term  $p_{\theta}(\theta)$  is the prior distribution of the parameter set. This represents all known information about the parameters prior to observing the data,  $\mathbf{y}$ . The term  $p_Y(\mathbf{y}|\theta)$  is the likelihood function of the parameter set given the data. The left-hand side of (A.1) is the posterior distribution of the parameters. This represents the updated information on the parameters having observed the data. New information on parameters, e.g., from further observations, can easily be assimilated into previous knowledge using the relationship between the prior and posterior distributions.

The choice of prior distribution allows subjective input into the process, and may incorporate any previously established information. Vague prior distributions may be used if little or no information is known *a priori*. When the prior and posterior distributions are of the same functional form, i.e., from the same family of distribution, the prior distribution is said to be conjugate to the likelihood. In such a setting only the parameters of the prior distribution change in the updating procedure, hence simplifying computation.

## Appendix B

## Double-Discount DLM Structure

Given the single-discount approach described in section 4.1.4.1 and equation 4.1.3, let any changes due to a second discount factor be denoted with the superscript  $(\delta)$ . Furthermore, assume  $\delta = 1$  for up to and including time t - 1, and  $\delta_t \in (0, 1)$ . Then the point estimate of  $\sigma_t^2$  in the double-discount model is

$$S_t^{(\delta)} = \frac{\delta_t d_{t-1} + S_{t-1} e_t^2 / Q_t}{\delta_t n_{t-1} + 1},$$

differing from the single-discount model only by the scaling of  $n_{t-1}$  and  $d_{t-1}$  by  $\delta_t$ . The posterior estimate for the variance of the parameters is also different:

$$\boldsymbol{C}_{t}^{(\delta)} = (S_{t}^{(\delta)}/S_{t-1})(\boldsymbol{R}_{t} - \boldsymbol{A}_{t}\boldsymbol{A}_{t}^{\mathrm{T}}Q_{t}) 
= (S_{t}^{(\delta)}/S_{t})\boldsymbol{C}_{t}.$$
(B.1)

Let  $N_t = (1/S_{t-1})(R_t - A_t A_t^{\mathrm{T}} Q_t)$ , which is the same for the single- and double-discount model. At time t+1 the above changes feed into the prior variance for the parameters and the forecast variance:

$$\mathbf{R}_{t+1}^{(\delta)} = (1/\lambda) \mathbf{C}_{t}^{(\delta)} 
= (1/\lambda) S_{t}^{(\delta)} \mathbf{N}_{t}, 
Q_{t+1}^{(\delta)} = \mathbf{X}_{t+1}^{\mathrm{T}} \mathbf{R}_{t+1}^{(\delta)} \mathbf{X}_{t+1} + S_{t}^{(\delta)} 
= S_{t}^{(\delta)} [(1/\lambda) \mathbf{X}_{t+1}^{\mathrm{T}} \mathbf{N}_{t} \mathbf{X}_{t+1} + 1].$$

The adaptive vector,  $A_{t+1}$ , however, remains unchanged:

$$\mathbf{A}_{t+1}^{(\delta)} = \mathbf{R}_{t+1}^{(\delta)} \mathbf{X}_{t+1} / Q_{t+1}^{(\delta)}$$

$$= [(1/\lambda) S_t^{(\delta)} \mathbf{N}_t \mathbf{X}_{t+1}] / S_t^{(\delta)} [(1/\lambda) \mathbf{X}_{t+1}^{\mathrm{T}} \mathbf{N}_t \mathbf{X}_{t+1} + 1]$$

$$= \mathbf{A}_{t+1},$$

as the  $S_t^{(\delta)}$  terms cancel. Hence

$$\mathbf{C}_{t+1}^{(\delta)} = (S_{t+1}^{(\delta)}/S_{t}^{(\delta)})(\mathbf{R}_{t+1}^{(\delta)} - \mathbf{A}_{t+1}^{(\delta)}(\mathbf{A}_{t+1}^{(\delta)})^{\mathrm{T}}Q_{t+1}^{(\delta)}) 
= S_{t+1}^{(\delta)}\{(1/\lambda)\mathbf{N}_{t} - \mathbf{A}_{t+1}^{(\delta)}(\mathbf{A}_{t+1}^{(\delta)})^{\mathrm{T}}[(1/\lambda)\mathbf{X}_{t+1}^{\mathrm{T}}\mathbf{N}_{t}\mathbf{X}_{t+1} + 1]\} 
= (S_{t+1}^{(\delta)}/S_{t+1})\mathbf{C}_{t},$$

exactly as in (B.1) but for t + 1. Note that  $S_t < S_t^{(\delta)}$  if

$$\frac{d_{t-1} + (d_{t-1}/n_{t-1})(e_t^2/Q_t)}{n_{t-1} + 1} < \frac{\delta d_{t-1} + (d_{t-1}/n_{t-1})(e_t^2/Q_t)}{\delta n_{t-1} + 1}$$

$$\Leftrightarrow \delta(e_t^2/Q_t - 1) < e_t^2/Q_t - 1$$

$$\Leftrightarrow |e_t/\sqrt{Q_t}| > 1.$$

The structure of the DLM implies that  $(e_t|D_{t-1}) \sim T_{n_{t-1}}(0,Q_t)$ , and so  $e_t/\sqrt{Q_t}$ , the standardised error, follows a standard  $T_{n_{t-1}}$  distribution. If the standardised error is outside the range (-1,1), which for large enough n is equivalent to one standard deviation from the mean, then the model adapts by increasing the point estimate of the observation error variance. Otherwise the point estimate will decrease, and hence artificially decreases the prediction interval of the forecast.

# Appendix C

## Sampling-Based Methods

Bayesian inference involves assessing the properties of posterior distributions, which may involve evaluating very complex integrals. For example, determining the expectation of a function of the parameters,  $g(\theta)$ , requires finding

$$\mathbb{E}[g(\boldsymbol{\theta}|Y)] = \frac{\int g(\boldsymbol{\theta})p(\boldsymbol{\theta})p(Y|\boldsymbol{\theta})d\boldsymbol{\theta}}{\int p(\boldsymbol{\theta})p(Y|\boldsymbol{\theta})d\boldsymbol{\theta}},$$

whose analytic evaluation, even approximately, may be impossible. A common approach to this problem is to use sampling based methods such as Markov Chain Monte Carlo (MCMC).

## C.1 Monte Carlo Integration

Monte Carlo integration uses random samples to evaluate integrals. For a given sample,  $\{\theta^{(i)}\}\$ , for i=1,...,n, from  $p(\theta|Y)$ , the expectation of  $g(\theta|Y)$  is estimated by the sample mean:

$$\mathbb{E}[g(\theta|Y)] \approx \frac{1}{n} \sum_{i=1}^{n} g(\theta^{(i)}).$$

Given independence of the  $\theta^{(i)}$ , the desired accuracy of the approximation may be achieved by choosing an appropriate value for n. However, it is not always possible to draw independent  $\theta^{(i)}$ . Dependent samples may instead be used to derive estimates of the characteristics of the population distribution if they are approximately distributed as the desired distribution; Markov chains are a method for achieving this.

### C.2 Markov Chains

A sequence,  $\{\theta^{(i)}\}$ , for i = 1, ..., n, is a Markov chain if it is generated from a distribution,  $p(\cdot|\cdot)$ , known as the transition kernel, with the property

$$p(\theta^{(i+1)}|\theta^{(i)}, \theta^{(i-1)}, \dots, \theta^{(1)}, \theta^{(0)}) = p(\theta^{(i+1)}|\theta^{(i)}).$$

Under appropriate conditions, the chain will forget its initial value,  $\theta^{(0)}$ , and converge to a unique stationary distribution,  $\pi(\cdot)$  (Gilks et al., 1996). A Markov chain thus generates dependent samples from  $\pi(\cdot)$  as n increases. Taking into account the time taken for the chain to forget its initial state (burn-in), the expectation is approximated by the delayed average,

$$\frac{1}{n-m} \sum_{i=m+1}^{n} g(\theta^{(i)}), \tag{C.1}$$

where values prior to burn-in time, m, are discarded. Markov chains may be constructed in a number of ways, discussed in the following sections. Monte Carlo estimation based on a Markov chain is known as MCMC.

### C.2.1 Metropolis-Hastings Algorithm

The Metropolis-Hastings (MH) algorithm is a general method for constructing a Markov chain with the desired stationary distribution. Defining  $\pi(\theta)$  to be the distribution of interest,  $q(\cdot)$  to be a proposal distribution, and the acceptance probability,  $\alpha$ , as:

$$\alpha(\theta, Z) = \min\left(1, \frac{\pi(Z)q(\theta|Z)}{\pi(\theta)q(Z|\theta)}\right),$$

the algorithm proceeds as follows:

- i) define iteration 0 (arbitrary starting point,  $\theta^{(0)}$ ), and set i = 0;
- ii) sample candidate, Z, from the proposal distribution,  $q(\cdot)$ ;
- iii) sample u from a standard uniform distribution, U(0,1);
- iv) set  $\theta^{(i+1)} = Z$  if  $\alpha(\theta^{(i)}, Z) > u$ , else  $\theta^{(i+1)} = \theta^{(i)}$ ;
- v) i = i + 1, return to step ii).

The algorithm is the Hastings (1970) generalisation of the method proposed in Metropolis et al. (1953). Originally the Metropolis approach considered only symmetric proposal distributions, where  $q(\theta|Z) = q(Z|\theta)$ , giving an acceptance probability of

$$\alpha(\theta, Z) = \min\left(1, \frac{\pi(Z)}{\pi(\theta)}\right). \tag{C.2}$$

The MH method works for any proposal distribution,  $q(\cdot)$ , but certain choices offer preferable results in terms of convergence (time taken to reach the stationary distribution) and mixing (how quickly samples explore the support of the stationary distribution). Hence identifying appropriate forms for the proposal distributions can minimise computation. Further details and wider discussion of the Metropolis-Hastings algorithm may be found in Gilks et al. (1996).

Often it is preferable to update  $\boldsymbol{\theta}$  component-wise rather than as a whole. This is known as single-component Metropolis-Hastings (SCMH). If the vector  $\boldsymbol{\theta}$  is divided into d components of possibly differing dimensions,  $\boldsymbol{\theta} = \{\theta_1, ..., \theta_d\}$ , then an iteration of SCMH involves d updating steps. Defining  $\theta_j^{(i)}$  to be the state of parameter  $\theta_j$  at the end of iteration i, step j of the  $(i+1)^{th}$  iteration involves updating  $\theta_j^{(i)}$ . A candidate,  $Z_j$ , is generated from a proposal,  $q_j(Z_j|\theta_j^{(i)},\boldsymbol{\theta}_{-j}^{(i+1)})$ , where  $\boldsymbol{\theta}_{-j}^{(i+1)} = \{\theta_1^{(i+1)},...,\theta_{j-1}^{(i+1)},\theta_{j+1}^{(i)},...,\theta_h^{(i)}\}$  is the vector of most recently sampled values of  $\boldsymbol{\theta}$ . The acceptance probability is given by

$$\alpha(Z_j; \theta_j^{(i)}, \boldsymbol{\theta}_{-j}^{(i+1)}) = \min\left(1, \frac{\pi(Z_j | \boldsymbol{\theta}_{-j}^{(i+1)}) q_j(\theta_j^{(i)} | Z_j, \boldsymbol{\theta}_{-j}^{(i+1)})}{\pi(\theta_j^{(i)} | \boldsymbol{\theta}_{-j}^{(i+1)}) q_j(Z_j | \theta_j^{(i)}, \boldsymbol{\theta}_{-j}^{(i+1)})}\right).$$
(C.3)

The term  $\pi(\theta_j^{(i)}|\boldsymbol{\theta}_{-j}^{(i+1)})$  is the full conditional distribution of  $\theta_j^{(i)}$  conditioning on  $\boldsymbol{\theta}_{-j}^{(i+1)}$ , given by

$$\pi(\theta_j^{(i)}|\boldsymbol{\theta}_{-j}^{(i+1)}) = \frac{\pi(\boldsymbol{\theta})}{\int \pi(\boldsymbol{\theta})d\theta_j^{(i)}}.$$
 (C.4)

The form of  $\boldsymbol{\theta}_{-j}^{(i+1)}$  presented here implies the elements of  $\boldsymbol{\theta}$  are updated sequentially, though this need not necessarily be the case. Correlated parameters may be updated as a group using SCMH to improve convergence and mixing, a process known as blocking.

### C.2.2 Gibbs Sampling

The Gibbs sampler (Geman and Geman, 1984) is a special case of SCMH with proposal distribution

$$q_j(Z_j|\theta_j, \boldsymbol{\theta}_{-j}) = \pi(Z_j|\boldsymbol{\theta}_{-j}), \tag{C.5}$$

where  $\pi(Z_j|\boldsymbol{\theta}_{-j})$  is the full conditional distribution as in (C.4). Gibbs sampling involves sampling from the full conditional distribution, and is most suitable when this is easily done. Substituting (C.5) into (C.3) gives an acceptance probability of one, hence Gibbs candidates are always accepted. Again, the order of updating may be random and need not necessarily involve all components during each iteration.

## C.3 Implementing MCMC

Assessing the performance of MCMC helps ensure that estimates derived from its output are appropriate. Practical considerations such as choice of starting values, length of burn-in, length of chain, and the number of chains are discussed in detail in Gilks et al. (1996), with many related references within. Valid inference based on MCMC output requires convergence of the chain to the stationary distribution, and a satisfactory sample size depends on a suitable chain length (including burn-in) and good mixing so that the entire support of the distribution is explored. Numerous diagnostics exist for determining convergence, with sometimes conflicting advice, e.g., Gelman and Rubin (1992) recommend running multiple chains, while Geyer (1992) recommends one long chain. No diagnostic has gained widespread recognition as a standard test for convergence; instead, a combination has been recommended (Cowles and Carlin, 1996). However, the large computational burden of MCMC introduces issues of time, resource and storage restrictions, meaning this is not always feasible.

#### C.3.1 Proposal Density

Given the computational intensity of MCMC, it is important to construct efficient chains that converge quickly to the stationary distribution and mix well. This involves consideration of the relationship between the proposal and stationary distributions, and the ease with which the proposal is sampled from. Often the scale of the proposal density (e.g., the variance of a normal distribution) must be specified. Gelman et al. (1996) recommend, in the case of a multivariate normal target distribution, the scale is tuned to return acceptance rates for candidates (i.e., candidates accepted divided by total number of iterations) of between 0.15–0.5. If the scale is too large, the algorithm will frequently choose values in low probability areas, returning a low acceptance rate; the chain will thus not move for many iterations and will require a large number of iterations to fully explore the target distribution. If the scale is too small, the algorithm will choose values in nearby high probability areas and so move frequently, returning a large acceptance rate; the chain will thus move in very small steps and will again require a large number of iterations to explore the target distribution.

#### C.3.2 Verification

Verification of MCMC performance may be assessed in a number of ways. Mean square error (MSE) and mean absolute deviation (MAD) are two general methods for assessing model performance which compare estimates to their true value. In the case of MCMC, this involves comparing a measure of the MCMC samples, e.g., the mean or median, to their respective verification values; for a set of parameters,  $\{\theta_i\}$ ,  $i = 1, \ldots, p$ , with

a measure of the associated MCMC sample,  $f(\theta_i)$ , and respective verification values,  $\{y_i\}$ ,

MSE = 
$$\frac{1}{p} \sum_{i=1}^{p} (f(\theta_i) - y_i)^2$$

and

MAD = 
$$\frac{1}{p} \sum_{i=1}^{p} |f(\theta_i) - y_i|$$
.

The continuous ranked probability score (CRPS) accounts for the entire predictive distribution rather than a single measure of an MCMC sample. CRPS compares the cumulative distribution function (cdf) of a set of MCMC samples to that of a verification value, and is defined as

$$CRPS(F, y) = -\int_{-\infty}^{\infty} [F(\theta) - \mathbb{I}(\theta \ge y)]^2 d\theta,$$

where  $F(\cdot)$  is the cdf of the MCMC samples and  $\mathbb{I}(x)$  is an indicator function taking the value of one if the argument, x, is true, and zero otherwise. This may be evaluated as (Gneiting and Raftery, 2007)

$$CRPS(F, y) = \frac{1}{2} \mathbb{E}_F |\theta^{(i)} - \theta^{(j)}| - \mathbb{E}_F |\theta^{(i)} - y|,$$

where  $\theta^{(i)}$  and  $\theta^{(j)}$  are two independent samples of a random variable with common cdf,  $F(\cdot)$ . This may be approximated by

$$C\hat{RPS}(F,y) = \frac{1}{n} \sum_{i=1}^{n} |\theta^{(i)} - y| - \frac{1}{2n^2} \sum_{i=1}^{n} \sum_{\substack{j=1\\j \neq i}}^{n} |\theta^{(i)} - \theta^{(j)}|,$$
 (C.1)

for a chain of length n. For p verification values, the overall CRPS is given by

$$C\hat{RPS}_p = \frac{1}{p} \sum_{i=1}^p CRPS(F_i, y_i).$$
 (C.2)

Smaller values of CRPS are preferred as this indicates the predictive cdf is closer to the observed cdf.

## References

- Abdul-Rasoul, M., Habib, H. and Al-Khouly, M. (2006) 'The honeymoon phase' in children with type 1 diabetes mellitus: frequency, duration, and influential factors. *Pediatric Diabetes*, 7, 101–107.
- Abu-Rimleh, A. and Garcia-Gabin, W. (2010) Feedforward-feedback multiple predictive controllers for glucose regulation in type 1 diabetes. *Computer Methods and Programs in Biomedicine*, **99**, 113–123.
- Agar, B. U., Erzen, M. and Cinar, A. (2005) Glucosim: Educational software for virtual experiments with patients with type 1 diabetes. In *Proceedings of the 2005 IEEE Engineering in Medicine and Biology Society, 27th Annual Conference.*
- Ahlborg, G., Wahren, J. and Felig, P. (1986) Splanchnic and peripheral glucose and lactate metabolism during and after prolonged arm exercise. *Journal of Clinical Investigation*, **77**, 690–699.
- Ainsworth, B. E., Haskell, W. L., Whitt, M. C., Irwin, M. L., Swartz, A. M., Strath, S. J., O'Brien, W. L., R., B. J. D., Schmitz, K. H., Emplaincourt, P. O., Jacobs Jnr., D. R. and Leon, A. S. (2000) Compendium of physical activities: an update of activity codes and MET intensities. *Medicine & Science in Sports & Exercise*, 32, S498S504.
- Akesen, E., Turan, S., Guran, T., Atay, Z., Save, D. and Bereket, A. (2011) Prevalence of type 1 diabetes mellitus in 6-18-yr-old school children living in Istanbul, Turkey. *Pediatric Diabetes*, **12**, 567–571.
- Akirav, E., Kushner, J. A. and Herold, K. C. (2008) Beta-cell mass and type 1 diabetes: Going, going, gone? *Diabetes*, **57**, 2883–2888.
- Andersen, K. E. and Højbjerre, M. (2005) A population-based Bayesian approach to the minimal model of glucose and insulin homeostasis. *Statistics in Medicine*, **24**, 2381–2400.
- Andre, D., Pelletier, R., Farringdon, J., Safier, S., Talbott, W., Stone, R., Vyas, N., Trimble, J., Wolf, D., Vishnubhatla, S., Boehmke, S., Stivoric, J. and Teller, A.

- (2006) The development of the Sensewear<sup>TM</sup> armband, a revolutionary energy assessment device to assess physical activity. *Body Media Inc.*
- Arleth, T., Andreassen, S., Federici, M. O. and Benedetti, M. M. (2000) A model of the endogenous glucose balance incorporating the characteristics of glucose transporters. Computer Methods and Programs in Biomedicine, 62, 219–234.
- Bantle, J. P., Neal, L. and Frankamp, L. M. (1993) Effects of the anatomical region used for insulin injections on glycaemia in type 1 diabetes subjects. *Diabetes Care*, **16**, 1592–1597.
- Bellazzi, R., Larizza, C., Magni, P., Montani, S. and Nicolao, G. D. (1999) Intelligent analysis of clinical time series by combining structural filtering and temporal abstractions. *Artificial Intelligence in Medicine*, **1620**, 261–270.
- Bellazzi, R., Nucci, G. and Cobelli, C. (2001) The subcutaneous route to insulindependent diabetes therapy. *IEEE Engineering in Medicine and Biology*, **51**, 54–64.
- Berger, M., Cuppers, H. J., Hegner, H., Jorgens, V. and Berchtold, P. (1982) Absorption kinetics and biologic effects of subcutaneously injected insulin preparations. *Diabetes Care*, **5**, 77–91.
- Bergman, R. N., Ider, Y. Z., Bowden, C. R. and Cobelli, C. (1979) Quantitative estimation of insulin sensitivity. *American Physiological Society*, **236**, 667–677.
- Bergman, R. N., Phillips, L. S. and Cobelli, C. (1981) Physiologic evaluation of factors controlling glucose tolerance in man. *Journal of Clinical Investigation*, **68**, 1456–1467.
- Bliss, M. (1982) The Discovery of Insulin. University of Chicago Press.
- Bloomfield, P. (1976) Fourier Analysis of Time Series: An Introduction. John Wiley & Sons.
- Bolie, V. W. (1961) Coefficients of normal blood glucose regulation. *Journal of Applied Physiology*, **16**, 783–788.
- Bolstad, W. M. (1988) The multiprocess dynamic linear model with biased perturbations: A real time model for growth hormone level. *Biometrika*, **75**, 685–692.
- Bremer, T. and Gough, G. A. (1999) Is blood glucose predictable from previous values? A solicitation for data. *Diabetes*, **48**, 445–451.
- Breton, M. and Kovatchev, B. (2008) Analysis, modeling, and simulation of the accuracy of continuous glucose sensors. *Journal of Diabetes and Science Technology*, **2**, 853–862.

- Breton, M. D. (2008) Physical activity the major unaccounted impediment to closed loop control. *Journal of Diabetes Science and Technology*, **2**, 169–174.
- Breton, M. D., Shields, D. P. and Kovatchev, B. P. (2008) Optimum subcutaneous glucose sampling and Fourier analysis of continuous glucose monitors. *Journal of Diabetes Science and Technology*, **2**, 495–500.
- Buse, J. B., Weyer, C. and Maggs, D. G. (2002) Amylin replacement with pramlintide in type 1 and type 2 diabetes: A physiological approach to overcome barriers with insulin therapy. *Clinical Diabetes*, **20**, 137–144.
- Butcher, J. C. (2008) Numerical Methods for Ordinary Differential Equations. Wiley, second edn.
- Carter, C. K. and Kohn, R. (1994) On Gibbs sampling for state space models. *Biometrika*, **81**, 541–553.
- van Cauter, E., Polonsky, K. S. and Scheen, A. J. (1997) Roles of circadian rhythmicity and sleep in human glucose regulation. *Endocrine Reviews*, **18**, 716–738.
- Cavan, D. A., Hejlesen, O. K., Hovorka, R., Evans, J. A., Metcalfe, J. A., Cavan, M. L., Halim, M., Andreassen, S., Carson, E. R. and Sonksen, P. H. (1999) Preliminary experience of the DIAS computer model in providing insulin dose advice to patients with insulin dependent diabetes. *Computer Methods and Programs in Biomedicine*, 56, 157–164.
- Cengiz, E. and Tamborlane, W. V. (2009) A tale of two compartments: Interstitial versus blood glucose monitoring. *Diabetes Technology & Therapeutics*, **11**, S11–S16.
- Cerny, F. J. and Burton, H. W. (2001) Exercise Physiology for Health Care Professionals. Human Kinetics Europe Ltd.
- Chatfield, C. (1992) The Analysis of Time Series. Chapman & Hall.
- Chib, S. and Greenberg, E. (1996) Markov chain Monte Carlo simulation methods in econometrics. *Econometric Theory*, **12**, 409–431.
- Cobelli, C., Bettini, F., Caumo, A. and Quon, M. J. (1998) Overestimation of minimal model glucose effectiveness in presence of insulin response is due to undermodeling. *Endocrinology and Metabolism*, 275, 1031–1036.
- Cobelli, C., Caumo, A. and Omenetto, M. (1999) Minimal model SG overestimation and SI underestimation: improved accuracy by a Bayesian two-compartment model. *Endocrinology and Metabolism*, 277, 481–488.

- Coderre, L., Kandror, K. V., Vallega, G. and Pilch, P. F. (1995) Identification and characterization of an exercise-sensitive pool of glucose transporters in skeletal muscle. Journal of Biological Chemistry, 270, 27584–27588.
- Couri, C. E. B., Oliveira, M. C. B., Stracieri, A. B. P. L., Moraes, D. A., Pieroni, F., Barros, G. M. N., Madeira, M. I. A., Malmegrim, K. C. R., Foss-Freitas, M. C., Simões, B. P., Martinez, E. Z., Foss, M. C., Burt, R. K. and Voltarelli, J. C. (2009) C-peptide levels and insulin independence following autologous nonmyeloablative hematopoietic stem cell transplantation in newly diagnosed type 1 diabetes mellitus. Journal of the American Medical Association, 301, 1573–1579.
- Cowles, M. K. and Carlin, B. P. (1996) Markov chain Monte Carlo convergence diagnostics: A comparative review. *Journal of the American Statistical Association*, 91, 883–904.
- Crawford, K. (2004) Validation of the Sensewear Pro 2 Armband to Assess Energy Expenditure of Adolescents During Various Modes of Activity. Ph.D. thesis, University of Pittsburgh.
- Dalla Man, C., Breton, M. D. and Cobelli, C. (2009) Physical activity into the meal glucose-insulin model of type 1 diabetes: *In Silico* studies. *Journal of Diabetes Science and Technology*, **3**, 56–67.
- Dalla Man, C., Camilleri, M. and Cobelli, C. (2006) A system model of oral glucose absorption: Validation on gold standard data. *IEEE Transactions on Biomedical Engineering*, **53**, 2472–2478.
- Dalla Man, C., Rizza, R. A. and Cobelli, C. (2007) Meal simulation model of the glucose-insulin system. *IEEE Transactions on Biomedical Engineering*, **54**, 1740–1749.
- Daniell, P. J. (1946) Discussion on the symposium on autocorrelation in time series. Supplement to the Journal of the Royal Statistical Society, 8, 88–90.
- DCCT Research Group, . (1993) The effect of intensive treatment of diabetes on the development and progression of long-term complications in insulin-dependent diabetes mellitus. New England Journal of Medicine, 329, 977–986.
- DCCT/EDIC Study Research Group, . (2005) Intensive diabetes treatment and cardio-vascular disease in patients with type 1 diabetes. *New England Journal of Medicine*, **353**, 2643–2653.
- De Gaetano, A. and Arino, O. (2000) Mathematical modelling of the intravenous glucose tolerance test. *Journal of Mathematical Biology*, **40**, 136–138.

- Derouich, M. and Boutayeb, A. (2002) The effect of physical exercise on the dynamics of glucose and insulin. *Journal of Biomechanics*, **35**, 911–917.
- Diabetes UK (2008) Diabetes. Beware the silent assassin. Tech. rep., Diabetes UK.
- Diggle, P. J. (1990) Time Series: A Biostatistical Introduction. Oxford Science.
- Dinneen, S., Alzaid, A., Turk, D. and Rizza, R. (1995) Failure of glucagon suppression contributes to postprandial hyperglycaemia in IDDM. *Diabetologia*, **38**, 337–343.
- Donner, H., Rau, H., Walfish, P. G., Braun, J., Siegmund, T., Finke, R., Herwig, J., Usadel, K. H. and Badenhoop, K. (1997) CTLA4 alanine-17 confers genetic susceptibility to Graves' disease and to type 1 diabetes mellitus. *The Journal of Clinical Endocrinology and Metabolism*, 82, 143–146.
- Dormand, J. R. and Prince, P. J. (1980) A family of embedded Runge-Kutta formulae.

  Journal of Computational and Applied Mathematics, 6, 19–26.
- Doucet, A., de Freitas, N. and Gordon, N. (2001) Sequential Monte Carlo Methods in Practice. Springer, first edn.
- Ehehalt, S., Dietz, K., Willasch, A. M. and Neu, A. (2012) Prediction model for the incidence and prevalence of type 1 diabetes in childhood and adolescence: evidence for a cohort-dependent increase within the next two decades in Germany. *Pediatric Diabetes*, **13**, 15–20.
- El Youssef, J., Castle, J. and Ward, W. K. (2009) A review of closed-loop algorithms for glycemic control in the treatment of type 1 diabetes. *Algorithms*, **2**, 518–532.
- Eren-Oruklu, M., Cinar, A., Quinn, L. and Smith, D. (2009) Adaptive control strategy for regulation of blood glucose levels in patients with type 1 diabetes. *Journal of Process Control*, **19**, 1333–1346.
- Fagot-Campagna, A., Narayan, K. M. V. and Imperatore, G. (2001) Type 2 diabetes in children. *BMJ*, **322**, 377–378.
- Frid, A. and Linde, B. (1993) Clinically important differences in insulin absorption from abdomen in IDDM. *Diabetes Research and Clinical Practice*, **21**, 137–141.
- Ganong, W. F. (2005) Review of Medical Physiology. McGraw-Hill Medical, 22nd edn.
- Gantt, J. A., Rochelle, K. A. and Gatzke, E. P. (2007) Type 1 diabetic patient insulin delivery using asymmetric PI control. *Chemical Engineering Communications*, **194**, 586–602.

- Gelman, A. (2006) Prior distributions for variance parameters in hierarchical models. Bayesian Analysis, 1, 515–533.
- Gelman, A., Roberts, G. O. and Gilks, W. R. (1996) Efficient Metropolis jumping rules. In *Bayesian Statistics* 5 (eds. J. M. Bernardo, J. O. Berger, A. P. Dawid and A. F. M. Smith), 599–607. Oxford University Press.
- Gelman, A. and Rubin, D. B. (1992) Inference from iterative simulation using multiple sequences. *Statistical Science*, **7**, 457–472.
- Geman, S. and Geman, D. (1984) Stochastic relaxation, Gibbs distributions, and the Bayesian restoration of images. *IEEE Transactions on Pattern Analysis and Machine Intelligence*, 6, 721–741.
- Geyer, C. J. (1992) Practical Markov chain Monte Carlo. Statistical Science, 7, 473–483.
- Gilks, W. R., Richardson, S. and Spiegelhalter, D. J. (1996) Markov Chain Monte Carlo in Practice. Chapman & Hall.
- Gneiting, T. and Raftery, A. E. (2007) Strictly proper scoring rules, prediction, and estimation. *Journal of the American Statistical Association*, **102**, 359–378.
- Godfrey, K. (1983) Compartmental Models and Their Application. Academic Press Inc.
- Gonzalez, E. L. M., Johansson, S., Wallander, M.-A. and Garcia-Rodriguez, L. A. (2009) Trends in the prevalence and incidence of diabetes in the UK: 1996-2005. Journal of Epidemiology and Community Health, 63, 332–336.
- Goodyear, L. J. and Kahn, B. B. (1998) Exercise, glucose transport, and insulin sensitivity. *Annual Review of Medicine*, **49**, 235–261.
- Gough, D. A., Kreutz-Delgado, K. and Bremer, T. M. (2003) Frequency characterization of blood glucose dynamics. *Annals of Biomedical Engineering*, **31**, 91–97.
- Harrison, P. J. and Stevens, C. F. (1976) Bayesian forecasting. *Journal of the Royal Statistical Society. Series B (Methodological)*, **38**, 205–247.
- Hastings, W. K. (1970) Monte Carlo sampling methods using Markov chains and their applications. *Biometrika*, **57**, 97–109.
- Hejlesen, O. K., Andreassen, S., Cavanb, D. A. and Hovorka, R. (1996) Analysing the hypoglycaemic counter-regulation: a clinically relevant phenomenon? *Computer Methods and Programs in Biomedicine*, **50**, 231–240.

- Hejlesen, O. K., Andreassen, S., Hovorka, R. and Cavan, D. A. (1997) DIAS the diabetes advisory system: an outline of the system and the evaluation results obtained so far. Computer Methods and Programs in Biomedicine, 54, 49–58.
- Henriksen, J. E., Djurhuus, M. S., Vaag, A., Thyme-Ronn, P., Knudsen, D., Hother-Nielsen, O. and Beck-Nielsen, H. (1993) Impact of injection sites for soluble insulin on glycaemic control in type 1 (insulin-dependent) diabetic patients treated with a multiple insulin injection regime. *Diabetologia*, 36, 752–758.
- Herbst, A., Bachran, R., Kapellen, T. and Holl., R. W. (2006) Effects of regular physical activity on control of glycemia in pediatric patients with type 1 diabetes mellitus. *Archives of Pediatrics and Adolescent Medicine*, **160**, 573577.
- Hernandez-Ordonez, M. and Campos-Delgado, D. U. (2008) An extension to the compartmental model of type 1 diabetic patients to reproduce exercise periods with glycogen depletion and replenishment. *Journal of Biomechanics*, **41**, 744–752.
- Hicks, D., Kirkland, F., Pledger, J., Burmiston, S. and Basi, M. (2011) Helping people with diabetes to manage their injectable therapies. *Primary Health Care*, **21**, 28–31.
- Hirota, K., Ishihara, H., Tsubo, T. and Matsuki, A. (1999) Estimation of the initial distribution volume of glucose by an incremental plasma glucose level at 3 min after i.v. glucose in humans. British Journal of Clinical Pharmacology, 47, 361–364.
- Hovorka, R. (2005a) Management of diabetes using adaptive control. *International Journal of Adaptive Control and Signal Processing*, **19**, 309–325.
- (2005b) Management of diabetes using adaptive control. *International Journal of Adaptive Control and Signal Processing*, **19**, 309–325.
- Hovorka, R., Canonico, V., Chassin, L. J., Haueter, U., Massi-Benedetti, M., Federici,
  M. O., Pieber, T. R., Schaller, H. C., Schaupp, L., Vering, T. and Wilinska, M. E.
  (2004) Nonlinear predictive control of glucose concentration in subjects with type 1 diabetes. *Physiological Measurement*, 25, 905–920.
- Hovorka, R., Shoajee-Moradie, F., Carroll, P. V., Chassin, L. J., Gowrie, I. J., Jackson, N. C., Tudor, R. S., Umpleby, A. M. and Jones, R. H. (2001) Partitioning glucose distribution/transport, disposal, and endogenous production during IVGTT. American Journal of Physiology Endocrinology and Metabolism, 282, E997–E1007.
- Hu, F. B. (2003) Sedentary lifestyle and risk of obesity and type 2 diabetes. *Lipids*, **38**, 103–108.
- Hyoty, H. (2002) Enterovirus infections and type 1 diabetes. *Annals of Medicine*, **34**, 138–147.

- Saez-de Ibarra, L. and Gallego, F. (1998) Factors related to lipohypertrophy in insulintreated diabetic patients: role of educational intervention. *Practical Diabetes International*, **15**, 9–11.
- Jenkins, D. J. A., Wolever, T. M. S., Taylor, R. H., Barker, H., Fielden, H., Baldwin, J. M., Bowling, A. C., Newman, H. C., Jenkins, A. L. and Goff, D. V. (1981) Glycemic Index of foods: a physiological basis for carbohydrate exchange. The American Journal of Clinical Nutrition, 34, 362–366.
- Jenkins, G. M. and Watts, D. G. (1968) Spectral Analysis and its Applications. Holden-Day.
- Johansen, K., Svendsen, R. A. and Lorup, B. (1984) Variations in renal threshold for glucose in type 1 (insulin-dependent) diabetes mellitus. *Diabetologia*, **26**, 180–182.
- Kalman, R. E. (1963) New methods in Wiener filtering theory. In *Proceedings of the First Symposium on Engineering Application of Random Function Theory and Probability* (eds. J. L. Bogdanoff and F. Kozin). New York: Wiley.
- Kameth, S., George, V. I. and Vidyasagar, S. (2006) A review of control algorithms for non invasive monitoring. *Journal of Automatic Control and Systems Engineering*, **6**, 17–22.
- Kellow, J., Costain, L. and Walton, R. (2007) The Calorie, Carb & Fat Bible 2008. Weight Loss Resources Ltd.
- Kendall, M. G., Stuart, A. and Ord, J. K. (1983) Advanced Theory of Statistics (Volume 3). Griffin.
- Klemp, P., Staberg, B., Madsbad, S. and Kolendorf, K. (1982) Smoking reduces insulin absorption from subcutaneous tissue. *British Medical Journal*, **284**, 237.
- Klonoff, D. C. (2005) Continuous glucose monitoring: Roadmap for 21st century diabetes therapy. *Diabetes Care*, **28**, 1231–1239.
- Koivisto, V. A. (1980) Sauna-induced acceleration in insulin absorption from subcutaneous injection site. *British Medical Journal*, **280**, 1411–1413.
- Koivisto, V. A., Fortney, S., Hendler, R. and Felig, P. (1981) A rise in ambient temperature augments insulin absorption in diabetic patients. *Metabolism*, **30**, 402–405.
- Kroop, H. S., Long, W. B., Alavi, A. and Hansell, J. R. (1979) Effect of water and fat on gastric emptying of solid meals. *Gastroenterology*, **77**, 997–1000.

- Lee, H. and Bequette, B. W. (2009) A closed-loop artificial pancreas based on model predictive control: Human-friendly identification and automatic meal disturbance rejection. *Biomedical Signal Processing and Control*, 4, 347–354.
- Lehmann, E. D. and Deutsch, T. (1991) A physiological model of glucose-insulin interaction. In *Proceedings of the 13th Annual International Conference of the IEEE Engineering in Medicine and Biology Society, IEEE Press.*
- (1992) A physiological model of glucose-insulin interaction in type 1 diabetes mellitus. *Journal of Biomedical Engineering*, **14**, 235–242.
- (1998) Compartmental models for glycaemic prediction and decision-support in clinical diabetes care: promise and reality. *Computer Methods and Programs in Biomedicine*, **56**, 193–204.
- Lehmann, E. D., Tarin, C., Bondia, J., Teufel, E. and Deutsch, T. (2007) Incorporating a generic model of subcutaneous insulin absorption into the AIDA v4 diabetes simulator. *Journal of Diabetes Science and Technology*, 1, 423–435.
- Lenart, P. J. and Parker, R. S. (2002) Modeling exercise effects in type 1 diabetes. In 15th Triennial World Congress, Barcelona, Spain.
- LeRoith, D., Taylor, S. I. and Olefsky, J. M. (2003) *Diabetes Mellitus: A Fundamental and Clinical Text*. Lippincott Williams and Wilkins, third (revised) edn.
- Liden, C., Wolowicz, M., Stivoric, J., Teller, A., Vishnubhatla, S., Pelletier, R. and Farringdon, J. (2002) Accuracy and reliability of the Sensewear armband as an energy expenditure assessment device. Internal analysis document; http://www.welnia.com/docs/Accuracy.pdf.
- Liden, C., Wolowicz, M., Stivoric, J., Teller, A., Vishnubhatla, S., Pelletier, R., Farringdon, J. and Boehmke, S. (2001) Benefits of the Sensewear armband over other physical activity and energy expenditure measurement techniques. Internal analysis document.
- Liu, D., Adamson, U., Lins, P. E. and Clausen-Sjobom, N. (1993) An analysis of the glucagon response to hypoglycaemia in patients with type 1 diabetes and in healthy subjects. *Diabetic Medicine*, **10**, 246–254.
- Marchetti, G., Barolo, M., Jovanovic, L., Zisser, H. and Seborg, D. E. (2008) A feedforward-feedback glucose control strategy for type 1 diabetes mellitus. *Journal of Process Control*, **18**, 149–162.
- Marliss, E. B. and Vranic, M. (2002) Intense exercise has unique effects on both insulin release and its roles in glucoregulation. *Diabetes*, **51**, S271–S283.

- Marmarelis, V. Z. (2004) Nonlinear Dynamic Modelling of Physiological Systems. Wiley-Interscience.
- Metropolis, N., Rosenbluth, A. W., Rosenbluth, M. N. and Teller, A. H. (1953) Equation of state calculations by fast computing machines. *Journal of Chemical Physics*, **21**, 1087–1092.
- Mosekilde, E., Jensen, K. S., Binder, C., Pramming, S. and Thorsteinsson, B. (1989) Modeling absorption kinetics of subcutaneous injected soluble insulin. *Journal of Pharmacokinetics and Biopharmaceutics*, **17**, 67–87.
- Muis, M. J., Bots, M. L., Bilo, H. J. G., Hoogma, R. P. L. M., Hoekstra, J. B. L., Grobbee, D. E. and Stolk, R. P. (2006) Determinants of daily insulin use in type 1 diabetes. *Journal of Diabetes and Its Complications*, **20**, 356–360.
- Naylor, J. N., Hodel, A. S., Morton, B. and Schumacher, D. (1995) Automatic control issues in the development of an artificial pancreas. In *Proceedings of the American Control Conference*, Seattle, Washington.
- NHS Information Centre (2011) National diabetes audit mortality analysis 2007-2008. Tech. rep., National Health Service.
- Nucci, G. and Cobelli, C. (2000) Models of subcutaneous insulin kinetics. a critical review. Computer Methods and Programs in Biomedicine, 62, 249–257.
- Ohlson, L.-O., Larsson, B., Bjrrntorp, P., Eriksson, H., Svirdsudd, K., Welin, L., Tibblin, G. and Wilhelmsen, L. (1988) Risk factors for type 2 (non-insulin-dependent) diabetes mellitus. Thirteen and one-half years of follow-up of the participants in a study of Swedish men born in 1913. *Diabetologia*, **31**, 798–805.
- Onkamo, P., Väänänen, S., Karvonen, M. and Tuomilehto, J. (1999) Worldwide increase in incidence of type 1 diabetes the analysis of the data on published incidence trends. *Diabetologia*, **42**, 1395–1403.
- Palerm, C. C., Zisser, H., Jovanovic, L. and Doyle III, F. J. (2008) A run-to-run control strategy to adjust basal insulin infusion rates in type 1 diabetes. *Journal of Process Control*, **18**, 258–265.
- Parker, R. S., Doyle, F. J., Ward, J. H. and Peppas, N. A. (2000) Robust H-infinity glucose control in diabetes using a physiological model. *AIChE Journal*, **46**, 2537–2549.
- Parker, R. S., III, F. J. D. and Peppas, N. A. (2001) The intravenous route to blood glucose control. *IEEE Engineering in Medicine and Biology*, **51**, 65–73.

- Petersen, K. F., Price, T. B. and Bergeron, R. (2005) Regulation of net hepatic glycogenolysis and gluconeogenesis during exercise: Impact of type 1 diabetes. *The Journal of Clinical Endocrinology & Metabolism*, 89, 46564664.
- Pickup, J. and Keen, H. (2001) Continuous subcutaneous insulin infusion in type 1 diabetes. *BMJ*, **322**, 1262–1263.
- Ploughmann, S., Hejlesen, O., Turner, B., Kerr, D. and Cavan, D. (2003) The effect of alcohol on blood glucose in type 1 diabetes-metabolic modelling and integration in a decision support system. *International Journal of Medical Informatics*, **70**, 337–344.
- Pocock, G. and Richards, C. D. (2006) *Human Physiology: The basis of medicine*. Oxford Core Texts, third edn.
- Pole, A., West, M. and Harrison, J. (1994) Applied Bayesian Forecasting and Time Series Analysis. Chapman & Hall, first edn.
- Priestley, M. B. (1981) Spectral Analysis and Time Series (Volume 1). Academic Press Inc.
- Puckett, W. R. (1992) Dynamic Modeling of Diabetes Mellitus. University of Wisconsin Madison.
- Quiroz, G. and Femat, R. (2010) Theoretical blood glucose control in hyper- and hypoglycemic and exercise scenarios by means of an  $H_{\infty}$  algorithm. *Journal of Theoretical Biology*, **263**, 154–160.
- Regittnig, W., Trajanoski, Z., Leis, H.-J., Ellmerer, M., Wutte, A., Sendlhofer, G., Schaupp, L., Brunner, G. A., Wach, P. and Pieber, T. R. (1999) Plasma and interstitial glucose dynamics after intravenous glucose injection. *Diabetes*, 48, 1070–1081.
- Riddell, M. C. and Iscoe, K. E. (2006) Physical activity, sport, and pediatric diabetes. *Pediatric Diabetes*, **7**, 60–70.
- Roep, B. O. (2003) The role of T-cells in the pathogenesis of type 1 diabetes: From cause to cure. *Diabetologia*, **46**, 305–321.
- Rollins, D. K., Bhandari, N. and Kotz, K. R. (2008) Critical modeling issues for successful feedforward control of blood glucose in insulin dependent diabetics. In *American Control Conference*, Seattle, Washington, 832-837.
- Roy, A. (2008) Dynamic Modeling of Free Fatty Acid, Glucose, and Insulin During Rest and Exercise in Insulin Dependent Diabetes Mellitus Patients. Ph.D. thesis, University of Pittsburgh.

- Roy, A. and Parker, R. S. (2006) Dynamic modeling of free fatty acid, glucose, and insulin: An extended "minimal model". *Diabetes Technology & Therapeutics*, 8, 617–626.
- (2007) Dynamic modeling of exercise effects on plasma glucose and insulin levels. Journal of Diabetes Science and Technology, 1, 338–347.
- Salzsieder, E., Albrecht, G., Fischer, U., Rutscher, A., Stephen, R. L. and Stoewhas, H. (1990) Assessment of individual pharmacokinetics and pharmacodynamics of insulin and its therapeutic consequences based on a model of the glucose-insulin system. In Annual International Conference of the IEEE Engineering in Medicine and Biology Society, vol. 12, no. 3.
- Salzsieder, E. and Rutscher, A. (1998) Identification of the parameters of a glucose/insulin control model based on individually monitored self-control data in diabetes care. Proceedings of the 20th Annual International Conference of the IEEE Engineering in Medicine and Biology Society, 20, 3123–3125.
- Scheen, A. J. and van Cauter, E. (1998) The roles of time of day and sleep quality in modulating glucose regulation: Clinical implications. *Hormone Research*, **49**, 191–201.
- Shapiro, A. M. J., Lakey, J. R. T., Ryan, E. A., Korbutt, G. S., Toth, E., Warnock, G. L., Kneteman, N. M. and Rajotte, R. V. (2000) Islet transplantation in seven patients with type 1 diabetes mellitus using a glucocorticoid-free immunosuppressive regimen. *New England Journal of Medicine*, **343**, 230–238.
- Shapiro, A. M. J., Ricordi, C., Hering, B. J., Auchincloss, H., Lindblad, R., Robertson, R. P., Secchi, A., Brendel, M. D., Berney, T., Brennan, D. C., Cagliero, E., Alejandro, R., Ryan, E. A., DiMercurio, B., Morel, P., Polonsky, K. S., Reems, J. A., Bretzel, R. G., Bertuzzi, F., Froud, T., Kandaswamy, R., Sutherland, D. E., Eisenbarth, G., Segal, M., Preiksaitis, J., Korbutt, G. S., Barton, F. B., Viviano, L., Seyfert-Margolis, V., Bluestone, J. and Lakey, J. R. (2006) International trial of the Edmonton protocol for islet transplantation. *New England Journal of Medicine*, 355, 1318–1330.
- Sheard, N. F., Clark, N. G., Brand-Miller, J. C., Franz, M. J., Pi-Sunyer, F. X., Mayer-Davis, E., Kulkarni, K. and Geil, P. (2004) Dietary carbohydrate (amount and type) in the prevention and management of diabetes. *Diabetes Care*, **27**, 2266–2271.
- Shin, J. J., Holtzclaw, K. R., Dangui, N. D., Kanderian Jnr, S., Mastrototaro, J. J. and Hong, P. I. (2006) Real time self-adjusting calibration algorithm. United States Patent; Patent No. US 7,029,444 B2; April 18, 2006.

- Siegel, J. A., Urbain, J. L., Adler, L. P., Charkes, N. D., Maurer, A. H., Krevsky, B., Knight, L. C., Fisher, R. S. and Malmud, L. S. (1988) Biphasic nature of gastric emptying. Gut, 29, 85–89.
- Soedamah-Muthu, S. S., Fuller, J. H., Mulnier, H. E., Raleigh, V. S., Lawrenson, R. A. and Colhoun, H. M. (2006) All-cause mortality rates in patients with type 1 diabetes mellitus compared with a non-diabetic population from the UK general practice research database, 1992-1999. *Diabetologia*, 49, 660–666.
- Sorensen, J. T. (1985) A Physiological Model of Glucose Metabolism in Man and its use to Design and Assess Improved Insulin Therapies for Diabetes. Massachusetts Institute of Technology.
- Soru, P., De Nicolao, G., Toffanin, C., Dalla Man, C., Cobelli, C. and Magni, L. (2012) MPC based artificial pancreas: Strategies for individualization and meal compensation. Annual Reviews in Control, 36, 118–128.
- Sparacino, G., Zanderigo, F., Corazza, S., Maran, A., Facchinetti, A. and Cobelli, C. (2007) Glucose concentration can be predicted ahead in time from continuous glucose monitoring sensor time-series. *IEEE Transactions on Biomedical Engineering*, 54, 931–937.
- Stumvoll, M., Chintalapudi, U., Perriello, G., Welle, S., Gutierrez, O. and Gerich, J. (1995) Uptake and release of glucose by the human kidney. Postabsorptive rates and responses to epinephrine. *Journal of Clinical Investigation*, **96**, 2528–2533.
- S., Sunseri, М., Liden, C., Farringdon, J., Pelletier, R., Safier, S. J., Teller, Α. and Vishnubhatla, The Sensewear arm-Stivoric, () sleep detection device. Internal analysis document: http://www.welnia.com/docs/SenseWearasSleepDetectionDevice.pdf.
- Tamborlane, W. V., Beck, R. W., Bode, B. W., Buckingham, B., Chase, H. P., Clemons, R., Fiallo-Scharer, R., Fox, L. A., Gilliam, L. K., Hirsch, I. B., Huang, E. S., Kollman, C., Kowalski, A. J., Laffel, L., Lawrence, J. M., Lee, J., Mauras, N., O'Grady, M., Ruedy, K. J., Tansey, M., Tsalikian, E., Weinzimer, S., Wilson, D. M., Wolpert, H., Wysocki, T. and Xing, D. (2008) Continuous glucose monitoring and intensive treatment of type 1 diabetes. New England Journal of Medicine, 359, 1464–1476.
- Tarin, C., Teufel, E., Pic, J., Bondia, J. and Pfleiderer, H.-J. (2005) Comprehensive pharmacokinetic model of insulin glargine and other insulin formulations. *IEEE Transactions on Biomedical Engineering*, **52**, 1994–2005.

- Teddy, S. D., Quek, C., Lai, E. M.-K. and Cinar, A. (2010) PSECMAC intelligent insulin schedule for diabetic blood glucose management under nonmeal announcement. *IEEE Transactions on Neural Networks*, **21**, 361–380.
- Teuscher, A. (2007) Insulin A Voice for Choice. S Karger AG.
- Thomas, M. C., Walker, M. K., Emberson, J. R., Thomson, D. A., Lawlor, D. A., Ebrahim, S. and Whincup, P. H. (2005) Prevalence of undiagnosed type 2 diabetes and impaired fasting glucose in older British men and women. *Diabetic Medicine*, **22**, 789–793.
- Thorell, A., Hirshman, M. F., Nygren, J., Jorfeldt, L., Wojtaszewski, J. F. P., Dufresne, S. D., Horton, E. S., Ljungqvist, O. and Goodyear, L. J. (1999) Exercise and insulin cause GLUT-4 translocation in human skeletal muscle. *Endocrinology and Metabolism*, 277, E733–E741.
- Toffolo, G., Bergman, R. N., Finegood, D. T., Bowden, C. R. and Cobelli, C. (1980) Quantitative estimation of  $\beta$ -cell sensitivity to glucose in the intact organism: A minimal model of insulin kinetics in the dog. *Diabetes*, **29**, 979–990.
- Tong, H. (1993) Non-linear Time Series. Oxford Science Publications.
- Trajanoski, Z., Wach, P., Kotanko, P., Ott, A. and Skraba, F. (1993) Pharmacokinetic model for the absorption of subcutaneously injected soluble insulin and monomeric insulin analogues. *Biomedizinische Technik*, **38**, 224–231.
- Valletta, J. J. (2011) Dynamic modelling of the effect of physical activity on capillary blood glucose concentration in people with type 1 diabetes. PhD Thesis.
- Valletta, J. J., Chipperfield, A. J. and Byrne, C. D. (2009) Gaussian process modelling of blood glucose response to free-living physical activity data in people with type 1 diabetes. In Conference Proceedings of IEEE Engineering in Medicine and Biology Society, 4913–4916.
- Waden, J., Tikkanen, H., Forsblom, C., Fagerudd, J., Pettersson-Fernholm, K., Lakka, T., Riska, M., Groop, P.-H. and on behalf of the FinnDiane Study Group (2005) Leisure time physical activity is associated with poor glycemic control in type 1 diabetic women. *Diabetes Care*, 28, 777–782.
- Weissberg-Benchell, J., Antisdel-Lomaglio, J. and Seshadri, R. (2003) Insulin pump therapy: a meta-analysis. *Diabetes Care*, **26**, 1079–1087.
- Wentholt, I. M. E., Hart, A. A. M., Hoekstra, J. B. L. and DeVries, J. H. (2007) Relationship between interstitial and blood glucose in type 1 diabetes patients: Delay

- and the push-pull phenomenon revisited. Diabetes Technology & Therapeutics, 9, 169–175.
- West, M. and Harrison, J. (1997) Bayesian Forecasting and Dynamic Models. Springer.
- Wild, S., Roglic, G., Green, A., Sicree, R. and King, H. (2004) Global prevalence of diabetes: Estimates for the year 2000 and projections for 2030. *Diabetes Care*, 27, 1047–1053.
- Wilinska, M. E., Chassin, L. J., Schaller, H. C., Schaupp, L., Pieber, T. R. and Hovorka, R. (2005) Insulin kinetics in type-1 diabetes: Continuous and bolus delivery of rapid acting insulin. *IEEE Transactions in Biomedical Engineering*, **52**, 3–12.
- Wolever, T. M. S. and Bolognesi, C. (1996) Prediction of glucose and insulin responses of normal subjects after consuming mixed meals varying in energy, protein, fat, carbohydrate and glycemic index. *The Journal of Nutrition*, **126**, 2807–2812.
- Wolfe, R. R., Nadel, E. R., Shaw, J. H., Stephenson, L. A. and Wolfe, M. H. (1986) Role of changes in insulin and glucagon in glucose homeostasis in exercise. *Journal of Clinical Investigation*, 77, 900–907.
- Wong, X.-W., Chase, J. G., Compte, A. J. L., Hann, C. E., Lin, J. and Shaw, G. M. (2009) An adaptive clinical type 1 diabetes control protocol to optimize conventional self-monitoring blood glucose and multiple daily-injection therapy. *International Journal of Adaptive Control and Signal Processing*, 23, 408–434.
- World Health Organisation (2008) World Health Organisation factsheet, no. 312. http://www.who.int/mediacentre/factsheets/fs312/en/.
- Worthington, D. R. L. (1997) Minimal model of food absorption in the gut. *Informatics* for Health and Social Care, 22, 35–45.
- Yamaguchi, M., Kaseda, C., Yamazaki, K. and Kobayashi, M. (2006) Prediction of blood glucose level of type 1 diabetics using response surface methodology and data mining. *Medical and Biological Engineering and Computing*, **44**, 451–457.
- Zajadacz, B., Skarpańska-Stejnborn, A., Brzenczek-Owczarzak, W., Juszkiewicz, A., Naczk, M. and Adach, Z. (2009) The influence of physical exercise on alterations in concentrations of neuropeptide Y, leptin and other selected hormonal and metabolic parameters in sportspeople. Biology of Sport, 26, 309–324.
- Zhao, Y., Jiang, Z., Zhao, T., Ye, M., Hu, C., Yin, Z., Li, H., Zhang, Y., Diao, Y., Li, Y., Chen, Y., Sun, X., Fisk, M. B., Skidgel, R., Holterman, M., Prabhakar, B. and Mazzone, T. (2012) Reversal of type 1 diabetes via islet cell regeneration following

immune modulation by cord blood-derived multipotent stem cells.  $BMC\ Medicine,$  10.

Zimmet, P. (1982) Type 2 (non-insulin-dependent) diabetes - an epidemiological overview. *Diabetologia*, **22**, 399–411.